Sclerochronology of Deep-Sea Bamboo Corals from the Northwest Atlantic: *Acanella arbuscula* and *Keratoisis* spp.

by

©

Laura F. Piccirillo

A Thesis submitted to the School of Graduate Studies in partial fulfillment
of the requirements for the degree of Master of Science

Environmental Science Program (Thesis-based) / Faculty of Science

Memorial University of Newfoundland and Labrador

March 2023

St. John's, Newfoundland and Labrador, Canada

Abstract

Deep-sea corals provide habitat for invertebrates and fish, have high longevities, and slow growth rates, making them vulnerable to anthropogenic disturbances. The bamboo corals *Acanella arbuscula* and *Keratoisis flexibilis* have been observed in the NW Atlantic, but growth rates and ages have not been heavily studied. Growth ring counts at the proteinaceous nodes of the coral skeletons were used for aging. Both species exhibited major and minor growth rings, but major rings represent annual growth in *A. arbuscula* and minor rings represent annual growth in *K. flexibilis*, determined by comparing age estimates from ring counts to radiometrically validated specimens of each species. Ages, radial, and axial growth rates ranged from 8-29 years, 0.025 – 0.160 mm/yr, and 1.87 – 16.1 mm/yr for *A. arbuscula,* and 89-168 years, 0.007-0.027 mm/yr, and 1.5-5.3 mm/yr for *K. flexibilis*. Geographic variations in *A. arbuscula* growth rates were observed, with the SE Baffin Shelf specimens growing the fastest because these specimens were youngest, and ontogenetic influence on growth rates was observed, causing younger colonies to grow faster. *K. flexibilis* growth rates were slower than *K. grayi,* and this inter-specific difference can be attributed to temperature, as the *K. flexibilis* samples were collected in colder waters.

General Summary

Deep-sea corals are found all throughout the world's oceans and are important components within their habitats because they provide shelter for other organisms. *Acanella arbuscula* and *Keratoisis flexibilis* are deep-sea bamboo corals that have been observed in the NW Atlantic, but average ages and growth rates for both species have not been determined. Similar to trees, some corals form annual growth rings that can be counted for ages. This study used growth ring counts in coral skeletons, and determined ages for *A. arbuscula* to be 8-29 years, radial growth rates of 0.025 – 0.160 mm/yr, and axial growth rates of 1.87 – 16.1 mm/yr. Ages for *K. flexibilis* were older (89-168 years), and radial and axial growth rates were slower (0.007-0.027 mm/yr; 1.5-5.3 mm/yr). Growth rates for both species are slow, which indicates they are vulnerable to anthropogenic disturbances, like bottom-contact fishing, because they are not able to recover quickly.

Table of Contents

List of Tables

List of Figures

List of Appendices

Abbreviations

DFO – Department of Fisheries and Oceans, Canada

MUN – Memorial University of Newfoundland and Labrador

NAFO – North Atlantic Fisheries Organization

ROV – remotely operated vehicle

Co-Authorship Statement

The work presented in this thesis was conducted and written by Laura Piccirillo. Original research planning and design were created by Evan Edinger and Meghan Burchell. Field work was carried out by Laura Piccirillo, Evan Edinger, and Bárbara Neves. Data chapter 2 is formatted for publication to Marine Ecology Progress Series or Deep-Sea Research I and co-authors are Laura Piccirillo, Evan Edinger, Bárbara Neves, Meghan Burchell, and Graham Layne. A portion of the lab preparation for Chapter 2 was conducted by Bárbara Neves and Vonda Wareham-Hayes, with the rest conducted by Laura Piccirillo. Chapter 3 is formatted for publication to Deep-Sea Research I and co-authors are Laura Piccirillo, Evan Edinger, Bárbara Neves, Meghan Burchell, Owen Sherwood, Shaomin Chen, and Graham Layne. Some lab work and analyses were conducted by Owen Sherwood and Shaomin Chen for Chapter 3, with the rest conducted by Laura Piccirillo. Input and advice on lab work techniques were provided from Evan Edinger, Meghan Burchell, Bárbara Neves, and Graham Layne for Chapters 2 and 3. Edits and comments for this thesis were provided from Evan Edinger, Meghan Burchell, and Graham Layne. Appendix 4-1 is a summary of the calcein staining experiment conducted in 2021 and was written by Laura Piccirillo, and will form part of a technical report in future work.

COVID-19 Impact Statement

The global COVID-19 pandemic interrupted various parts of completing this thesis in a timely and efficient manner. Firstly, I interviewed and was encouraged to apply for this MSc position in January of 2020, yet due to the pandemic beginning in March of 2020, everything was put on hold, and I did not end up applying until June of 2020, only three months before beginning my program. Next, due to travel restrictions and being an international student, I was unable to move to St. John's until March of 2021, six months after the start of my program in September, 2020. I then had to isolate for three days at my port of entry into Canada (Montreal), followed by a 14-day isolation at Memorial University (MUN). I completed all of my coursework remotely, as all classes during Fall and Winter of 2020-2021 were carried out virtually.

Closures at MUN and limits to on-campus access for research activities postponed my start to lab work until May of 2021. I was also supposed to participate in a research cruise in May of 2020 to begin collecting samples for my project, but this cruise ended up being pushed to a later date and shortened in length, so I was not able to collect samples for my project until July of 2021. I luckily was still able to participate in a research cruise in July/August of 2021, which was a phenomenal learning experience and something I am very grateful for.

Due to the Omicron breakout in December of 2021, I was unable to travel to The Bedford Institute of Oceanography in Halifax, NS for sediment core processing, which had originally been scheduled for January of 2022. Additionally, I was unable to travel to ETH Zürich, which had originally been scheduled for February of 2022, for LA-AMS-^{14}C

measurements on bamboo corals for my studies. A new laser ablation radiocarbon system was planned to be used for my samples at ETH Zürich, but due to the travel restrictions and university guidelines, we instead had to ship my samples overseas. This delayed my measurements originally, and measurements were also delayed due to one of our collaborators in Switzerland testing positive for COVID-19. The first radiocarbon measurements were carried out on March 25, 2022, nearly five weeks after the original set date, all due to COVID restrictions and complications. Because of the delays and complications, the LA-AMS-^{14}C measurements are not included in either data chapters of this thesis, but are included as appendices, which will be co-published with the ETH Zürich scientists in future work.

I was supposed to participate in an additional research cruise in August of 2022, on board the Atlantic Condor focused on deep-sea habitats on the Scotian Shelf and offshore SW Newfoundland, but was unable to after testing positive for COVID-19 only one day before the cruise was departing Halifax.

Lastly, impacts of the COVID-19 pandemic felt by many graduate students included increased financial stress due to higher prices of travel, and risks of traveling and contracting COVID-19, and then having to pay for isolation accommodations. Similar to all people, the unwavering stress of contracting COVID-19 during daily activities and exposing friends, family, professors, and peers, had an obvious hindrance on academic performance and the proper graduate school experience. Amidst all of these complications and hardships, it does give a larger sense of pride in overcoming these obstacles and being able to successfully complete my program during a global pandemic.

CHAPTER 1: General Introduction

Deep-sea corals serve as key components within their environment, providing habitat for fish and invertebrates, and increasing the overall complexity of the surrounding ecosystem (Krieger and Wing 2002; Buhl-Mortensen and Mortensen 2004; Pierrejean et al. 2020). In the NW Atlantic and eastern Canadian Arctic, a group of corals informally termed "gorgonians" (Octocorallia sub-class) are composed of calcium carbonate and proteinaceous skeletons, and these corals are typically observed as solitary colonies or forming coral forests, but not usually reefs (Wareham and Edinger 2007; Kenchington et al. 2016). However, reef habitats in the NW Atlantic have been observed composed of the scleractinian coral *Lophelia pertusa* at the Stone Fence on the Scotian Shelf (Buhl-Mortensen et al. 2017), and in Greenlandic waters off SE Greenland (Kenchington et al. 2017). Other types of deep-sea corals documented in the region include antipatharians (black corals) (Wareham and Edinger 2007), pennatulaceans (sea pens) (Baker et al. 2012), and alcyonaceans (soft corals) (Table 1-1) (Mortensen et al. 2006; Wareham and Edinger 2007; Kenchington et al. 2016). Gorgonian corals are members of the Cnidaria phylum, Anthozoan class, Octocoral sub-class, and Alcyonaceans order (Table 1-1). Divisions below order are dependent on the type of gorgonian coral, with bamboo corals being members of the Calcaxonia and Holaxonia sub-orders (Table 1-1) (Watling et al. 2011; Roberts and Cairns 2014; Heestand Saucier et al. 2021). Bamboo coral taxonomy is continuously evolving, and recent studies have suggested three subfamilies within the Isididae family be elevated to the family level, including the sub-family Keratoisididae (Table 1-1) (Heestand Saucier et al. 2021; Watling et al. 2022).

Deep-sea coral research in the NW Atlantic, and globally, has been increasing in response to the development of manned and unmanned submersible vehicles, specifically remotely operated vehicles (ROV). Prior to these technological advancements, deep-sea corals were minimally studied due to their remote locations and the challenges of deep-sea exploration efforts (Roberts and Hirshfield 2004). Deep-sea corals mainly exist on the continental shelf, slope, and on seamounts in depths greater than 200m and occasionally exceeding 4000m, but have been observed in shallower depths as well.

In the Atlantic, both scleractinian and gorgonian corals are present (Hall-Spencer et al. 2007; Buhl-Mortensen et al. 2015). Growth rate, aging, and paleoceanographic studies have focused more on scleractinians (Frank et al. 2004; Pons-Branchu et al. 2005; Robinson et al. 2007) and large gorgonians (Heikoop et al. 2002; Sherwood et al. 2005; Sherwood et al. 2008), and less on small gorgonians and bamboo corals (Sherwood and Edinger 2009; Hill et al. 2011; Farmer et al. 2015). Bamboo corals have been studied more frequently in the Pacific and Gulf of Alaska (Roark et al. 2005; Tracey et al. 2007; Andrews et al. 2009; Sherwood et al. 2009). This study focuses on determining ages and growth rates for the understudied, small bamboo coral *Acanella arbuscula* from the NW Atlantic, and the bamboo coral *Keratoisis flexibilis* from the eastern Canadian Arctic, which was observed forming dense patches (Neves et al. 2015), but has not been studied for longevity.

Table 1-1. Taxonomic diagram of deep-sea bamboo corals with recent revisions shown (Heestand Saucier et al. 2021).

Class	Sub-Class	Order	Sub-Order	Family
Anthozoa	Octocorallia	Helioporacea		
		Alcyonacea	Protoalcyonaria	
			Stolonifera	
			Alcyoniina	
			Scleraxonia	
			Holaxonia	Isididae
				Chelidonisididae
			Calcaxonia	Mopseidae
				Keratoisididae
				Isidoidae
				Ellisellidae
				Dendrobrachiidae
		Pennatulacea		

1.1 ECOLOGICAL ROLE OF DEEP-SEA CORALS

Deep-sea corals are often referred to as ecosystem engineers, as they perform essential ecosystem functions, alter sedimentation patterns, and increase the overall complexity of benthic environments (Buhl-Mortensen and Mortensen 2004; Buhl-Mortensen et al. 2010). Ecosystem functions include providing substrate and feedings sites for other organisms, along with nutrient cycling (Roberts et al. 2009; Buhl-Mortensen et al. 2010), which includes providing shelter and feeding sites for highly sought-after commercially fished species and invertebrates in particular (Boulard et al. 2022; Edinger et al. 2007; Buhl-Mortensen and Mortensen 2005). Many studies have noted observations of fish and invertebrate species interacting with deep-sea corals, and gorgonians especially (Krieger and Wing 2002; Roberts and Hirshfield 2004; Westerman et al. 2021).

1.1.1 *Environmental significance & conservation importance*

Most deep-sea corals globally are threatened by a variety of natural and anthropogenic disturbances. Commercial fishing activities, specifically bottom trawling, are detrimental to deep-sea corals because they are sessile organisms, often with robust skeletons that are long-lived and slow-growing (Roberts and Hirshfield 2004; Shester et al. 2021). Since the 1970s, trawling efforts have been even more detrimental for deep-sea coral habitats because of migration in fishing activity to deeper waters due to depleted fish stocks in shallower waters, with about 40 percent of trawling grounds existing on continental slopes and margins (Roberts and Hirshfield 2004; Roberts and Cairns 2014). In the NW Atlantic, the cod moratorium in 1992 (Schrank 2005) led to deeper fishing activities in recent years. Little is known regarding the impact of destruction from fishing activities on deep-sea coral species, as recovery patterns have been minimally studied. Many species have long lifespans and slow growth rates, which makes them particularly vulnerable to disturbance events (Hall-Spencer et al. 2002; Lacharité and Metaxas 2013; Beazley et al. 2021). Effects of deep-sea coral disturbances are still not well understood for many species, therefore, studies are focusing on deep-sea coral growth patterns, growth rates, and ages by studying growth rings in coral skeletons.

Sclerochronology was first suggested as a field of study analogous to dendrochronology in Buddemeier et al. (1974), which defined it as "the study of growth patterns in calcareous exoskeletons or shells". The study of sclerochronology involves marine organisms such as corals and mollusks and is a tool to develop high resolution

chronologies that can be used in paleoclimate studies and to study growth rates and longevity in marine invertebrates (Oschmann 2009; Peharda et al. 2021).

Expansion in the oil and gas industry also poses risks to deep-sea corals, as they are at a higher risk for destruction with increased mining, drilling, and exploration in deep-sea habitats (Roberts and Cairns 2014). Deep-sea coral habitats affected by oil spills have also been observed to exhibit increased stress levels and declining health (White et al. 2012), meaning effects of oil and gas extraction can also harm corals not directly impacted by the mining and extraction process, but also by oil spills. The expansion of oil and gas industries and bottom-contact fishing is particularly worrisome for Arctic habitats, where melting ice sheets are allowing for increased anthropogenic activity in previously unexplored areas (Andersen et al. 2017). Therefore; Arctic benthic environments are important to study and understand given the increasing threats to establish baseline conditions prior to further anthropogenic activity in the area.

Finally, as with most environments and species on Earth, climate change also poses a threat to deep-sea corals, due to variation in the pH of ocean waters. It is estimated that over 80% of warming during the last 40 years has been absorbed by oceans, making ocean temperature change a concern (Robert and Cairns 2014). Greenhouse gas emissions are also causing gradual ocean acidification due to oceanic uptake of atmospheric CO_2 (Roberts and Cairns 2014). The CO_2 uptake by oceans is causing declines in pH, with pH set to fall up to 0.4 units by 2100, as well as declines in carbonate ion concentration (Turley et al. 2007). As corals are formed from calcium carbonate crystal structures, the decline in carbonate ion concentration has the potential to limit growth for many benthic calcifiers,

which could decrease suitable habitat available for other marine organisms (Turley et al. 2007; Tittensor et al. 2010). The current threats to deep-sea corals have made them a component of Vulnerable Marine Ecosystems (VMEs) listed by the United Nations, and coastal regions are required to identify and protect VMEs (Rogers and Gianni 2010; Roberts and Cairns 2014).

1.1.2   Scientific Significance

Global research on various types of deep-sea corals is advancing due to increased access to study these species within their habitats (Frank et al. 2011; Hitt et al. 2020; Marriott et al. 2020). Deep-sea corals are important components of various paleoclimate studies, as they provide high-resolution archives of past climate variation (Adkins et al. 2003; Sherwood et al. 2008; Sherwood et al. 2009; Robinson et al. 2014; Peharda et al. 2021). To realize the full potential of these paleoceanographic studies, an understanding of growth rates and ages for the deep-sea coral species is important for reliable chronologies (Roark et al. 2006; Farmer et al. 2015). Additionally, growth rates and ages of deep-sea coral species are key indicators of species vulnerability to both natural and anthropogenic disturbance events, such as fishing activities, as slow growth rates suggest slow recovery times after disturbance (Roark et al. 2006; Sherwood and Edinger 2009; Neves et al. 2015b). Many deep-sea coral species have extreme longevities and slow growth rates, as most live for decades to centuries, and very few species live for up to thousands of years (Roark et al. 2009). This study focuses on understanding growth rates, ages, and growth patterns for two abundant deep-sea coral species in the NW Atlantic

(*Acanella arbuscula; Keratoisis flexibilis*) in order to inform conservation and management efforts in light of the anthropogenic activities potentially damaging deep-sea coral ecosystems.

1.2 DEEP-SEA CORALS IN THE NW ATLANTIC & LABRADOR SEA

1.2.1 Distribution & abundance

Prior to the early 2000's, location and abundance of deep-sea coral species in Atlantic Canada were primarily based on fishermen observations (Gass and Willison 2005). The first studies focused on distribution of deep-sea corals in this area were based on a combination of the fishermen observations, with trawl survey information from DFO or other bottom trawl surveys, and fishermen's local ecological knowledge (LEK) (Gass and Willison 2005; Colpron et al. 2010; Murillo et al. 2011). Since these early studies, scientific surveys have expanded in the region, and now include underwater technology that allows for studying deep-sea coral distribution in a less invasive and destructive form (Mortensen and Buhl-Mortensen 2004; Baker et al. 2012; Neves et al. 2015a).

In the NW Atlantic, octocorals have been noted to exist with over 20 alcyonacean species observed and around 11 pennatulaceans (Edinger et al. 2007; Wareham and Edinger 2007; Murillo et al. 2011; Neves et al. 2015b; Neves et al. 2018). Additionally, scleractinian and antipatharian species have been observed, however they are far less abundant in the NW Atlantic (Wareham and Edinger 2007; Murillo et al. 2011). Octocorals can be found in both shallow and deep waters (Pérez et al. 2016), with the only shallow-water octocorals in the NW Atlantic being the Nephtheid soft coral group (Wareham and

Edinger 2007). Deep-sea corals in the NW Atlantic are primarily found at depths >200 meters on the continental shelf or slope, which are the most suitable habitats for coral growth because of water temperature, current strength, and substrate type (Wareham and Edinger 2007; Baker et al. 2012).

Particular areas of high coral abundance and species richness include the Southwest (SW) Grand Banks, the Flemish Pass and Flemish Cap, the Labrador Shelf area, and the Southeast (SE) Baffin Island Shelf in Davis Strait (Wareham and Edinger 2007) (Fig. 1-1). Regions focused on in this study will be the SW Grand Banks, the Northern Labrador Shelf, and two areas off the SE Baffin Island Shelf (Davis Strait and Disko Fan) (Fig. 1-1).
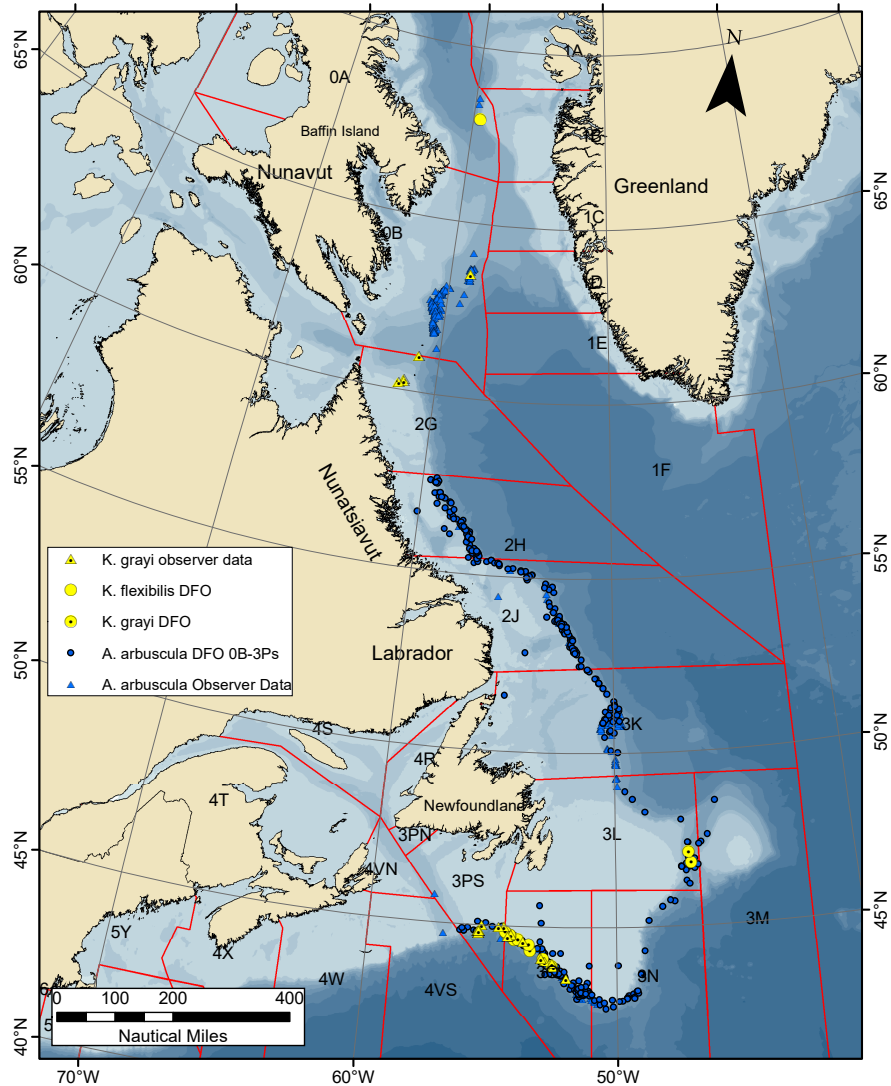
Figure 1-1. Map of the NW Atlantic showing the distribution of *A. arbuscula*, *K. flexibilis*, and *K. grayi* from DFO trawl surveys and observer data. Red lines indicate NAFO zones.

1.2.2 Growth rate & aging studies

Due to limited information about deep-sea coral species in the NW Atlantic, information on growth forms, life history traits (growth rates, ages), and size metrics for most species are minimal. These characteristics are of interest because longevity and

growth rates are among the most important predictors regarding the sensitivity of different species to anthropogenic disturbances (Gass and Willison 2005).

Many studies have been done worldwide regarding deep-sea coral growth rates and ages, focusing on different types of corals including scleractinians (Roark et al. 2006), black corals (Roark et al. 2006; Hitt et al. 2020), and large gorgonian corals (Andrews et al. 2002; Aranha et al. 2014). Growth rate and ages of deep-sea corals in the NW Atlantic have been studied for large gorgonians (Risk et al. 2002; Sherwood et al. 2005; Sherwood and Edinger 2009), particularly the large gorgonian species *Primnoa resedaeformis*, including its associated fauna (Buhl-Mortensen and Mortensen 2005). Annual growth rings have been confirmed in *P. resedaeformis* colonies, making this species easier to age based on annual growth ring counts (Sherwood et al. 2005). Annual growth rings have been determined for the large gorgonian species *Keratoisis grayi* as well, based on radiometric dating techniques (Sherwood and Edinger 2009). Sea pens from the NW Atlantic have also been studied, such as *Halipteris finmarchica* (Neves et al. 2015b) and *Umbellula encrinus* (Neves et al. 2018). These studies emphasized the slow growth rates and abundant nature of the two sea pen species, which encouraged conservation efforts. Additionally, other studies in the NW Atlantic include aging and growth rates of deep-sea scleractinian corals collected from the New England Seamounts (Robinson et al. 2007), and the eastern coast of Canada (Risk et al. 2002; Hamel et al. 2010).

One of the most widespread deep-sea coral species in the NW Atlantic is the small bamboo coral, *Acanella arbuscula* (Fig. 1-1) (Wareham and Edinger 2007). Other gorgonians present include the bamboo coral *Keratoisis flexibilis,* however both bamboo

10

coral species have not been studied for ages and growth rates (Fig. 1-1) despite observations of both species (Wareham and Edinger 2007; Sherwood and Edinger 2009; Neves et al. 2015). *Keratoisis grayi* has been studied for aging, yet ages and growth rates for *Keratoisis flexibilis* still need to be confirmed because of their different growth forms (Fig. 1-2).
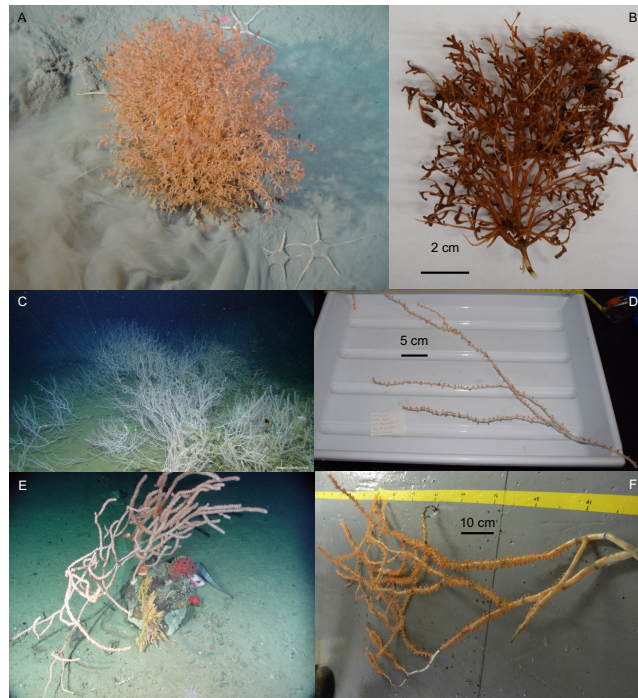
Figure 1-2. A) *A. arbuscula* colony imaged *in situ* and B) *A. arbuscula* colony imaged once collected. C) *Keratoisis flexibilis* imaged *in situ* at Disko Fan and D) imaged once collected. E) *Keratoisis grayi* imaged *in situ* in the SW Grand Banks and F) imaged once collected.

1.2.3 Geographic & bathymetric growth rate variation

Environmental variables, such as temperature, primary productivity, and current strength, can alter growth rates of deep-sea corals within the same species and among similar species (Tracey et al. 2007; Thresher 2009; Neves et al. 2015b). Bathymetric

variations have also been documented to influence growth rates of deep-sea corals (Thresher 2009), as food availability in deep waters is likely to be less than in shallow environments. Previous geographic studies have compared sea pen growth rates of *Halipteris finmarchica* from the NW Atlantic with *Halipteris willemoesi* colonies from the Bering Sea, which showed statistically faster diametric growth for the Pacific species, possibly due to environmental factors, such as primary productivity differences (Wilson et al. 2002; Neves et al. 2015b). A temperature effect on radial growth rates of *Keratoisis* corals from different regions has also been documented (Thresher 2009; Farmer et al. 2015; Thresher et al. 2016).

Previous studies have not focused on geographic variation in growth rates within one specific region, which is of interest to understand how ocean conditions can influence growth rates. It is also important for conservation measures because it indicates the slowest-growing organisms within a region and allows for more effective marine spatial planning (DFO Marine Spatial Planning 2021). Therefore, growth rates and ages of *A. arbuscula* colonies collected from different locations in the NW Atlantic are compared in this study to determine how environmental variables may impact growth rates in the species. Additionally, *A. arbuscula* colonies from the same approximate location are studied for intra-location variability in longevity and growth rates, which has not been extensively studied and is important for understanding fine-scale environmental effects or ontogenetic variability within the species. A comparison of growth rates for *K. flexibilis* and *K. grayi* was also conducted, as *Keratoisis* colonies are located all throughout the

region and in different water temperatures, which led to an interest in how environmental variables like bottom temperature may affect growth rates within the genus.

1.3 BAMBOO CORAL SYSTEMATICS & MORPHOLOGY

1.3.1 Systematics

Bamboo corals are members of the Alcyonacean order within the Octocorallia subclass (Table 1-1). Recent revisions to bamboo coral taxonomy suggest that most deepwater bamboo corals found in the NW Atlantic should be within one family (Keratoisididae), which was previously a sub-family of Isididae (Heestand Saucier et al. 2021). The genera *Acanella* and *Keratoisis* are both within the Keratoisididae family.

1.3.2 Morphology

Bamboo corals have eight divisions of the polyp, and are a specific type of gorgonian coral. Bamboo corals have been noted to exist in both shallow, warm waters and deep, cold water environments, and are characterized by their alternating proteinaceous nodes composed of gorgonin with calcareous internodes composed of magnesian calcite (Fig. 1-3) (Watling et al. 2011). They have been observed anchoring onto hard substrate, such as boulders (Edinger et al. 2011) and also in soft sediment, such as muddy habitats (Fig. 1-2) (Baker et al. 2012; Neves et al. 2015a). The two-part skeleton composed of organic (gorgonin) and inorganic (calcite) material is well separated in bamboo corals, which makes them important recorders of marine conditions and past climate variations (Sherwood et al. 2008).
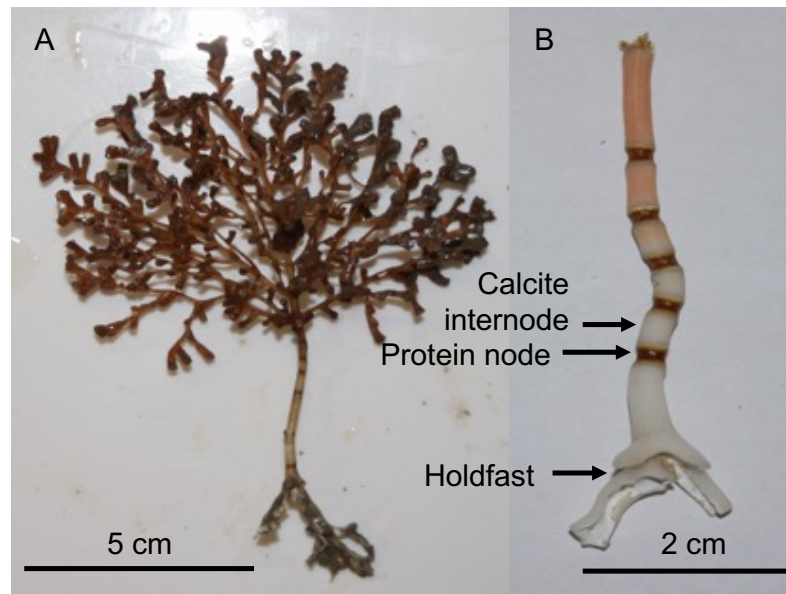
Figure 1-3. A) Colony of *A. arbuscula* and B) close-up image of the base of an *A. arbuscula* colony, highlighting the alternating calcite internodes and proteinaceous nodes, with a root-like holdfast for anchoring the colonies in muddy environments or soft sediment.

1.3.3 Growth rate & aging experiments/techniques

Different techniques have been applied to study ages and growth rates of deep-sea bamboo corals. These include counts of concentric growth rings assumed or confirmed to be annual inside the skeletons of the corals, particularly at the proteinaceous nodes (Noé and Dullo 2006; Noé et al. 2008; Sherwood and Edinger 2009; Thresher 2009), radiocarbon dating and bomb-radiocarbon peak matching (Roark et al. 2005; Sherwood et al. 2008; Sherwood et al. 2009; Farmer et al. 2015), and other radiometric dating techniques or geochemistry validations, such as ^{210}Pb dating (Andrews et al. 2009; Sherwood and Edinger 2009) and elemental peak matching (Thresher et al. 2009). U-Th dating has been used in conjunction with ^{14}C dating on solitary scleractinian corals in the Labrador Sea, but not bamboo corals (Maccali et al. 2020). Additionally, new *in situ* techniques for studying

growth rates and ages are developing, which stain corals with calcein solution (Lartaud et al. 2013; Lartaud et al. 2017), alizarin red (Lartaud et al. 2017), or toluidine blue (Marschal et al. 2004). The effectiveness of staining is still being explored, as calcein solution was used in a portion of this study to stain bamboo corals *in situ*, but these colonies have not been recovered (see appendix 4-1).

1.4 *ACANELLA ARBUSCULA & KERATOISIS* SPECIES

Two of the most abundant genera of bamboo corals in the NW Atlantic, which are members of the Keratoisididae family, are *Acanella* and *Keratoisis* (Fig. 1-1, 1-2) (Watling et al. 2011; Heestand Saucier et al. 2021). The species *Acanella arbuscula* and *Keratoisis flexibilis* are the focus of this study, and both species exhibit alternating calcitic internodes with proteinaceous gorgonin nodes and have been typically observed as conspicuous components in muddy environments.

1.4.1 *Distribution in NW Atlantic*

Acanella arbuscula was previously noted to be the most abundant, and one of the most widespread gorgonian species to exist in the NW Atlantic along the shelf edge and slope, and is typically small and bush-like, and red in color (Wareham and Edinger 2007). The species has also been observed in the NE Atlantic (van den Beld et al. 2017) and along the Mid-Atlantic Ridge (Mortensen et al. 2008), and is considered a cosmopolitan species. Hotspots for the species in the NW Atlantic have been noted to be off of SE Baffin Island (Davis Strait), near the Hawke Channel closure, off the Labrador margin and NE

Newfoundland Shelf, and in the SW Grand Banks (Fig. 1-1) (Wareham and Edinger 2007).

A. arbuscula colonies have also been observed at a wide range of depths in the NW

Atlantic, ranging from 100 - 2000m (Baker et al. 2012). It has been suggested that *A.*

arbuscula is potentially more easily disturbed by gillnets or bottom trawl nets, as instead

of attaching to hard substrates, this species has been observed using a root-like holdfast in

muddy bottoms, which may make it easier for the species to be caught and removed from

their habitat (Fig. 1-2, 1-3) (Gass and Willison 2005). *A. arbuscula* colonies have not been

observed forming reefs in any region in the NW Atlantic, but seem to grow as solitary

colonies, and *A. arbuscula* is also considered a species that can form aggregations of small

gorgonian corals (Baker et al. 2012).

     Keratoisis flexibilis has only been observed in SE Baffin Bay at the Disko Fan site

(Neves et al. 2015a), while *Keratoisis grayi* (synonym *K. ornata*) colonies have been

observed in the SW Grand Banks and off Nova Scotia, with one specimen collected in NE

Saglek Bank as well (Fig. 1-1) (Wareham and Edinger 2007; Sherwood and Edinger 2009;

Baker et al. 2019). There have also been dense accumulations of a *Keratoisis* species not

identified to the species level observed in Flemish Pass, with similarities in growth forms

to both *K. grayi* and *K. flexibilis*. *K. flexibilis* have been observed having thinner coral

skeletons and forming dense forests at Disko Fan on the SE Baffin Shelf (Neves et al.

2015a), which are notable distinctions from the solitary growth form observed in the SW

Grand Banks for *K. grayi*, which tend to have thicker skeletons (Fig. 1-2) (Sherwood and

Edinger 2009). Additionally, *K. flexibilis* has been observed only in muddy environments

(Neves et al. 2015a), while *K. grayi* has only been observed attached to hard substrates like

rocks or boulders (Wareham and Edinger 2007). Both species of *Keratoisis* are large gorgonian corals with vulnerable, branch-like structures, causing them to be easily disturbed by fishing activities (Edinger et al. 2007; Neves et al. 2015a).

1.4.2   Growth rate & age studies on A. arbuscula & Keratoisis spp.

A. arbuscula has been under-studied, and despite the species having the most observances from scientific studies and fisheries data in the NW Atlantic, when compared to other gorgonian corals in the region, the amount of information currently known about the life history of the species is minimal (Fig. 1-1). Previous research on the growth rates and longevity of *A. arbuscula* from the NW Atlantic used growth ring counts and bomb-^{14}C dating on one colony collected from the Davis Strait area at 526m depth (Sherwood and Edinger 2009). Due to the small size of *A. arbuscula*, with coral diameters rarely larger than 4mm, the previous study had difficulty analyzing the age and growth rates of the species. As of now, the species age is constrained to 40-60 years (<100 years) and it was suggested that *A. arbuscula* samples form annual growth rings (Sherwood and Edinger 2009). Additionally, reproductive traits for *A. arbuscula* have been explored for colonies from The Gully and Flemish Cap (Beazley and Kenchington 2012). Therefore; additional research is necessary to determine more accurate age and growth rate estimates for the species, which will lead to a better understanding of its vulnerability to disturbances (Edinger et al. 2007; Beazley and Kenchington 2012).

The existence of dense *K. flexibilis* colonies in the eastern Canadian Arctic is a more recent discovery (Gass and Willison 2005; DFO 2007; Neves et al. 2015a), and

growth rates and ages for this species have not been studied. However, *K. grayi* colonies have been focused on in previous growth rate and aging studies from the NW Atlantic, making data on this species readily available. A colony of *K. grayi* collected from the SW Grand Banks at 601m depth has a well-constrained age of 94 years, a radial growth rate of 0.074 mm/yr^{-1}, and axial growth rate of 0.93 cm/yr^{-1} (Sherwood and Edinger 2009). Other samples of *K. grayi* previously analyzed from the NW Atlantic show slightly different ages and growth rates, ranging from 138 – 200 yrs (Sherwood and Edinger 2009). Colonies of *K. grayi* in Sherwood and Edinger 2009 were aged with bomb-^{14}C, ^{14}C, and ^{210}Pb.

With colonies of the two different species of *Keratoisis* existing in different areas and exhibiting different growth forms, comparisons of growth rates and ages within the genus based on geography, bathymetry, ocean conditions, and substrate type is of particular interest, as this has been studied for *Keratoisis* species in a broader context (Thresher 2009). A similar comparison has been analyzed in the region, as geographic variation studies of the large gorgonian corals *Primnoa resedaeformis* and *Primnoa pacifica* have concluded that radial growth rates can differ based on geography (Sherwood and Edinger 2009; Aranha et al. 2014). Primary productivity differences between regions are likely to affect growth rate differences observed in similar species (Aranha et al. 2014).

Axial and radial growth patterns in both species have not been studied, so it is unknown if growth rates continue at the same speed throughout each colonies lifespan. A previous study on sea pens have described varying growth rates throughout the lifespan of a colony (Neves et al. 2015), but this has not been recorded in many other deep-sea coral species.

1.5 CONSERVATION MOTIVATION FOR *ACANELLA ARBUSCULA &* *KERATOISIS FLEXIBILIS*

Fishing activities in the NW Atlantic have been ongoing for decades, long before research on deep-sea corals began, with records from fishermen of abundant coral bycatch during fishing activities (Gass and Willison 2005). While this information is useful for identifying coral hot-spots in the region, it is also troublesome since the full extent and abundance of deep-sea corals cannot be fully understood due to the continued removal of corals in previous decades by fishing activities. Therefore, prevention of further destructions to deep-sea coral species in the NW Atlantic is important.

To better understand the deep-sea bamboo coral species *Acanella arbuscula* and *Keratoisis flexibilis*, a better understanding of how long the species live and how fast they grow is of utmost importance. This research aims to determine ages and growth rates for the species, and compare these geographically and bathymetrically to understand how oceanographic conditions can alter growth rates within each species, and to be able to predict growth rates of both species in other regions. With more information on the species, conservation measures to protect deep-sea corals from bottom-contact fishing will be better advised, and will focus on the slowest growing *A. arbuscula* colonies in the NW Atlantic.

Information on longevity and growth rates for both bamboo coral species will be utilized by the Marine Spatial Planning program at DFO, as the *A. arbuscula* portion of this study is supported and funded by DFO for identifying vulnerable marine ecosystems (VMEs) in the NW Atlantic (DFO 2017; DFO Marine Spatial Planning 2021). Area-based conservation measures could be effectively advised and implemented with data from this

study based on growth rate and longevity. If geographic and bathymetric variation is determined for each species, this data will also be applicable in conservation measures, as the most vulnerable organisms of each species could be identified in the region, based on the slowest growth rates and oldest longevities.

Marine protected areas have been validated to succeed in encouraging recruitment of deep-sea corals, as the implementation of a conservation area for *Lophelia pertusa* reefs in Atlantic Canada, named the "*Lophelia* Coral Conservation Area" was established to protect deep-sea corals and the benthic fauna associated with the corals (Beazley et al. 2021). Contrasting this, recruitment of two deep-sea gorgonian species (*Primnoa resedaeformis* and *Paragorgia arborea*) was shown to vary based on reproductive modes of each species, and very few recruits of *P. arborea* succeeded in growing (Lacharité and Metaxas 2013). This study highlighted the need for consideration of early life history stage growth patterns in each individual species when implementing marine protected areas, as some species do not recruit as successfully as others.

Keratoisis grayi was previously determined to be a highly vulnerable species because of old ages and slow growth rates (Sherwood and Edinger 2009). Studying *K. flexibilis* ages and growth rates in the eastern Canadian Arctic is necessary to compare the two *Keratoisis* species. In particular, since they demonstrate different growth forms and thrive in different regions of the NW Atlantic, they may also grow at different rates (Fig. 1-2) (Neves et al. 2015a). I aim to determine ages and growth rates for *K. flexibilis* colonies, and compare these to previously determined data for *K. grayi* colonies to better advise conservation efforts on *Keratoisis* hot-spots in the region.

1.6   THESIS OUTLINE

Included in this thesis are four chapters, with the first chapter being an introductory chapter and chapter four being general conclusions and future work. There are two chapters formatted for publication (chapters 2 and 3), focused on studying the ages and growth rates of the deep-sea bamboo corals *Acanella arbuscula* and *Keratoisis flexibilis* collected in the NW Atlantic using sclerochronology techniques (i.e. growth ring counts), with supplementary AMS-^{14}C for *K. flexibilis*.

Chapter 2, entitled "The small bamboo coral *Acanella arbuscula* in the Northwest Atlantic and Eastern Canadian Arctic: geographic and bathymetric comparisons of growth rates and age", compares determined growth rates and ages geographically and bathymetrically in the NW Atlantic for *A. arbuscula* colonies. The growth rate and longevity analyses were conducted with growth ring counts. A majority of the samples analyzed in this chapter were collected in NAFO zones 0B, 2H, and 3O by DFO scientific bottom trawl surveys. Additional samples were collected during the 2021 *Amundsen* scientific mission off the SE Baffin Slope in Davis Strait at a depth of ~1300m.

Chapter 3 entitled "Slow growth rates for *Keratoisis flexibilis* in muddy Arctic environments" focuses on growth rate and longevity for colonies of *K. flexibilis* previously observed forming coral fields at Disko Fan (Neves et al. 2015a). These ages and growth rates are compared to previously determined growth rates and ages for *K. grayi* from the NW Atlantic (Sherwood and Edinger 2009), and also to *Keratoisis* colonies in different regions. The *K. flexibilis* samples analyzed were collected during the 2021 *Amundsen* scientific mission at Disko Fan at a depth of ~900m. Additional colonies used were

collected at Disko Fan in 2018 with a box core. These samples were sub-sampled for AMS-^{14}C to determine axial growth rates and ages of *K. flexibilis* fragments.

Chapter 4 summarizes main findings from both data chapters, future work that is planned with both species, as well as new scientific questions that can be asked based on the results from this study.

The appendices will not be included as supplementary material in publications, but are instead documenting important sample preparation methods and additional datasets that are relevant to each chapter. Appendices 2-5 and 3-5 summarize raw LA-AMS radiocarbon dating results conducted at ETH Zürich on bamboo corals utilized in this study, but these data were not analyzed in this thesis because of delays and complications due to COVID-19. The LA-AMS radiocarbon data will be utilized in future work to confirm ages from this study on both bamboo coral species, as the technique is still experimental on bamboo corals, and was used because sample diameters and growth rings are too small in both species within this thesis for traditional radiometric dating techniques.

Appendix 4-1 is a summary of the methods used to stain bamboo corals with calcein solution *in situ* for the first time in Canadian waters, which was conducted on the *Amundsen* in 2021. This experiment is attempting to determine growth ring periodicity in *A. arbuscula* and *K. flexibilis*, and stained corals will be collected in a few years. Once results are available from this study, appendix 4-1 will be a component of a technical report on the staining procedure and results.

1.7   Literature Cited

Adkins JF, Boyle EA, Curry WB, Lutringer A. 2003. Stable isotopes in deep-sea corals and a new mechanism for "vital effects". Elsevier Science Ltd. 67: 1129 – 1143.

Andersen JH, Berzaghi F, Christensen T, Geertz-Hansen O, Mosbech A, Stock A, Zinglersen KB, Wisz MS. 2017. Potential for cumulative effects on human stressors on fish, sea birds and marine mammals in Arctic waters. Estuarine, Coastal and Shelf Science. 184: 202-206.

Andrews AH, Cordes EE, Mahoney MM, Munk K, Coale KH, Cailliet GM, Heifetz J. 2002. Age, growth and radiometric age validation of a deep-sea, habitat-forming gorgonian (*Primnoa resedaeformis*) from the Gulf of Alaska. Hydrobiologia. 471: 101-110.

Andrews AH, Stone RP, Lundstrom CC, DeVogelaere. 2009. Growth rate and age determination of bamboo corals from the northeastern Pacific Ocean using refined ^{210}Pb dating. Marine Ecology Progress Series. 397: 173-185.

Aranha R, Edinger E, Layne G, Piercey G. 2014. Growth rate variation and potential paleoceanographic proxies in *Primnoa pacifica*: Insights from high-resolution trace element micro-analysis. Deep-Sea Research II. 99: 213-226.

Baker KD, Snelgrove PVR, Fifield DA, Edinger EN, Wareham VE, Haedrich RL, Gilkinson KD. 2019. Small-scale patterns in the distribution and condition of bamboo coral, *Keratoisis grayi*, in submarine canyons on the Grand Banks, Newfoundland. Frontiers in Marine Science. 6: article 374.

Baker KD, Wareham VE, Snelgrove PVR, Haedrich RL, Fifield DA, Edinger EN, Gilkinson KD. 2012. Distributional patterns of deep-sea coral assemblages in three submarine canyons off Newfoundland, Canada. Marine Ecology Progress Series. 445: 235-249.

Beazley LI, Kenchington EL. 2012. Reproductive biology of the deep-water coral *Acanella arbuscula* (Phylum Cnidaria: Class Anthozoa: Order Alcyonacea), northwest Atlantic. Deep-Sea Research I. 68: 92-104.

Beazley L, Kenchington E, Korabik M, Fenton D, King M. 2021. Other effective area-based conservation measure promotes recovery in a cold-water coral reef. Global Ecology and Conservation. 26.

Boulard M, Lawton P, Baker K, Edinger E (in review). 2022. The effect of small-scale habitat features on groundfish density in deep-sea soft-bottom ecosystems. Deep-Sea Research Part I.

Buddemeier RW, Maragos JE, Knutson DW. 1974. Radiographic studies of reef coral exoskeletons: rates and patterns of coral growth. J. exp. mar. Biol. Ecol. 14: 179-200.

Buhl-Mortensen P, Gordon Jr. DC, Buhl-Mortensen L, Kulka DW. 2017. First description of a *Lophelia pertusa* reef complex in Atlantic Canada. Deep-Sea Research Part I. 126: 21-30.

Buhl-Mortensen L, Mortensen PB. 2004. Symbiosis in Deep-Water Corals. Symbiosis. 37: 33-61.

Buhl-Mortensen L, Mortensen PB. 2005. Distribution and diversity of species associated with deep-sea gorgonian corals off Atlantic Canada. Cold-water corals and ecosystems. 849-879.

Buhl-Mortensen L, Olafsdottir SH, Buhl-Mortensen P, Burgos JM, Ragnarsson SA. 2015. Distribution of nine cold-water coral species (Scleractinia and Gorgonacea) in the cold temperate North Atlantic: effects of bathymetry and hydrography. Hydrobiologia. 759: 39-61.

Buhl-Mortensen L, Vanreusel A, Gooday AJ, Levin LA, Priede IG, Buhl-Mortensen P, Gheerardyn H, King NJ, Raes M. 2010. Biological structures as a source of habitat heterogeneity and biodiversity on the deep ocean margins. Marine Ecology. 31: 21-50.

Colpron E, Edinger E, Neis B. 2010. Mapping the distribution of deep-sea corals in the Northern Gulf of St. Lawrence using both scientific and local ecological knowledge. DFO Can. Sci. Advis. Sec. Res.

DFO. 2007. Development of a closed-area in NAFO 0A to protect narwhal over-wintering grounds, including deep-sea corals. DFO Can. Sci. Advis. Sec. Sci. Resp. 2007/002.

DFO Marine Spatial Planning. 2021. doi:https://www.dfo-mpo.gc.ca/oceans/management-gestion/msp-psm/index-eng.html

Edinger E, Baker K, Devillers R, Wareham V. 2007. Coldwater corals off Newfoundland and Labrador: Distribution and Fisheries Impacts. WWF-Canada.

Edinger EN, Sherwood OA, Piper DJW, Wareham VE, Baker KD, Gilkinson KD, Scott DB. 2011. Geological features supporting deep-sea coral habitat in Atlantic Canada. Continental Shelf Research. 31: S69-S84.

Farmer JR, Robinson LF, Hönisch B. 2015. Growth rate determinations from radiocarbon in bamboo corals (genus *Keratoisis*). Deep-Sea Research I. 105: 26-40.

Fisheries and Oceans Canada (DFO). 2017. Guidance on the level of protection of significant areas of coldwater corals and sponge-dominated communities in Newfoundland and Labrador waters. DFO Canadian Science Advisory Secretariat Science Response 2017/030.

Frank N, Freiwald A, Correa ML, Wienberg C, Eisele M, Hebbeln D, Van Rooij D, Henriet J-P, Colin C, van Weering T, de Haas H, Buhl-Mortensen P, Roberts JM, De Mol B, Douville E, Blamart D, Hatté. 2011. Northeastern Atlantic cold-water coral reefs and climate. Geology. 39: 743-746.

Frank N, Paterne M, Ayliffe L, van Weering T, Henriet JP, Blamart D. 2004. Eastern North Atlantic deep-sea corals: tracing upper intermediate water $\Delta^{14}C$ during the Holocene. Earth and Planetary Science Letters. 219: 297-309.

Gass SE, Willison JHM. 2005. An assessment of the distribution of deep-sea corals in Atlantic Canada by using both scientific and local forms of knowledge. Cold-Water Corals and Ecosystems - Erlangen Earth Conference Series.

Hall-Spencer J, Allain V, Fosså JH. 2002. Trawling damage to Northeast Atlantic ancient coral reefs. The Royal Society. 269: 507-511

Hall-Spencer J, Rogers A, Davies J, Foggo A. 2007. Deep-sea coral distribution on seamounts, oceanic islands, and continental slopes in the Northeast Atlantic. Bulletin of Marine Science. 81(3): 135-146.

Hamel JF, Sun Z, Mercier A. 2010. Influence of size and seasonal factors on the growth of the deep-sea coral *Flabellum alabastrum* in mesocosm. Coral Reefs. 29: 521-525.

Heestand Saucier E, France SC, Watling L. 2021. Toward a revision of the bamboo corals: Part 3, deconstructing the Family Isididae. Zootaxa. 5047(3): 247-272.

Heikoop JM, Hickmott DD, Risk MJ, Shearer CK, Atudorei V. 2002. Potential climate signals from the deep-sea gorgonian coral *Primnoa resedaeformis*. Hydrobiologia. 471: 117-124.

Hill TM, Spero HJ, Guilderson T, LaVigne M, Clague D, Macalello S, Jang N. 2011. Temperature and vital effect controls on bamboo coral (*Isididae*) isotope geochemistry: A test of the "lines method". Geochemistry, Geophysics, Geosystems (G^3). 12(4).

Hitt NT, Sinclair DJ, Fallon SJ, Neil HI, Tracey DM, Komugabe-Dixson A, Marriott P. 2020. Growth and longevity of New Zealand black corals. Deep-Sea Research Part I. 162.

Kenchington E, Beazley L, Lirette C, Murillo FJ, Guijarro J, Wareham V, Gilkinson K, Koen Alonso M, Benoît H, Bourdages H, Sainte-Marie B, Treble M, Siferd T. 2016. Delineation of coral and sponge significant benthic areas in eastern Canada using kernel density analyses and species distribution models. DFO Can. Sci. Advis. Sec. Res. Doc.

Kenchington E, Yashayaev I, Tendal OS, Jørgensbye H. 2017. Water mass characteristics and associated fauna of a recently discovered *Lophelia pertusa* (Scleractinia: Anthozoa) reef in Greenlandic waters. Polar Biol. 40: 321-337.

Krieger KJ, Wing BL. 2002. Megafauna associations with deepwater corals (*Primnoa* spp.) in the Gulf of Alaska. Hydrobiologia. 471: 83-90.

Lacharité M, Metaxas A. 2013. Early life history of deep-water gorgonian corals may limit their abundance. PLOS One. 8(6).

Lartaud F, Meistertzheim AL, Peru E, Le Bris N. 2017. *In situ* growth experiments of reef building cold-water corals: The good, the bad and the ugly. Deep-sea Research I. 121: 70-78.

Lartaud F, Pareige S, De Rafelis M, Feuillassier L, Bideau M, Peru E, Romans P, Alcala F, Le Bris N. 2013. A new approach for assessing cold-water coral growth *in situ* using fluorescent calcein staining. Aquatic Living Resources. 26: 187-196.

Maccali J, Hillaire-Marcel C, Ménabréaz L, Ghaleb B, Blénet A, Edinger E, Hélie JF, Preda M. 2020. Late Quaternary sporadic development of *Desmophyllum dianthus* deep-coral populations in the southern Labrador Sea with specific attention to their ^{14}C and ^{230}Th-dating. Marine Chemistry. 224.

Marriott P, Tracey DM, Bostock H, Hitt N, Fallon SJ. 2020. Ageing Deep-Sea Black Coral *Bathypathes patula*. Frontiers in Marine Science. 7:479.

Marschal C, Garrabou J, Harmelin JG, Pichon M. 2004. A new method for measuring growth and age in the precious red coral *Corallium rubrum* (L.). Coral Reefs. 23: 423-432.

Mortensen PB, Buhl-Mortensen L. 2004. Distribution of deep-water gorgonian corals in relation to benthic habitat features in the Northeast Channel (Atlantic Canada). Marine Biology. 144: 1223-1238.

Mortensen PB, Buhl-Mortensen L, Gordon Jr DC. 2006. Distribution of deep-water corals in Atlantic Canada. Proc 10th Int Coral Reef. 1: 1832-1848.

Mortensen PB, Buhl-Mortensen L, Gebruk AV, Krylova EM. 2008. Occurrence of deep-water corals on the Mid-Atlantic Ridge based on MAR-ECO data. Deep-Sea Research II. 55: 142-152.

Murillo FJ, Muñoz PD, Altuna A, Serrano A. 2011. Distribution of deep-water corals of the Flemish Cap, Flemish Pass, and the Grand Banks of Newfoundland (Northwest Atlantic Ocean): interaction with fishing activities. ICES Journal of Marine Science. 68(2): 319-332.

Neves B de M, Edinger E, Hillaire-Marcel C, Saucier EH, France SC, Treble MA, Wareham VE. 2015a. Deep-water bamboo coral forests in a muddy Arctic environment. Mar Biodiv. 45:867-871.

Neves B de M, Edinger E, Layne GD, Wareham VE. 2015b. Decadal longevity and slow growth rates in the deep-water sea pen *Halipteris finmarchica* (Sars, 1851) (Octocorallia: Pennatulacea): implications for vulnerability and recovery from anthropogenic disturbance. Hydrobiologia. 759:147-170.

Neves B de M, Edinger E, Wareham Hayes V, Devine B, Wheeland L, Layne G. 2018. Size metrics, longevity, and growth rates in *Umbellula encrinus* (Cnidaria: Pennatulacea) from the eastern Canadian Arctic. Arctic Science. 00: 1-28.

Noé SU, Dullo W-Chr. 2006. Skeletal morphogenesis and growth mode of modern and fossil deep-water isidid gorgonians (Octocorallia) in the West Pacific (New Zealand and Sea of Okhotsk). Coral Reefs. 25: 303-320.

Noé SU, Lembke-Jene L, Dullo W-Chr. 2008. Varying growth rates in bamboo corals: sclerochronology and radiocarbon dating of a mid-Holocene deep-water gorgonian skeleton (*Keratoisis* sp.: Octocorallia) from Chatham Rise (New Zealand). Facies. 54: 151-166.

Oschmann W. 2009. Sclerochronology: editorial. Int J Earth Sci (Geol Rundsch). 98: 1-2.

Peharda M, Schöne BR, Black BA, Corrège T. 2021. Advances of sclerochronology research in the last decade. Palaeogeography, Palaeoclimatology, Palaeoecology. 570(110371).

Pérez CD, Neves B de M, Cordeiro RT, Williams GC, Cairns SD. 2016. Diversity and distribution of Octocorallia. The Cnidaria, Past, Present, and Future. 109-123.

Pierrejean M, Grant C, Neves BM, Chaillou G, Edinger E, Blanchet FG, Maps F, Nozais C, Archambault P. 2020. Influence of deep-water corals and sponge gardens on infaunal community composition and ecosystem functioning in the Eastern Canadian Arctic. Frontiers in Marine Science. 7: 495.

Pons-Branchu E, Hillaire-Marcel C, Deschamps P, Ghaleb B, Sinclair DJ. 2005. Early diagenesis impact on precise U-series dating of deep-sea corals: Example of a 100-200-

year old *Lophelia pertusa* sample from the northeast Atlantic. Geochimica et Cosmochimica Acta. 69(20): 4865-4879.

Risk MJ, Heikoop JM, Snow MG, Beukens R. 2002. Lifespans and growth patterns of two deep-sea corals: *Primnoa resedaeformis* and *Desmophyllum cristagalli*. Hydrobiologia. 471: 125-131.

Roark EB, Guilderson TP, Dunbar RB, Fallon SJ, Mucciarone DA. 2009. Extreme longevity in proteinaceous deep-sea corals. PNAS 106(13): 5204-5208.

Roark EB, Guilderson TP, Dunbar RB, Ingram BL. 2006. Radiocarbon-based ages and growth rates of Hawaiian deep-sea corals. Marine Ecology Progress Series. 327: 1-14.

Roark EB, Guilderson TP, Flood-Page S, Dunbar RB, Ingram BL, Fallon SJ, McCulloch M. 2005. Radiocarbon-based ages and growth rates of bamboo corals from the Gulf of Alaska. Geophysical Research Letters. 32: L04606.

Roberts JM, Cairns SD. 2014. Cold-water corals in a changing ocean. Current Opinion in Environmental Sustainability. 7:118-126.

Roberts JM, Wheeler A, Freiwald A, Cairns S. 2009. Cold-water corals: The biology and geology of deep-sea coral habitats. Cambridge University Press.

Roberts S, Hirshfield M. 2004. Deep-Sea Corals: Out of Sight, but No Longer out of Mind. Frontiers in Ecology and the Environment. 2:123-130.

Robinson LF, Adkins JF, Frank N, Gagnon AC, Prouty NG, Roark EB, van de Flierdt T. 2014. The geochemistry of deep-sea coral skeletons: A review of vital effects and application for palaeoceanography. Deep-Sea Research II. 99: 184-198.

Robinson LF, Adkins JF, Scheirer DS, Fernandez DP, Gagnon A, Waller RG. 2007. Deep-sea scleractinian coral age and depth distributions in the Northwest Atlantic for the last 225,000 years. Bulletin of Marine Science. 81(3): 371-391.

Rogers AD, Gianni M. 2010. The implementation of UNGA resolutions 61/105 and 64/72 in the management of deep-sea fisheries on the high seas. Prepared for the Deep-Sea Conservation Coalition.

Schrank WE. 2005. The Newfoundland fishery: ten years after the moratorium. Marine Policy. 29: 407-420.

Sherwood OA, Edinger EN. 2009. Ages and growth rates of some deep-sea gorgonian and antipatharian corals of Newfoundland and Labrador. Can. J. Fish. Aquat. Sci. 66:142 152.

Sherwood OA, Edinger EN, Guilderson TP, Ghaleb B, Risk MJ, Scott DB. 2008. Late Holocene radiocarbon variability in Northwest Atlantic slope waters. Earth and Planetary Science Letters. 275: 146-153.

Sherwood OA, Scott DB, Risk MJ, Guilderson TP. 2005. Radiocarbon evidence for annual growth rings in the deep-sea octocoral *Primnoa resedaeformis*. Marine Ecology Progress Series. 301: 129-134.

Sherwood OA, Thresher RE, Fallon SJ, Davies DM, Trull TW. 2009. Multi-century time-series of ^{15}N and ^{14}C in bamboo corals from deep Tasmanian seamounts: evidence for stable oceanographic conditions. Marine Ecology Progress Series. 397: 209-218.

Shester GG, Enticknap B, Mecum B, Blacow-Draeger A, Brock T, Murray S. 2021. A win-win for deep-sea corals and fishing: increasing seafloor protections while restoring fishing opportunities off the United States West Coast. Frontiers in Marine Science. 7:525619.

Thresher RE. 2009. Environmental and compositional correlates of growth rate in deep-water bamboo corals (Gorgonacea; Isididae). Marine Ecology Progress Series. 397: 187-196.

Thresher RE, Fallon SJ, Townsend AT. 2016. A "core-top" screen for trace element proxies of environmental conditions and growth rates in the calcite skeletons of bamboo corals (Isididae). Geochimica et Cosmochimica Acta. 193: 75-99.

Thresher RE, MacRae CM, Wilson NC, Fallon S. 2009. Feasibility of age determination of deep-water bamboo corals (Gorgonacea: Isididae) from annual cycles in skeletal composition. Deep-Sea Research I. 56: 442-449.

Tittensor DP, Baco AR, Hall-Spencer JM, Orr JC, Rogers AD. 2010. Seamounts as refugia from ocean acidification for cold-water stony corals. Marine Ecology. 31: 212-225.

Tracey DM, Neil H, Marriott P, Andrews AH, Cailliet GM, Sánchez JA. 2007. Age and growth of two genera of deep-sea bamboo corals (family Isididae) in New Zealand waters. Bulletin of Marine Science. 81(3): 393-408.

Turley CM, Roberts JM, Guinotte JM. 2007. Corals in deep-water: will the unseen hand of ocean acidification destroy cold-water ecosystems? Coral reefs. 26:445-448.

van den Beld IMJ, Bourillet JF, Arnaud-Haond S, Chambure LD, Davies JS, Guillaumont B, Olu K, Menot L. 2017. Cold-water coral habitats in submarine canyons of the Bay of Biscay. Frontiers in Marine Science. 4(118).

Wareham VE, Edinger EN. 2007. Distribution of deep-sea corals in the Newfoundland and Labrador region, Northwest Atlantic Ocean. Bulletin of Marine Science. 81:289-313.

Watling L, France SC, Pante E, Simpson A. 2011. Biology of Deep-Water Octocorals. In: Lesser M, editor. Advances in Marine Biology. Elsevier. pp. 41-122.

Watling L, Heestand Saucier E, France SC. 2022. Towards a revision of the bamboo corals (Octocorallia): Part 4, delineating the family Keratoisididae. Zootaxa. 5093(3): 337-375.

Westerman R, Neves B de M, Ahmed M, Holovachov O. 2021. *Aborjinia corallicola* sp. n., a new nematode species (Nematoda: Marimermithidae) associated with the bamboo coral *Acanella arbuscula* (Johnson). Syst Parasitol.

White HK, Hsing P-Y, Cho W, Shank TM, Cordes EE, Quattrini AM, Nelson RK, Camilli R, Demopoulos AWJ, German CR, Brooks JM, Roberts HH, Shedd W, Reddy CM, Fisher CR. 2012. Impact of the *Deepwater Horizon* oil spill on a deep-water coral community in the Gulf of Mexico. PNAS. 109(50): 20303-20308.

Wilson MT, Andrews AH, Brown AL, Cordes EE. 2002. Axial rod growth and age estimation of the sea pen, *Halipteris willemoesi* Kölliker. Hydrobiologia. 471: 133-142.

CHAPTER 2: The small bamboo coral *Acanella arbuscula* in the Northwest Atlantic and Eastern Canadian Arctic: geographic and bathymetric comparisons of growth rates and age

Author list: Laura Piccirillo[1], Evan Edinger[1,2,3,4], Bárbara de Moura Neves[3,5], Meghan Burchell[1,6], Graham D. Layne[4]

[1]Environmental Science Program, [2]Department of Geography, [3]Department of Biology, [4]Department of Earth Sciences Memorial University of Newfoundland and Labrador, St. John's NL, [5]Northwest Atlantic Fisheries Center, Department of Fisheries & Oceans Canada, St. John's NL, [6]Department of Archaeology, Memorial University of Newfoundland and Labrador, St. John's NL

ABSTRACT

In the Northwest Atlantic, deep-sea bamboo corals are abundant and widespread, yet the life-history traits of the small bamboo coral, *Acanella arbuscula,* have not been extensively studied. A total of 115 colonies of *A. arbuscula* were analyzed to examine the relationship between age, location, and depth, and how different environmental conditions influence growth rates. Colonies collected from [Northwest Atlantic Fisheries Organization (NAFO) zones] the SW Grand Banks [3O], Northern Labrador shelf [2H], and SE Baffin shelf [0B], ranging from depths of 178-1354m, were cross-sectioned at the proteinaceous nodes of their skeletons, and examined at magnifications up to 258x to determine age and growth rate using growth ring counts. Annual growth ring formation was confirmed for major growth rings, from comparisons of a previous bomb-^{14}C analysis of *A. arbuscula*, and age comparisons with coral size metrics. Minor (sub-annual) growth rings were observed at variable rates between specimens, and the cause of their formation is unknown. Specimens ranged from 8-29 years, with radial growth rates of 0.025 – 0.160 mm/yr and axial growth rates of 1.87 – 16.1 mm/yr. The youngest and fastest growing colonies were from NAFO zone 0B and the oldest and slowest growing were from NAFO zone 3O. Age, stem diameter, and height were plotted with two different sigmoid growth curves, Gompertz and logistic, to examine the consistency of growth through the coral's lifespan. A multi-factor ANOVA with ontogenetic and environmental (temperature, chlorophyll-a concentrations) variables revealed that radial and axial growth rates decrease through a coral's lifespan, explaining why the fastest growing colonies were also the youngest, located in the most northern location.

2.1 INTRODUCTION

Deep-sea corals are widely distributed, key components within benthic ecosystems, and have been gaining more attention in recent decades because of technological advancements and knowledge of benthic habitat disturbances due to anthropogenic activities (Roberts and Cairns 2014). The knowledge on deep-sea coral distribution was previously limited to some scientific data and fishermen observations, but with developments in technology it is possible to have greater access to study deep-sea corals in their natural environments (Roberts and Hirshfield 2004). Many studies have focused on longevity and growth rates of different species, which have proven long longevities and slow growth rates in many deep-sea coral species, which suggest a higher vulnerability to disturbance events. Geographic and bathymetric variation regarding longevity and growth patterns have garnered more attention because anthropogenic threats to deep-sea corals are not uniformly distributed (Roberts and Cairns 2014).

Bamboo corals are a type of "gorgonian" Alcyonacean octocoral with cosmopolitan distribution, characterized by alternating calcite internodes and proteinaceous gorgonin nodes. The genus *Acanella* is one of the most widespread, with nine species observed across the North and South Atlantic, and in the Pacific (Watling et al. 2011). *Acanella arbuscula* in particular is the most commonly observed gorgonian species in Atlantic Canada, ranging from waters off Nova Scotia to locations on the SE Baffin Shelf (Baker et al. 2012; Buhl-Mortensen et al. 2015), and it has been noted as the most abundant gorgonian species in the NW Atlantic (Wareham and Edinger 2007). *A. arbuscula* has also been documented in other places in the North Atlantic, such as south of Iceland, in Irish

waters, and in the Bay of Biscay, commonly in muddy habitats (Buhl-Mortensen et al. 2015; van den Beld et al. 2017), and also in the South Atlantic off Brazil (Cordeiro et al. 2020).

Environmental variables likely play an important role in determining the distribution and growth rates of *A. arbuscula* colonies, as has been observed and suggested for other gorgonians (Tracey et al. 2007; Aranha et al. 2014). Studies on other bamboo (*Keratoisis*) corals comparing multiple species have suggested that higher ambient temperatures (Thresher 2009) and more productive waters (Tracey et al. 2007), which increases food content for benthic organisms, cause deep-sea corals to grow faster. In addition to environmental variables, ontogenetic controls also likely influence longevity and growth rates throughout a colony's lifespan, but this has not been studied in-depth for corals, and specifically not for *A. arbuscula*. Ontogeny concerns how an organism develops, and can be studied using Gompertz and logistic growth curves, which are sigmoid growth curves commonly used in bivalve studies (Urban 2002), and they have also been used with sea pens (K. Greeley MSc Thesis, Memorial University 2021). Comparisons of linear, logarithmic, or exponential regressions with sigmoidal growth curves can give better insight to growth rate variation throughout the lifespan of the species, and addresses ontogenetic influences on growth rates of an organism.

The three main objectives of this study focused on the bamboo coral *Acanella arbuscula* from the NW Atlantic are to determine age and growth rate of the species using sclerochronology, including determining if major or minor growth band structures in the coral skeletons represent annual growth banding. Next, we wanted to understand how

growth rates and ages vary in the region based on location and depth, focusing on the SW Grand Banks, offshore Northern Labrador, and Baffin Bay. We compared colonies from all three locations using previously collected scientific trawl survey samples, and additional samples collected in 2021 with a remotely operated vehicle. Lastly, we aim to understand what is driving geographic and bathymetric variations in growth rates and ages within the species, focusing on environmental factors such as chlorophyll-a concentration to measure productivity, bottom-water temperature, and also possible ontogenetic factors.

2.1.1 Acanella arbuscula

The depth range documented for the species in the North Atlantic ranges from 100-2,000m based on trawl survey data (Gass and Willison 2005; Wareham and Edinger 2007; Buhl-Mortensen et al. 2015), and the species has been reported to exist in coral fields in the NW Atlantic (Baker et al. 2012). The typical temperature range the species has been observed in is 1°C-12°C (Wareham and Edinger 2007; van den Beld et al. 2017), and this temperature range possibly limits the species' distribution (Buhl-Mortensen et al. 2015). The species is usually observed anchored in muddy sediment with a root-like holdfast, which contributes to its wide distribution because colonies are not limited by hard substrate only (Wareham and Edinger 2007). However, the species has also been observed anchoring to boulders, cobbles, and gravel (Baker et al. 2012).

The wide distribution of *A. arbuscula* in the NW Atlantic has led to frequent occurrences of the species reported in fisheries bycatch. *A. arbuscula* colonies are abundant at the SE Baffin Shelf based on observer samples and records (Wareham and

Edinger 2007), and this location is also noted for high density of large and small gorgonian corals based on bycatch in the Greenland halibut fishery (Edinger et al. 2007). Data from April 2004 – January 2006 reported 237 occurrences of *A. arbuscula* colonies observed within fisheries bycatch, most commonly by mobile fishing gear and gillnets (Wareham and Edinger 2007). It has been suggested that the species is more susceptible to disturbance from fishing gear because the colonies frequently anchor in muddy sediment, which are more trawlable bottoms, compared to most large gorgonian species that anchor to hard substrate only, which is believed to be more secure for a colony and likely experiences less fishing activity (Gass and Willison 2005).

Growth rates and longevity for *A. arbuscula* colonies are still not well understood, as the only previous study from the region analyzed a single *A. arbuscula* colony for age and growth rates (Sherwood and Edinger 2009). Because of the small size of *A. arbuscula* skeletons collected from the SE Baffin Shelf in this study, the analytical methods applied in Sherwood and Edinger (2009) could not be used on the colonies collected with a ROV for this study. However, age for the colony studied in Sherwood and Edinger (2009) was determined to be 30-40 years, radial growth rate was >0.02 mm/yr, and axial (linear) growth rate was >3 mm/yr, based on observing the end of the bomb-^{14}C peak in the specimen. The study also observed concentric growth rings at the proteinaceous node of the *A. arbuscula* specimen; therefore, Sherwood and Edinger (2009) also reported ages and growth rates based on growth ring counts, which were: 30 years, 0.07mm/yr for radial growth rate, and 10 mm/yr for axial growth rate. Furthermore, Sherwood and Edinger

(2009) suggested that growth bands are annual in *A. arbuscula* colonies, but it was not proven because of limited samples and unclear growth rings.

The age and growth rates determined from Sherwood and Edinger (2009) indicates that *A. arbuscula* is a slow-growing species, and also moderately long-lived, yet this needs to be confirmed through further analyses of more *A. arbuscula* specimens. Other bamboo corals from the NW Atlantic had radial growth rates of 0.012-0.078 mm/yr for *Keratoisis* sp. (Farmer et al. 2015), and ages of 94-200 years, radial growth rates of 0.053-0.075 mm/yr, and a axial growth rate of 9.3 mm/yr for *Keratoisis grayi* colonies (Sherwood and Edinger 2009).

2.2 MATERIALS & METHODS

2.2.1 DFO trawl survey samples: Study area & sampling

Most of the *A. arbuscula* colonies used in this study were collected by DFO scientific bottom-trawl surveys (n = 105) from 2004-2018 in the NW Atlantic and NW Labrador Sea (Fig. 2-1; Table 2-1). The colonies analyzed from the DFO sample set were chosen based on geographic location, depth, and quality. The locations were selected to capture geographic variation: SE Baffin Shelf (Davis Strait), the Northern Labrador Sea, and the SW Grand Banks, corresponding to North Atlantic Fisheries Organization (NAFO) zones 0B, 2H, and 3O, respectively (Fig. 2-1). These NAFO zones differ in oceanographic conditions, and the sample size and bathymetric range to choose from within each zone was substantial. Samples with thicker stem diameters were favored, as these corals are easier to analyze for growth rings. Samples collected in DFO bottom-trawl surveys were

measured for height, width, stem length, root length, and wet weight at DFO. Stem length differs from height because only the base stem was measured, instead of the entire colony. The samples were also noted for how much tissue remained and if any associated fauna remained on the skeleton for use in a different study (Neves and Hayes, in prep). Only the bases of these colonies were preserved for aging and growth rate analyses when the samples were processed at DFO, and the basal section was determined as the location on the stem where tissue was not deposited. Basal sections of the samples were photographed and measured for stem diameter with calipers before sectioning.
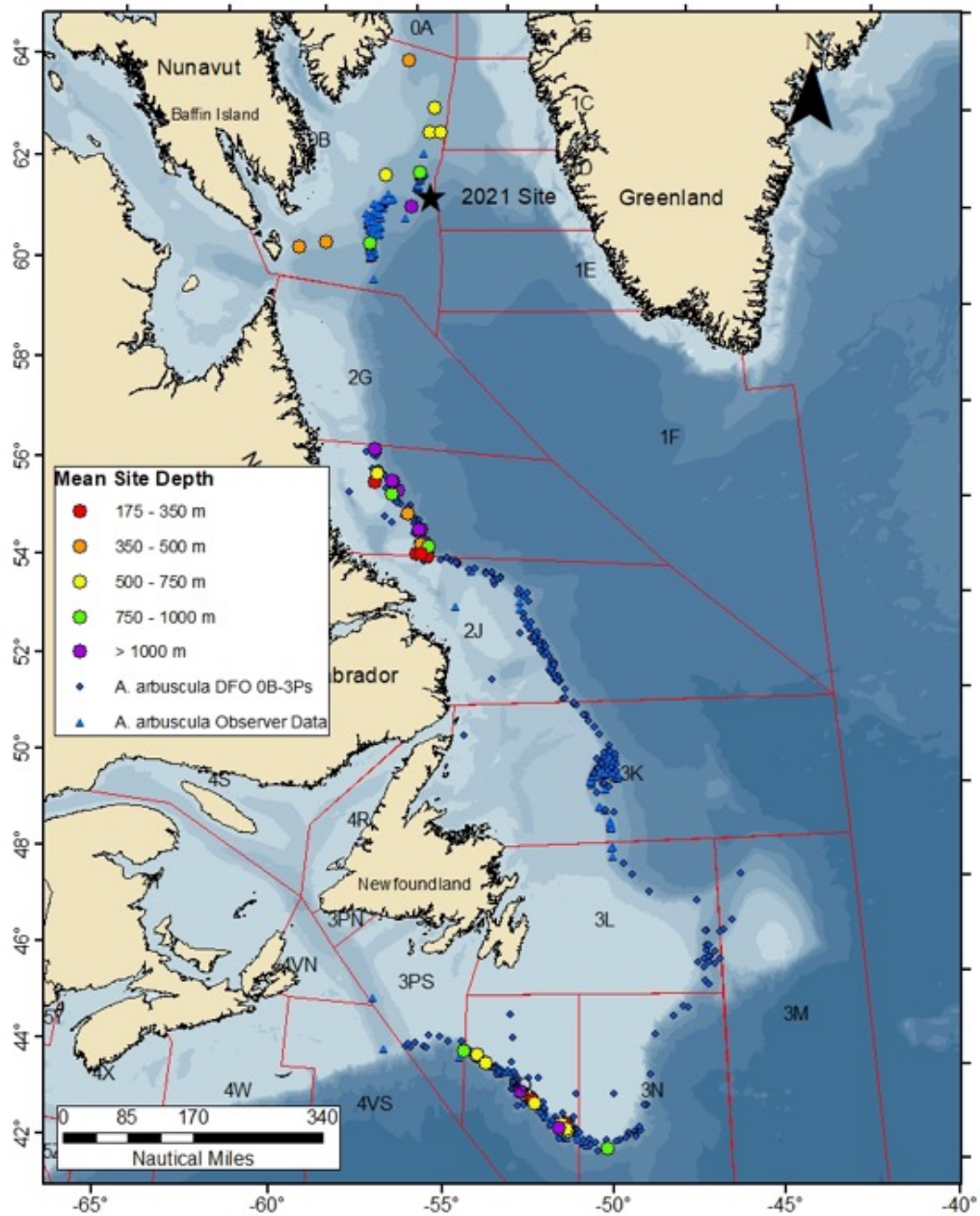
Figure 2-1. *Acanella arbuscula* samples used in the geographic and bathymetric comparison study are shown here in the NW Atlantic. Multi-colored circles represent samples used, with the color indicating depth of the sample. Small blue circles and triangles represent other *A. arbuscula* samples observed in the area, but not used in the study. The 2021 ROV dive site to collect additional *A. arbuscula* samples is indicated by the black star.

2.2.2 Sampling with ROV in 2021

Additional *A. arbuscula* colonies used were collected with the new *"Astrid"* ROV aboard the Canadian scientific icebreaker *CCGS Amundsen* in 2021. The ROV dive was conducted on July 29, 2021 on the SE Baffin Shelf (Davis Strait) at ~1300m depth (63° 20.6094N, 58° 11.5092W), and lasted ~12 hours. This location was chosen for the ROV survey based on previous substantial fisheries bycatch of *A. arbuscula* colonies in this area. The ROV dive included a transect of ~1400m length ranging in depth from 1336-1293m (Fig. 2-2). Ten *A. arbuscula* colonies were collected for this study and all samples were photographed on the seafloor before collection (Fig. 2-3a; Table 2-2). The corals were immediately photographed on deck and measured for height, width, stem diameter, and wet weight. Any associated fauna found on the colonies were removed and will be used for other studies. The samples were stored in plastic bags at -20°C.
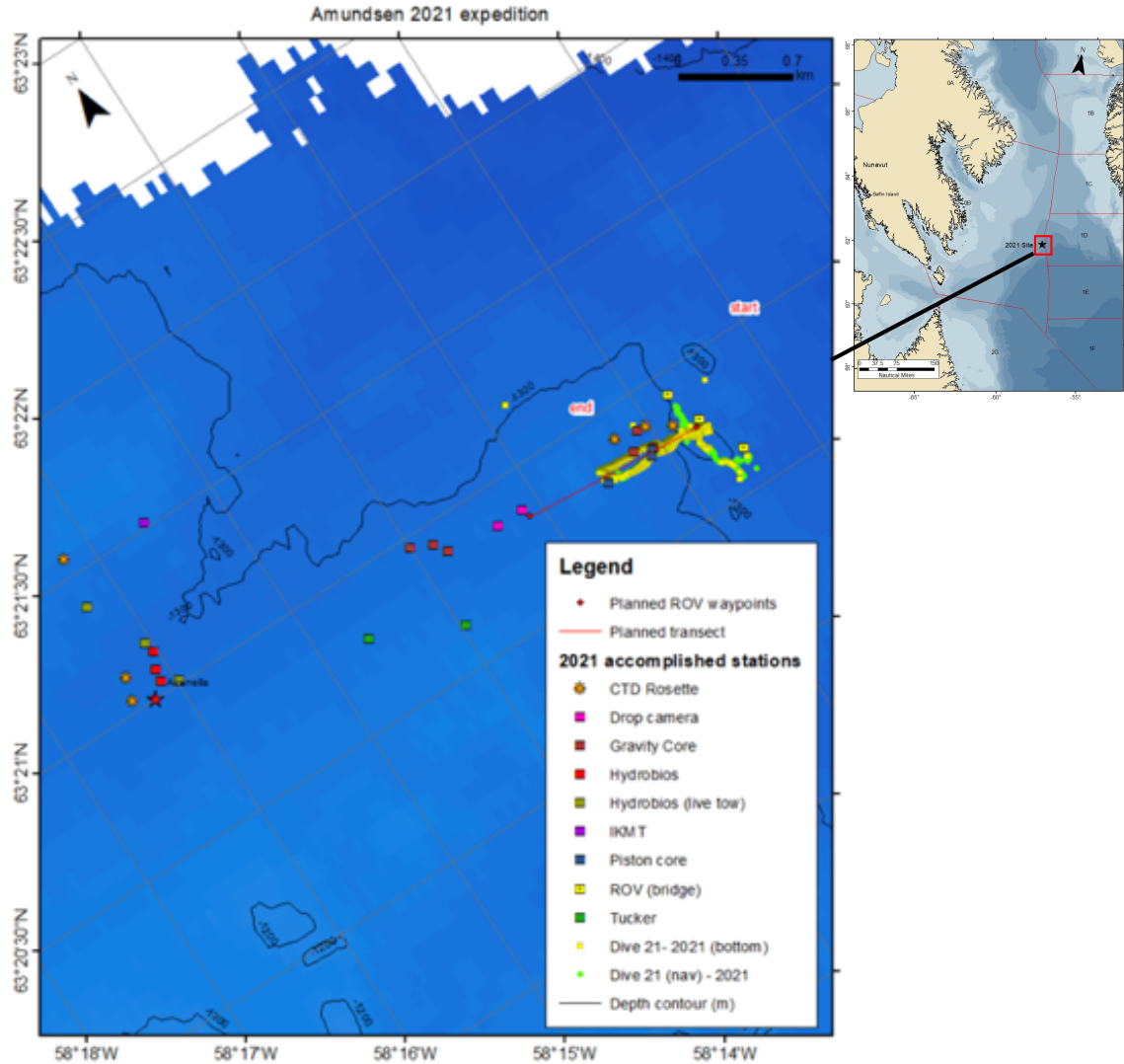
Figure 2-2. Map showing the 2021 ROV dive at the Davis Strait site on the SE Baffin Shelf, with the planned dive transect shown in red and the completed dive transect on the seafloor shown in yellow. Other operations conducted at or near the dive site are also indicated on the map (*Amundsen* 2021 Leg 2 Cruise Report).

2.2.3 Sample preparation sclerochronology (growth ring counting)

Samples collected in 2021 were photographed and re-measured for height, width, stem diameter, and wet weight on return to MUN. Basal sections of samples from DFO trawl surveys were imaged and stem diameter was measured with calipers before

sectioning. Growth ring counting is most successful at the proteinaceous nodes of the bamboo coral skeleton; therefore, samples were examined for the thickest location of the stem with a proteinaceous node present. The corals were first cut into pieces ~2-5cm in height near the location to be analyzed for growth ring counts. Most colonies collected in 2021 were sectioned twice per colony, so some colonies have two age/growth rate estimates based on different proteinaceous nodes of the colony (Table 2-2). Cut pieces were placed in 1" Buehler SamplKups ™ with the proteinaceous node parallel to the base of the sample cup. Samples were embedded in epoxy using Buehler EpoKwick FC Hardener and Resin and left to dry for >12 hours at room temperature.

Once dried, samples were cut at the proteinaceous node of the coral skeleton using a Buehler IsoMet Low-Speed Saw, with the blade cooled with 100% isopropyl alcohol. Samples were grinded and polished on a Buehler MetaServ 250 Grinder-Polisher using 400–800 grit Buehler CarbiMet silicon carbide grinding papers. Samples were then polished with a TexMet C polishing cloth and Buehler MicroPolish Alumina (0.3µm) solution to remove adhering material, and finally cleaned ultrasonically in isopropyl alcohol or water after the final polishing step. The samples were analyzed and photographed for growth ring counts on a Zeiss AxioZoom V.16 Telecentric Microscope using reflected white light and fluorescence under 16-258x.

In attempt to increase the clarity of growth rings, different sample preparation methodologies were experimented with, such as fluorescence microscopy, staining with Mutvei's solution (Schöne et al. 2005), thin section preparation, and etching in 5% HCl, but only fluorescence microscopy proved successful (Fig. 2-4).

Fluorescence microscopy used a Zeiss AxioZoom V.16 Telecentric Microscope with the same cross-sections used for reflected white light images. Different lighting colors and excitation/emission wavelengths were tested, including green light (excitation wavelength: 488, emission wavelength: 509) and blue light (excitation wavelength: 353, emission wavelength: 465), and samples were imaged under 16-258x.

2.2.4 Growth ring counting

ImageJ software was used to count growth rings and measure sample diameters (Schneider et al. 2012). Growth ring counts and measurements were done at the proteinaceous nodes, where growth rings are best visible. Stem diameter was measured with ImageJ before ring counting was completed. The measured stem diameter is indicated in Tables 2-1 and 2-2, as this measurement was most representative of the node being analyzed. The thickest portion of the skeleton, which we attempted to measure before sectioning each colony, was occasionally difficult to locate, due to the thin and fragile nature of these coral skeletons. The complexity of measuring an accurate stem diameter on small samples with calipers meant the stem diameter measured with ImageJ was likely to be more accurate when estimating age and growth rate than the initial field or lab measurement using calipers.

The *A. arbuscula* samples exhibited both major and minor growth banding (Fig. 2-3b, Fig. 2-5). Both structures were counted as it was unknown which structure represented annual banding (Sherwood and Edinger 2009). Major rings were defined as the larger growth band structures, often with 5-10 minor growth bands within each major band.

Minor growth bands were the finest banding seen in the sample image (Fig. 2-3). Three independent counters produced a set of major and minor growth ring counts for all of the samples, to minimize observer bias in the data. Each counter was given the same set of instructions and a brief tutorial on how to count the growth rings before producing the data. Each counter used ImageJ for the growth ring counts. SE was determined with the following formula:

$$\text{Standard deviation (x1, x2, x3) / sqrt (3)}$$

2.2.5 Determining age and growth rates

After collecting all growth ring count data from the three independent counters, major and minor ring counts were averaged separately from the three counters. Size metrics were compared with age and growth rate calculated from the growth ring counts, including an additional size metric termed "area", which was calculated by multiplying height and width of each colony. All size metric data were plotted with linear, logarithmic, and exponential regressions against age based on major and minor rings to determine annual growth increments. The data analysis process was first conducted for the *A. arbuscula* samples collected in scientific trawl surveys only, and then repeated including colonies collected in 2021. This methodology has been successfully applied in a sea pen study, which compared "major rings" and "all rings" with total sea pen length for the best R^2 value (K. Greeley MSc Thesis, Memorial University 2021).

Age calculated from major and minor rings was used instead of average major and minor ring counts due to inconsistency in sample clarity and calcite material inside and outside growth rings in some samples. The inconsistency means that the whole sample

radius was not included for growth ring counts in each sample, depending on the node width and sample clarity. Therefore, for all samples with calcite material inside or outside the continuum of visible growth rings marked by proteinaceous material ("inner" and "outer" calcite as displayed in Fig. 2-3c), age was calculated by extrapolating the growth rate linearly across the sample radius.

An *A. arbuscula* sample (1591) collected from NAFO zone 0B (SE Baffin Shelf) at 526m depth, analyzed for growth rates, age, and bomb-^{14}C was compared with the *A. arbuscula* samples of this study to confirm which growth band structure represented annual growth (Sherwood and Edinger 2009). The sample from the previous study had an age, radial, and axial growth rates, and radius and height measurements. Sample 1591 was aged with bomb-^{14}C and growth ring counts, which were major ring counts due to only reflected light microscopy being used, meaning minor growth rings were not observed. Linear regressions were calculated using sample 1591 and the specimens aged with growth ring counts from this study. The slope of the regression lines, along with the R^2 and p-values were used to determine if major or minor growth rings were best representative of annual banding

After interpreting which growth band structure was most likely to represent annual banding, radial and axial growth rates were calculated based on this interpretation. Radial growth rate was calculated by dividing the radius, which was measured using ImageJ, by the age determined from major growth band counts. The full sample radius was measured by taking four radial measurements from the concentric center of the growth rings to the outside edge of the samples, and then averaging these four measurements to account for

asymmetrical cross-sections. Axial growth rate was calculated by dividing the height of
each colony by the determined age.
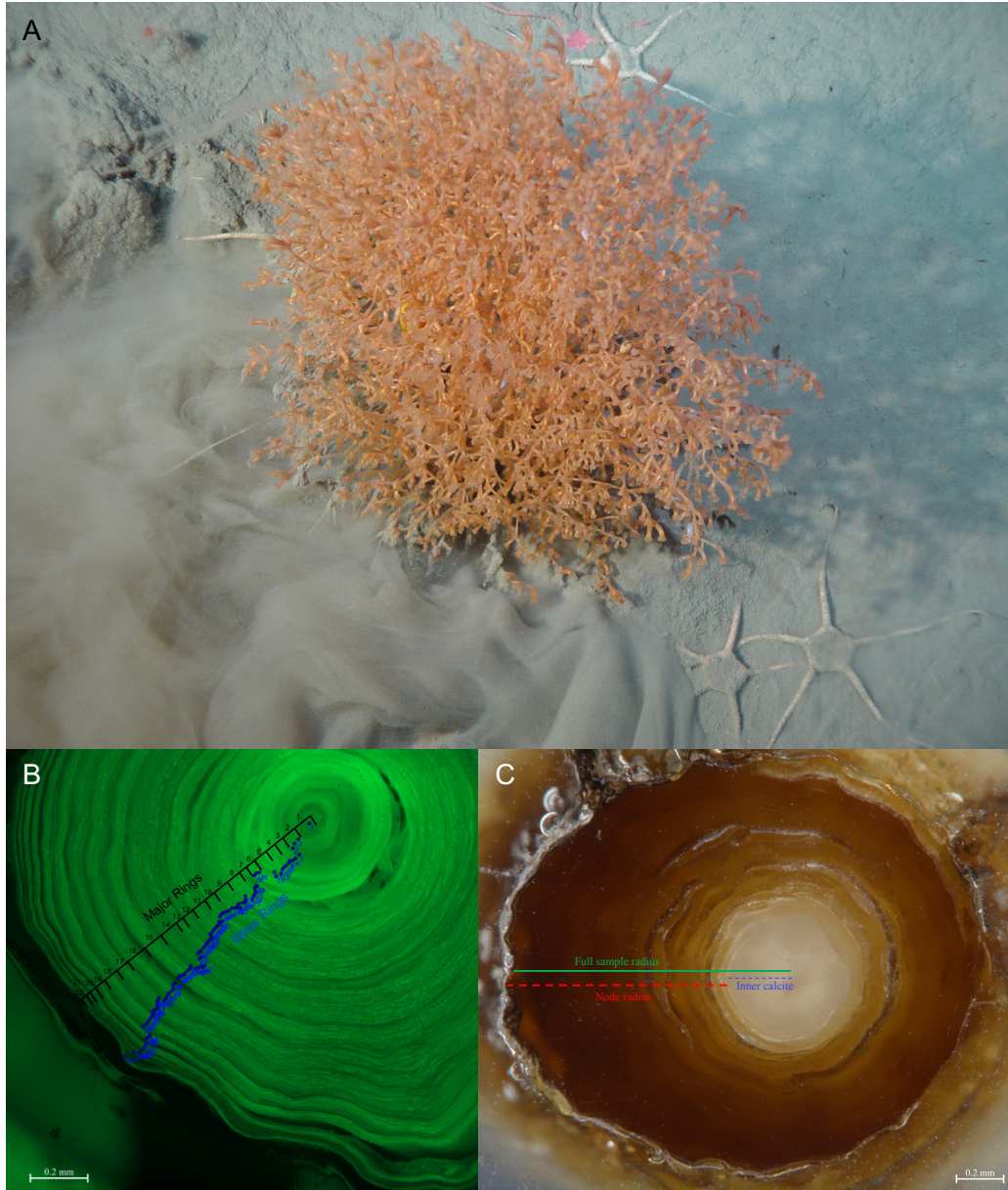
Figure 2-3. A) *A. arbuscula* colony photographed on a muddy seafloor. B) *A. arbuscula*
sample 836_18_1 imaged with fluorescence, with major and minor growth ring
differentiation labeled. This sample exhibited 22 major rings and 107 minor rings. C) *A.
arbuscula* sample 460_16_4 with measurements indicating the inner calcite section, the
node radius (or distance where ring counts were performed) and the full sample radius,
which is the node radius + inner/outer calcite layers.
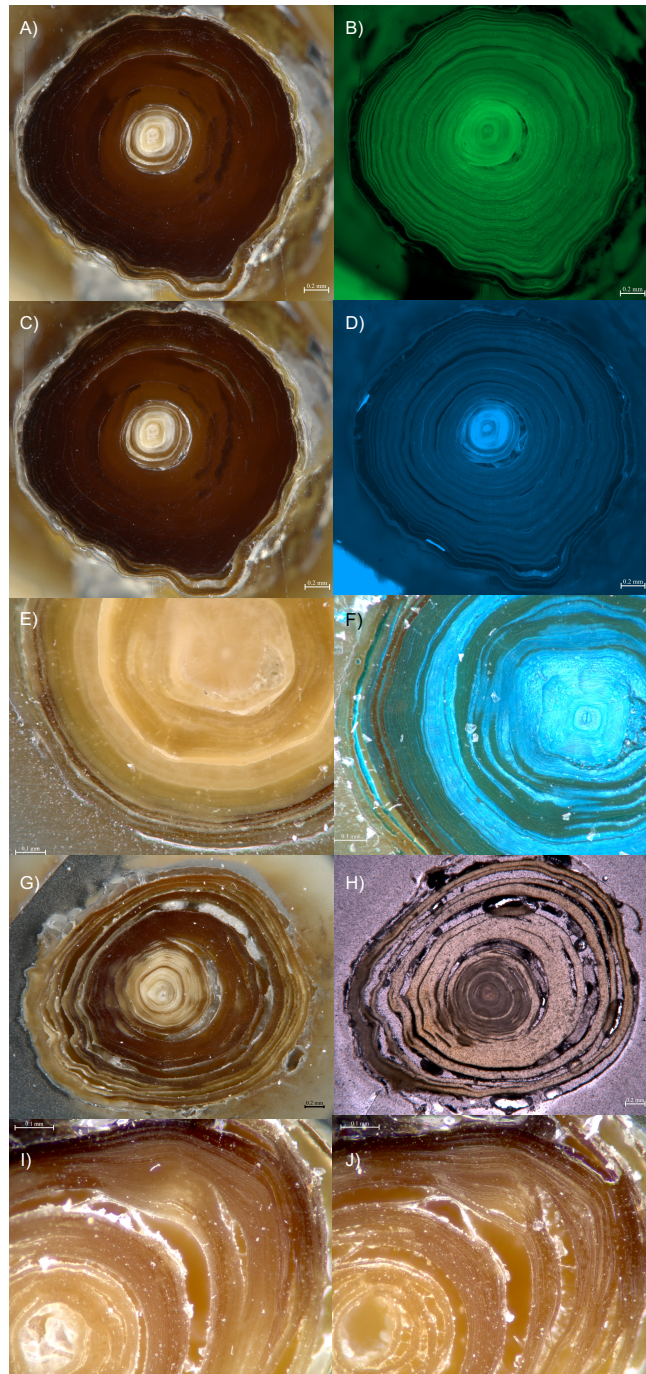
Figure 2-4. *Acanella arbuscula* cross-sections at the proteinaceous node of the skeletons, comparing reflected white light in thick section (A, C, E, G, I) with green fluorescence (B), blue fluorescence (D), a thick section stained with Mutvei's stain for 1 hour (F), a ~100μm thin section imaged with transmitted light, and J) a thick section etched in 5% diluted HCl for 1-2 minutes. Images A, B, C, D: sample 836_18_1. Images E and F: sample R21-23_a. Images G and H: AC 09_1. Images I and J: R21-20_b.
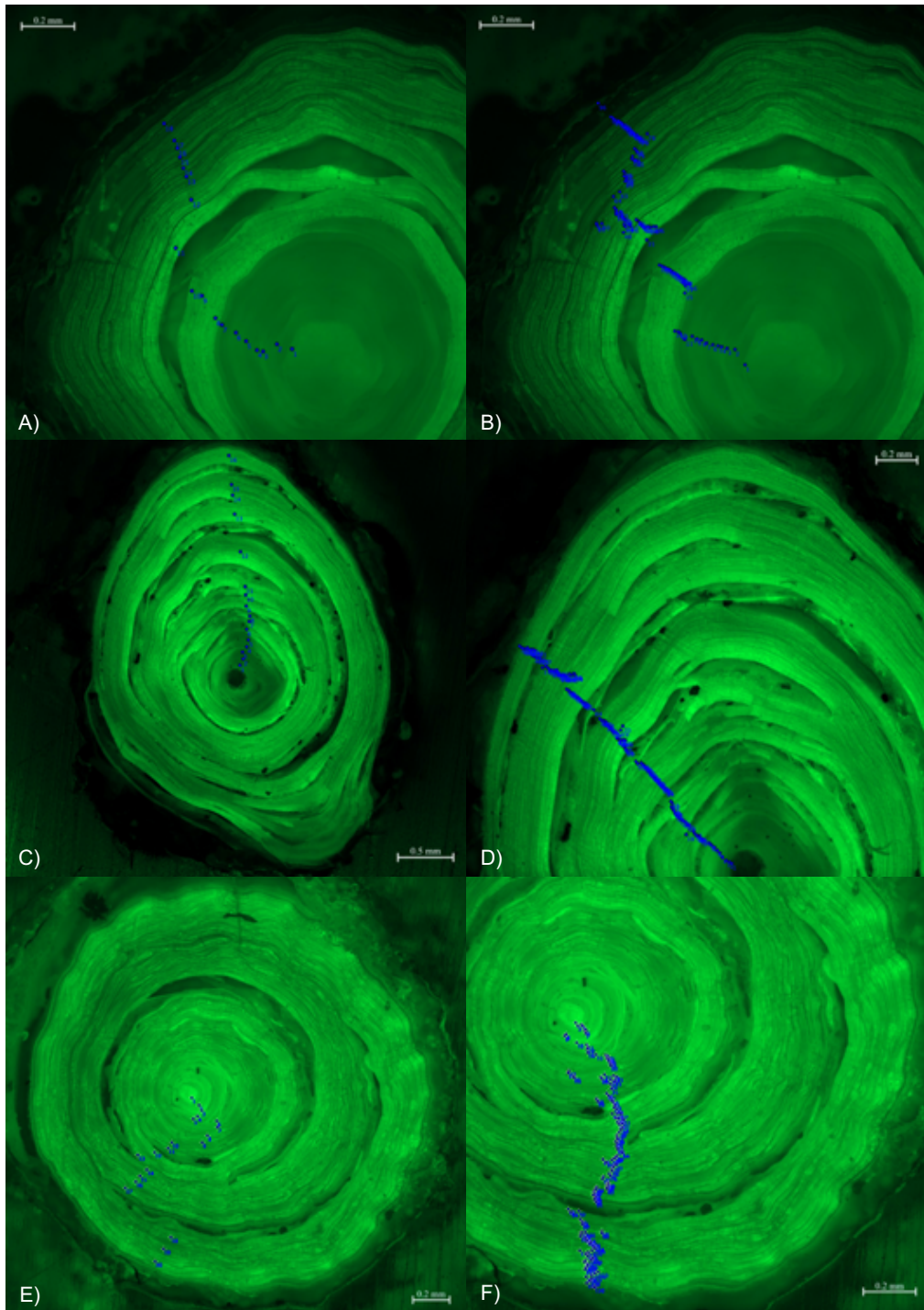
Figure 2-5. *Acanella arbuscula* specimens 7_177_1 (A&B), 8_118_1 (C&D), and 932_67_1 (E&F), showing major growth ring counts (A, C, E) compared to minor growth ring counts (B, D, F) imaged with fluorescence. Growth ring counts shown are only from one ring counter.

2.2.6 Geographic and bathymetric comparisons

Age, radial, and axial growth rates were compared geographically and bathymetrically for samples collected in scientific trawl surveys (Fig. 2-1). For the geographic comparisons, samples were divided based on NAFO zone (0B, 2H, 3O), and one-way ANOVA tests were completed for size metrics, age, and growth rates. Each analysis was first tested for normality and homogeneity before performing the one-way ANOVA. Specimens collected in 2021 from Davis Strait were also included in some of the geographic analyses to compare these samples with those collected in trawl surveys. The 2021 samples were first analyzed independently by performing regressions for size metrics and major/minor growth rings but were sampled from within NAFO zone 0B. When geographic comparisons were conducted, similarities between samples from 0B and Davis Strait were anticipated (Fig. 2-1).

Bathymetric comparisons were analyzed for age, radial, and axial growth rate. All trawl survey specimens were first analyzed bathymetrically, followed by analyzing for bathymetric relationships within each NAFO zone. These analyses included regressions and one-way ANOVA tests.

Many *A. arbuscula* samples collected in 2021 were aged twice from two different proteinaceous nodes. Multiple age estimates from a single colony were averaged to maintain the consistency of only one age estimate per colony (Table 2-2).

Some colonies analyzed for growth rates and ages were from the same approximate location. With these specimens, intra-location variation was analyzed for comparisons of

ages, radial, and axial growth rates. The intra-location comparisons were only conducted for trip/sets with 5 colonies measured for growth rates and age (Table 2-1).

2.2.7 Ontogenetic tests (Gompertz and logistic growth curves)

Regional differences observed in growth rate could be a result of ontogenetic control, which can be tested using Gompertz and logistic functions. These sigmoid functions are defined by slow growth in early stages, followed by increased growth rates, and finally slowed growth approaching an asymptote with increased age, which gives a sigmoidal shape to the growth curves (Winsor 1932; Sebens 1987). The only difference between the two functions is that logistic growth is symmetrical between the two asymptotes, while the Gompertz function is asymmetrical (Winsor 1932). Gompertz fits have been used previously to model coral growth in the deep-sea soft coral *Anthomastus ritteri* (Cordes et al. 2001), have been suggested for the sea pen species *Halipteris finmarchica* based on slow diametric growth rates in early years of this species' life (Neves et al. 2015), and are commonly used in studies on vertebrates (Sebens 1987). Gompertz functions are used when modelling population growth structures (Finch and Pike 1996) and when modelling tumor growth rates (Lo 2010). The Gompertz equation is defined as:

$$(1) \qquad f(t) = ae^{-be^{-ct}}$$

where a = asymptote, b = displacement on the x-axis, and c = growth rate. The logistic equation is defined as:

$$(2) \qquad f(t) = L / (1 + e^{-k(x-x_0)})$$

where L = asymptote, k = growth rate, and x_0 = the sigmoid midpoint.

We applied both growth curves to age compared with stem diameter, height, wet weight (provided by DFO), and area (height * width) to better understand how radial and axial growth rates may change throughout the lifespan of this species. Gompertz and logistic growth curves were fit to age based on major rings only, and were generated for all colonies together, and for colonies collected in scientific trawl surveys only. The R^2 values from these functions were compared to the regression fits produced, and growth coefficients from the sigmoid growth curves were compared with average growth rates from each NAFO zone.

2.2.8 Environmental data

To measure productivity differences in each NAFO zone, chlorophyll-a concentrations were extracted from the satellites MODIS (Moderate Resolution Imaging Spectroradiometer) and SeaWiFS (Sea-viewing Wide Field-of-view Sensor) at 4km resolution in daily increments (Clay et al. 2021). MODIS data were used from 2003-2021 and SeaWiFS data for 1997-2010. The overlapping years from both sensors were compared to understand variance when using different satellites. Afterwards, only MODIS data were used in analyses from 2003-2021 to keep consistency in the satellite and SeaWiFS data from 1997-2002 were included to extend the record. The different regions used for geographic variation (NAFO zones 3O, 2H, and 0B) were created in the chlorophyll visualization program using custom polygons. Data was not available for most of NAFO zone 0B in PhytoFit Chlorophyll Visualization (Clay et al. 2021) because of its northern location. Therefore, data from the pre-defined polygon "North Central Labrador

Shelf" (NCLS) was used for NAFO zone 0B instead (Clay et al. 2021) (Fig. 2-6). Mean, median, standard deviation, maximum, and minimum chlorophyll were generated for each defined polygon in daily increments, along with percent coverage. Phytoplankton bloom parameters were also extracted from 1997-2021 for the start day, end day, duration, magnitude, and amplitude (Clay et al. 2021).

One-way ANOVA tests compared the mean and median daily average chlorophyll concentrations, and bloom duration, amplitude, and magnitude from 1997–2021 for each location. Inter-annual variation was not analyzed using a time series because we were not interested in how chlorophyll concentrations varied over time.

Mean, median, and standard deviation of daily chlorophyll values from 1997-2021 were averaged for each colonies' estimated growth years only for specimens collected in trawl surveys. Growth years were determined by subtracting age (calculated from major growth ring counts) from the year of collection within scientific trawl surveys. Phytoplankton bloom data (start, max, end, duration, amplitude, magnitude) were also averaged for growth years of each colony. Some colonies' growth years extended earlier than the available chlorophyll data. In these cases, data were averaged to the earliest year with data (1997) until the year of collection.

Multi-factor ANOVA tests were completed to determine geographic and bathymetric variation observed in growth rates and ages, which included environmental and ontogenetic variables into the ANOVA tests.
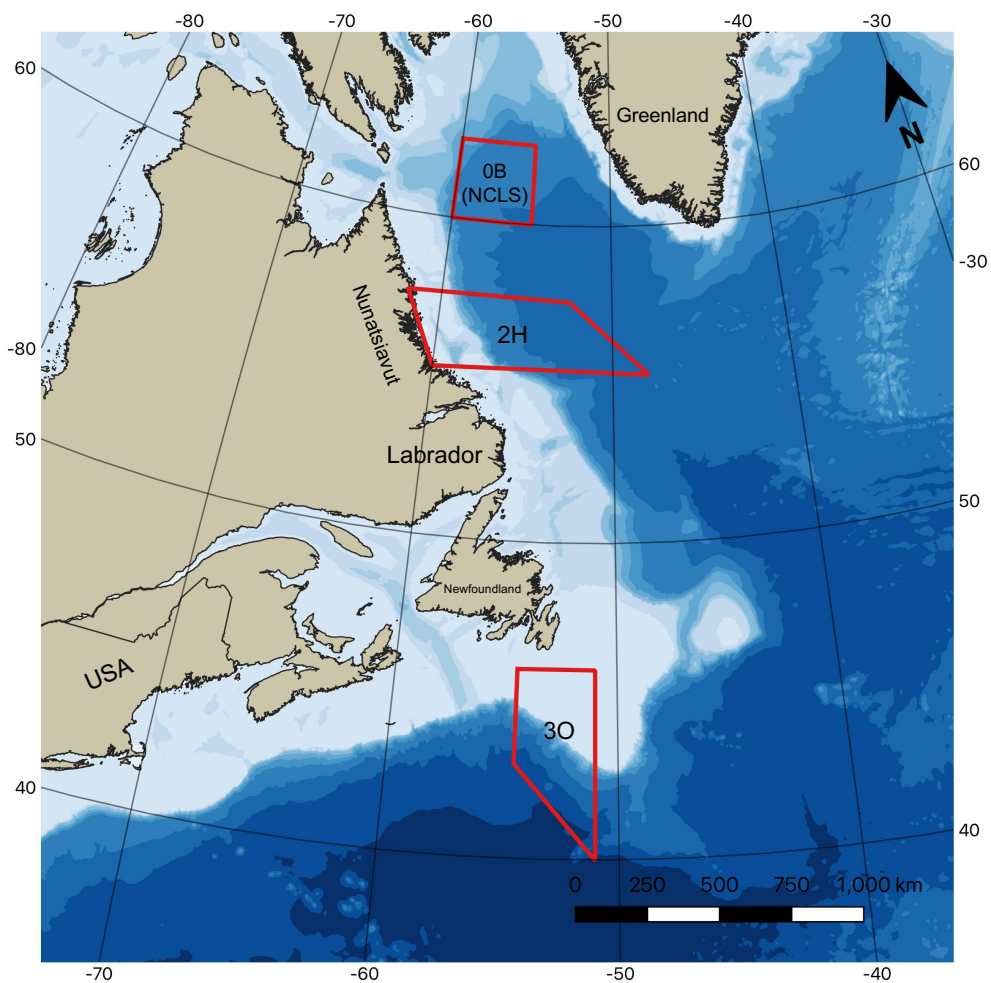
Figure 2-6. Map of the NW Atlantic with red shapes indicating the polygons used for chlorophyll and phytoplankton bloom data (Clay et al. 2021). NCLS indicates the North Central Labrador Shelf, which was used as a proxy for NAFO zone 0B since data was not available in the real location of NAFO zone 0B, due to its northern location.

Table 2-1. *Acanella arbuscula* samples collected by scientific trawl surveys from 2004 - 2018.

Trip	Set	Subsample No.	Year	Latitude	Longitude	NAFO Zone	Depth	BTemp	Height	Width	Diameter
7	177	1	2015	64.5741	-58.5205	0B	686	2.68	155	50	2.12
7	177	2	2015	64.5741	-58.5205	0B	686	2.68			2.01
7	22	1	2015	64.6131	-57.9640	0B	729	3.9	85	80	2.30
8	150	1	2016	61.6909	-63.8428	0B	481	2.67	30.42	17.62	2.21
8	150	2	2016	61.6909	-63.8428	0B	481	2.67	50.33	24.49	2.23
8	150	3	2016	61.6909	-63.8428	0B	481	2.67	60.61	32.81	3.36
270	9	1	2004	62.0333	-60.6667	0B	841		80	65	1.74
270	86	1	2004	62.9500	-59.0000	0B	1060		185	160	2.65
8	96	1	2016	66.0606	-60.1152	0B	447	1.26			2.28
8	153	1	2016	61.8989	-62.6805	0B	467	2.68			2.54
8	118	1	2016	63.6956	-58.7827	0B	848	3.65			3.30
8	118	2	2016	63.6956	-58.7827	0B	848	3.65	205	122	3.28
8	118	3	2016	63.6956	-58.7827	0B	848	3.65	140	104	1.93
8	118	4	2016	63.6956	-58.7827	0B	848	3.65			2.13
101	124	1	2006	65.1308	-58.4517	0B	511	3.14	220	115	2.34
101	124	2	2006	65.1308	-58.4517	0B	511	3.14	99	111	1.92
103	117	1	2008	63.5396	-60.4051	0B	585	3.11	137.31	47.88	2.44
103	117	2	2008	63.5396	-60.4051	0B	585	3.11	162	71	2.10
103	117	3	2008	63.5396	-60.4051	0B	585	3.11	96.91	64.43	1.89
119	13	1	2013	55.4725	-57.1983	2H	178	1.1	175	110	3.06
975	6	1	2010	55.4500	-56.7775	2H	181	1.5	62.22	39.54	2.55
975	36	1	2010	56.9225	-59.0967	2H	243	2.1	55	55	2.51
975	33	1	2010	56.9992	-58.4325	2H	1312	3.9	40	75	1.73
817	13	1	2008	55.6075	-57.0217	2H	252	0.9	110	140	3.00
817	13	2	2008	55.6075	-57.0217	2H	252	0.9	110	110	2.21
817	13	3	2008	55.6075	-57.0217	2H	252	0.9	75	100	2.35
817	13	4	2008	55.6075	-57.0217	2H	252	0.9			2.16
817	13	5	2008	55.6075	-57.0217	2H	252	0.9	70	100	1.49

817	12	1	2008	55.7375	-56.9525	2H	1042	4	85	90	1.57
817	12	2	2008	55.7375	-56.9525	2H	1042	4	85	70	1.64
817	12	3	2008	55.7375	-56.9525	2H	1042	4	90	95	1.86
817	29	2	2008	56.3325	-57.6908	2H	413	4.8	167	85	2.57
817	20	1	2008	56.0142	-57.2258	2H	1274	3.8	78	90	1.80
680	10	1	2006	57.6483	-59.2492	2H	1052	4.1	80	55	2.49
679	17	1	2006	55.7008	-57.0592	2H	471	3.3	55.47	35.41	1.16
679	17	3	2006	55.7008	-57.0592	2H	471	3.3	68.5	47.67	1.67
190	11	1	2018	55.4792	-57.0117	2H	179	1.4	145	210	3.43
190	11	2	2018	55.4792	-57.0117	2H	179	1.4	75	35	1.48
190	11	3	2018	55.4792	-57.0117	2H	179	1.4		45	1.95
163	1	1	2016	56.0042	-57.1208	2H	1354	3.6	150	95	3.06
163	18	1	2016	56.8017	-58.1758	2H	1284	3.7	80	115	1.86
163	19	1	2016	56.9800	-58.3717	2H	1321	3.6	100	110	2.24
120	12	1	2013	57.1217	-59.0325	2H	523	4.6			1.14
106	7	1	2012	55.6525	-56.7900	2H	867	blank	108	65	1.70
95	19	1	2011	56.7208	-58.3700	2H	960	4.2	67.67	46.68	0.99
95	19	2	2011	56.7208	-58.3700	2H	960	4.2	102	91	1.73
943	20	1	2010	43.6800	-52.3383	3O	624	4.2	185	180	2.50
943	27	1	2010	43.1025	-51.4158	3O	667	4.1	63	65	1.62
943	27	2	2010	43.1025	-51.4158	3O	667	4.1	139	107	2.07
943	27	3	2010	43.1025	-51.4158	3O	667	4.1	104	76	1.65
933	18	1	2010	43.2375	-51.5125	3O	604	4.4	135	160	3.17
933	18	2	2010	43.2375	-51.5125	3O	604	4.4	160	110	4.32
933	18	3	2010	43.2375	-51.5125	3O	604	4.4	135	90	2.10
933	18	4	2010	43.2375	-51.5125	3O	604	4.4	130	50	1.88
933	18	5	2010	43.2375	-51.5125	3O	604	4.4	75	65	1.85
932	67	1	2010	44.0750	-52.9092	3O	582	4.7	143	122	2.31
915	8	1	2009	43.1042	-51.3958	3O	647	4	125	70	2.21
915	8	2	2009	43.1042	-51.3958	3O	647	4	140	90	2.33

915	8	3	2009	43.1042	-51.3958	3O	647	4	120	120	2.06
915	8	4	2009	43.1042	-51.3958	3O	647	4	130	90	1.70
915	8	5	2009	43.1042	-51.3958	3O	647	4	113	84	1.44
905	23	1	2009	43.7692	-52.3983	3O	337	7.4	230	90	2.80
905	23	2	2009	43.7692	-52.3983	3O	337	7.4	230	110	3.03
905	39	1	2009	43.0783	-51.3425	3O	596	4.8	80.04	53.73	1.59
905	39	2	2009	43.0783	-51.3425	3O	596	4.8	90.17	62.99	2.44
905	39	3	2009	43.0783	-51.3425	3O	596	4.8	90.58	72.89	1.80
905	39	4	2009	43.0783	-51.3425	3O	596	4.8	93.15	79.54	1.96
905	39	5	2009	43.0783	-51.3425	3O	596	4.8	56.69	44.96	1.98
905	38	1	2009	43.1250	-51.3808	3O	598	5.1	50	55	1.26
905	38	2	2009	43.1250	-51.3808	3O	598	5.1	100	34	1.40
905	38	3	2009	43.1250	-51.3808	3O	598	5.1	116	67	2.10
905	38	4	2009	43.1250	-51.3808	3O	598	5.1	95	43	1.47
905	38	5	2009	43.1250	-51.3808	3O	598	5.1	71	68	1.43
894	1	1	2009	44.7650	-54.5067	3O	768	4.3	107.04	86.93	1.84
894	1	2	2009	44.7650	-54.5067	3O	768	4.3			2.56
894	1	3	2009	44.7650	-54.5067	3O	768	4.3			2.02
894	1	4	2009	44.7650	-54.5067	3O	768	4.3	35.08	26.01	2.99
894	1	5	2009	44.7650	-54.5067	3O	768	4.3	84.48	57.97	2.34
894	9	1	2009	43.9258	-52.7517	3O	887	4.2	120	145	3.30
894	10	1	2009	43.9367	-52.7817	3O	1020	4.2	77.6	92.04	1.94
836	18	1	2008	43.8517	-52.5850	3O	573	4.5	176	63	2.32
836	18	2	2008	43.8517	-52.5850	3O	573	4.5	220	104	2.32
836	18	3	2008	43.8517	-52.5850	3O	573	4.5	216	72	3.46
836	18	4	2008	43.8517	-52.5850	3O	573	4.5	130	77	2.22
836	18	5	2008	43.8517	-52.5850	3O	573	4.5	143	61	2.79
760	37	1	2007	43.8758	-52.5942	3O	600	4.3	163	117	4.50
760	37	2	2007	43.8758	-52.5942	3O	600	4.3	170	215	6.43
760	37	3	2007	43.8758	-52.5942	3O	600	4.3	230	85	2.65

Trip	Set	Subsample	Year	Latitude	Longitude	NAFO zone	Depth	BTemp	Height	Width	Diameter
760	37	4	2007	43.8758	-52.5942	3O	600	4.3	93	85	3.24
760	37	5	2007	43.8758	-52.5942	3O	600	4.3	176	197	3.61
760	31	1	2007	44.6958	-54.1075	3O	719	4.3	155	130	2.59
760	31	2	2007	44.6958	-54.1075	3O	719	4.3	140	40	2.73
760	31	3	2007	44.6958	-54.1075	3O	719	4.3	205	130	2.48
760	31	4	2007	44.6958	-54.1075	3O	719	4.3			2.82
760	31	5	2007	44.6958	-54.1075	3O	719	4.3	180	145	2.88
750	23	1	2007	43.1475	-51.6008	3O	1153	3.9	53	17	1.00
750	23	2	2007	43.1475	-51.6008	3O	1153	3.9	70	40	1.68
750	23	3	2007	43.1475	-51.6008	3O	1153	3.9	43	41	1.25
750	23	4	2007	43.1475	-51.6008	3O	1153	3.9	75	55	1.03
479	18	1	2017	44.6883	-54.1083	3O	702	4.6	192	74.26	2.52
460	13	1	2015	43.2758	-51.4033	3O	224	8.5	180	100	2.08
460	16	1	2015	43.0717	-51.2950	3O	574	4.5	139.75	37.03	2.95
460	16	2	2015	43.0717	-51.2950	3O	574	4.5	130.87	78.91	2.24
460	16	3	2015	43.0717	-51.2950	3O	574	4.5	127.26	60.42	1.92
460	16	4	2015	43.0717	-51.2950	3O	574	4.5	118.7	45.61	1.92

Notes and units: Sample numbers = trip_set_subsample no. Latitude and Longitude: decimal degrees. Depth: m. BTemp (Bottom temperature): °C. Height: mm. Width: mm. Diameter: mm. NAFO zone: North Atlantic Fisheries Organization zone. Blanks in the table represent values that are not available or were not measured.

Table 2-2. *Acanella arbuscula* samples collected in 2021 at Davis Strait.

Sample	Subsample No.	Year	Latitude	Longitude	Depth	Height	Width	Diameter
R21-8	b2	2021	63 20.793	58 11.9094	1314	90	80	0.995
R21-9	a	2021	63 20.7918	58 11.9112	1314	110	90	1.008
R21-9	b	2021	63 20.7918	58 11.9112	1314	110	90	1.104
R21-10	b	2021	63 20.793	58 11.9472	1314	100	120	1.288
R21-10	c	2021	63 20.793	58 11.9472	1314	100	120	1.332
R21-15	a	2021	63 20.8008	58 12.456	1299	120	100	1.189
R21-15	b	2021	63 20.8008	58 12.456	1299	120	100	1.226
R21-16	a	2021	63 20.8038	58 12.4638	1299	130	120	1.627
R21-16	b	2021	63 20.8038	58 12.4638	1299	130	120	1.601
R21-17	a	2021	63 20.802	58 12.4644	1298	105	40	1.414
R21-17	b	2021	63 20.802	58 12.4644	1298	105	40	1.55
R21-20	a	2021	63 20.7996	58 12.4794	1297	100	80	1.23
R21-20	b	2021	63 20.7996	58 12.4794	1297	100	80	1.55
R21-21	a	2021	63 20.8002	58 12.4812	1297	110	100	1.19
R21-21	b	2021	63 20.8002	58 12.4812	1297	110	100	1.138
R21-23	a	2021	63 20.799	58 12.4824	1297	120	80	1.374
R21-23	b	2021	63 20.799	58 12.4824	1297	120	80	1.832
R21-25	a	2021	63 20.7876	58 12.4578	1299	150	150	1.664
R21-25	b	2021	63 20.7876	58 12.4578	1299	150	150	1.501

Notes and units: Latitude and longitude: decimal degrees minutes. Depth: m. Height: mm. Width: mm. Diameter: mm. All of the samples except "R21-8b2" were averaged together depending on sample colony, as these colonies were all sub-sampled two times. Averaged values were used for data analysis so each colony only had one age/growth rate estimate.

2.3 RESULTS

2.3.1 Growth ring characteristics

A. arbuscula samples exhibited both major and minor growth ring structures (Fig. 2-3b). The major rings were defined as the larger ring structures and minor rings were defined as the smallest observed ring structures. Minor growth bands observed represent a sub-annual growth increment, but further study on these growth rings was not completed in this study.

Growth ring clarity amongst the samples was not consistent. Samples showed separation of proteinaceous growth rings, with material in between, likely not protein. This material was often 'blurry', and it is possible that sample preparation effected clarity, as growth rings in bamboo corals are hygroscopic. The material separating the protein was not identified, but is likely calcite or epoxy. Calcite material was frequently observed on the outside of the proteinaceous portion of the skeleton when cross-sectioned. The samples with this calcite material had to be measured differently radially to accurately calculate growth rates (Fig. 2-3c). Similarly, if the skeleton had calcite material near the center of the skeleton, this portion was not measured when calculating growth rates. Both the outside portion of calcite and the inner axis portion were taken into consideration when calculating the age of the samples because growth rings could not be counted across the full radius, meaning the coral continued growing after the final protein ring was deposited (Fig. 2-3c). Outer or inner calcite were measured on these samples to extrapolate the growth rate, and calculate an accurate age estimate. Another common observation was non-concentric growth rings and inconsistent clarity of growth rings across a thick section.

This clarity variation was likely due to the process of preparing specimens because their small skeletons and fragile material did not always allow for a flat surface due to the various steps of prepping the samples for epoxy, cutting the samples, and grinding/polishing the specimens. Throughout these preparation steps, there are many opportunities for the sample surface to become uneven, which impacts the readability of growth rings.

Clarity variation amongst samples led to high standard errors of major and minor growth ring counts for some specimens (Fig. 2-7). Standard error represents disagreement amongst the three growth ring counters, which evaluates the consistency of growth ring counts and the possible uncertainty of the growth ring counting method. Calculations were conducted removing samples with high standard errors, which is further explained in appendix 2-6.
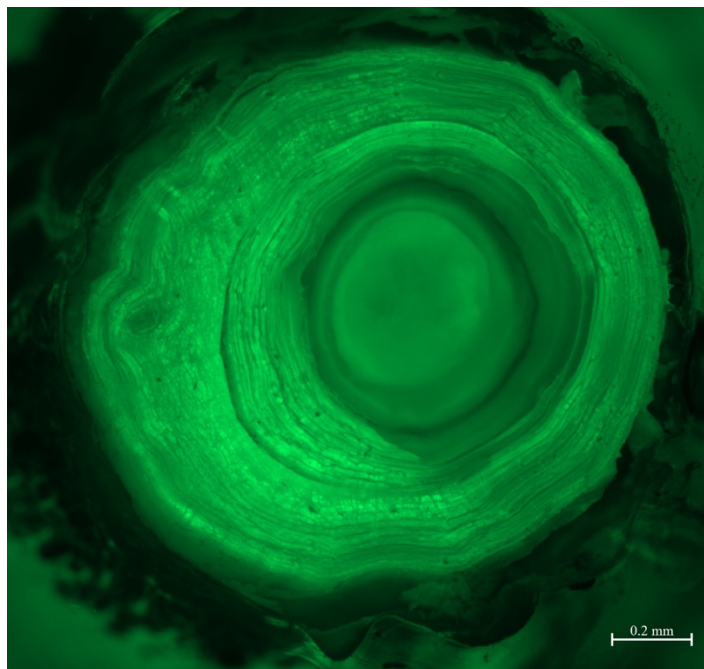
Figure 2-7. *Acanella arbuscula* sample 905_38_5 imaged with fluorescence. Standard error determined from three growth ring counters was 1.5 for major rings and 12.6 for minor rings.

2.3.2 Radiometrically validated sample comparison (major/minor rings)

Sample 1591 from Sherwood and Edinger (2009), collected from NAFO zone 0B (SE Baffin Shelf) at 526m depth was previously analyzed and aged with bomb-^{14}C and growth ring counts. This specimen showed stronger relationships with ages based on major rings for samples from this study, aged with growth ring counts (Fig. 2-8). Analyses were conducted for age based on major and minor growth rings with height and radius, as these two size metrics were available for sample 1591 (Sherwood and Edinger 2009) (Fig. 2-8).
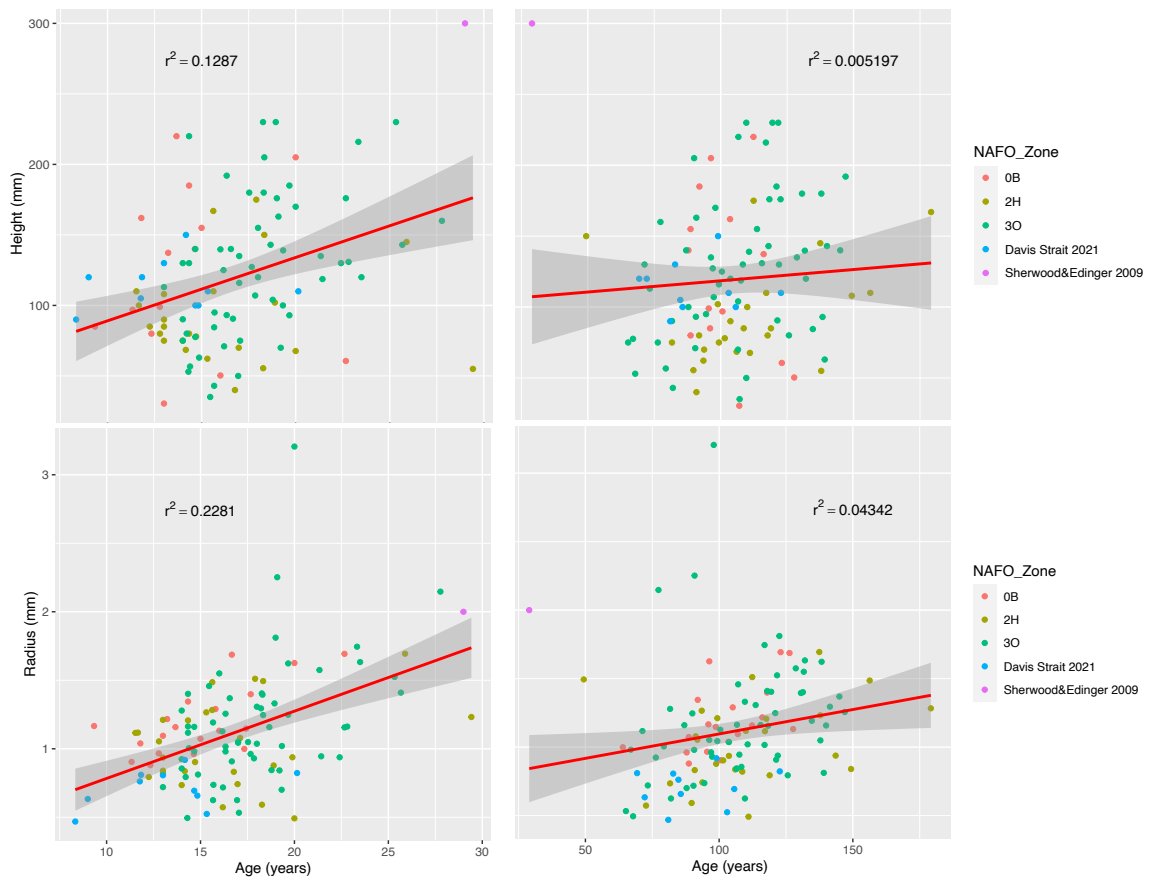
Figure 2-8. *Acanella arbuscula* samples from this study and sample 1591 (Sherwood and Edinger 2009), plotted for age based on major (left panel) and minor rings (right panel) with height and radius. Red lines indicate linear regression models with a 95% confidence interval shown in grey.

2.3.3 Size metrics and age (major/minor rings)

Age based on major rings for scientific trawl samples showed stronger relationships with size metrics than age based on minor rings for all metrics except root length and wet weight (Fig. 2-9; Table 2-3). Each size metric was analyzed with a linear, logarithmic, and exponential regression for the highest R^2 value, and the strongest fit regression was then plotted for each variable (Fig. 2-9) (Table 2-3). Wet weight data was used with caution because samples were stored frozen, but often lost water weight while the weighing process was ongoing, and colonies had varying amounts of tissue on the skeletons and variations in associated fauna attached. Size metric data for samples collected in 2021 were similarly compared based on linear, logarithmic, or exponential regressions, and age based on major rings showed stronger relationships than age based on minor rings for 3 of the 5 size metrics (Table 2-3) Based on these comparisons and the radiometrically dated sample from Sherwood and Edinger (2009), major rings were determined to represent annual growth. Size metric analyses with all samples (scientific trawl survey and ROV samples from 2021) showed the same trends of age based on major rings exhibiting stronger regressions with size metrics than age based on minor rings (Table 2-3).
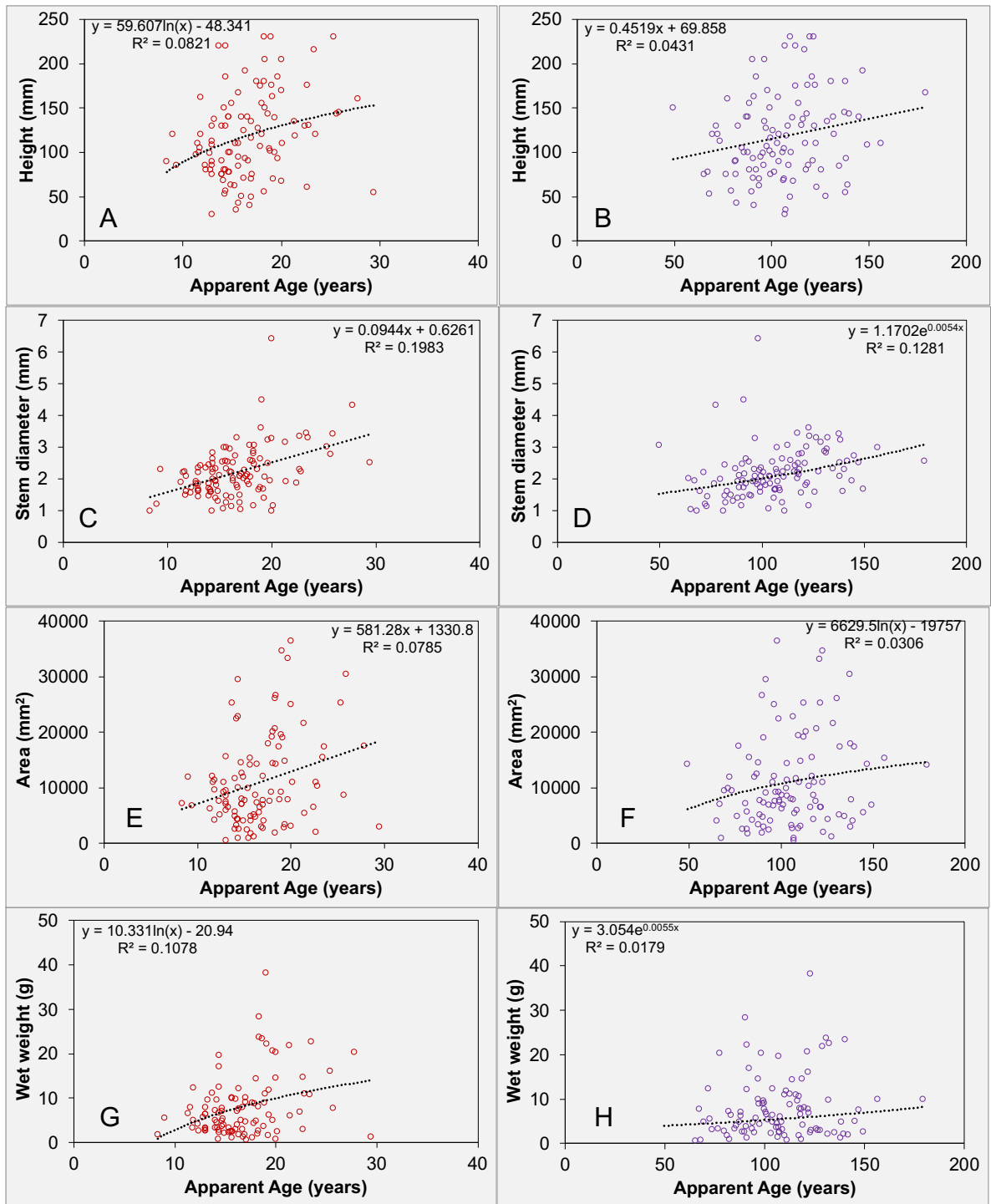
Figure 2-9. Size metrics and age for all *A. arbuscula* samples (n = 115) plotted with linear, logarithmic, or exponential regressions. A) Height (major rings), B) height (minor rings), C) stem diameter (major rings), D) stem diameter (minor rings), E) area (major rings), F) area (minor rings), G) wet weight (major rings), H) wet weight (minor rings).

2.3.4 Growth rates and ages: geographic and bathymetric comparisons

Age based on major growth rings (termed "age" for the remainder of chapter 2) was used as the age estimate and to determine radial and axial growth rates. Ages for the 105 colonies from trawl surveys ranged from 9-29 years, with both a mean and median value of 17 years (Table 2-4). Radial growth rates ranged from 0.025 – 0.160 mm/yr and axial growth rates ranged from 1.9 – 16.1 mm/yr (Table 2-4). *A. arbuscula* colonies collected in 2021 with the ROV (n = 10) showed ages ranging from 8-20 years, with a mean of 13 years and a median of 14 years (Table 2-5). Radial growth rates ranged from 0.034 – 0.071 mm/yr and axial growth rates ranged from 5.8 – 13.4 mm/yr (Table 2-5).

Geographic comparisons for samples collected in trawl surveys indicated a strong relationship between NAFO zone and age (p = 0.0046), radial growth rate (p = 0.0146), and axial growth rate (p = 0.01904). The youngest colonies were in NAFO zone 0B and the oldest colonies were in NAFO zone 3O, while radial and axial growth rates showed the fastest growth rates in NAFO zone 0B, and similar yet slightly slower growth rates in NAFO zones 2H and 3O (Table 2-4).

A. arbuscula samples collected in 2021 were included in a separate analysis, which also showed significant relationships between NAFO zone and age and growth rates (Fig. 2-10). The age of samples collected from Davis Strait (2021), within NAFO zone 0B were most similar to samples from NAFO zone 0B, however radial growth rates were slowest in the Davis Strait samples compared to all NAFO zones, while the axial growth rates were similar to NAFO zone 0B (Fig. 2-10).

Linear regression of bathymetric depth against age showed a weak but significant decline in age with depth ($R^2 = 0.109$; $p = 0.0003$). No relationship with radial growth rate ($R^2 = 0.02$; $p = 0.13$) or axial growth rate ($R^2 = 0.014$; $p = 0.26$) was observed (Fig. 2-9).
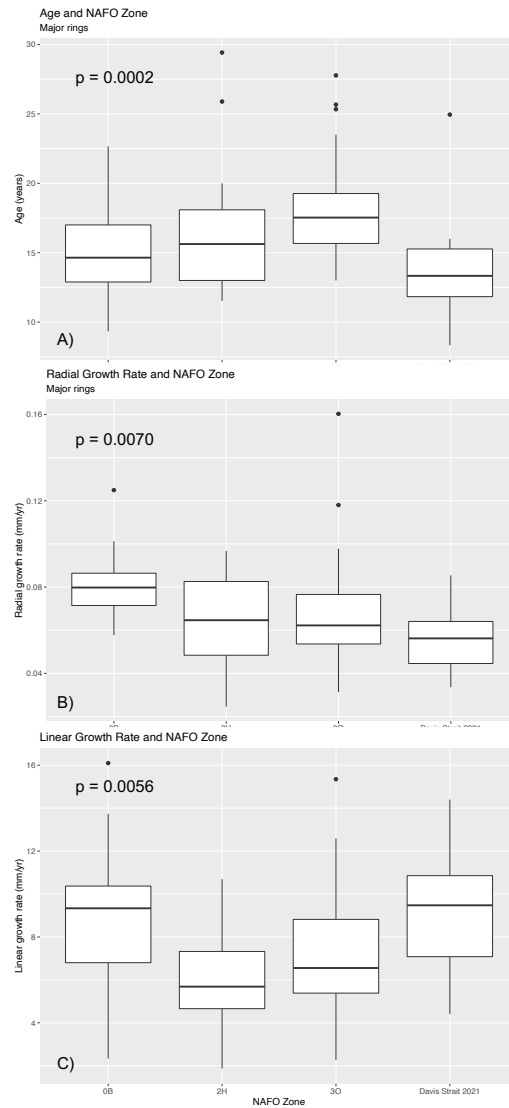
Figure 2-10. All *Acanella arbuscula* samples compared for age (A) and growth rates (B&C) within each NAFO zone and for the samples collected in 2021 with the ROV, sampled from within NAFO zone 0B. The black line within each box plot represents the median value, the boxes represent the interquartile range (25th-75th percentiles), and the vertical lines represent the minimum and maximum values excluding outliers, which are indicated by the black points.
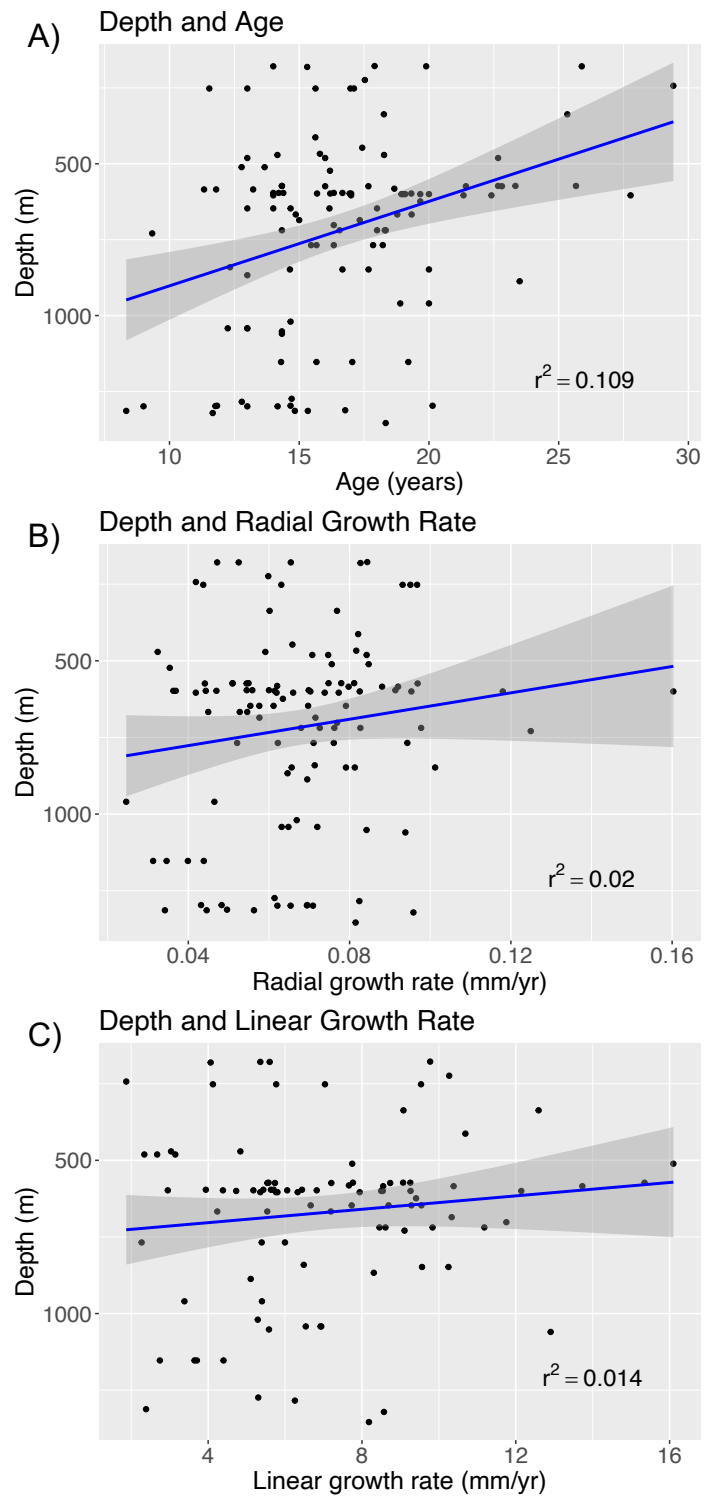
Figure 2-11. All *Acanella arbuscula* samples compared for age (A) and growth rates (B&C) with depth. The blue line indicates the linear regression best fit line with the grey shading representing 95% confidence intervals.

2.3.5 Intra-location analyses of size metrics, growth rates, & ages

Nine different trawls had five colonies analyzed for growth rates and ages, meaning size metrics, growth rates, and ages between different colonies from the same approximate location could be compared. Each location analyzed except for trip/set 817_13, was from within NAFO zone 3O. Wide ranges were observed for some colonies sampled from the same location, while others showed good consistency between samples (Fig. 2-12). The largest age range was 14-28 years for trip/set 933_18, while the smallest range was for trip/set 760_37 with a range of 19-20 years (Fig. 2-12; Table 2-6). The higher end of age variability observed within trip/sets was equal to variability observed within NAFO zones, while most trip/sets showed lower ranges of variation than observed within NAFO zones (Table 2-6). Similarly, radial and axial growth rate ranges were mostly less than the range observed within NAFO zone regions, however the trip/sets with more variable growth rates showed similar ranges to the NAFO zone region growth rate ranges (Table 2-6).
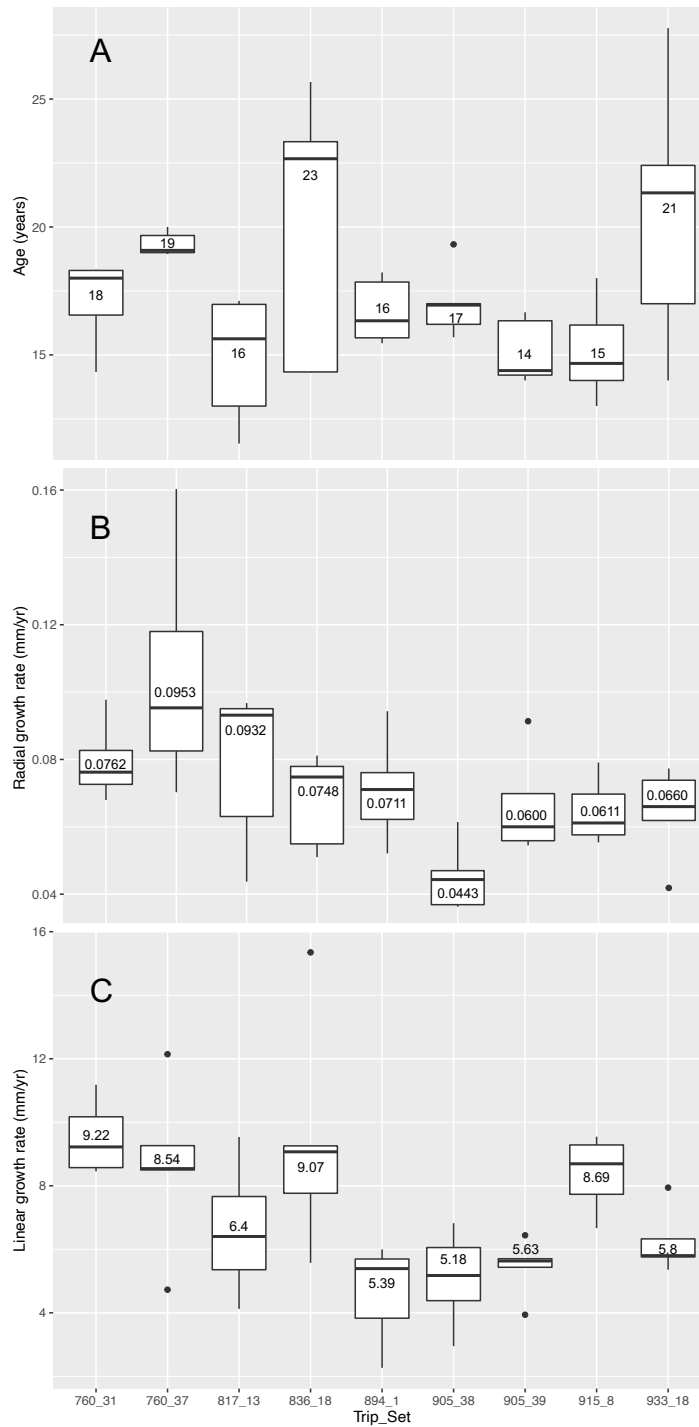
Figure 2-12. *Acanella arbuscula* samples analyzed for intra-location variation, showing the A) age determined from major ring counts and the trip/set, B) radial growth rate and the trip/set, and C) axial growth rate and the trip/set. Numbers on each plot represent the median value of ages or growth rates for each location based on 5 colonies.

2.3.6 Gompertz and logistic growth models

Stem diameter, height, area (height * width), and wet weight were compared with age using Gompertz and logistic growth models to better understand any possible ontogenetic influence observable in the axial and radial growth rates (Fig. 2-13). Gompertz growth curves fit for height versus age of all *A. arbuscula* samples showed a slightly higher R^2 value than when fit to a logarithmic growth curve, and the logistic growth curve fitting increased the R^2 value slightly for these parameters (Fig. 2-14; Table 2-3). Growth rate coefficients indicate 0.084 mm/yr for axial growth in the Gompertz model and 0.121 mm/yr in the logistic model (Table 2-3), which are showing growth rates during the later stages of the organism's life, since we did not analyze any colonies younger than 8 years. We compared these growth rates to average axial growth rates within each NAFO zone, which were 8.81 mm/yr (NAFO zone 0B), 6.06 mm/yr (NAFO zone 2H), and 7.10 mm/yr (NAFO zone 3O) (Table 2-4), and axial growth rate determined from a linear regression was 3.942 mm/yr (Table 2-3). Growth rates reported here prove that sampling a wide age structure is necessary to understand growth rate changes throughout a colonies lifespan.

The Gompertz growth curve for stem diameter and age showed a similar R^2 value with a linear regression, and the logistic function showed the same R^2 value as the Gompertz function (Fig. 2-14; Table 2-3). Comparisons of growth rate coefficients indicate 0.027 mm/yr for the Gompertz function and 0.069 mm/yr for the logistic function, compared to average radial growth rates of 0.081 mm/yr (NAFO zone 0B), 0.065 mm/yr (NAFO zone 2H), and 0.066 mm/yr (NAFO zone 3O). Radial growth rate determined from a linear regression was 0.087 mm/yr (Table 2-3).

Gompertz and logistic growth models for area (height * width) showed improved goodness of fit compared to a linear regression, based on slightly higher R^2 values (Fig. 2-15; Table 2-3). Growth rate coefficients for the Gompertz and logistic functions were 0.1 mm^2/yr and 0.17 mm^2/yr, respectively, compared to a growth rate coefficient of 581.3 mm^2/yr for the linear regression (Table 2-3).

Gompertz and logistic models plotted for wet weight also showed slight improvements in goodness of fit compared to logarithmic regressions (Fig. 2-15; Table 2-3). Growth rate coefficients for the linear regression was 0.6 g/yr, compared to 0.14 g/yr and 0.24 g/yr for the Gompertz and logistic functions, respectively (Table 2-3).
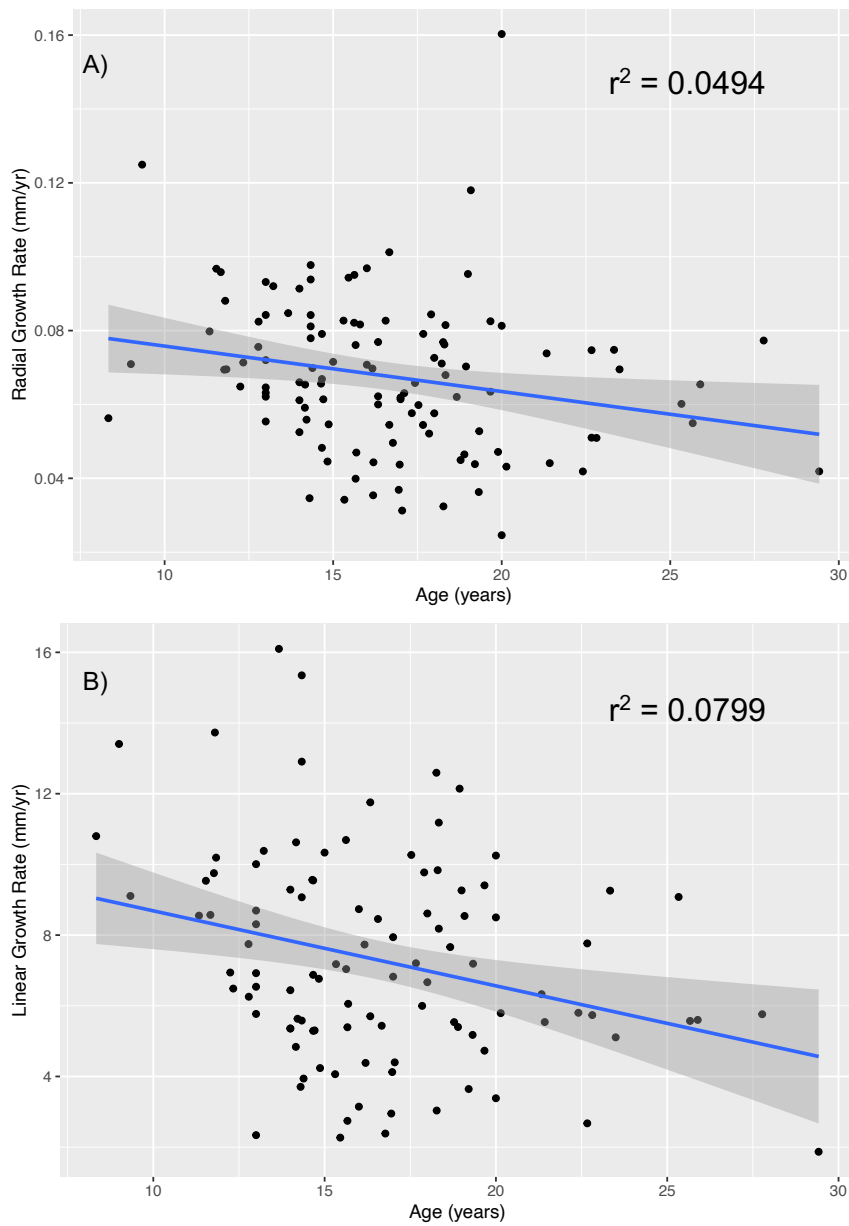
Figure 2-13. Age compared with A) radial growth rate and B) axial growth rate for all *A. arbuscula* colonies. Blue lines indicate linear regression best-fit lines, with the grey shading representing 95% confidence intervals.
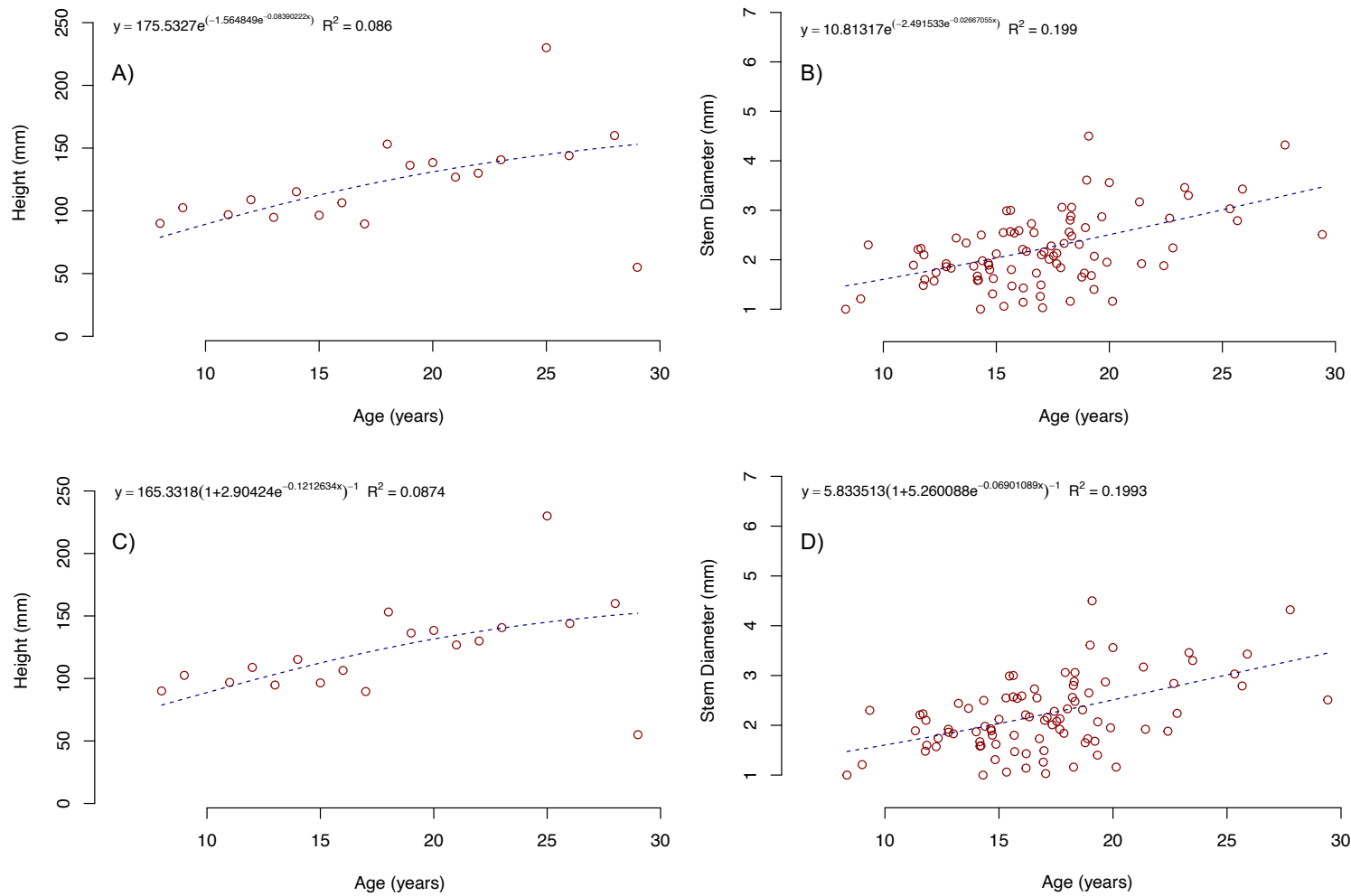
Figure 2-14. Age of all *A. arbuscula* samples, fit with Gompertz growth curves for A) height and B) stem diameter. Data fit to logistic growth curves are also shown for C) height and D) stem diameter.
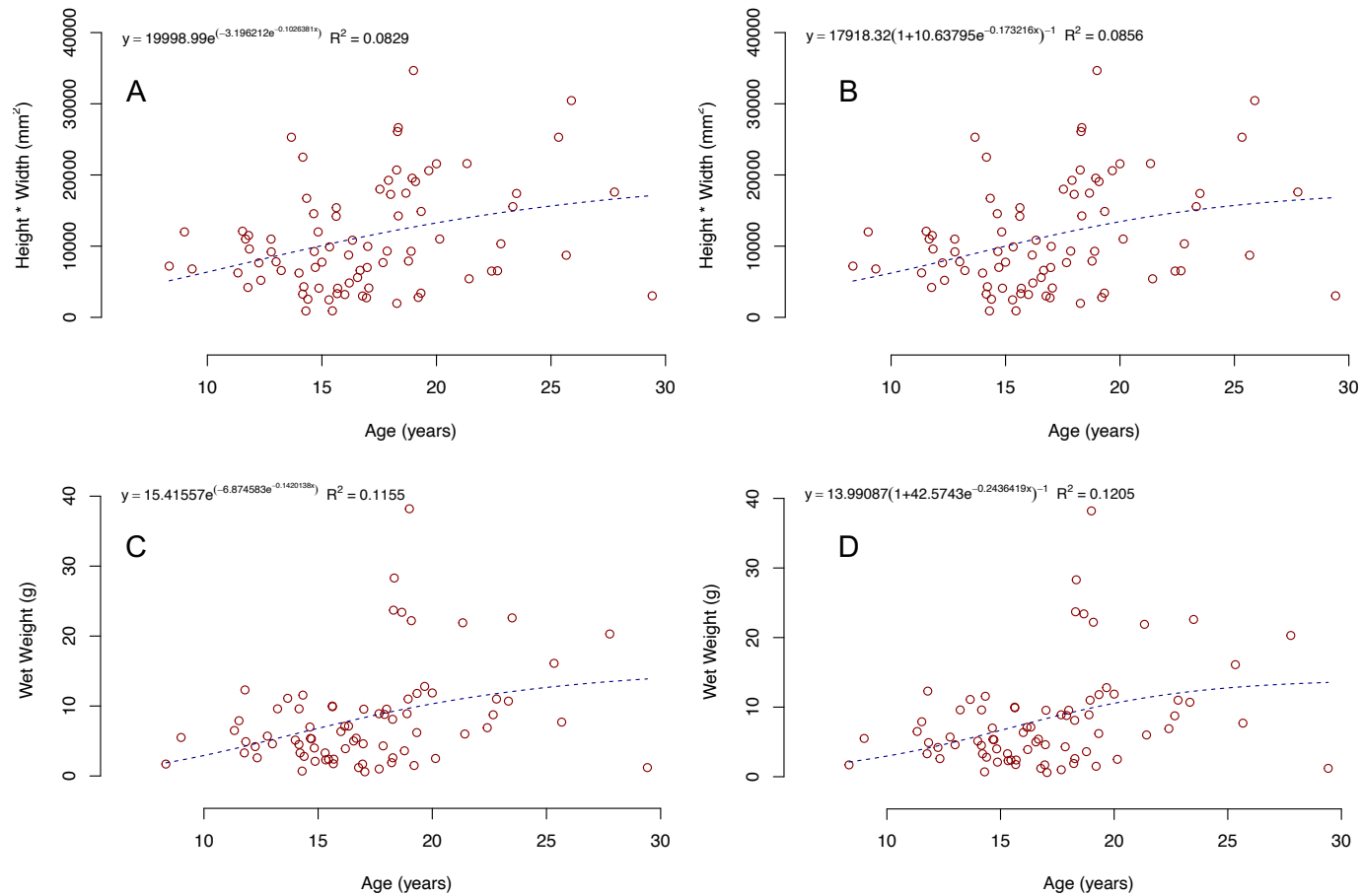
Figure 2-15. Height * width (area) compared to age for all *A. arbuscula* samples in this study with A) a Gompertz regression and B) a logistic regression. Wet weight compared to age for all *A. arbuscula* samples in this study with C) a Gompertz regression and D) a logistic regression.

2.3.7 Chlorophyll-a and phytoplankton bloom (geographic comparisons)

Using custom polygons for NAFO zones 3O and 2H, and the NCLS as an approximate location for NAFO zone 0B, mean daily average chlorophyll concentrations varied significantly by location ($p = 3.44 \times 10^{-6}$), as did median daily average chlorophyll concentrations ($p = 2.21 \times 10^{-5}$) based on 1-way ANOVA analyses (Table 2-7). The calculated mean daily average chlorophyll concentrations were highest in NAFO zone 0B and lowest in NAFO zone 3O, and median daily average chlorophyll concentrations followed the same pattern (Fig. 2-16). Standard deviation was calculated for each day from 1997-2021 and averaged for a mean standard deviation each year of the daily chlorophyll concentrations within each zone. Standard deviation values did not vary significantly based on location determined by an ANOVA test ($p = 0.72$). However, the standard deviations from the satellite SeaWiFS (1997-2002) were consistently higher than standard deviations from the MODIS satellite (2003-2021) (Table 2-8).

Phytoplankton bloom results indicated, on average, longer bloom periods for NAFO zone 3O (94 days), and the shortest bloom periods for NAFO zone 0B (31 days) (Table 2-8). 1-way ANOVA analyses indicated that location was significant regarding the duration of the bloom ($p = 2.09 \times 10^{-15}$) (Table 2-7). The bloom start period was consistently earlier in NAFO zone 3O from 1997-2021, starting on average at Julian day 65. Average bloom start days for NAFO zones 0B and 2H were day 113 and 133 of the year, respectively (Fig. 2-17) (Table 2-8).

Both amplitude and magnitude were significant in 1-way ANOVA tests for location ($p = 0.0136$; 0.0388) (Table 2-7). NAFO zone 0B had the highest average magnitude of

57.6 mg/m^3*days for 1997-2021, with a comparable magnitude determined for NAFO zone

3O of 51.0 mg/m^3*days, while NAFO zone 2H had a much lower average magnitude of

23.8 mg/m^3*days (Fig. 2-16; Table 2-8). Amplitude followed a similar pattern, with the

highest average amplitude for 1997-2021 determined for NAFO zone 0B (4.4 mg/m^3) and

a comparable value for NAFO zone 3O (3.0 mg/m^3). NAFO zone 2H showed the lowest

amplitude value of 1.6 mg/m^3. Some years are missing phytoplankton bloom data,

including 1997 for all locations, as this was the first year that the SeaWiFS satellite was in

use (Clay et al. 2021). Other missing years represent unavailable data, which is most

common for NAFO zone 0B (NCLS) because of its northern location.
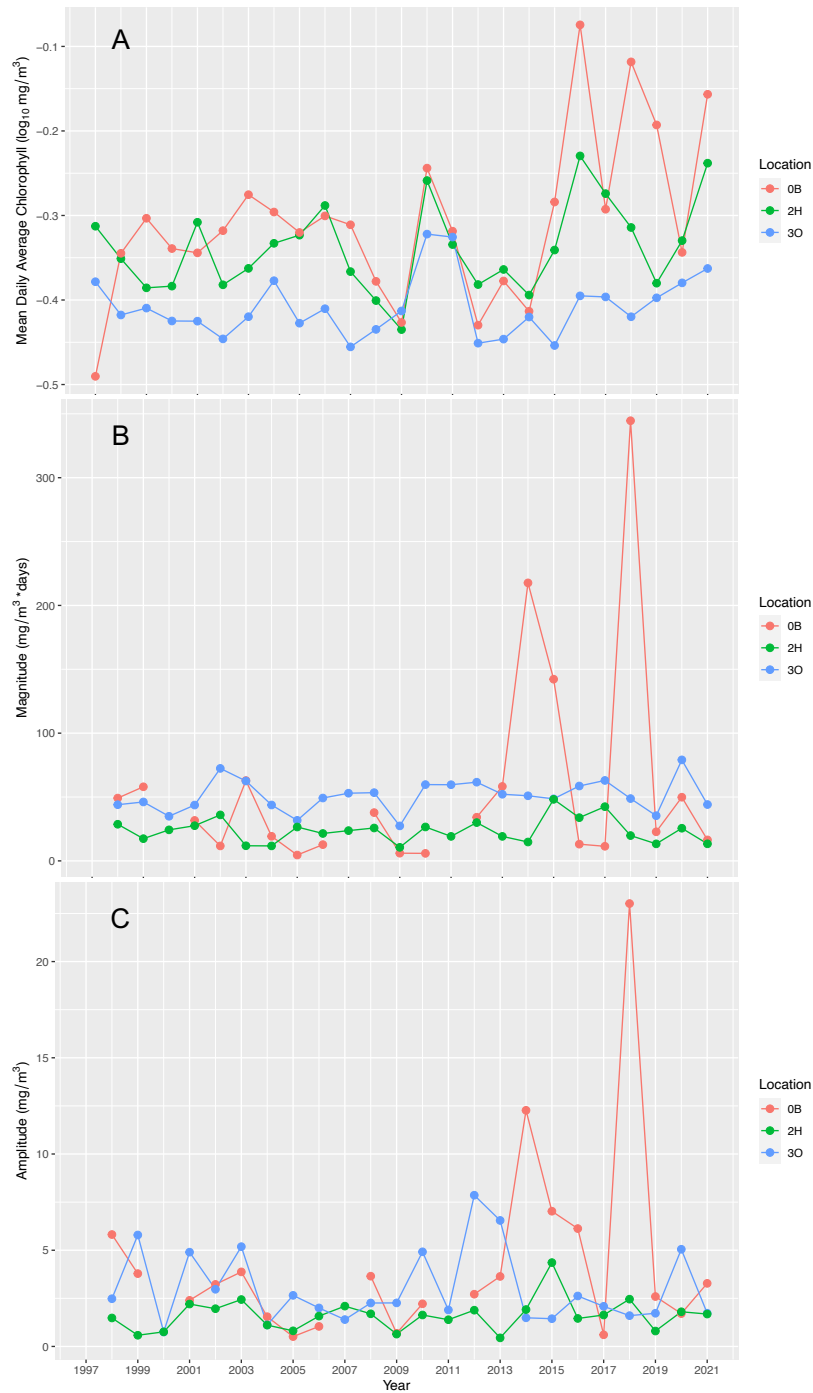
Figure 2-16. A) Mean daily average chlorophyll concentrations, B) median average chlorophyll concentrations, C) phytoplankton bloom magnitude, and D) phytoplankton bloom amplitude for NAFO zones 0B (NCLS), 2H, and 3O from 1997 – 2021. Chlorophyll values for 1997–2002 are from the SeaWiFS satellite and 2003-2021 are from the MODIS satellite (Clay et al. 2021).
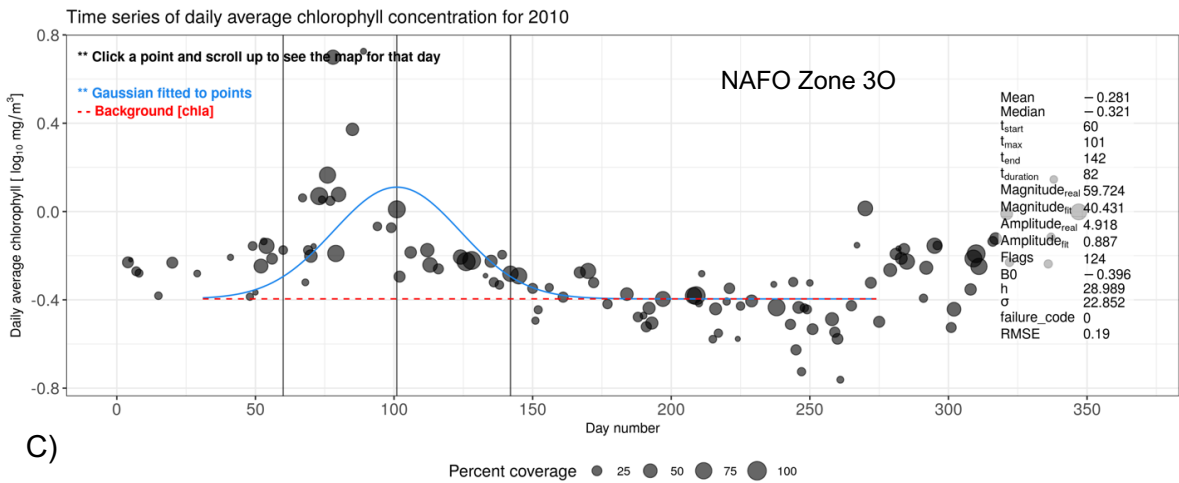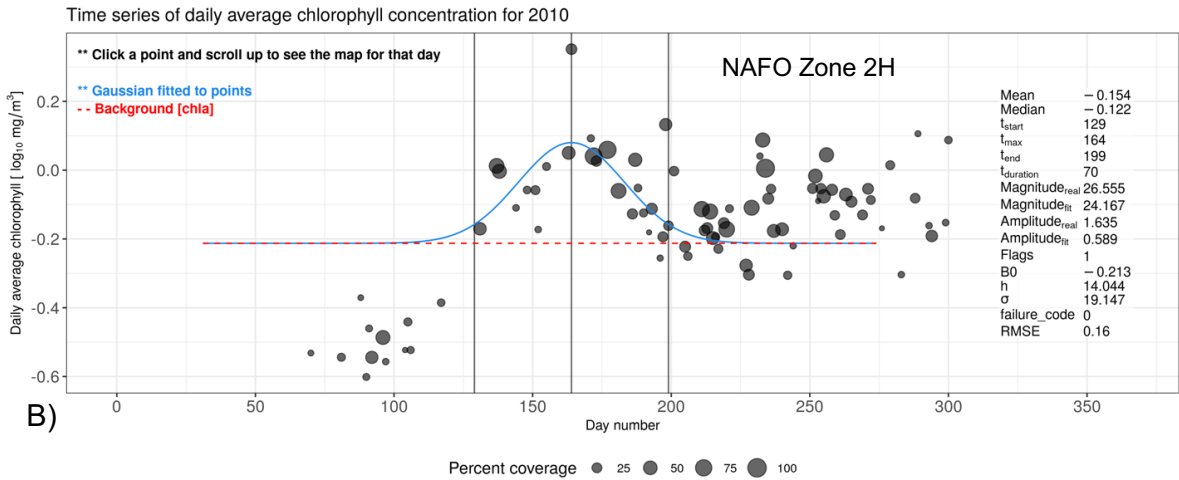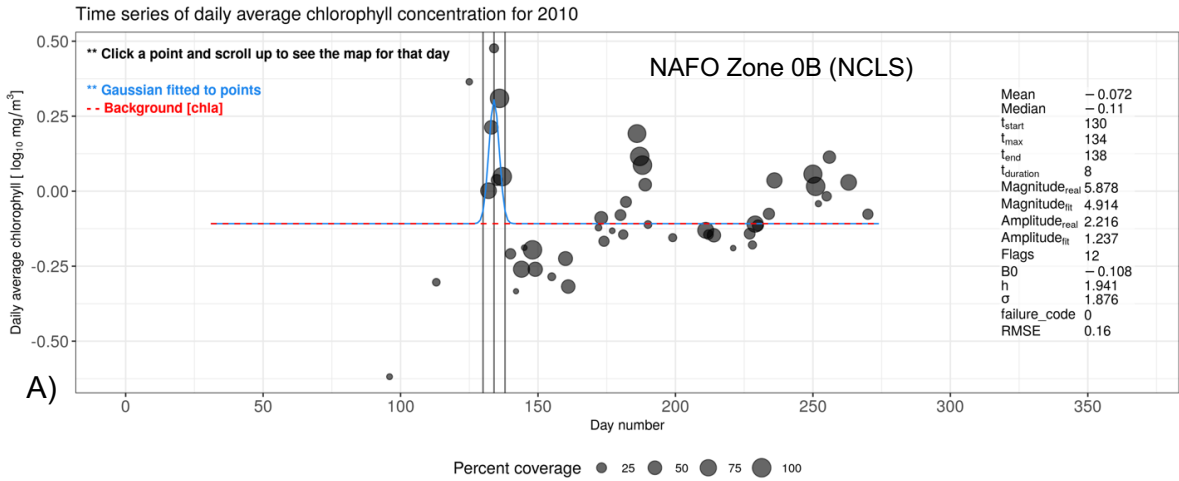
Figure 2-17. Examples of phytoplankton bloom diagrams for A) NAFO zone 0B (NCLS), B) NAFO zone 2H, and C) NAFO zone 3O from 2010 (MODIS Satellite). Black vertical lines indicate bloom start, max, and end (Clay et al. 2021).

2.3.8 Multi-factor data analysis

Multi-factor statistics were used to help understand the drivers of observed geographic and bathymetric variation in growth rates and age. Linear regression models comparing age and radial growth rate for all colonies in the study showed a negative correlation ($R^2 = 0.0494$; $p = 0.017$), and axial growth rate also showed a negative correlation with age ($R^2 = 0.0799$; $p = 0.0037$) (Fig. 2-11).

Multi-factor ANOVA analyses indicated that age for all colonies was strongly related to NAFO zone ($p = 0.00013$) and depth ($p = 0.014$). In terms of environmental variables, age did not show strong relation to bottom temperature ($p = 0.07$), but age was related to mean daily average chlorophyll ($p = 0.0038$), phytoplankton bloom amplitude ($p = 0.017$), phytoplankton bloom magnitude ($p = 0.0027$), and bloom duration ($p = 0.018$) (Table 2-9).

ANOVA analyses for radial growth rate showed that the only variable related was age ($p = 0.034$). No environmental variables included in this study showed strong trends with radial growth rate, such as bottom temperature ($p = 0.41$), depth ($p = 0.13$), mean daily average chlorophyll concentration ($p = 0.07$), bloom amplitude ($p = 0.96$), bloom magnitude ($p = 0.15$), and bloom duration ($p = 0.86$) (Table 2-9).

Axial growth rate showed relation with bloom amplitude ($p = 0.0014$). However, mean daily average chlorophyll was not as strong ($p = 0.17$), along with bloom magnitude ($p = 0.14$), bloom duration ($p = 0.56$), depth ($p = 0.26$), and bottom temperature ($p = 0.37$). Age was related in terms of axial growth rate ($p = 0.0045$), making bloom amplitude and age the only variables showing strong relation to axial growth rate (Table 2-8).

Table 2-3. Regression analyses and growth rate coefficients (major and minor rings; scientific trawl specimens only, 2021 samples, and all samples together).

Size Metric *Scientific trawl samples*	Regression Type & R² value *Major rings*					Growth rate coefficient *Major rings*			Regression Type & R² value *Minor rings*		
	Lin	Log	Exp	Gomp	Logistic	Lin	Gomp	Logistic	Lin	Log	Exp
Height	0.0893	**0.0955**	0.0737	0.1001	0.1019	3.94	0.13	0.17	**0.0459**	0.0439	0.0444
Width	**0.04**	0.0378	0.0229	-	-	-	-	-	0.0175	**0.018**	0.0131
Area	0.09	**0.0938**	0.0558	0.0998	0.1038	660.5	0.15	0.23	0.034	0.0341	**0.0356**
Wet weight	0.0963	**0.1004**	0.0443	0.108	0.1135	0.62	0.17	0.27	0.0084	0.0105	**0.0147**
Stem diameter	**0.1644**	0.1508	0.1371	0.1828	0.1831	0.087	0.01	0.05	0.0599	0.0564	**0.1048**
Stem length	0.0025	**0.0058**	0.0052	-	-	-	-	-	0.0011	**0.0012**	0.0001
Root length	0.0007	0.0006	**0.0013**	-	-	-	-	-	0.0303	0.0329	**0.0339**
2021 ROV samples											
Height	0.0085	**0.0212**	0.0127	-	-	-	-	-	0.0014	0.0015	**0.0017**
Width	0.0698	**0.0765**	0.0709	-	-	-	-	-	0.0251	**0.0286**	0.0263
Area	0.0402	0.0533	**0.0611**	-	-	-	-	-	0.0126	**0.0152**	0.0131
Wet weight	**0.0057**	0.00002	0.0039	-	-	-	-	-	0.0368	0.0316	**0.0708**
Stem diameter	0.00005	**0.0134**	0.001	-	-	-	-	-	**0.0689**	0.0648	0.06
All samples											
Height	0.0814	**0.0821**	0.0595	0.086	0.0874	3.5	0.084	0.121	-	-	-
Width	**0.0284**	0.0249	0.0134	-	-	-	-	-	-	-	-
Area	**0.0785**	0.0776	0.0403	0.0829	0.0856	581.3	0.1	0.17	-	-	-
Wet weight	0.1068	**0.1078**	0.0504	0.1155	0.1205	0.6	0.14	0.24	-	-	-
Stem diameter	**0.1983**	0.1884	0.1793	0.199	0.199	0.09	0.027	0.069	-	-	-

Notes: Lin = linear regression, Log = logarithmic regression, Exp = exponential regression, Gomp = Gompertz growth model. Bolded R^2 values represent best fit regression for each size metric when comparing linear, logarithmic, or exponential regressions.

Table 2-4. Results for *Acanella arbuscula* colonies collected in DFO trawl surveys.

Trip	Set	Subsample No.	NAFO Zone	Depth	BTemp	Diameter	Major Rings (± SE)	Minor Rings (± SE)	Minor/ Major	Age	R Growth Rate	A Growth Rate	Q
7	177	1	0B	686	2.68	2.12	15 ± 2.5	89 ± 3.8	6	15	0.072	10.33	3
7	177	2	0B	686	2.68	2.01	17 ± 1.3	64 ± 4.7	4	17	0.058		3
7	22	1	0B	729	3.9	2.30	9 ± 0.7	96 ± 3.2	10	9	0.125	9.11	2
8	150	1	0B	481	2.67	2.21	13 ± 0.6	107 ± 3.0	8	13	0.084	2.34	2
8	150	2	0B	481	2.67	2.23	16 ± 1.0	128 ± 1.8	8	16	0.071	3.15	3
8	150	3	0B	481	2.67	3.36	23 ± 1.2	123 ± 4.0	5	23	0.075	2.67	2
270	9	1	0B	841		1.74	12 ± 0.9	89 ± 3.3	7	12	0.071	6.49	3
270	86	1	0B	1060		2.65	14 ± 2.3	92 ± 2.0	6	14	0.094	12.91	1
8	96	1	0B	447	1.26	2.28	16 ± 1.5	91 ± 4.5	6	17	0.066		1
8	153	1	0B	467	2.68	2.54	15 ± 1.2	102 ± 4.4	7	16	0.082		3
8	118	1	0B	848	3.65	3.30	17 ± 1.2	126 ± 9.3	8	17	0.101		3
8	118	2	0B	848	3.65	3.28	20 ± 2.5	96 ± 4.3	5	20	0.081	10.25	1
8	118	3	0B	848	3.65	1.93	14 ± 0.9	82 ± 4.7	6	15	0.066	9.56	2
8	118	4	0B	848	3.65	2.13	16 ± 1.2	109 ± 8.6	7	18	0.079		2
101	124	1	0B	511	3.14	2.34	14 ± 0.9	112 ± 6.5	8	14	0.085	16.10	2
101	124	2	0B	511	3.14	1.92	12 ± 0.6	90 ± 3.8	7	13	0.076	7.75	3
103	117	1	0B	585	3.11	2.44	12 ± 0.9	108 ± 2.8	9	13	0.092	10.38	1
103	117	2	0B	585	3.11	2.10	10 ± 0.9	91 ± 2.0	9	12	0.088	13.73	1
103	117	3	0B	585	3.11	1.89	11 ± 1.2	101 ± 6.9	9	11	0.080	8.55	3
			0B							**15**	**0.081**	**8.81**	
119	13	1	2H	178	1.1	3.06	16 ± 0.7	98 ± 6.4	6	18	0.084	9.77	1
975	6	1	2H	181	1.5	2.55	12 ± 0.3	75 ± 1.9	6	15	0.083	4.06	2
975	36	1	2H	243	2.1	2.51	24 ± 0.3	114 ± 1.5	5	29	0.042	1.87	0
975	33	1	2H	1312	3.9	1.73	14 ± 0.9	78 ± 8.1	5	17	0.050	2.38	2
817	13	1	2H	252	0.9	3.00	9 ± 1.7	87 ± 8.2	10	16	0.095	7.04	0
817	13	2	2H	252	0.9	2.21	11 ± 0.9	108 ± 4.8	10	12	0.097	9.54	1
817	13	3	2H	252	0.9	2.35	13 ± 0	99 ± 0.9	8	13	0.093	5.77	2

817	13	4	2H	252	0.9	2.16	16 ± 1.7	85 ± 3.4	5	17	0.063		1
817	13	5	2H	252	0.9	1.49	14 ± 0.6	77 ± 6.5	6	17	0.044	4.12	1
817	12	1	2H	1042	4	1.57	10 ± 0.3	100 ± 2.4	10	12	0.065	6.94	1
817	12	2	2H	1042	4	1.64	13 ± 0.6	109 ± 5.2	8	13	0.063	6.54	2
817	12	3	2H	1042	4	1.86	13 ± 0.6	104 ± 4.9	8	13	0.072	6.92	1
817	29	2	2H	413	4.8	2.57	11 ± 0.9	122 ± 1.2	11	16	0.082	10.69	2
817	20	1	2H	1274	3.8	1.80	14 ± 1.5	94 ± 1.8	7	15	0.061	5.30	2
680	10	1	2H	1052	4.1	2.49	14 ± 0.9	118 ± 5.0	8	14	0.084	5.58	3
679	17	1	2H	471	3.3	1.16	15 ± 2.0	74 ± 1.5	5	18	0.032	3.04	1
679	17	3	2H	471	3.3	1.67	12 ± 0.9	92 ± 0.9	7	14	0.059	4.84	2
190	11	1	2H	179	1.4	3.43	14 ± 0	74 ± 4.6	5	26	0.065	5.60	0
190	11	2	2H	179	1.4	1.48	14 ± 0.6	82 ± 11.7	6	14	0.053	5.36	1
190	11	3	2H	179	1.4	1.95	15 ± 2.2	111 ± 4.1	7	20	0.047		2
163	1	1	2H	1354	3.6	3.06	16 ± 0.7	44 ± 1.5	3	18	0.082	8.18	0
163	18	1	2H	1284	3.7	1.86	13 ± 1.5	91 ± 6.6	7	13	0.082	6.26	0
163	19	1	2H	1321	3.6	2.24	12 ± 0.3	110 ± 6.1	9	12	0.096	8.57	3
120	12	1	2H	523	4.6	1.14	15 ± 3.1	67 ± 2.6	4	16	0.035		1
106	7	1	2H	867		1.70	13 ± 0.0	149 ± 4.8	11	13	0.065	8.31	2
95	19	1	2H	960	4.2	0.99	20 ± 1.2	111 ± 7.6	6	20	0.025	3.38	1
95	19	2	2H	960	4.2	1.73	17 ± 0.6	89 ± 6.2	5	19	0.047	5.40	3
			2H							**16**	**0.065**	**6.06**	
943	20	1	3O	624	4.2	2.50	20 ± 0.9	121 ± 5.2	6	20	0.064	9.41	2
943	27	1	3O	667	4.1	1.62	13 ± 0.0	122 ± 4.8	9	15	0.055	4.24	1
943	27	2	3O	667	4.1	2.07	19 ± 1.9	111 ± 11.4	6	19	0.053	7.19	2
943	27	3	3O	667	4.1	1.65	16 ± 0.9	93 ± 0.7	6	19	0.045	5.54	2
933	18	1	3O	604	4.4	3.17	21 ± 1.2	129 ± 3.3	6	21	0.074	6.33	1
933	18	2	3O	604	4.4	4.32	22 ± 1.9	60 ± 2.7	3	28	0.077	5.76	0
933	18	3	3O	604	4.4	2.10	17 ± 0.6	96 ± 2.9	6	17	0.062	7.94	3
933	18	4	3O	604	4.4	1.88	14 ± 2.2	78 ± 1.2	5	22	0.042	5.80	2
933	18	5	3O	604	4.4	1.85	14 ± 0.6	76 ± 1.5	5	14	0.066	5.36	1

932	67	1	3O	582	4.7	2.31	19 ± 1.3	140 ± 5.1	8	19	0.062	7.66	2
915	8	1	3O	647	4	2.21	14 ± 1.2	87 ± 1.7	6	16	0.070	7.73	1
915	8	2	3O	647	4	2.33	15 ± 0.9	87 ± 3.0	6	15	0.079	9.55	1
915	8	3	3O	647	4	2.06	18 ± 2.0	104 ± 0.9	6	18	0.058	6.67	1
915	8	4	3O	647	4	1.70	14 ± 1.0	108 ± 4.9	8	14	0.061	9.29	2
915	8	5	3O	647	4	1.44	13 ± 1.2	73 ± 4.3	6	13	0.055	8.69	0
905	23	1	3O	337	7.4	2.80	16 ± 0.6	105 ± 3.2	7	18	0.077	12.59	2
905	23	2	3O	337	7.4	3.03	25 ± 0.9	122 ± 4.3	5	25	0.060	9.08	3
905	39	1	3O	596	4.8	1.59	11 ± 0.3	94 ± 4.1	9	14	0.056	5.63	1
905	39	2	3O	596	4.8	2.44	14 ± 2.1	82 ± 3.7	6	14	0.091	6.44	0
905	39	3	3O	596	4.8	1.80	17 ± 0.7	121 ± 4.8	7	17	0.055	5.43	3
905	39	4	3O	596	4.8	1.96	16 ± 0.9	91 ± 7.3	6	16	0.060	5.70	1
905	39	5	3O	596	4.8	1.98	12 ± 0.9	64 ± 5.2	6	14	0.070	3.94	0
905	38	1	3O	598	5.1	1.26	11 ± 1.2	73 ± 2.2	6	17	0.037	2.95	2
905	38	2	3O	598	5.1	1.40	18 ± 0.9	80 ± 4.3	5	19	0.036	5.18	2
905	38	3	3O	598	5.1	2.10	17 ± 0.6	99 ± 3.4	6	17	0.061	6.82	1
905	38	4	3O	598	5.1	1.47	15 ± 1.2	88 ± 1.5	6	16	0.047	6.06	1
905	38	5	3O	598	5.1	1.43	12 ± 1.5	67 ± 12.6	6	16	0.044	4.38	1
894	1	1	3O	768	4.3	1.84	15 ± 0.3	84 ± 1.5	5	18	0.052	6.00	2
894	1	2	3O	768	4.3	2.56	14 ± 1.0	109 ± 3.0	8	18	0.071		3
894	1	3	3O	768	4.3	2.02	16 ± 0.3	117 ± 2.6	7	16	0.062		3
894	1	4	3O	768	4.3	2.99	14 ± 0.7	99 ± 4.7	7	15	0.094	2.27	1
894	1	5	3O	768	4.3	2.34	16 ± 1.7	135 ± 12.2	9	16	0.076	5.39	1
894	9	1	3O	887	4.2	3.30	22 ± 1.0	124 ± 4.7	6	23	0.070	5.11	0
894	10	1	3O	1020	4.2	1.94	15 ± 1.3	67 ± 4.0	5	15	0.067	5.29	1
836	18	1	3O	573	4.5	2.32	23 ± 1.2	118 ± 5.8	5	23	0.051	7.76	3
836	18	2	3O	573	4.5	2.32	14 ± 2.7	107 ± 3.2	7	14	0.081	15.35	2
836	18	3	3O	573	4.5	3.46	23 ± 0.7	117 ± 5.0	5	23	0.075	9.26	3
836	18	4	3O	573	4.5	2.22	14 ± 0.7	71 ± 6.1	5	14	0.078	9.07	1
836	18	5	3O	573	4.5	2.79	26 ± 0.7	118 ± 6.4	5	26	0.055	5.57	3

760	37	1	3O	600	4.3	4.50	18 ± 1.5	86 ± 0.3	5	19	0.118	8.54	0
760	37	2	3O	600	4.3	6.43	20 ± 3.5	98 ± 7.5	5	20	0.160	8.50	0
760	37	3	3O	600	4.3	2.65	17 ± 2.0	100 ± 4.2	6	19	0.070	12.14	2
760	37	4	3O	600	4.3	3.24	20 ± 3.8	138 ± 1.5	7	20	0.083	4.73	2
760	37	5	3O	600	4.3	3.61	13 ± 1.2	86 ± 3.5	6	19	0.095	9.26	0
760	31	1	3O	719	4.3	2.59	18 ± 1.2	114 ± 2.3	6	18	0.073	8.61	3
760	31	2	3O	719	4.3	2.73	14 ± 0.9	120 ± 3.4	9	17	0.083	8.46	3
760	31	3	3O	719	4.3	2.48	18 ± 0.9	90 ± 3.6	5	18	0.068	11.18	2
760	31	4	3O	719	4.3	2.82	14 ± 0.9	131 ± 3.5	9	14	0.098		2
760	31	5	3O	719	4.3	2.88	15 ± 0.9	105 ± 6.9	7	18	0.076	9.84	3
750	23	1	3O	1153	3.9	1.00	13 ± 1.5	62 ± 3.8	5	14	0.035	3.71	1
750	23	2	3O	1153	3.9	1.68	15 ± 1.9	81 ± 5.0	6	19	0.044	3.64	1
750	23	3	3O	1153	3.9	1.25	16 ± 0.9	82 ± 8.5	5	16	0.040	2.74	1
750	23	4	3O	1153	3.9	1.03	15 ± 1.5	57 ± 7.9	4	17	0.031	4.40	1
479	18	1	3O	702	4.6	2.52	16 ± 1.8	147 ± 2.5	9	16	0.077	11.76	3
460	13	1	3O	224	8.5	2.08	12 ± 0.3	97 ± 5.0	8	18	0.060	10.27	2
460	16	1	3O	574	4.5	2.95	16 ± 1.0	132 ± 3.8	8	16	0.097	8.73	0
460	16	2	3O	574	4.5	2.24	16 ± 0.7	79 ± 3.3	5	23	0.051	5.74	1
460	16	3	3O	574	4.5	1.92	18 ± 0.9	97 ± 4.0	5	18	0.055	7.20	3
460	16	4	3O	574	4.5	1.92	16 ± 0.9	79 ± 1.9	5	21	0.044	5.54	2
			3O							**18**	**0.066**	**7.1**	

Notes and units: NAFO (North Atlantic Fisheries Organization), Depth - m, BTemp (Bottom temperature) - °C, Diameter – mm, SE (standard error), Age (major ring growth rate / radius) – years, R growth rate (radial growth rate) – mm/yr based on major rings, A growth rate (axial growth rate) – mm/yr, Q (quality assessment) – scale 0-3. Blank values indicate unavailable information. Bolded values represent the mean ages and growth rates for each NAFO zone.

Table 2-5. Results for *Acanella arbuscula* samples collected in 2021 at Davis Strait.

Sample	Subsample No.	NAFO Zone	Depth	Diameter	Major Rings (± SE)	Minor Rings (± SE)	Minor/ Major	Age	R Growth Rate	A Growth Rate
R21-8	b2	0B	1314	0.995	8 ± 1.9	81 ± 5.2	10	8	0.056	10.80
R21-9	a	0B	1314	1.008	15 ± 4.0	125 ± 28.8	8	15	0.034	7.33
R21-9	b	0B	1314	1.104	16 ± 1.9	81 ± 14.8	5	16	0.035	7.02
R21-10	b	0B	1314	1.288	16 ± 4.1	100 ± 7.2	6	16	0.041	6.38
R21-10	c	0B	1314	1.332	14 ± 1.5	71 ± 5.0	5	14	0.048	7.14
R21-15	a	0B	1299	1.189	8 ± 1.2	63 ± 2.9	8	8	0.078	14.40
R21-15	b	0B	1299	1.226	10 ± 1.9	81 ± 3.5	8	10	0.064	12.41
R21-16	a	0B	1299	1.627	13 ± 0.3	70 ± 5.0	6	13	0.064	10.26
R21-16	b	0B	1299	1.601	13 ± 2.4	95 ± 9.0	7	13	0.060	9.75
R21-17	a	0B	1298	1.414	8 ± 0.9	86 ± 7.3	10	8	0.085	12.60
R21-17	b	0B	1298	1.55	8 ± 0.3	46 ± 6.7	6	15	0.053	6.91
R21-20	a	0B	1297	1.23	16 ± 3.5	85 ± 5.9	5	16	0.038	6.25
R21-20	b	0B	1297	1.55	13 ± 1.8	126 ± 12.4	9	13	0.059	7.50
R21-21	a	0B	1297	1.19	20 ± 4.2	115 ± 10.3	6	25	0.034	4.41
R21-21	b	0B	1297	1.138	15 ± 0.9	102 ± 9.2	7	15	0.053	7.17
R21-23	a	0B	1297	1.374	13 ± 0.9	47 ± 3.5	4	13	0.054	9.47
R21-23	b	0B	1297	1.832	11 ± 0.6	92 ± 11.3	8	11	0.085	10.91
R21-25	a	0B	1299	1.664	9 ± 0.9	73 ± 2.5	8	15	0.056	10.00
R21-25	b	0B	1299	1.501	13 ± 2.6	72 ± 4.7	5	13	0.075	11.25

Notes and units: Colonies with 2 sub-samples were averaged for major/minor rings, diameter, age, radial growth rate, and axial growth rate. This applied to all samples except R21-8_b2. NAFO (North Atlantic Fisheries Organization). Depth – m. Diameter – mm. SE (standard error). Age – years. R growth rate (radial growth rate) – mm/year. A growth rate (axial growth rate) – mm/yr. Both radial and axial growth rates are based on major rings and sample radius or height.

Table 2-6. *Acanella arbuscula* samples used for intra-location variation analyses in size metrics and growth rates/age compared to NAFO zone age and growth rate variations.

TripSet	NAFO Zone	Year	Depth	BTemp	Min Rgrowth Rate	Max Rgrowth Rate	Min Agrowth Rate	Max Agrowth Rate	Min Age	Max Age
817_13	2H	2008	252	0.9	0.044	0.097	4.12	9.54	12	17
760_31	3O	2007	719	4.3	0.068	0.098	8.46	11.18	14	18
760_37	3O	2007	600	4.3	0.070	0.160	4.73	12.14	19	20
836_18	3O	2008	573	4.5	0.051	0.081	5.57	15.35	14	26
894_1	3O	2009	768	4.3	0.052	0.094	2.27	6.00	15	18
905_38	3O	2009	598	5.1	0.036	0.061	2.95	6.82	16	19
905_39	3O	2009	596	4.8	0.055	0.091	3.94	6.44	14	17
915_8	3O	2009	647	4	0.055	0.079	6.67	9.55	13	18
933_18	3O	2010	604	4.4	0.042	0.077	5.36	7.94	14	28
-	**0B**	-	-	-	**0.058**	**0.125**	**2.34**	**16.1**	**9**	**23**
-	**2H**	-	-	-	**0.025**	**0.097**	**1.87**	**10.69**	**12**	**29**
-	**3O**	-	-	-	**0.031**	**0.160**	**2.27**	**15.35**	**13**	**28**

Notes and units: NAFO (North Atlantic Fisheries Organization), Depth - m, BTemp (Bottom temperature) - °C, Min and Max R growth rate (minimum and maximum radial growth rate) – mm/yr based on major rings, Min and Max A growth rate (minimum and maximum axial growth rate) – mm/yr, Min and Max Age (minimum and maximum age) – years. Age and growth rate ranges for all samples within each NAFO zone are indicated in the bottom rows in bold.

Table 2-7. Results of one-way ANOVA tests for chlorophyll and bloom measurements with NAFO zones as the explanatory variable.

Measurement	p-value	f-value
Mean daily avg. chl ($\log_{10}$ mg/m^3)	3.44×10^{-6}	15.06
Median daily avg. chl ($\log_{10}$ mg/m^3)	2.21×10^{-5}	12.49
Bloom magnitude (mg/m^3 * days)	0.039	3.41
Bloom amplitude (mg/m^3)	0.014	4.59
Bloom duration (days)	2.09×10^{-15}	58.91

Table 2-8. Chlorophyll and phytoplankton bloom data from 1997-2021 for NAFO zones 3O, 2H, and 0B (NCLS).

Location	Year	Mean Chl	Median Chl	SD Chl	Bloom Start	Bloom Max	Bloom End	Bloom Duration	Magnitude	Amplitude
3O	1997	-0.3784	-0.3748	0.1994						
3O	1998	-0.4177	-0.4190	0.1861	69	112	155	86	43.9834	2.4799
3O	1999	-0.4096	-0.4173	0.2067	60	102	144	84	46.1244	5.7920
3O	2000	-0.4248	-0.4198	0.1888	60	109	158	98	34.9271	0.7515
3O	2001	-0.4250	-0.4214	0.1830	60	110	160	100	43.7136	4.8994
3O	2002	-0.4460	-0.4562	0.2034	60	114	168	108	72.4035	2.9711
3O	2003	-0.4198	-0.4238	0.1350	92	121	150	58	62.5369	5.1854
3O	2004	-0.3772	-0.3791	0.1362	72	131	190	118	43.7628	1.1187
3O	2005	-0.4274	-0.4210	0.1332	75	106	137	62	31.7436	2.6547
3O	2006	-0.4103	-0.4062	0.1272	62	117	172	110	49.2129	2.0014
3O	2007	-0.4554	-0.4569	0.1189	60	116	172	112	52.9870	1.3961
3O	2008	-0.4348	-0.4371	0.1201	60	111	162	102	53.4127	2.2573
3O	2009	-0.4130	-0.4149	0.1386	60	91	122	62	27.3889	2.2628
3O	2010	-0.3220	-0.3176	0.1493	60	101	142	82	59.7235	4.9176
3O	2011	-0.3255	-0.3279	0.1455	60	103	146	86	59.6287	1.8963
3O	2012	-0.4511	-0.4448	0.1391	68	105	142	74	61.6059	7.8591

3O	2013	-0.4463	-0.4458	0.1358	70	108	146	76	52.1648	6.5482
3O	2014	-0.4201	-0.4227	0.1405	77	132	187	110	50.9712	1.4889
3O	2015	-0.4538	-0.4515	0.1308	60	129	198	138	48.5849	1.4423
3O	2016	-0.3951	-0.3926	0.1477	60	117	174	114	58.6204	2.6232
3O	2017	-0.3964	-0.3909	0.1250	60	115	170	110	62.9770	2.0853
3O	2018	-0.4198	-0.4199	0.1364	60	115	170	110	48.7872	1.6006
3O	2019	-0.3974	-0.4033	0.1312	60	92	124	64	35.3708	1.7245
3O	2020	-0.3797	-0.3788	0.1498	73	120	167	94	79.0787	5.0500
3O	2021	-0.3627	-0.3625	0.1349	60	110	160	100	44.1083	1.7275
2H	1997	-0.3127	-0.3426	0.2253						
2H	1998	-0.3511	-0.3705	0.2123	129	159	189	60	28.6764	1.4800
2H	1999	-0.3856	-0.3996	0.1946	139	174	209	70	17.3994	0.5817
2H	2000	-0.3836	-0.4026	0.1992	148	176	204	56	24.2916	0.7582
2H	2001	-0.3080	-0.3247	0.2184	139	153	167	28	27.5425	2.2044
2H	2002	-0.3820	-0.3963	0.1968	151	181	211	60	35.9976	1.9614
2H	2003	-0.3626	-0.3747	0.1275	131	142	153	22	11.8330	2.4369
2H	2004	-0.3329	-0.3379	0.1262	148	158	168	20	11.7251	1.1091
2H	2005	-0.3233	-0.3311	0.1391	122	153	184	62	26.5149	0.8121
2H	2006	-0.2882	-0.3054	0.1562	111	141	171	60	21.4516	1.5771
2H	2007	-0.3664	-0.3700	0.1207	151	166	181	30	23.6976	2.0952
2H	2008	-0.4007	-0.4097	0.1138	104	136	168	64	25.7476	1.6965
2H	2009	-0.4350	-0.4437	0.1259	139	170	201	62	10.6012	0.6413
2H	2010	-0.2587	-0.2658	0.1283	129	164	199	70	26.5550	1.6349
2H	2011	-0.3344	-0.3421	0.1343	137	159	181	44	19.1735	1.3894
2H	2012	-0.3817	-0.3875	0.1204	119	147	175	56	29.9863	1.8842
2H	2013	-0.3639	-0.3732	0.1281	101	159	217	116	19.1704	0.4462
2H	2014	-0.3942	-0.3940	0.1167	134	145	156	22	14.7785	1.9168

2H	2015	-0.3409	-0.3552	0.1375	124	150	176	52	48.1809	4.3573
2H	2016	-0.2295	-0.2345	0.1436	151	177	203	52	33.8358	1.4552
2H	2017	-0.2742	-0.2879	0.1596	130	164	198	68	42.4387	1.6339
2H	2018	-0.3142	-0.3218	0.1393	149	169	189	40	19.8234	2.4574
2H	2019	-0.3801	-0.3859	0.1118	137	150	163	26	13.3330	0.8010
2H	2020	-0.3297	-0.3423	0.1376	138	166	194	56	25.5559	1.8021
2H	2021	-0.2381	-0.2496	0.1541	124	140	156	32	13.3582	1.6835
0B	1997	-0.4903	-0.4826	0.2080						
0B	1998	-0.3448	-0.3544	0.2079	95	118	141	46	49.1666	5.8153
0B	1999	-0.3033	-0.3181	0.2022	107	128	149	42	58.0091	3.7854
0B	2000	-0.3391	-0.3468	0.2055						
0B	2001	-0.3442	-0.3591	0.2109	111	131	151	40	31.6625	2.3963
0B	2002	-0.3180	-0.3310	0.2069	113	117	121	8	11.7049	3.2245
0B	2003	-0.2754	-0.2869	0.1147	112	131	150	38	62.8750	3.8742
0B	2004	-0.2959	-0.2964	0.1256	119	132	145	26	19.2551	1.5459
0B	2005	-0.3201	-0.3247	0.0953	109	118	127	18	4.5738	0.5119
0B	2006	-0.3005	-0.3068	0.1312	101	111	121	20	12.7219	1.0409
0B	2007	-0.3110	-0.3109	0.1231						
0B	2008	-0.3779	-0.3839	0.1167	115	139	163	48	37.7904	3.6513
0B	2009	-0.4266	-0.4395	0.1114	133	139	145	12	6.0234	0.6853
0B	2010	-0.2440	-0.2544	0.1386	130	134	138	8	5.8780	2.2158
0B	2011	-0.3186	-0.3254	0.1217						
0B	2012	-0.4298	-0.4369	0.1027	91	124	157	66	34.1835	2.7156
0B	2013	-0.3775	-0.3858	0.1108	119	135	151	32	58.2819	3.6380
0B	2014	-0.4133	-0.4220	0.1136	104	124	144	40	217.6518	12.2706
0B	2015	-0.2840	-0.2920	0.1142	111	137	163	52	142.2466	7.0273
0B	2016	-0.0745	-0.0774	0.1524	125	127	129	4	13.0857	6.1251

0B	2017	-0.2926	-0.3015	0.1177	125	141	157	32	11.4174	0.6064
0B	2018	-0.1183	-0.1172	0.1516	91	112	133	42	344.6072	23.0146
0B	2019	-0.1929	-0.2014	0.1559	124	134	144	20	22.7750	2.5933
0B	2020	-0.3437	-0.3550	0.1024	121	144	167	46	49.8433	1.7070
0B	2021	-0.1566	-0.1562	0.1422	121	125	129	8	16.4123	3.2787

Notes & units: Chl = chlorophyll. SD = standard deviation. Bloom start, max, end, and duration in days out of 365. Mean, median, and standard deviation of chlorophyll units = $\log_{10}$ mg/m^3. Magnitude of bloom units = mg/m^3 * days. Amplitude of bloom units = mg/m^3. Missing data cells represents unavailable data.

Table 2-9. Multi-factor geographic and bathymetric ANOVA tests for age, radial, and axial growth rate.

Variable	Age			R Growth Rate			A Growth Rate		
	p-value	f-value	d.f	p-value	f-value	d.f	p-value	f-value	d.f
Age (years)	-	-	-	**0.034**	9.08	1	**0.0045**	8.45	1
NAFO zone (location)	**0.0002**	7.16	3	**0.007**	4.25	3	**0.0056**	4.45	3
Depth (m)	**0.014**	6.24	1	0.13	2.31	1	0.26	1.46	1
BTemp (°C)	0.07	3.37	1	0.41	0.67	1	0.37	0.82	1
Mean daily avg. chl ($\log_{10}$ mg/m^3)	**0.0038**	8.76	1	0.07	3.29	1	0.17	1.89	1
Bloom magnitude (mg/m^3 * days)	**0.0027**	9.42	1	0.15	2.06	1	0.14	2.24	1
Bloom amplitude (mg/m^3)	**0.017**	5.89	1	0.96	0.0027	1	**0.0014**	10.81	1
Bloom duration (days)	**0.018**	5.8	1	0.86	0.03	1	0.56	0.34	1

Notes & units: D.f = degrees of freedom, chl = chlorophyll. R Growth Rate = radial growth rate (mm/yr) and A Growth Rate = axial growth rate (mm/yr). Bold values are p-values <0.05.

2.4 DISCUSSION

2.4.1 Growth ring characteristics

A. arbuscula is a particularly understudied bamboo coral species, likely due to its small size, which made applying sclerochronology techniques to the species difficult. Fluorescence microscopy increased growth ring clarity substantially, and was the only technique that assisted with growth ring visualization. Some observed characteristics at the proteinaceous nodes included calcite overgrowth on the outside of protein material, and growth ring expansion or inconsistent spacing between growth rings, which may have resulted from sample preparation techniques or hygroscopic proteinaceous layers. Due to the large sample size in this study, growth rate and age estimates are indicative of the likely longevity and growth speed for this cosmopolitan species, which is of utmost importance for implementation of proper conservation measures wherever the species is located.

2.4.2 Annual periodicity of major growth rings

Previous studies have recorded annual growth banding in gorgonian corals in Eastern Canadian waters, such as the large gorgonian coral *Primnoa resedaeformis* (Risk et al. 2002; Sherwood et al. 2005), the bamboo coral *Keratoisis ornata* (cf. *grayi*), and the antipatharian coral *Stauropathes arctica* (Sherwood and Edinger 2009). Major and minor growth banding was observed in *A. arbuscula* colonies, which displayed age estimates of 8-29 years from major ring counts and 49-179 years from minor ring counts. A bomb-^{14}C dated *A. arbuscula* colony (Sherwood & Edinger 2009) validated major growth rings to represent 1 year, based on goodness of fit for the bomb-^{14}C dated sample when compared

to samples aged by major growth ring counts in this study (Fig. 2-8). Age estimates based on major and minor growth band counts compared to size metrics further validated the conclusion of major rings representing annual growth, as age based on major growth rings showed improved regression fits (Fig. 2-9). Therefore, all age estimates and growth rate calculations were based on major growth ring counts.

The driving factor behind minor growth band formation for *A. arbuscula* was not evident. However, examples of larger, more dominant banding patterns along with a finer banding pattern have been recorded in bamboo corals (Roark et al. 2005; Tracey et al. 2007), the gorgonian corals *Primnoa pacifica* (Aranha et al. 2014) and *Primnoa resedaeformis* (Risk et al. 2002), the black coral *Bathypathes patula* (Marriott et al. 2020), and in sea pens (Neves et al. 2015; K. Greeley MSc Thesis, Memorial University 2021). In Roark et al. (2005), it was suggested that sub-annual growth rings in the proteinaceous nodes and calcite internodes of bamboo corals from the Gulf of Alaska were formed because of variations in food supply following lunar cycles. Sub-annual growth bands in the gorgonian coral *Primnoa pacifica* from the NE Pacific were attributed to primary productivity fluctuations on sub-annual intervals, which was supported by trace element variations recorded on sub-annual intervals (Mg/Ca and Sr/Ca) (Aranha et al. 2014). Mg/Ca and Sr/Ca variations from this study were determined to not represent temperature variations, and instead reflect growth rate changes in coral skeletons, possibly from multiple increases in food availability per year. In depth analysis regarding the cause of minor growth band formation for *A. arbuscula* was not completed in this study, but should be considered in future work.

2.4.3 Growth rates and ages

Ages ranged from 8-29 years, which is much younger than previously reported longevities of large gorgonians, bamboo corals, and antipatharians in the NW Atlantic, but similar to longevities reported of some sea pens. Previously reported bamboo coral ages off Newfoundland and Labrador include <100 years for an *A. arbuscula* colony bomb-^{14}C dated, and 30 years for the same colony aged by growth ring counts, and 94-200 years for *Keratoisis grayi* colonies (Sherwood and Edinger 2009). A study on *Keratoisis* colonies from the Davidson Seamount off the western coast of the US reported colony ages of 98 and >145 years, and for a sample from the Gulf of Alaska an age of 116 years, while an *Isidella* colony from the Gulf of Alaska reported an age of 53 years (Andrews et al. 2009). Bamboo corals not identified as to genus or species from the Gulf of Alaska displayed ages between 75-126 years (Roark et al. 2005) (Fig. 2-18). *A. arbuscula* longevity is not as long as other bamboo coral species, and not anywhere near the extreme longevity observed for some species of deep-sea corals, such as the black coral *Leiopathes* sp., which have displayed ages up to 4265 years (Roark et al. 2009) (Fig. 2-18). When specimens were being chosen for analysis, samples with larger stem diameters were preferred, meaning it is unlikely that younger ages were caused by sampling bias. The longevities determined in this study do compare to some sea pen species, with reported ages of 13-22 years for *Halipteris finmarchica* from the NW Atlantic (Neves et al. 2015), 2-75 years for *Umbellula encrinus* from the eastern Canadian Arctic (Neves et al. 2018), and 6-48 years for *Halipteris willemoesi* from the Eastern Bering Sea (Wilson et al. 2002) (Fig. 2-18).

Radial and axial growth rates for *A. arbuscula* are comparable with other bamboo corals from similar and different areas, which suggests that deep-sea bamboo corals are slow growing organisms regardless of oceanographic region (Fig. 2-18). Radial growth rates of *A. arbuscula* ranged from 0.0246 – 0.1603 mm/yr, and axial growth rates ranged from 1.87 – 16.1 mm/yr (Tables 2-4; 2-5). An *A. arbuscula* colony off Newfoundland and Labrador displayed radial growth rates of >0.02 mm/yr and axial growth rates of >3 mm/yr based on bomb-^{14}C data, and 0.07 mm/yr and 10 mm/yr based on growth ring counts, respectively (Sherwood and Edinger 2009). *Keratoisis grayi* colonies from the same study recorded radial growth rates of 0.053-0.075 mm/yr and an axial growth rate of 9.3 mm/yr. *Keratoisis* specimens from the NW Atlantic displayed radial growth rates of 0.012-0.078 mm/yr (Farmer et al. 2015), bamboo corals from the Gulf of Alaska displayed radial growth rates of 0.05-0.16 mm/yr (Roark et al. 2005), and *Keratoisis* colonies from the Gulf of Alaska and Davidson Seamount displayed radial growth rates of 0.051-0.10 mm/yr and axial growth rates of 2.8–13.8 mm/yr (Andrews et al. 2009) (Fig. 2-18).
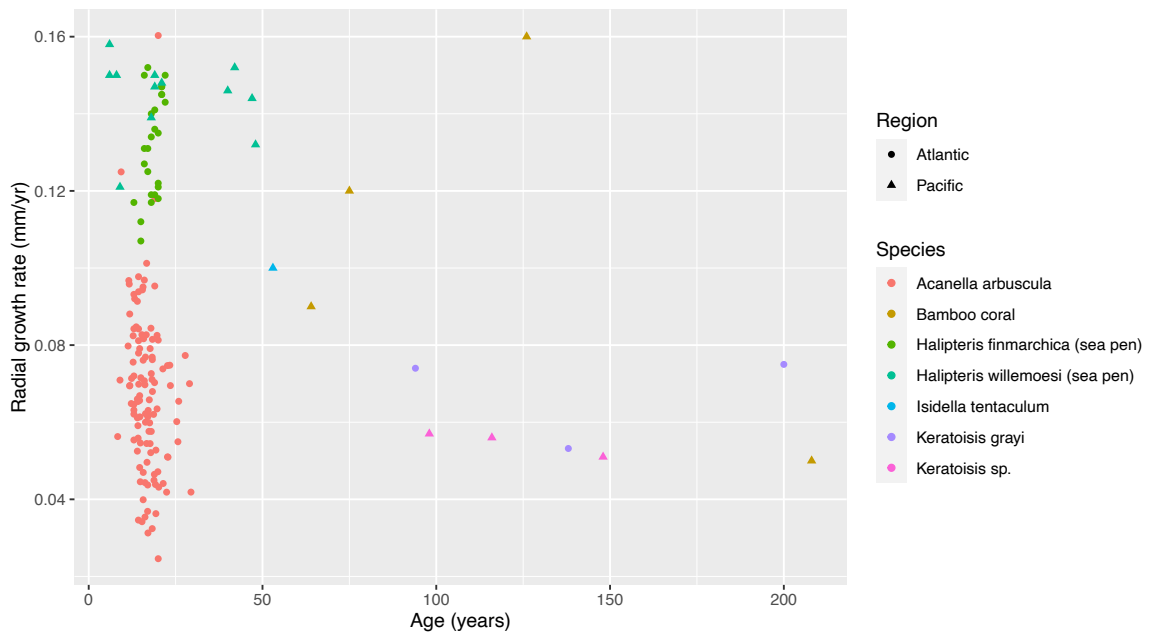
Figure 2-18. Comparisons of ages and radial growth rates for different species of bamboo corals and sea pens. *Acanella arbuscula* (this study), *Keratoisis grayi* (Sherwood and Edinger 2009), bamboo corals (Roark et al. 2005), *Keratoisis* sp. (Andrews et al. 2009), *Isidella tentaculum* (Andrews et al. 2009), *Halipteris finmarchica* (Neves et al. 2015), *Halipteris willemoesi* (Wilson et al. 2002).

2.4.4 Intra-location differences in ages and growth rates

Of the nine locations used for inter-colony variation, locations with consistency for ages also displayed wide ranges of radial growth rates and axial growth rates (Fig. 2-10; Table 2-6). Most trip/sets showed age and growth rate ranges less than the ranges observed within each NAFO zone, yet some showed equal ranges of both ages and growth rates as each region (Table 2-6). The narrower age and growth rate gap for specimens from the same trip/set is to be expected, because this indicates that samples from the same approximate location will have similar growth rates, if they are the same species. However, other trip/sets did present large ranges of growth rates, which reflects the ontogenetic influence on growth rates in the species as well. The variations in age and growth rates for

colonies from the same location highlights the need for deep-sea coral studies to analyze a large sample set, instead of assuming one coral is representative of a population.

Extensive research on deep-sea corals regarding inter-colony variation from the same sampling location without geochemical proxies has not been completed. Previous studies considering inter-colony variation in deep-sea corals incorporated geochemical proxies, such as $\delta^{13}C$ and $\delta^{15}N$, which showed strong trends for inter-colony $\delta^{13}C$ for the gorgonian *Primnoa* from similar locations, indicating similar temporal patterns, but did not show strong trends for $\delta^{15}N$ values (Sherwood et al. 2005). A study analyzing *Keratoisis* samples compared both intra-colony and inter-colony relations using Mg, Sr, and Ca transects, which showed inter-colony variation from the same site were reproducible and likely reflected environmental controls, and not biological controls (Thresher et al. 2007). Inter-colony variation in growth rates for the tropical corals *Porites* spp. (Felis et al. 2003) and *Porites australiensis* (Hayashi et al. 2013) have also been studied to understand how growth rate variation effects the accuracy of geochemical proxies.

The variation in growth rates for colonies sampled within the same scientific trawl set indicates that ontogenetic processes may be causing wide ranges of growth rates. Since there are limited coral studies on inter-colony variation of growth rates for specimens from the same location, studies focused on other organisms were explored to compare our findings with. A study on the green-lipped mussel *Perna canaliculus* (Ibarrola et al. 2017) demonstrated intra-family growth rate variations for specimens grown in a controlled setup. This eliminates the possibility of environmental influence; therefore, growth rate variations within each family were attributed to genetic differences, including both

anatomical and physiological differences, which were measured in depth for fast and slow growing specimens (Ibarrola et al. 2017). The lack of studies on intra-location comparisons of growth rates for deep-sea corals highlights an increased need to focus on fine scale differences in growth rate patterns for organisms of the same species, ideally sampled from the same locations.

2.4.5 Ontogenetic controls of growth rates

Ontogenetic factors may cause inconsistent growth rates throughout the species' lifespan; therefore, ontogenetic variation was further explored, as axial and radial growth rates both decreased with age (Fig. 2-13). This suggests that axial and radial growth rates are not consistent throughout the lifespan of the species, which has been observed in other studies on the bamboo coral *Keratoisis* (Andrews et al. 2009; Farmer et al. 2015). Height and radius of the large gorgonian coral *Primnoa resedaeformis* have also shown to be best fit with age using logarithmic functions, suggesting axial and radial growth rates slow as the species ages (Sherwood and Edinger 2009). Improvements were observed when using the Gompertz and logistic models compared to linear or logarithmic models of stem diameter, height, wet weight, and area, with age, which suggests that *A. arbuscula* colonies reach asymptotic stages of growth axially and radially (Figs. 2-15; 2-15). Further determinations of whether Gompertz or logistic growth models were better fit with *A. arbuscula* data was not concluded in this study because colonies <8 years in age were not analyzed.

Multi-factor analyses including environmental and ontogenetic variables showed that ontogenetic control likely caused most of the geographic growth rate variance observed because of the difference in ages from each NAFO zone, supported by the improvement of fit with Gompertz and logistic growth functions (Table 2-9). Radial growth rate only showed significance with age and not any environmental variables, while axial growth rate showed significance with age, and bloom amplitude. The significance of bloom amplitude with axial growth rate is likely due to an increased food supply in high bloom years (Sebens 1987; Gooday 2002).

Age showed significant relations with location, depth, mean chlorophyll, and bloom amplitude, magnitude, and duration. Youngest ages were observed in NAFO zone 0B, which is also where chlorophyll concentration, and bloom magnitude and amplitude were highest. Because phytoplankton delivery is lagged to deep-sea environments (Gooday 2002), bloom duration may not be important for deep-sea coral success, but higher amplitude and magnitude likely increase total food delivery to the seafloor. This is possibly why highest chlorophyll concentrations, and bloom amplitude and magnitude were observed in the location with the youngest colonies, because new specimens may be inhabiting the area due to the increased food productivity.

2.4.6 Environmental variables and growth rates

The influence of environmental variables like productivity and bottom temperature, which vary geographically and bathymetrically, on growth rates and ages for *A. arbuscula* was studied. The oldest colonies were located in NAFO zone 3O (most southern location),

while these colonies also displayed slower radial growth rates than the other locations (Fig. 2-10). The youngest colonies, found in NAFO zone 0B (most northern location), were also the fastest growing, both radially and axially, with the samples from Davis Strait growing at a similar axial growth rate to NAFO zone 0B samples, but not radial growth rate (Fig. 2-10). NAFO zone 2H displayed ages in between the other two NAFO zones, and the slowest axial growth rates (Fig. 2-10). The observed trends of the fastest growing colonies in the northernmost location and the slower growing colonies in more southern locations were not expected because samples in warmer waters were anticipated to be growing faster based on knowledge of how ambient temperature effects growth rates in most organisms, including bamboo corals noted in a previous study to show increased radial growth rates in warmer waters (Thresher 2009). Because bottom temperature did not explain the observed results, other environmental variables were explored, like chlorophyll concentration and phytoplankton bloom parameters, to evaluate differences in productivity between regions.

Chlorophyll concentration between 1997-2021 showed the highest mean and median daily average concentrations for NAFO zone 0B and the lowest for NAFO zone 3O, which varied significantly by location (Tables 2-7; 2-8) (Clay et al. 2021). Some caution should be expressed for data allocated to NAFO zone 0B, as the location for the data was not identical to NAFO zone 0B because chlorophyll data is not yet available for this region. The closest designated area was used instead as a proxy (NCLS) (Clay et al. 2021). Additionally, chlorophyll concentration did not show a strong relationship with

growth rates, despite the observed data of highest chlorophyll concentrations in regions with the faster growing corals.

Benthic organisms rely on particulate organic matter, often in the form of phytodetritus, to infiltrate into deeper waters as their main food source (Gooday 2002). Temperate locations observe bi-annual phytoplankton bloom periods in spring and fall (Demarcq et al. 2012), while locations in higher latitudes usually observe one phytoplankton bloom period in early or late spring (Ardyna et al. 2014). This means that in areas with increased food supply, or increased intensity or possibly frequency of phytoplankton blooms, it is expected that the corals may be able to grow faster. The mean and median chlorophyll concentration supports this, as the highest daily average chlorophyll concentrations were observed in NAFO zone 0B, where the corals were growing the fastest both radially and axially. The lowest mean and median chlorophyll concentration values were in NAFO zone 3O, which was also the location with the slowest radial growth rates observed.

Phytoplankton bloom data showed varying regions with the highest amplitude and magnitude per year, with some years highest in NAFO zone 3O, and some highest in NAFO zone 0B (Fig. 2-16) (Clay et al. 2021). Overall, the average mean amplitude and magnitude of phytoplankton bloom was highest for NAFO zone 0B, but comparable values were observed for NAFO zone 3O, while values were much lower for NAFO zone 2H (Fig. 2-16; Table 2-8). Bloom duration was earliest and longest in NAFO zone 3O, with a later start and shorter duration in NAFO zone 0B, likely because of ice cover delays (Fig. 2-17) (Ardyna et al. 2014; Clay et al. 2021).

Comparisons of bloom fit data with daily chlorophyll concentrations year to year indicated chlorophyll concentrations returning to pre-bloom levels and possibly slightly lower, after the bloom was completed (Fig. 2-17). In NAFO zones 0B and 2H, where bloom periods were later and shorter, chlorophyll concentrations post-bloom remain high, sometimes nearing the bloom maximum, but at a slower rate (Fig. 2-17) (Clay et al. 2021). The elevated post-bloom concentrations could contribute to the faster growth rates we observed in NAFO zone 0B, as the increased concentrations later in the year are a large contribution to the overall higher mean chlorophyll concentrations noted for NAFO zone 0B. It has also been suggested that recent declines of sea ice in higher latitude waters are causing increased productivity in these areas and possibly bi-annual phytoplankton blooms in both spring and fall (Ardyna et al. 2014). This idea could explain why we observed the youngest coral colonies growing more northward, as these are possibly new specimens in the location because of recent increases in productivity, which leads to greater survivorship of young coral colonies. However, chlorophyll concentration did not show a strong relationship with growth rates in statistical analyses, despite the observed data of highest chlorophyll concentrations in regions with the faster growing corals.

2.4.7 Bathymetric variation in age and growth rates

Only age was significantly related to depth, and radial and axial growth rates showed weak negative trends with depth (Fig. 2-11). The negative trend for radial and axial growth rates with depth were expected, as it has been documented that bamboo corals decrease in radial growth rate with increasing depth (Thresher 2009), and a similar negative

trend of growth rates and depth has been documented for black corals off Hawaii (Roark et al. 2006). It is likely that corals are able to grow faster in shallower waters due to increased food and warmer waters. However, the oceanographic conditions in the NW Atlantic may distribute food resources more readily to deeper environments, as most of the specimens in this study were collected from depths where either the Irminger water (200-500 m) or the Labrador Sea water (500-1000 or 2000 m) are located (Radice et al. 2016). Labrador Sea and NW Atlantic water is known to be well-mixed due to winter convection, which creates a homogeneous water mass located throughout the Labrador Sea (Yashayaev 2007). A study on the deep-sea scleractinian coral *Desmophyllum dianthus* in the New England Seamounts highlights how the North Atlantic Deep Water causes no stratigraphic differences in the water column in terms of nutrients and temperature (Robinson et al. 2007). A homogeneous water mass is more likely to equally distribute food resources due to stronger mixing patterns; therefore, allowing corals to thrive equally at different depths.

The observation of increasing coral ages in shallower waters indicates that deeper colonies may not survive as long or these colonies were removed in previous decades by fisheries activities. The latter potential impact is unlikely, as fishing efforts have been focused in shallower waters in previous decades, and are only recently starting to move into deeper waters due to depleted fish stocks and improved technologies (Roberts and Hirshfield 2004). A previous study on sea pens documented positive relationships of deep-sea coral ages and depth (Neves et al. 2015), while both negative and positive relationships of large gorgonian colony sizes and depth have also been observed over a narrower depth range (Watanabe et al. 2009).

2.5 CONCLUSIONS

A. arbuscula colonies ranged from 8-29 years in age, 0.0246 – 0.1603 mm/yr for radial growth rates, and 1.87 – 16.1 mm/yr for axial growth rates. This species exhibited major and minor growth banding, which is a common observation in other gorgonian coral species (Risk et al. 2002; Roark et al. 2005; Tracey et al. 2007). Our data suggested that major growth bands were representative of annual growth banding, but the driver behind minor growth band formation was not determined and should be studied further in future work.

Age and growth rates varied amongst the three regions compared, being the SE Baffin Shelf (NAFO zone 0B), Northern Labrador Sea (NAFO zone 2H), and the SW Grand Banks (NAFO zone 3O), however the growth rate ranges observed in this study were similar to previously reported growth rates for bamboo corals from the NW Atlantic (Sherwood and Edinger 2009; Farmer et al. 2015). The fastest growing and youngest colonies were located in NAFO zone 0B, while the oldest and slowest growing colonies were found in NAFO zone 3O. Our study suggests that ontogenetic variations had strong influences on axial and radial growth rates. Further investigation into the details of previous fishing activities, such as the Greenland Halibut fishery off the SE Baffin Shelf (Wareham and Edinger 2007), and *A. arbuscula* bycatch return frequency for each region should be studied to reveal differences in fishing pressures that could relate to longevity variation observed regionally and bathymetrically.

Similar to most deep-sea coral species, *A. arbuscula* specimens proved to be slow-growing organisms, with varying growth rates by geographic location. Longevity was less

than most deep-sea coral studies have reported, however we may have sampled primarily younger colonies because older colonies have been removed by bottom trawling efforts in previous decades. Reported slow growth rates make *Acanella arbuscula* a particularly vulnerable species to disturbance events, as the likelihood of recovery and recruitment for the species is unknown. Immediate efforts to protect the species from further disturbances should be encouraged.

2.6 LITERATURE CITED

Andrews AH, Stone RP, Lundstrom CC, DeVogelaere. 2009. Growth rate and age determination of bamboo corals from the northeastern Pacific Ocean using refined ^{210}Pb dating. Marine Ecology Progress Series. 397: 173-185.

Aranha R, Edinger E, Layne G, Piercey G. 2014. Growth rate variation and potential paleoceanographic proxies in *Primnoa pacifica*: Insights from high-resolution trace element micro-analysis. Deep-Sea Research II. 99: 213-226.

Ardyna M, Babin M, Gosselin M, Devred E, Rainville L, Tremblay J-E. 2014. Recent Arctic Ocean sea ice loss triggers novel fall phytoplankton blooms. Geophysical Research Letters. 41: 6207-6212.

Baker KD, Wareham VE, Snelgrove PVR, Haedrich RL, Fifield DA, Edinger EN, Gilkinson KD. 2012. Distributional patterns of deep-sea coral assemblages in three submarine canyons off Newfoundland, Canada. Marine Ecology Progress Series. 445: 235-249.

Buhl-Mortensen L, Olafsdottir SH, Buhl-Mortensen P, Burgos JM, Ragnarsson SA. 2015. Distribution of nine cold-water coral species (Scleractinia and Gorgonacea) in the cold temperate North Atlantic: effects of bathymetry and hydrography. Hydrobiologia. 759: 39-61.

Clay S, Layton C, Devred E. 2021. BIO-RSG/PhytoFit: First release (v1.0.0). Zenodo.

Cordeiro RTS, Neves BM, Kitahara MV, Arantes RCM, Perez CD. 2020. First assessment on Southwestern Atlantic equatorial deep-sea coral communities. Deep-sea Research I. 163: 103344.

Cordes EE, Nybakken JW, VanDykhuizen G. 2001. Reproduction and growth of *Anthomastus ritteri* (Octocorallia: Alcyonacea) from Monterey Bay, California, USA. Marine Biology. 138: 491-501.

Demarcq H, Reygondeau G, Alvain S, Vantrepotte V. 2012. Monitoring marine phytoplankton seasonality from space. Remote Sensing of Environment. 117: 211-222.

Edinger E, Baker K, Devillers R, Wareham V. 2007. Coldwater corals off Newfoundland and Labrador: Distribution and Fisheries Impacts. WWF-Canada.

Farmer JR, Robinson LF, Hönisch B. 2015. Growth rate determinations from radiocarbon in bamboo corals (genus *Keratoisis*). Deep-Sea Research I. 105: 26-40.

Felis T, Pätzold J, Loya Y. 2003. Mean oxygen-isotope signatures in *Porites* spp. corals: inter-colony variability and correction for extension-rate effects. Coral Reefs. 22: 328-336.

Finch CE, Pike MC. 1996. Maximum life span predictions from the Gompertz mortality model. Journal of Gerontology: Biological Sciences. 51A(3): B183-B194.

Gass SE, Willison JHM. 2005. An assessment of the distribution of deep-sea corals in Atlantic Canada by using both scientific and local forms of knowledge. Cold-Water Corals and Ecosystems - Erlangen Earth Conference Series.

Gooday AJ. 2002. Biological responses to seasonally varying fluxes of organic matter to the ocean floor: a review. Journal of Oceanography. 58: 305-332.

Greeley K. 2021. MSc Thesis. Memorial University of Newfoundland.

Hayashi E, Suzuki A, Nakamura T, Iwase A, Ishimura T, Iguchi A, Sakai K, Okai T, Inoue M, Araoka D, Murayama S, Kawahata H. 2013. Growth-rate influences on coral climate proxies tested by a multiple colony culture experiment. Earth and Planetary Science Letters. 362: 198-206.

Ibarrola I, Hilton Z, Ragg NLC. 2017. Physiological basis of inter-population, inter-familiar and intra-familiar differences in growth rate in the green-lipped mussel *Perna canaliculus*. Aquaculture. 479: 544-555.

Lo CF. 2010. A modified stochastic Gompertz model for tumour cell growth. Computational and mathematical methods in medicine. 11(1): 3-11.

Marriott P, Tracey DM, Bostock H, Hitt N, Fallon SJ. 2020. Ageing Deep-Sea Black Coral *Bathypathes patula*. Frontiers in Marine Science. 7: 479.

Neves B de M, Edinger E, Layne GD, Wareham VE. 2015. Decadal longevity and slow growth rates in the deep-water sea pen *Halipteris finmarchica* (Sars, 1851) (Octocorallia: Pennatulacea): implications for vulnerability and recovery from anthropogenic disturbance. Hydrobiologia. 759: 147-170.

Neves B de M, Edinger E, Wareham Hayes V, Devine B, Wheeland L, Layne G. 2018. Size metrics, longevity, and growth rates in *Umbellula encrinus* (Cnidaria: Pennatulacea) from the eastern Canadian Arctic. Arctic Science. 00: 1-28.

Radice VZ, Quattrini AM, Wareham VE, Edinger EN, Cordes EE. 2016. Vertical water mass structure in the North Atlantic influences the bathymetric distribution of species in the deep-sea coral genus *Paramuricea*. Deep-Sea Research I. 116: 253-263.

Risk MJ, Heikoop JM, Snow MG, Beukens R. 2002. Lifespans and growth patterns of two deep-sea corals: *Primnoa resedaeformis* and *Desmophyllum cristagalli*. Hydrobiologia. 471: 125-131.

Roark EB, Guilderson TP, Dunbar RB, Fallon SJ, Mucciarone DA. 2009. Extreme longevity in proteinaceous deep-sea corals. PNAS. 106(13): 5204-5208.

Roark EB, Guilderson TP, Dunbar RB, Ingram BL. 2006. Radiocarbon-based ages and growth rates of Hawaiian deep-sea corals. Marine Ecology Progress Series. 327: 1-14.

Roark EB, Guilderson TP, Flood-Page S, Dunbar RB, Ingram BL, Fallon SJ, McCulloch M. 2005. Radiocarbon-based ages and growth rates of bamboo corals from the Gulf of Alaska. Geophysical Research Letters. 32: L04606.

Roberts JM, Cairns SD. 2014. Cold-water corals in a changing ocean. Current Opinion in Environmental Sustainability. 7:118-126.

Roberts S, Hirshfield M. 2004. Deep-Sea Corals: Out of Sight, but No Longer out of Mind. Frontiers in Ecology and the Environment. 2: 123-130.

Robinson LF, Adkins JF, Scheirer DS, Fernandez DP, Gagnon A, Waller RG. 2007. Deep-sea scleractinian coral age and depth distributions in the Northwest Atlantic for the last 225,000 years. Bulletin of Marine Science. 81(3): 371-391.

Schneider CA, Rasband WS, Eliceiri KW. 2012. NIH image to ImageJ: 25 years of image analysis. Nat Methods. 9(7): 671-675.

Schöne BR, Dunca E, Fiebig J, Pfeiffer M. 2005. Mutvei's solution: An ideal agent for resolving microgrowth structures of biogenic carbonates. Paleogeography, Paleoclimatology, Paleoecology. 228: 149-166.

Sebens KP. 1987. The ecology of intermediate growth in animals. Ann. Rev. Ecol. Syst. 18: 371-407.

Sherwood OA, Edinger EN. 2009. Ages and growth rates of some deep-sea gorgonian and antipatharian corals of Newfoundland and Labrador. Can. J. Fish. Aquat. Sci. 66: 142 152.

Sherwood OA, Heikoop JM, Scott DB, Risk MJ, Guilderson TP, McKinney RA. 2005. Stable isotopic composition of deep-sea gorgonian corals *Primnoa* spp.: a new archive of surface processes. Marine Ecology Progress Series. 301: 135-148.

Sherwood OA, Scott DB, Risk MJ, Guilderson TP. 2005. Radiocarbon evidence for annual growth rings in the deep-sea octocoral *Primnoa resedaeformis*. Marine Ecology Progress Series. 301: 129-134.

Thresher RE. 2009. Environmental and compositional correlates of growth rate in deep-water bamboo corals (Gorgonacea; Isididae). Marine Ecology Progress Series. 397: 187-196.

Thresher RE, MacRae CM, Wilson NC, Gurney R. 2007. Environmental effects on the skeletal composition of deep-water gorgonians (*Keratoisis* spp.; Isididae). Bulletin of Marine Science. 81(3): 409-422.

Tracey DM, Neil H, Marriott P, Andrews AH, Cailliet GM, Sánchez JA. 2007. Age and growth of two genera of deep-sea bamboo corals (family Isididae) in New Zealand waters. Bulletin of Marine Science. 81(3): 393-408.

Urban HJ. 2002. Modeling growth of different developmental stages in bivalves. Marine Ecology Progress Series. 238: 109-114.

van den Beld IMJ, Bourillet JF, Arnaud-Haond S, Chambure LD, Davies JS, Guillaumont B, Olu K, Menot L. 2017. Cold-water coral habitats in submarine canyons of the Bay of Biscay. Frontiers in Marine Science. 4(118).

Wareham VE, Edinger EN. 2007. Distribution of deep-sea corals in the Newfoundland and Labrador region, Northwest Atlantic Ocean. Bulletin of Marine Science. 81:289-313.

Watanabe S, Metaxas A, Sameoto J, Lawton P. 2009. Patterns in abundance and size of two deep-water gorgonian octocorals, in relation to depth and substrate features off Nova Scotia. Deep-Sea Research I. 56: 2235-2248.

Watling L, France SC, Pante E, Simpson A. 2011. Biology of Deep-Water Octocorals. In: Lesser M, editor. Advances in Marine Biology. Elsevier. pp. 41-122.

Wilson MT, Andrews AH, Brown AL, Cordes EE. 2002. Axial rod growth and age estimation of the sea pen, *Halipteris willemoesi* Kölliker. Hydrobiologia. 471: 133-142.

Winsor CP. 1932. The Gompertz curve as a growth curve. Proceedings of the National Academy of Sciences. 18(1).

Yashayaev I. 2007. Hydrographic changes in the Labrador Sea, 1960-2005. Progress in Oceanography. 73: 242-276.

Appendix 2-1. Lab equipment used during sample preparation

Figure A2-1.1. Buehler IsoMet Low-Speed Saw.

Figure A2-1.2. Buehler MetaServ 250 Grinder-Polisher.
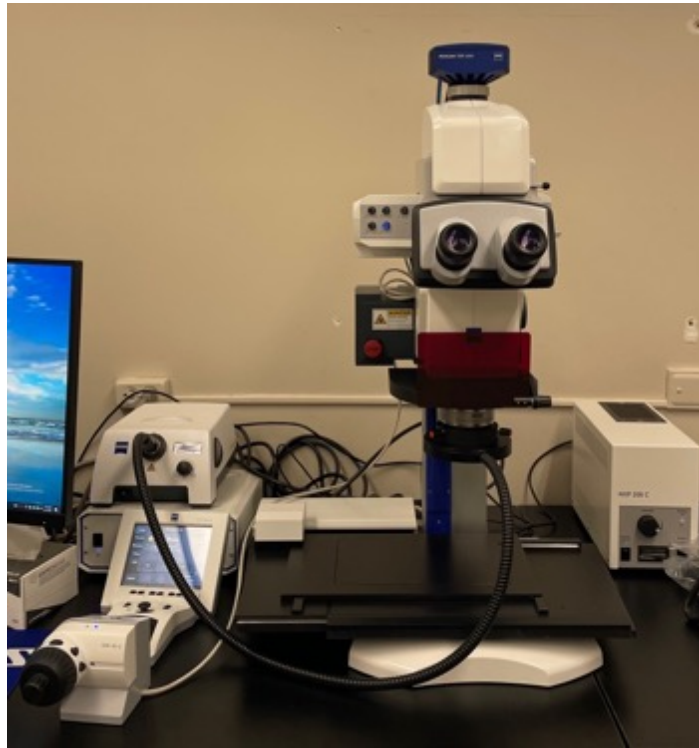
Figure A2-1.3. Zeiss AxioZoom V.16 Telecentric Microscope.

Appendix 2-2. Full sample preparation experiments

In attempt to increase the clarity of growth rings in *A. arbuscula* samples, different sample preparation methodologies were experimented with, such as fluorescence microscopy, staining the samples with Mutvei's solution (Schöne et al. 2005), thin section preparation, and etching in 5% HCl.

Fluorescence microscopy was experimented with, as it is similar to ultraviolet light, which has been proven to increase growth ring clarity in other cold-water coral species (Aranha et al. 2014; Neves et al. 2015, 2018). Fluorescence microscopy was used on a Zeiss AxioZoom V.16 Telecentric Microscope. The same cross-sections used for reflected white light images were also used with fluorescence microscopy. Different lighting colors

and excitation/emission wavelengths were tested, such as green light (excitation wavelength: 488, emission wavelength: 509) and blue light (excitation wavelength: 353, emission wavelength: 465). Samples were not kept under fluorescence for prolonged periods of time, as this can damage the samples.

Mutvei's stain, which is composed of alcian blue, glutaraldehyde, acetic acid, and DI water, was used to stain two *A. arbuscula* samples that were collected in 2021, in attempt to improve growth ring clarity (Schöne et al. 2005). Mutvei's solution was created following procedures outlined in Schöne et al. (2005), and is a form of etching that causes growth ring structures to have a 3D appearance, making growth ring counts easier to complete. *A. arbuscula* sample R21-25b was originally stained for 40 minutes in Mutvei's solution, followed by an additional 1 hour, while sample R21-23a was stained for 1 hour only. Both samples were allowed to dry before imaging under reflected light. The staining with Mutvei's solution was conducted at 37-40°C using a hotplate, and the solution was continuously stirred as the samples were staining. The solution is kept in a refrigerator to preserve the effectiveness of the stain.

Four thin sections of *A. arbuscula* samples were created to experiment with transmitted light and growth ring visibility. Two different methodologies were followed to compare visualization in the different approaches. Two *A. arbuscula* samples (R21-17a and R21-21b) in thick sections were first glued with epoxy to 1mm glass slides after being grinded and polished, and then cut with a Buehler IsoMet Low-Speed Saw to an epoxy thickness of about 1mm. The samples were grinded down to 100-200 μm using $400-800$ grit Buehler CarbiMet silicon carbide grinding papers on a Buehler MetaServ 250 Grinder-

Polisher. Samples were then polished using a TexMet C polishing cloth. All grinding and polishing were done using a mixture of water and isopropyl alcohol for the grinding liquid. There was difficulty keeping the surface of the sample uniform in thickness due to grinding and polishing pressure being applied by hand. The samples were analyzed with a Zeiss AxioZoom V.16 Telecentric Microscope using transmitted light.

The second thin section methodology was completed by Matt Crocker of the CREAIT Network (Memorial University), which followed standard methodology used for petrographic thin sections. This approach included two *A. arbuscula* samples (AC 01_1a and AC 09_1), which were not used in the growth rate and aging portion of this study. These samples were first prepared in thick section, and then grinded with 220 – 600 silicon carbide grinding papers before mounting on the glass slides with Epo-Tek 301 epoxy. A Struers Discoplan Saw was used to continue grinding the samples until they were about 150 μm, and they were then grinded additionally by hand with 600 grit silicon carbide grinding paper on a glass plate. Matt did not grind the thin sections to the normal thickness of a petrographic thin section (30-80 μm), as it would have likely removed too much proteinaceous material for the growth rings to be visible.

Etching in 5% HCl was the final approach in attempting to increase growth ring clarity. Multiple *A. arbuscula* samples were etched by placing the exposed node surface, in thick sections, in 5% HCl for about 1-2 minutes, after all grinding and polishing was complete. The samples were allowed to dry before being analyzed and imaged with a Zeiss AxioZoom V.16 Telecentric Microscope using reflected white light.

Appendix 2-3. Successful and unsuccessful visualization techniques

Fluorescence microscopy increased growth ring clarity substantially in most samples and was used in the remainder of the study. Comparison images of the same sample with reflected light versus fluorescence show the difference in visualization capabilities of growth rings with the fluorescence. The sample images used for the growth ring counts were chosen based on image clarity with respect to growth ring visualization, meaning some growth rings were counted under reflected white light, yet most were counted under fluorescence. Both green (excitation wavelength: 488, emission wavelength: 509) and blue (excitation wavelength: 353, emission wavelength: 465) fluorescence were experimented with, with most samples imaged with green fluorescence.

Mutvei's solution was used to stain two *A. arbuscula* samples for 40 minutes - 1 hour and 40 minutes. Mutvei's solution was absorbed in one of the samples (R21-23a), causing an increase in growth ring clarity. However, it did not work on the other sample stained (R21-25b), as the proteinaceous node portion of the skeleton did not seem to absorb the stain, causing there to be no etched or 3D appearance in the growth rings.

Thin section preparation of four *A. arbuscula* samples showed no substantial improvement in clarity of growth rings in thick sections when compared to the thin sections. It was challenging to keep the sample thickness level and uniform when working with small coral skeleton diameters in thin sections. Only some samples showed improvement in portions of the node diameter, but not uniformly across the growth rings. Thin section samples were also difficult to fully clean after thin section preparation.

The final approach to improve growth ring clarity was etching with 5% HCl for 1-2 minutes in thick sections. 10 *A. arbuscula* samples were etched with 5% HCl, and results varied for each sample. Some samples show that etching does slightly improve growth ring clarity by emphasizing growth ring structures. However, the effects were not consistent between samples; therefore, etching was only attempted on samples that were difficult to image with reflected white light and fluorescence. Based on the results of comparing image quality in the different techniques, fluorescence imaging was used along with reflected white light for the remainder of the study.

Appendix 2-4. Comparison images of different sample preparation techniques
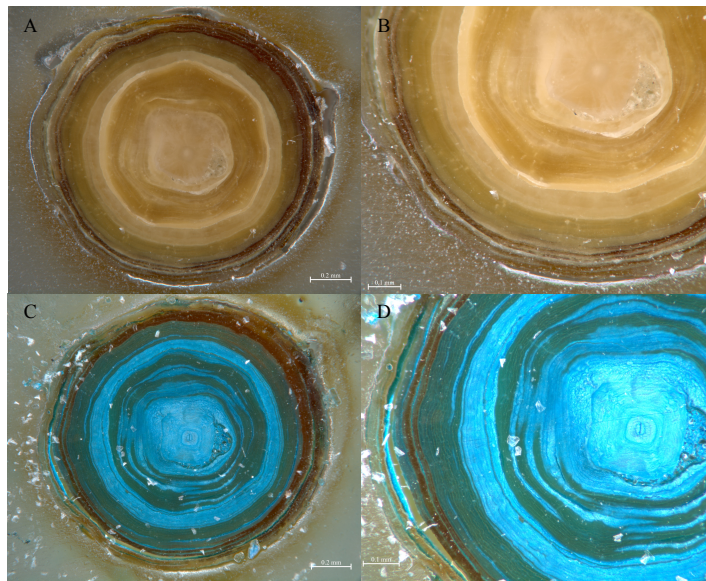
Figure A2-4.1. *A. arbuscula* sample R21-23a A) in thick section imaged with reflected white light, B) zoomed in photo imaged with reflected white light, C) thick section stained with Mutvei's solution for 1 hour, D) zoomed in photo of the rings, stained for 1 hour.
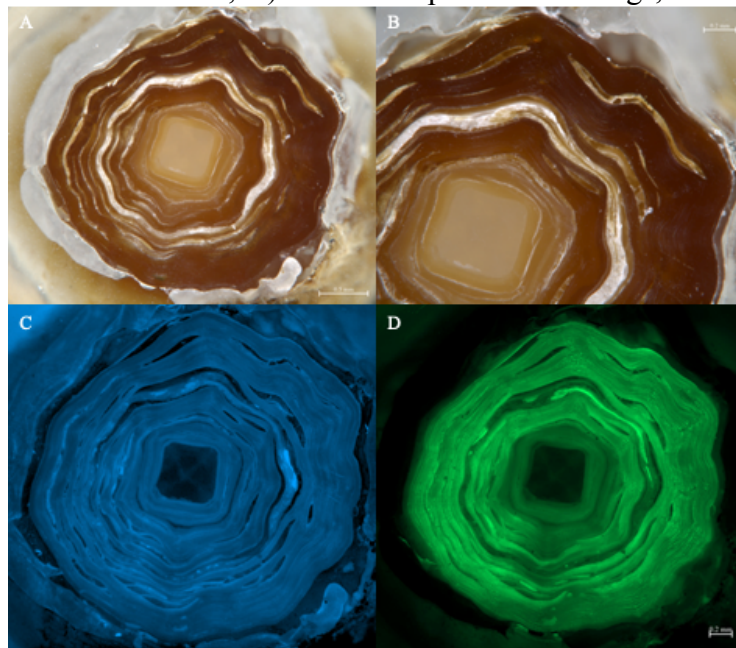
Figure A2-4.2. *A. arbuscula* sample 760_31_5 in thick section imaged with A) reflected white light, B) reflected white light zoomed in, C) blue fluorescence (excitation wavelength: 353, emission wavelength: 465), and D) green fluorescence (excitation wavelength: 488, emission wavelength: 509). All photos are the same thick section.
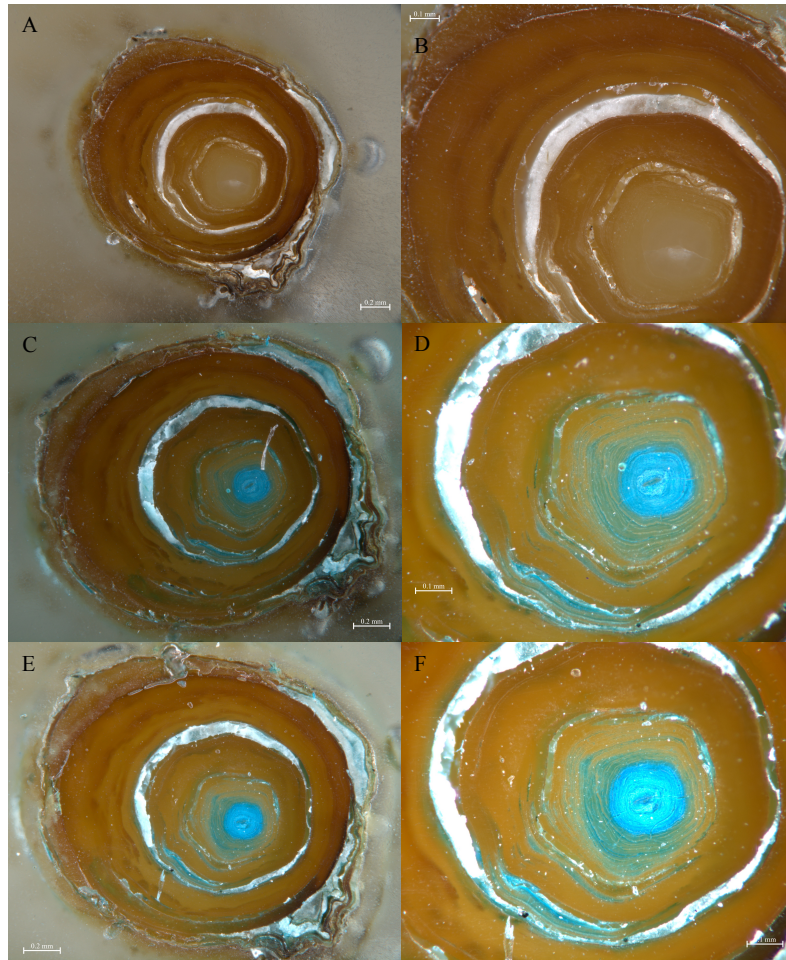
Figure A2-4.3. *A. arbuscula* sample R21-25b A) in thick section imaged with reflected white light, B) zoomed in photo imaged with reflected white light, C) thick section stained with Mutvei's solution for 40 minutes, D) zoomed in thick section stained for 40 minutes, E) thick section stained for 1 hour and 40 minutes, and F) zoomed in image of the rings for the 1 hour and 40 minute stained sample.
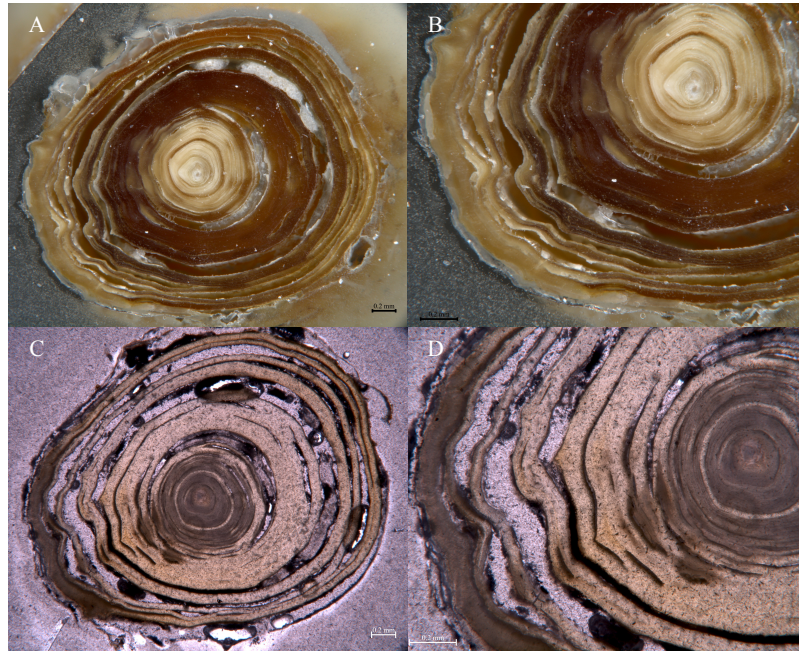
Figure A2-4.4. *A. arbuscula* sample AC 09_1 A) in thick section imaged with reflected white light, B) zoomed in thick section imaged with reflected white light, C) in thin section, ~100 μm thick, imaged with transmitted light, and D) zoomed in thin section at ~100 μm thick of the growth rings, imaged with transmitted light.
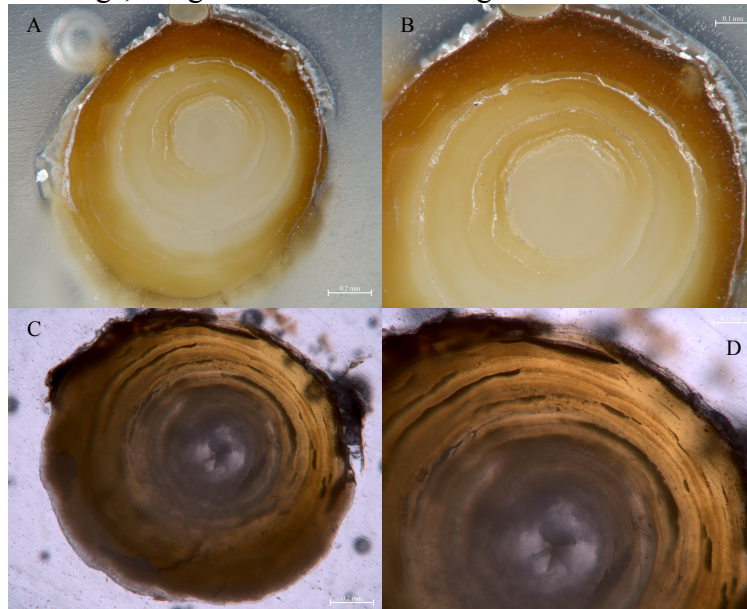
Figure A2-4.5. *A. arbuscula* sample R21-17a A) in thick section imaged with reflected white light, B) zoomed in thick section imaged with reflected white light, C) in thin section imaged with transmitted light, and D) zoomed in thin section of the growth rings, imaged with transmitted light.
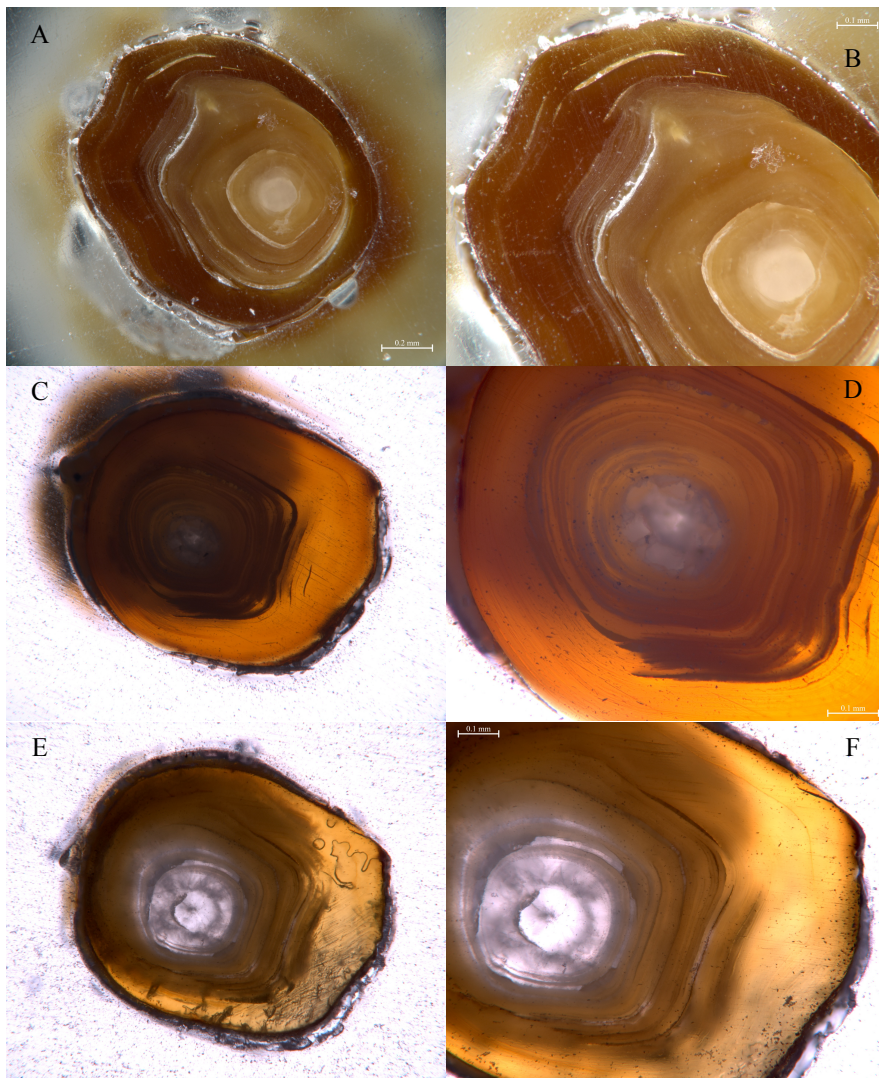
Figure A2-4.6. *A. arbuscula* sample R21-21b A) in thick section imaged with reflected white light, B) zoomed in thick section imaged with reflected white light, C) in thin section, ~500 μm thick, imaged with transmitted light, D) zoomed in thin section at ~500 μm thick of the growth rings, imaged with transmitted light, E) thin section at ~100 μm thick imaged with transmitted light, and F) zoomed in at ~100 μm thick imaged with transmitted light.
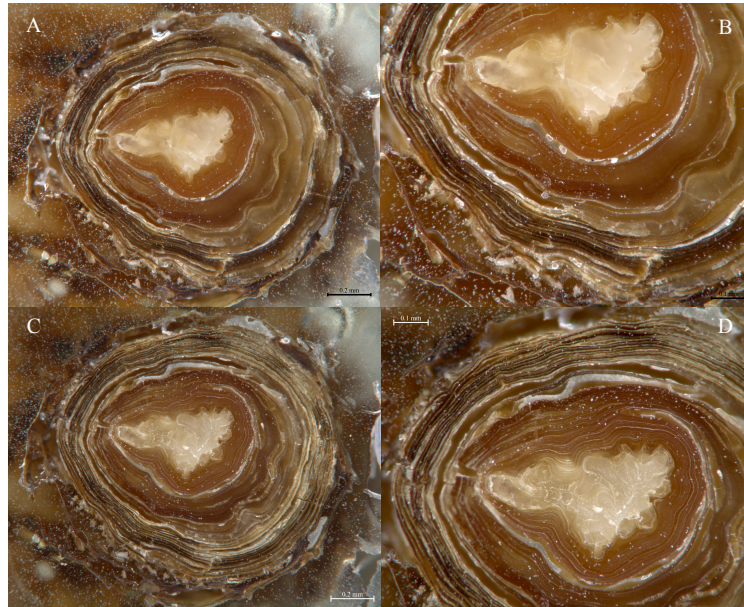
Figure A2-4.7. *A. arbuscula* sample AC 03_1 A) in thick section imaged with reflected white light, B) zoomed in thick section imaged with reflected white light, C) thick section after etching in 5% HCl for 1-2 minutes, imaged with reflected white light, and D) zoomed in thick section after etching, imaged with reflected white light.
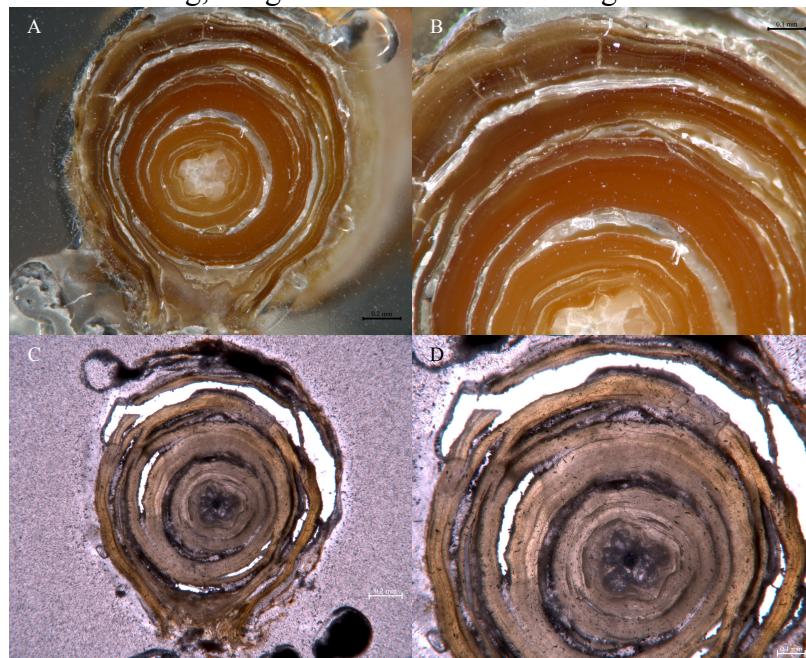
Figure A2-4.8. *A. arbuscula* sample AC 01_1a A) in thick section imaged with reflected white light, B) zoomed in thick section imaged with reflected white light, C) in thin section, ~100 μm thick, imaged with transmitted light, and D) zoomed in thin section at ~100 μm thick of the growth rings, imaged with transmitted light.

117
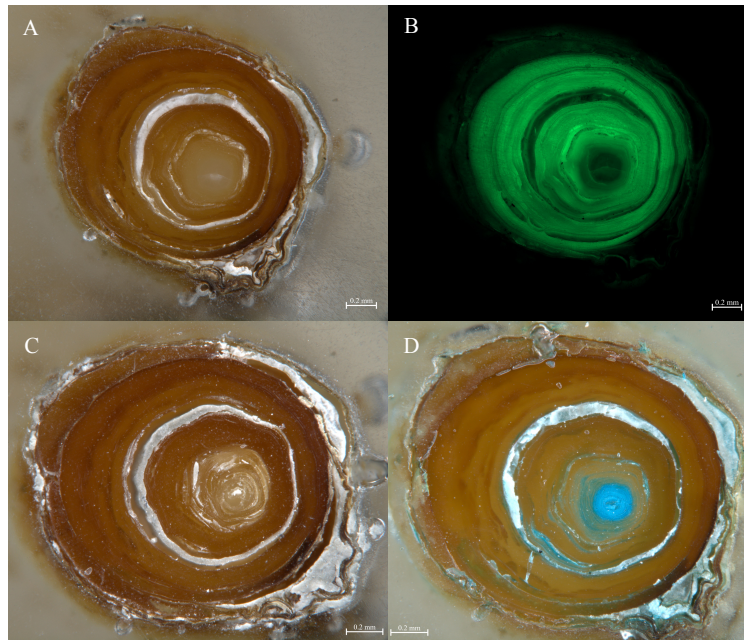
Figure A2-4.9. *A. arbuscula* sample R21-25b A) in thick section imaged with reflected white light, B) in thick section imaged with green fluorescence, C) in thick section after etching in 5% HCl, imaged with reflected white light, and D) in thick section after staining with Mutvei's solution for 1 hour and 40 minutes, imaged with reflected white light.
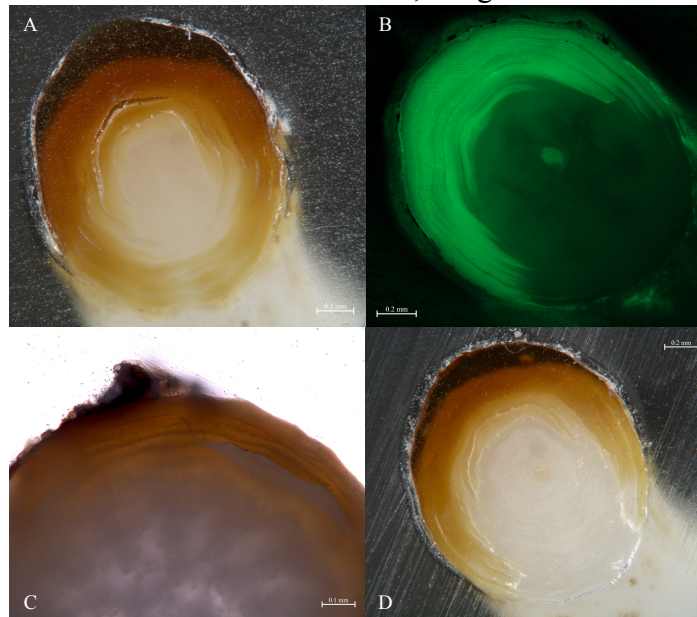
Figure A2-4.10. *A. arbuscula* sample R21-17b A) in thick section imaged with reflected white light, B) in thick section imaged with fluorescence, C) in thin section imaged with transmitted light, and D) in thick section after etching in 5% HCl, imaged with reflected white light.

The first thin section methodology of completing all grinding/polishing by hand, did not show improvements in clarity, as it was challenging to keep the sample thickness level and uniform. Samples showed some improvement in portions of the node diameter, but not uniformly across the growth rings. The other thin section methodology completed by M. Crocker showed some growth ring clarity improvements, but none substantial enough to continue with thin section preparation for the remainder of the study. These samples were also difficult to fully clean and remove grinding material after thin section preparation, so they do not appear as clean as the thick sections. Additionally, since skeleton diameters of *A. arbuscula* are small, creating clear and level thin sections was challenging.
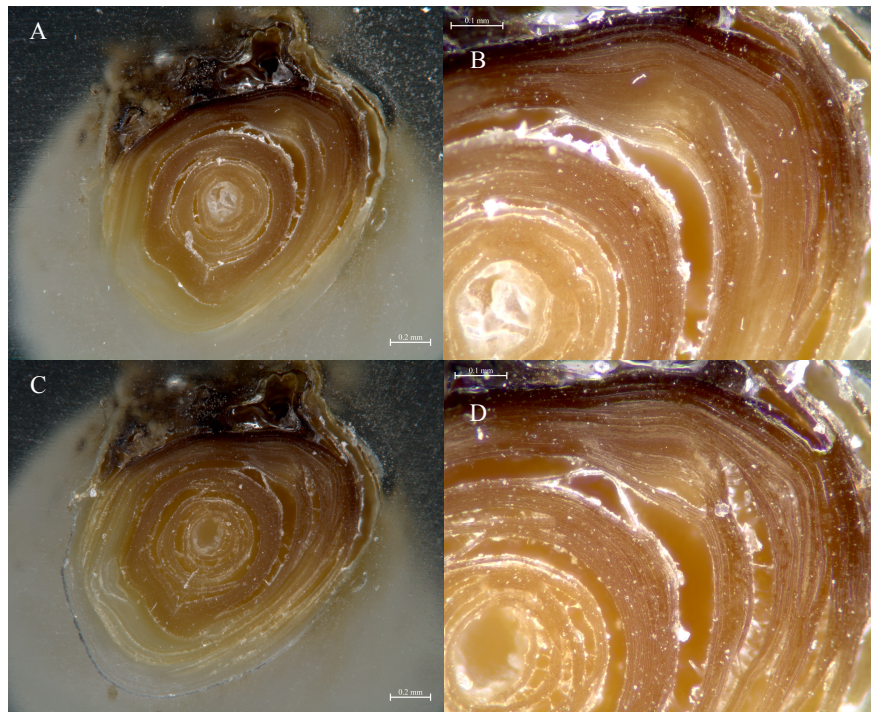
Figure A2-4.11. *A. arbuscula* sample R21-20b A) in thick section imaged with reflected white light, B) zoomed in thick section imaged with reflected white light, C) thick section after etching in 5% HCl for 1-2 minutes, imaged with reflected white light, and D) zoomed in thick section after etching, imaged with reflected white light.

Appendix 2-5. LA-AMS Radiocarbon Methods & Initial Results

To determine annual from sub-annual growth ring formation in the species, and validate age and growth rate estimates, bomb-^{14}C data acquired by laser ablation accelerated mass spectrometry (LA-AMS) was used. LA-AMS on these samples was conducted at ETH Zürich in the Laboratory of Ion Beam Physics by our collaborators Dr. Caroline Welte and Dr. Melina Wertnik, located in Zürich, Switzerland. This approach to radiocarbon measurements was chosen because of the small size of the *A. arbuscula* samples, meaning they did not have enough mass for traditional AMS radiocarbon analyses. The laser ablation approach allows for smaller samples like these to be analyzed. However, this approach is still experimental with bamboo corals; therefore, measurements and data processing for the bomb-^{14}C data is ongoing and will not be included in this chapter.
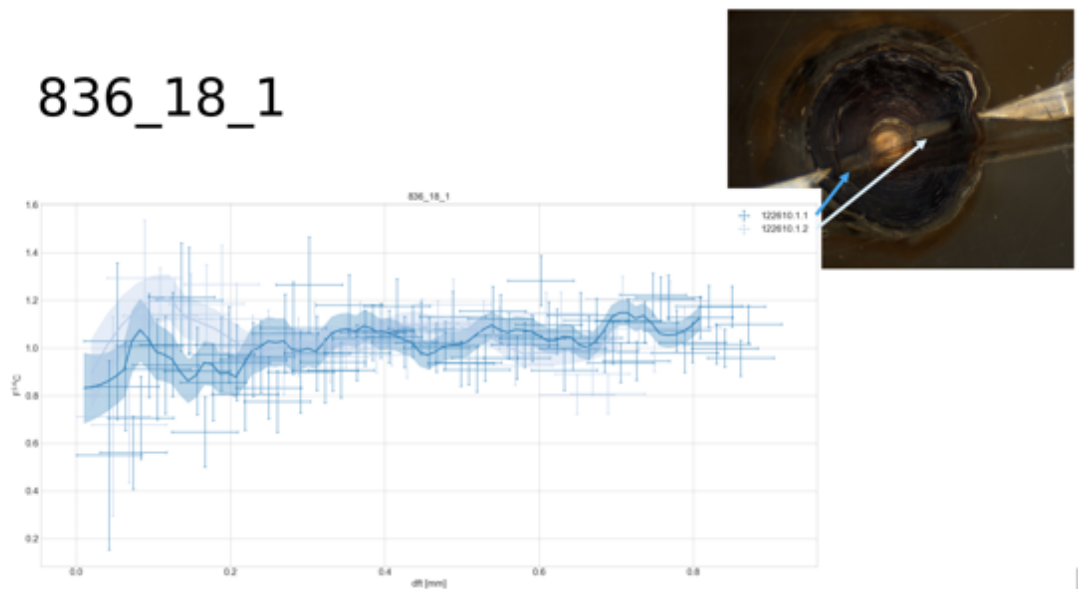
Figure A2-5.1. LA-AMS results for *A. arbuscula* sample 838_18_1 (prepared by C. Welte and M. Wertnik of ETH Zürich).

Table A2-5.1. LA-AMS results for *A. arbuscula* sample 836_18_1.

Label	dft_mm	spot_mm	F14C	F14Cerror	sg	sg_err	C12corr
836_18_1			-0.04197	-0.00136			0.065867
836_18_1			1.943317	0.748954			0.049453
836_18_1			0.59682	0.448076			0.044102
836_18_1			0.306104	0.342422			0.041428
836_18_1			1.016237	0.607019			0.040008
836_18_1			0.688858	0.51162			0.038831
836_18_1			0.68139	0.50614			0.039886
836_18_1			0.497452	0.299637			0.079382
836_18_1			1.028399	0.467082			0.06684
836_18_1			0.217413	0.231366			0.060091
836_18_1			0.736667	0.432604			0.054762
836_18_1			1.079001	0.54552			0.051769
836_18_1	0	0.085	0.55017	0.397241			0.050388
836_18_1	0.010358	0.086	1.028129	0.328712	0.833226	0.14454	0.133488
836_18_1	0.020716	0.086	0.837753	0.185283	0.836622	0.134197	0.340551
836_18_1	0.031074	0.086	0.56089	0.152871	0.845965	0.125818	0.336121
836_18_1	0.041432	0.085	0.706879	0.174106	0.861255	0.119402	0.3245
836_18_1	0.05179	0.086	1.009722	0.217603	0.88249	0.114949	0.295648
836_18_1	0.062148	0.086	0.91115	0.211516	0.909672	0.11246	0.28298
836_18_1	0.072506	0.086	0.928539	0.20496	1.030797	0.126117	0.305785
836_18_1	0.082864	0.085	1.014172	0.218489	1.077026	0.127884	0.293525
836_18_1	0.093222	0.086	1.21445	0.227493	1.0397	0.123126	0.32347
836_18_1	0.10358	0.086	1.200348	0.221092	0.985161	0.114838	0.338393
836_18_1	0.113938	0.086	0.903096	0.182742	0.973209	0.108379	0.37326
836_18_1	0.124296	0.085	0.647065	0.147081	0.953995	0.101882	0.416424
836_18_1	0.134654	0.086	0.85627	0.161009	0.901576	0.094315	0.45771
836_18_1	0.145012	0.086	0.974548	0.153945	0.862098	0.089146	0.569725
836_18_1	0.15537	0.086	1.014423	0.160156	0.885773	0.088277	0.546414
836_18_1	0.165728	0.085	0.937578	0.158094	0.938646	0.089362	0.518574
836_18_1	0.176086	0.086	0.805079	0.148983	0.932436	0.087362	0.501787
836_18_1	0.186444	0.086	0.951146	0.154086	0.892829	0.083067	0.554773
836_18_1	0.196802	0.086	0.963802	0.150436	0.896118	0.083801	0.588567
836_18_1	0.20716	0.085	0.832358	0.130178	0.878753	0.083897	0.680397
836_18_1	0.217519	0.086	0.774567	0.129157	0.93442	0.08929	0.640585
836_18_1	0.227877	0.086	1.060678	0.165329	0.989395	0.095241	0.531938
836_18_1	0.238235	0.086	1.084217	0.193536	1.004263	0.099073	0.39814
836_18_1	0.248593	0.085	0.899174	0.171969	1.028464	0.100818	0.421204
836_18_1	0.258951	0.086	1.265664	0.199357	1.02342	0.099254	0.438517

836_18_1	0.269309	0.086	0.978273	0.156443	1.02944	0.094125	0.552127
836_18_1	0.279667	0.086	0.9055	0.135234	0.994549	0.085107	0.687116
836_18_1	0.290025	0.085	0.941635	0.122129	0.989132	0.07699	0.875082
836_18_1	0.300383	0.086	0.907601	0.117797	0.99839	0.072165	0.906456
836_18_1	0.310741	0.086	1.179135	0.127792	0.985175	0.067502	0.998077
836_18_1	0.321099	0.086	0.980382	0.117055	1.023223	0.067558	0.990015
836_18_1	0.331457	0.086	1.041529	0.117914	1.062737	0.067783	1.036045
836_18_1	0.341815	0.085	1.064991	0.116972	1.075541	0.067336	1.079622
836_18_1	0.352173	0.086	1.073217	0.113931	1.079836	0.066139	1.144741
836_18_1	0.362531	0.086	1.047971	0.110114	1.070137	0.064818	1.197751
836_18_1	0.372889	0.086	1.17631	0.114546	1.092773	0.064692	1.240374
836_18_1	0.383247	0.085	1.025272	0.107206	1.08198	0.063774	1.238326
836_18_1	0.393605	0.086	1.069495	0.108912	1.058437	0.062696	1.24843
836_18_1	0.403963	0.086	1.082929	0.110251	1.062298	0.062297	1.232468
836_18_1	0.414321	0.086	1.020935	0.106198	1.054059	0.061467	1.253795
836_18_1	0.424679	0.085	1.001281	0.101575	1.034352	0.060015	1.344675
836_18_1	0.435037	0.086	1.010445	0.100988	1.02527	0.058728	1.373127
836_18_1	0.445395	0.086	1.132237	0.103851	0.982851	0.056755	1.453593
836_18_1	0.455753	0.086	0.934723	0.094479	0.970632	0.055678	1.455208
836_18_1	0.466111	0.085	0.939526	0.093155	0.985523	0.055704	1.504463
836_18_1	0.476469	0.086	0.909206	0.092878	1.006756	0.056134	1.464805
836_18_1	0.486827	0.086	0.957614	0.095815	1.012763	0.056023	1.446896
836_18_1	0.497185	0.086	1.154343	0.102967	1.016033	0.055809	1.506959
836_18_1	0.507543	0.085	1.121717	0.101287	1.026277	0.055878	1.513756
836_18_1	0.517901	0.086	1.051315	0.096579	1.054876	0.056432	1.56236
836_18_1	0.528259	0.086	0.959382	0.091309	1.07889	0.056581	1.597876
836_18_1	0.538617	0.086	1.013261	0.093915	1.095825	0.056546	1.592733
836_18_1	0.548975	0.085	1.040204	0.096771	1.076575	0.055631	1.539257
836_18_1	0.559333	0.086	1.283069	0.105013	1.065435	0.054945	1.610001
836_18_1	0.569691	0.086	1.098429	0.09486	1.077008	0.054935	1.691631
836_18_1	0.580049	0.086	1.069101	0.093394	1.074527	0.054597	1.702055
836_18_1	0.590407	0.085	0.907291	0.085722	1.069482	0.054023	1.717328
836_18_1	0.600765	0.086	0.998227	0.09035	1.04979	0.053074	1.697282
836_18_1	0.611123	0.086	1.138004	0.095846	1.030874	0.052446	1.717271
836_18_1	0.621481	0.086	1.042735	0.091143	1.031878	0.052209	1.742824
836_18_1	0.63184	0.085	1.116495	0.092509	1.048516	0.05226	1.809318
836_18_1	0.642198	0.086	0.985949	0.086591	1.044562	0.051693	1.826912
836_18_1	0.652556	0.086	1.020672	0.08766	1.012137	0.050237	1.845737
836_18_1	0.662914	0.086	0.936925	0.082384	1.002551	0.049228	1.919899
836_18_1	0.673272	0.085	1.112765	0.089582	1.028904	0.049065	1.92435

836_18_1	0.68363	0.086	0.946034	0.080264	1.070265	0.049554	2.045072
836_18_1	0.693988	0.086	1.108954	0.085875	1.128076	0.050659	2.0879
836_18_1	0.704346	0.086	1.223858	0.089808	1.148066	0.051053	2.105614
836_18_1	0.714704	0.086	1.206827	0.090479	1.148235	0.051234	2.043197
836_18_1	0.725062	0.085	1.212177	0.09317	1.123533	0.05089	1.933325
836_18_1	0.73542	0.086	1.073895	0.087332	1.1362	0.051391	1.95523
836_18_1	0.745778	0.086	0.980228	0.082517	1.10564	0.05073	2.000734
836_18_1	0.756136	0.086	1.024068	0.084156	1.061196	0.049505	2.007545
836_18_1	0.766494	0.085	1.128198	0.087331	1.054135	0.049064	2.051757
836_18_1	0.776852	0.086	1.175256	0.087448	1.057012	0.048708	2.133817
836_18_1	0.78721	0.086	1.014769	0.081591	1.069826	0.04844	2.119078
836_18_1	0.797568	0.086	0.999131	0.079631	1.092578	0.048257	2.192364
836_18_1	0.807926	0.085	1.173824	0.085992	1.125267	0.048161	2.20457
836_18_1	0.818284	0.086	0.957838	0.075508			2.342123
836_18_1	0.828642	0.086	1.0994	0.077903			2.524457
836_18_1			0.741805	0.391939			0.071929
836_18_1			0.507768	0.385525			0.051681
836_18_1			-0.03507	-0.00129			0.043655
836_18_1			0.673778	0.501094			0.040251
836_18_1			-0.03417	-0.00133			0.037451
836_18_1			0.361353	0.394221			0.035606
836_18_1			0.366909	0.398265			0.033884
836_18_1			0.391398	0.423321			0.033235
836_18_1			0.549583	0.410245			0.048317
836_18_1			0.146895	0.166212			0.081941
836_18_1			0.218126	0.232938			0.057731
836_18_1			0.263054	0.276295			0.04937
836_18_1	0	0.095	0.712821	0.418813			0.056828
836_18_1	0.020026	0.097	0.678517	0.2442	0.89216	0.140799	0.160335
836_18_1	0.040053	0.097	1.294564	0.242607	1.008285	0.128769	0.305086
836_18_1	0.060079	0.097	1.135698	0.199739	1.098439	0.11787	0.393626
836_18_1	0.080105	0.095	1.122305	0.170958	1.162619	0.108103	0.530932
836_18_1	0.100132	0.097	1.142481	0.168341	1.200827	0.099467	0.557031
836_18_1	0.120158	0.097	1.185421	0.164421	1.213063	0.091963	0.605705
836_18_1	0.140184	0.097	1.266882	0.165056	1.131896	0.085457	0.642898
836_18_1	0.160211	0.095	1.12314	0.145324	1.106423	0.082156	0.735664
836_18_1	0.180237	0.097	1.006888	0.128395	1.079543	0.079112	0.847597
836_18_1	0.200263	0.097	1.031176	0.12844	1.038227	0.074551	0.865324
836_18_1	0.220289	0.097	0.925197	0.122058	0.996606	0.070161	0.862314
836_18_1	0.240316	0.095	1.00532	0.120831	0.985423	0.066989	0.955324

836_18_1	0.260342	0.097	1.071753	0.119822	1.000288	0.065251	1.036307
836_18_1	0.280368	0.097	0.96431	0.106096	1.020244	0.063352	1.19155
836_18_1	0.300395	0.097	1.020548	0.104523	1.014205	0.060339	1.295768
836_18_1	0.320421	0.095	1.087006	0.105984	1.023489	0.058445	1.343469
836_18_1	0.340447	0.097	0.992457	0.097824	1.013101	0.05688	1.440977
836_18_1	0.360474	0.097	1.022373	0.096742	1.035728	0.056814	1.518114
836_18_1	0.3805	0.097	0.970772	0.09573	1.055388	0.057127	1.473186
836_18_1	0.400526	0.095	1.102949	0.103788	1.064126	0.056936	1.419521
836_18_1	0.420553	0.097	1.095753	0.101419	1.088186	0.0568	1.479618
836_18_1	0.440579	0.097	1.184429	0.103284	1.094981	0.056237	1.540406
836_18_1	0.460605	0.097	1.017263	0.092051	1.079546	0.054666	1.669969
836_18_1	0.480632	0.095	1.107943	0.093699	1.071181	0.052935	1.752872
836_18_1	0.500658	0.097	1.08386	0.089882	1.082529	0.05152	1.866802
836_18_1	0.520684	0.097	0.926649	0.082774	1.069971	0.050075	1.889023
836_18_1	0.540711	0.097	1.055404	0.086195	1.05171	0.049703	1.981752
836_18_1	0.560737	0.097	1.143336	0.090387	1.002708	0.049442	1.948071
836_18_1	0.580763	0.095	1.144733	0.090768	0.974234	0.049762	1.932721
836_18_1	0.600789	0.097	0.803288	0.081967	0.980256	0.050758	1.668248
836_18_1	0.620816	0.097	0.892203	0.092169	0.980083	0.050611	1.460978
836_18_1	0.640842	0.097	0.808247	0.084136	0.986186	0.050299	1.59708
836_18_1	0.660868	0.095	1.205582	0.095768	0.998563	0.049824	1.824664
836_18_1	0.680895	0.097	1.08191	0.087203	1.017216	0.049185	1.985294
836_18_1	0.700921	0.097	0.981255	0.08028	1.042144	0.048383	2.131704
836_18_1	0.720947	0.097	1.196937	0.08576			2.273078
836_18_1	0.740974	0.095	1.086481	0.082153			2.248261

Appendix 2-6. Alternate data analysis tests and results

Differences were observed in growth ring quality amongst samples, so an alternate analysis was completed with the trawl survey samples to separate the highest quality samples and determine if data patterns were stronger. To assess image and sample quality, a quality scale was used on each sample, based on clarity of growth rings and ability to measure an accurate stem diameter from the cross-section images. Each sample was given a number 0-3, meaning the following: 0; growth rings are not legible and measurements for diameter/radius are inconsistent across the axis, sample should be removed from data analysis, 1; growth rings are legible, but are read with great difficulty, and material between the growth rings makes it difficult to attain an accurate diameter/radius measurement, 2; growth rings are legible and likely accurate, stem diameter measurement is uniform both laterally and longitudinally, 3; growth rings are very legible and pronounced, and no difficulty in counting growth rings. Due to weak relationships observed between size metrics (height, width, stem diameter, area), and both major and minor rings, we assigned a quality measurement for each sample, and attempted analyses again only with samples given a quality rating of 2-3.

Another attempt to analyze the data and observe stronger relationships between size metrics and major/minor growth rings with the DFO trawl survey samples included removing samples with a standard error (SE) greater than the median SE for major/minor ring counts (averaged counts from the 3 counters). SE was determined with the following formula:

$$\text{Standard deviation } (x1, x2, x3) / \sqrt{3}$$

Any sample with a SE greater than the median SE (0.9 for major rings; 4.0 for minor rings), was removed for the additional sample analyses. All size metric comparison analyses described above were calculated again without these samples. After all approaches were completed, R^2 and p-values were compared for the different analysis approaches used.

Due to the weak relationships observed with the size metric data and all colonies, the highest quality samples were analyzed separately. The best quality samples (n = 56, "Q" rating of 2 or 3) from the DFO sample set, compared with size metric data, showed stronger relationships based on R^2 values for some of the size metrics, which varied for age based on major or minor rings. The size metrics that showed improved relationships included height for both age estimates, area for age based on minor rings, stem diameter for age based on minor rings, root length for both age estimates, and stem length for age based on minor rings. The type of regression that had the highest R^2 value was not consistent between the analysis with all colonies and the analysis of only the "quality" samples.

Further comparisons were made between samples with a SE less than or equal to 0.9 for major rings and a SE less than or equal to 4.0 for minor rings (now termed the "standard error" calculation). Based on the standard error calculations, R^2 values were also higher for some of the size metrics with age estimates when compared to the calculations with all colonies. These included height for both age estimates, width for both age estimates, area for both age estimates, stem diameter for age based on major rings , root length for both age estimates, and stem length for both age estimates. The standard error

analyses also showed different types of regressions with the highest R^2 values when compared to analyses with all colonies.

Based on the three different analyses of size metrics and *A. arbuscula* colonies (all colonies, quality, and standard error), the highest R^2 value from all three analyses varied for each size metric. The only size metric with all colonies showing the highest R^2 value for both age estimates was wet weight, which may not be the most reliable size metric. The quality calculations showed the highest R^2 values for height and stem diameter with age based on major rings, and root length and stem length with age based on minor rings. Standard error calculations showed the highest R^2 values for width, area, and stem diameter with age based on minor rings. Quality and standard error analyses also showed significant relationships for age and radial growth rate with these analyses having stronger significance values, while axial growth rate analyses were not significant for the quality assessment and were significant yet showed a weaker relationship for standard error.

Additional analyses with select colonies from the overall sample set (quality, standard deviation) showed similar trends of higher significance values for R^2 calculations based on major ring count determinations of age. Exceptions to this included four size metrics for the quality calculations and one size metric for the standard deviation calculation. With these exceptions, R^2 values were higher for age based on minor ring counts when compared to the size metrics. However, the age based on major ring counts showed higher significance values within the overall sample set and also within the majority of the additional calculations.

Figure A2-6.1. *Acanella arbuscula* samples from this study compared with height in different analyses. Top row of plots represent age based on major rings and the bottom row of plots represent age based on minor rings. The columns are labeled as which analysis was conducted for each plot, with "All colonies" representing the entire dataset (circle points), "Quality" representing samples with quality ratings of 2 or 3 on a 0-3 scale (triangle points), and "Standard Error" representing samples with a major ring standard error less than or equal to the median of 0.9, and a minor ring standard error less than or equal to the median of 4.0 (square points).
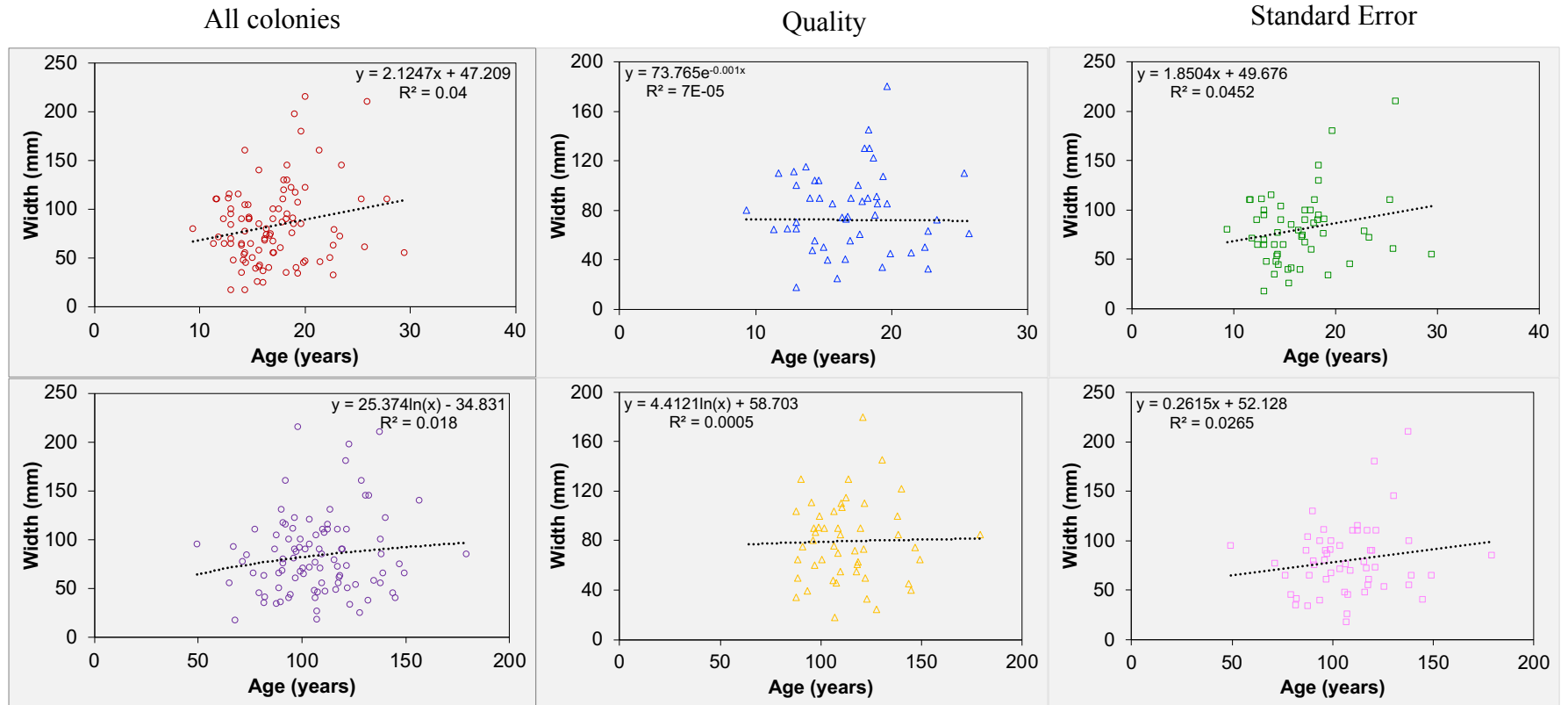
Figure A2-6.2. *Acanella arbuscula* samples from this study compared with width in different analyses. Top row of plots represent age based on major rings and the bottom row of plots represent age based on minor rings. The columns are labeled as which analysis was conducted for each plot, with "All colonies" representing the entire dataset (circle points), "Quality" representing samples with quality ratings of 2 or 3 on a 0-3 scale (triangle points), and "Standard Error" representing samples with a major ring standard error less than or equal to the median of 0.9, and a minor ring standard error less than or equal to the median of 4.0 (square points).
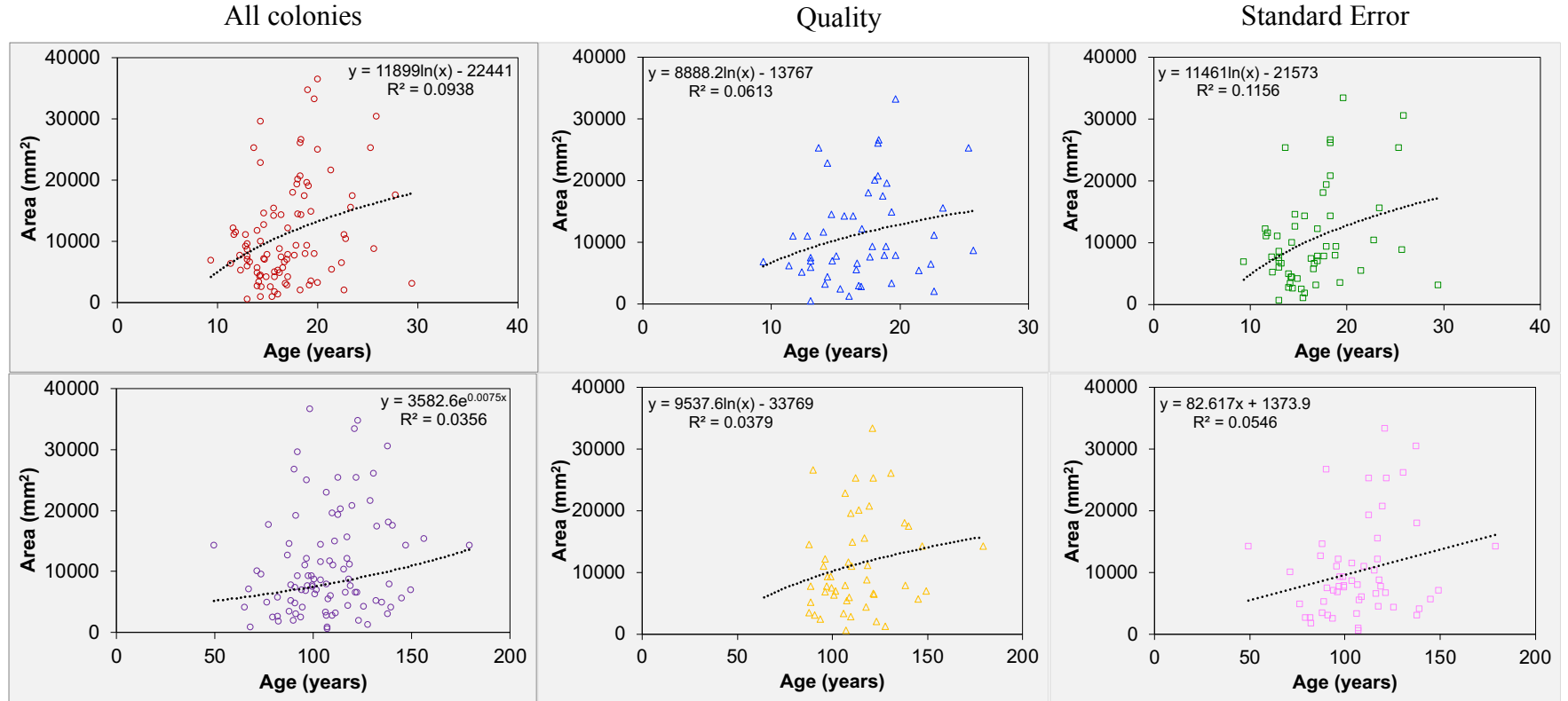
Figure A2-6.3. *Acanella arbuscula* samples from this study compared with area (height * width) in different analyses. Top row of plots represent age based on major rings and the bottom row of plots represent age based on minor rings. The columns are labeled as which analysis was conducted for each plot, with "All colonies" representing the entire dataset (circle points), "Quality" representing samples with quality ratings of 2 or 3 on a 0-3 scale (triangle points), and "Standard Error" representing samples with a major ring standard error less than or equal to the median of 0.9, and a minor ring standard error less than or equal to the median of 4.0 (square points).
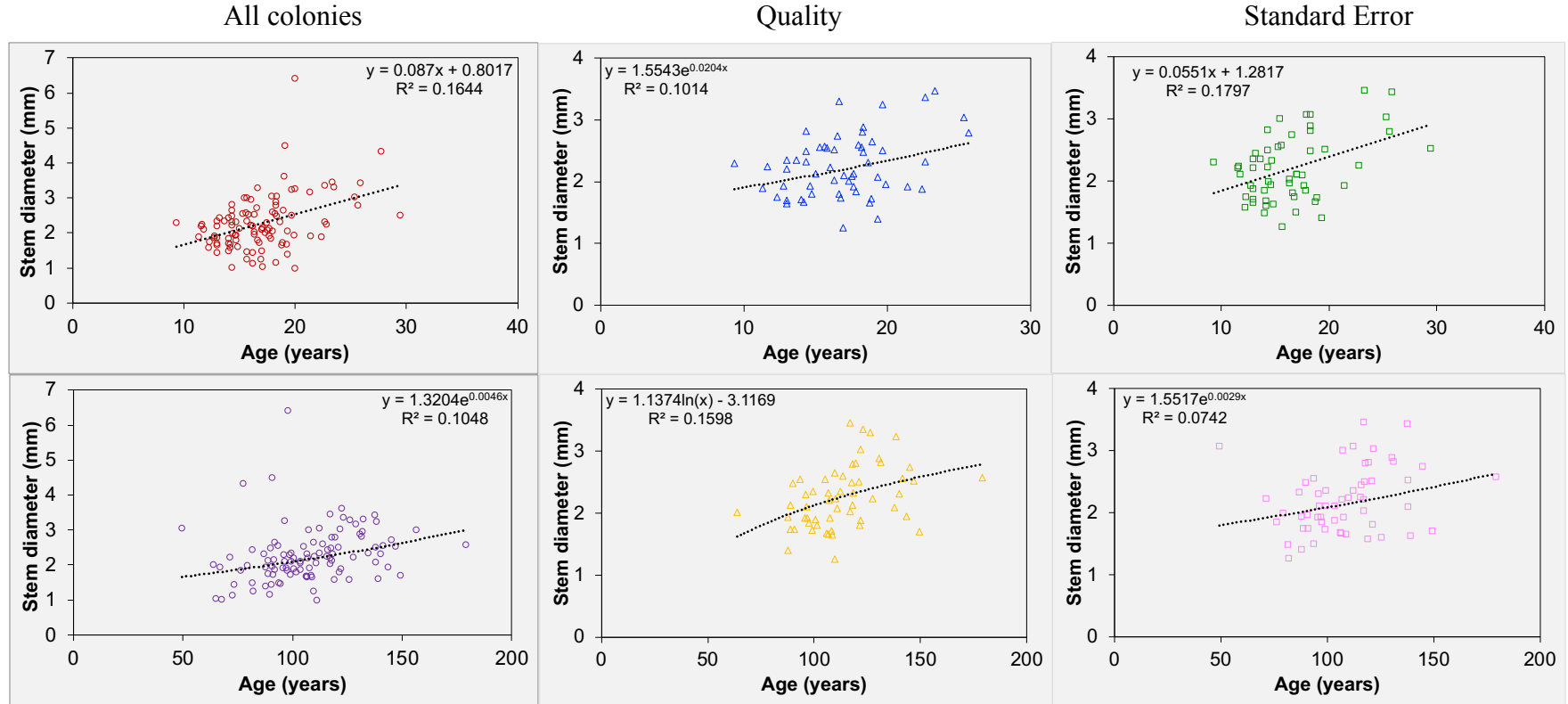
Figure A2-6.4. *Acanella arbuscula* samples from this study compared with stem diameter in different analyses. Top row of plots represent age based on major rings and the bottom row of plots represent age based on minor rings. The columns are labeled as which analysis was conducted for each plot, with "All colonies" representing the entire dataset (circle points), "Quality" representing samples with quality ratings of 2 or 3 on a 0-3 scale (triangle points), and "Standard Error" representing samples with a major ring standard error less than or equal to the median of 0.9, and a minor ring standard error less than or equal to the median of 4.0 (square points).
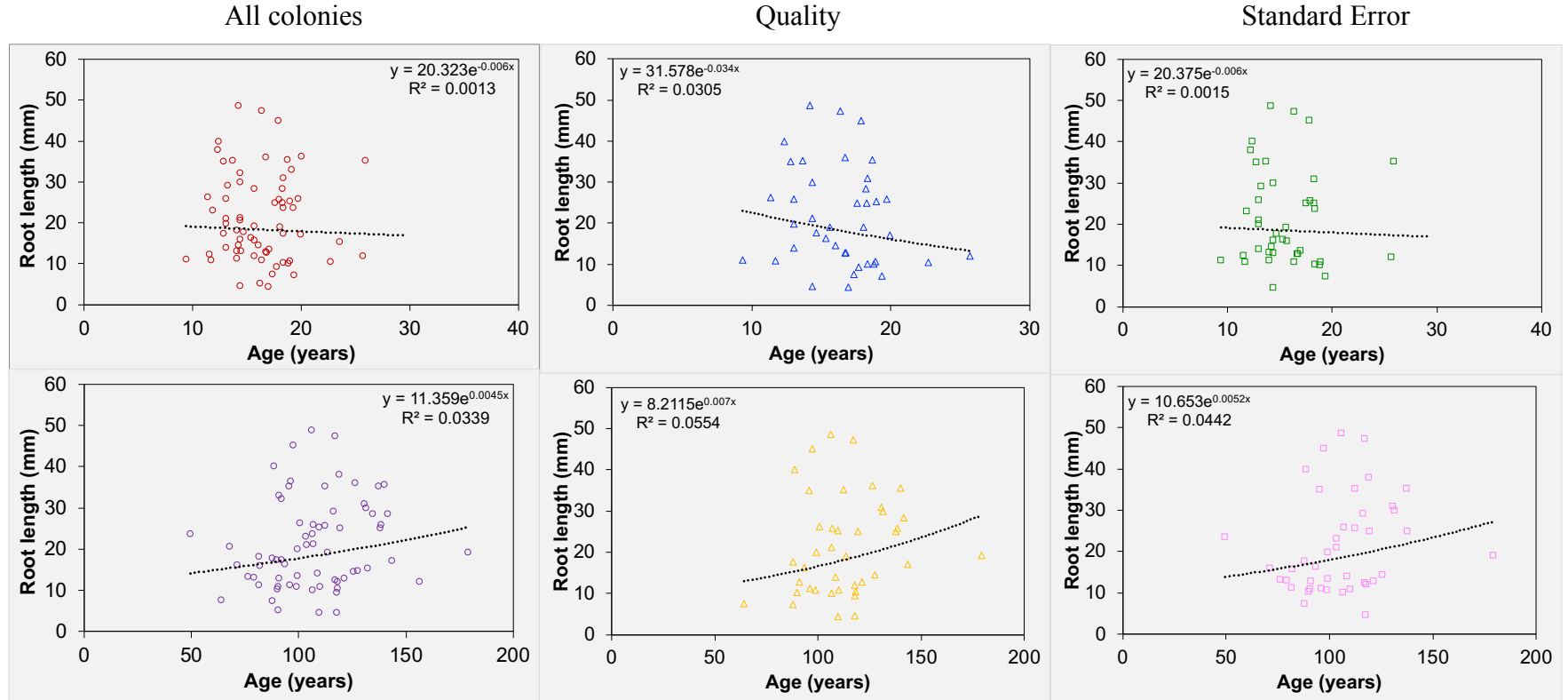
Figure A2-6.5. *Acanella arbuscula* samples from this study compared with colony root length in different analyses. Top row of plots represent age based on major rings and the bottom row of plots represent age based on minor rings. The columns are labeled as which analysis was conducted for each plot, with "All colonies" representing the entire dataset (circle points), "Quality" representing samples with quality ratings of 2 or 3 on a 0-3 scale (triangle points), and "Standard Error" representing samples with a major ring standard error less than or equal to the median of 0.9, and a minor ring standard error less than or equal to the median of 4.0 (square points).
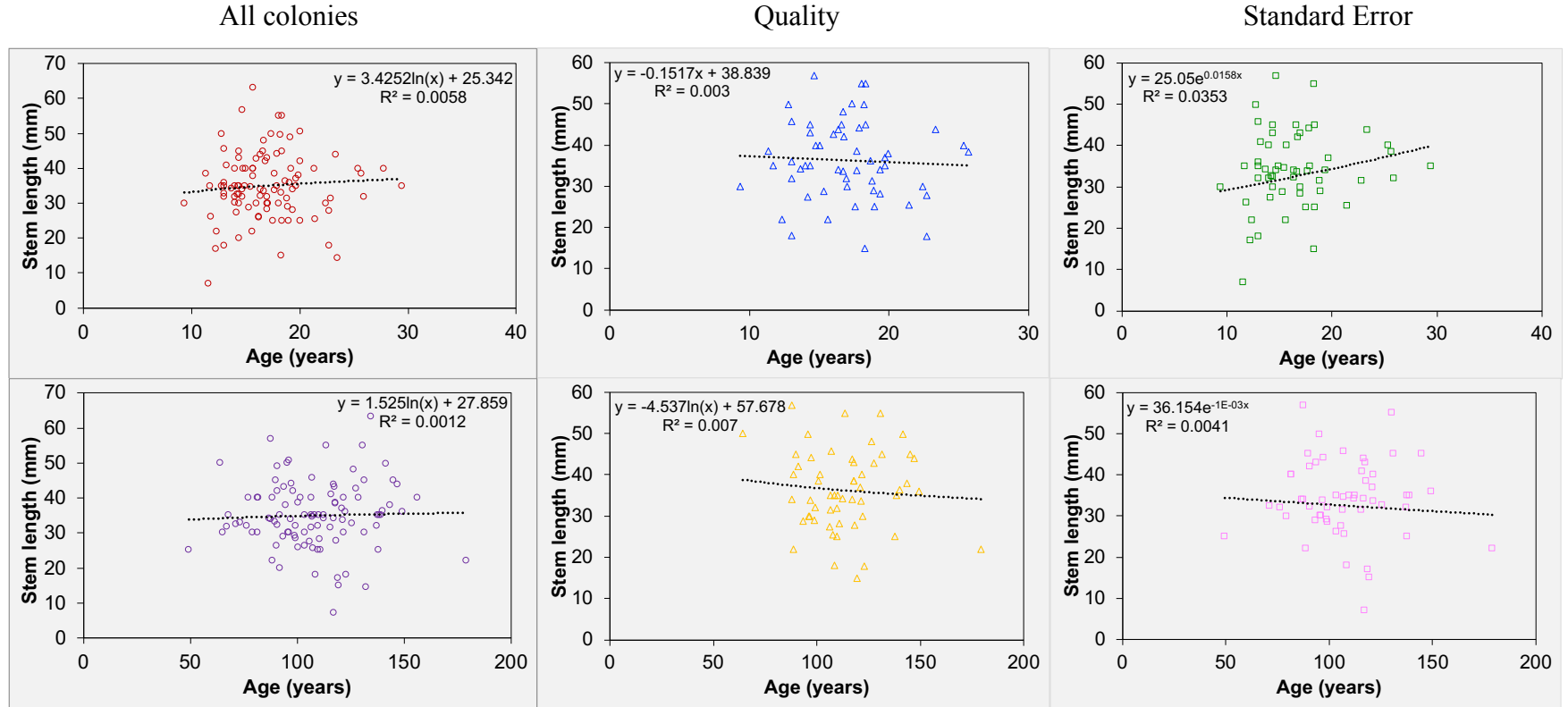
Figure A2-6.6. *Acanella arbuscula* samples from this study compared with colony stem length in different analyses. Top row of plots represent age based on major rings and the bottom row of plots represent age based on minor rings. The columns are labeled as which analysis was conducted for each plot, with "All colonies" representing the entire dataset (circle points), "Quality" representing samples with quality ratings of 2 or 3 on a 0-3 scale (triangle points), and "Standard Error" representing samples with a major ring standard error less than or equal to the median of 0.9, and a minor ring standard error less than or equal to the median of 4.0 (square points).
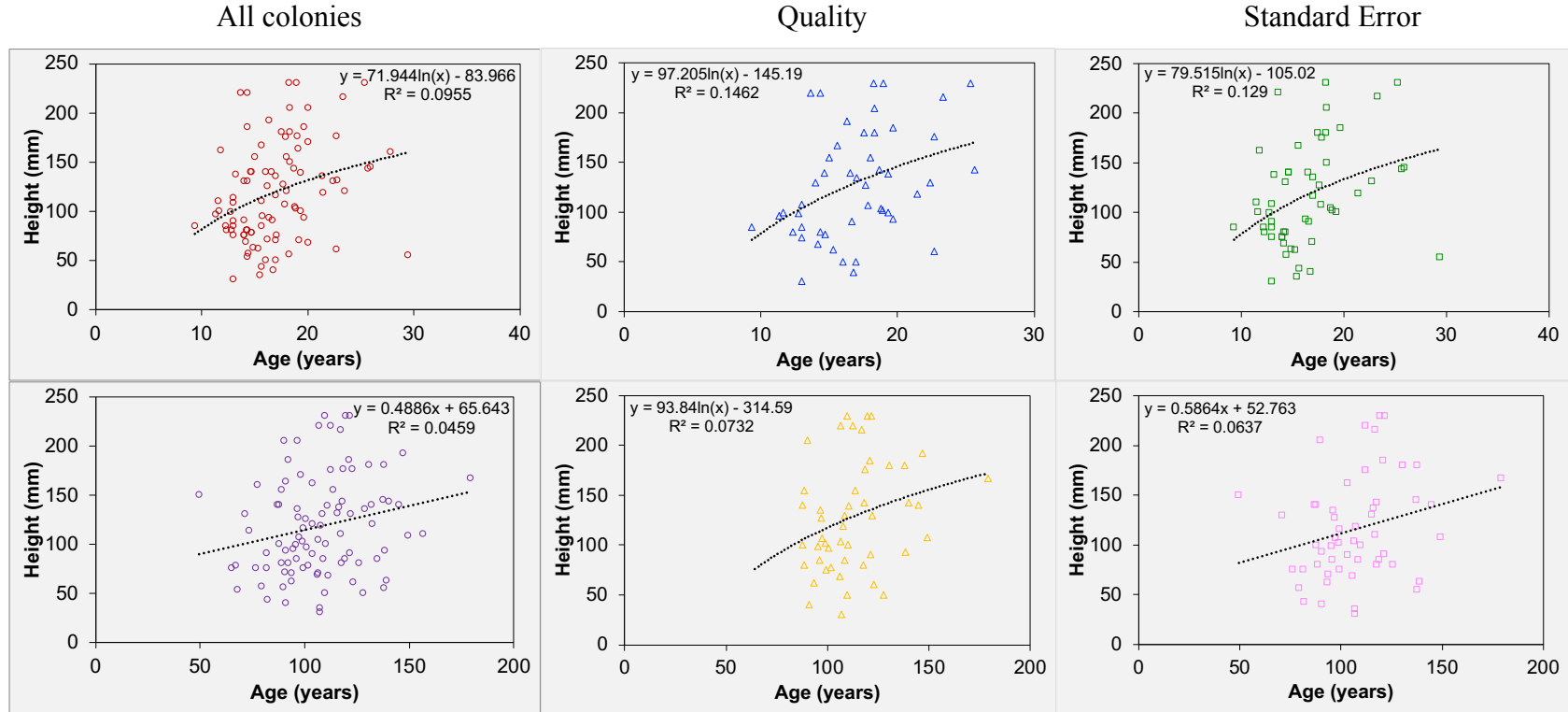
133
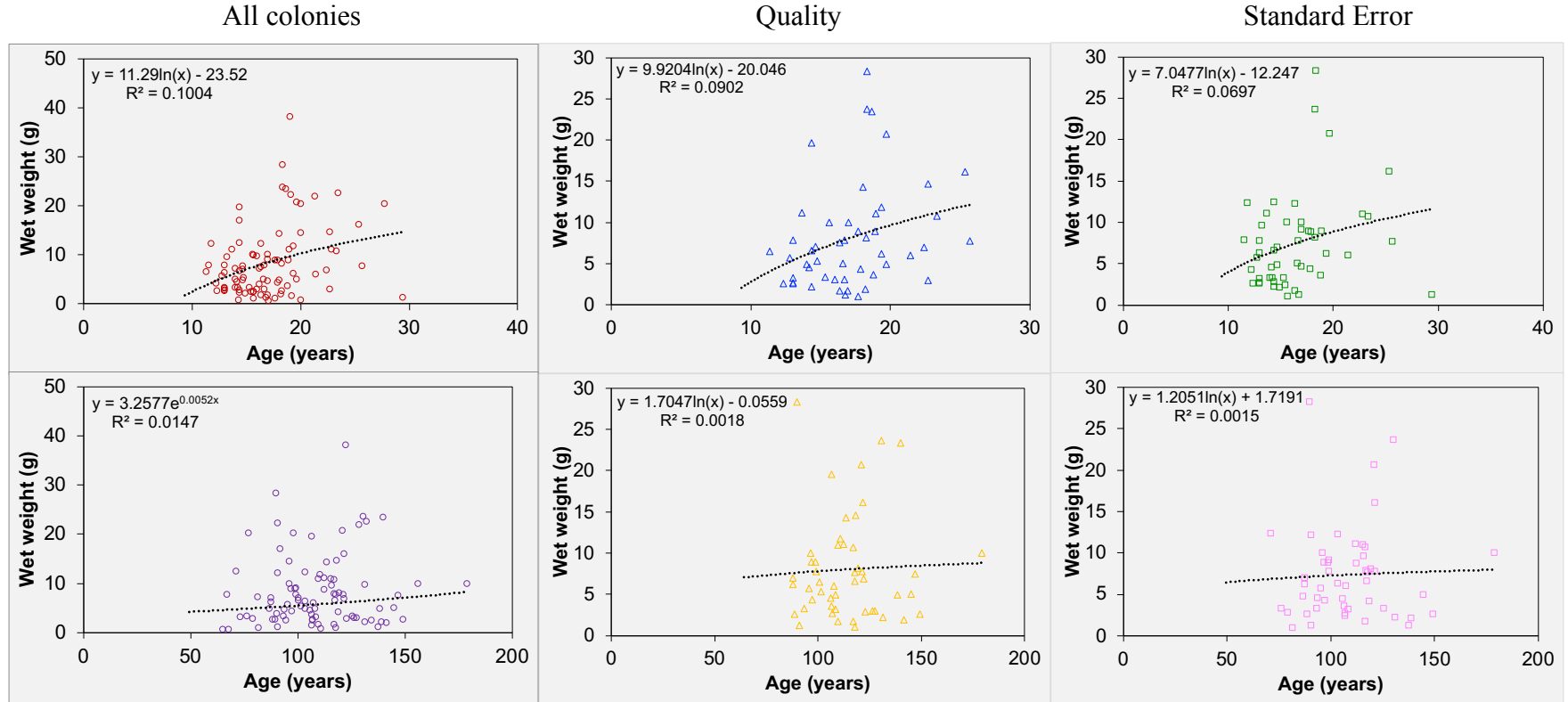
Figure A2-6.7. *Acanella arbuscula* samples from this study compared with wet weight in different analyses. Top row of plots represent age based on major rings and the bottom row of plots represent age based on minor rings. The columns are labeled as which analysis was conducted for each plot, with "All colonies" representing the entire dataset (circle points), "Quality" representing samples with quality ratings of 2 or 3 on a 0-3 scale (triangle points), and "Standard Error" representing samples with a major ring standard error less than or equal to the median of 0.9, and a minor ring standard error less than or equal to the median of 4.0 (square points).
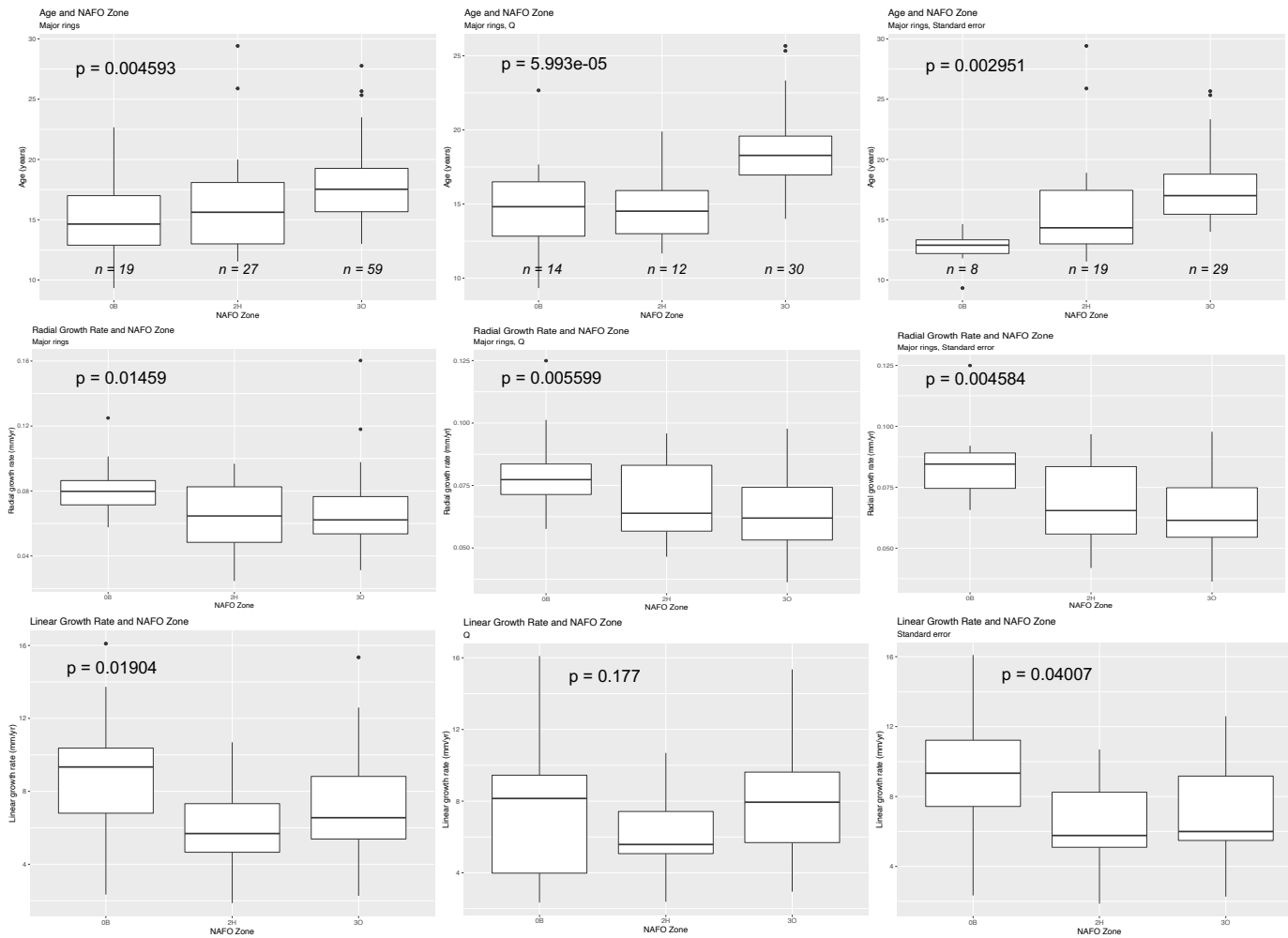
Figure A2-6.8. All *Acanella arbuscula* colonies in the left column, quality samples in the middle column, and standard error in the right column, compared with age, radial growth rate, and axial growth rate for NAFO zones 0B, 2H, and 3O. The black line within each box plot represents the median value.

Table A2-6.1. Age, radial, and axial growth rate analyzed with ANOVA tests for variance between NAFO zones.

ANOVA Test	Age & NAFO zone			R Growth & NAFO zone			A Growth & NAFO zone		
	F	P	D.f	F	P	D.f	F	P	D.f
All samples (major)	5.68	0.0046	2	4.41	0.0146	2	4.14	0.0190	2
Quality (major)	11.75	<0.0005	2	5.72	0.0056	2	1.80	0.177	2
Standard error (major)	6.52	0.0030	2	5.97	0.0046	2	3.43	0.0401	2

Notes & units: For description on ANOVA tests listed, see full methodology in appendices. F = f value, P = p value, and D.f = degrees of freedom. R Growth = radial growth rate (mm/yr) and A Growth = axial growth rate (mm/yr). Major indicates age/growth rate was determined from major ring counts.

Appendix 2-7. Size metric data with apparent age
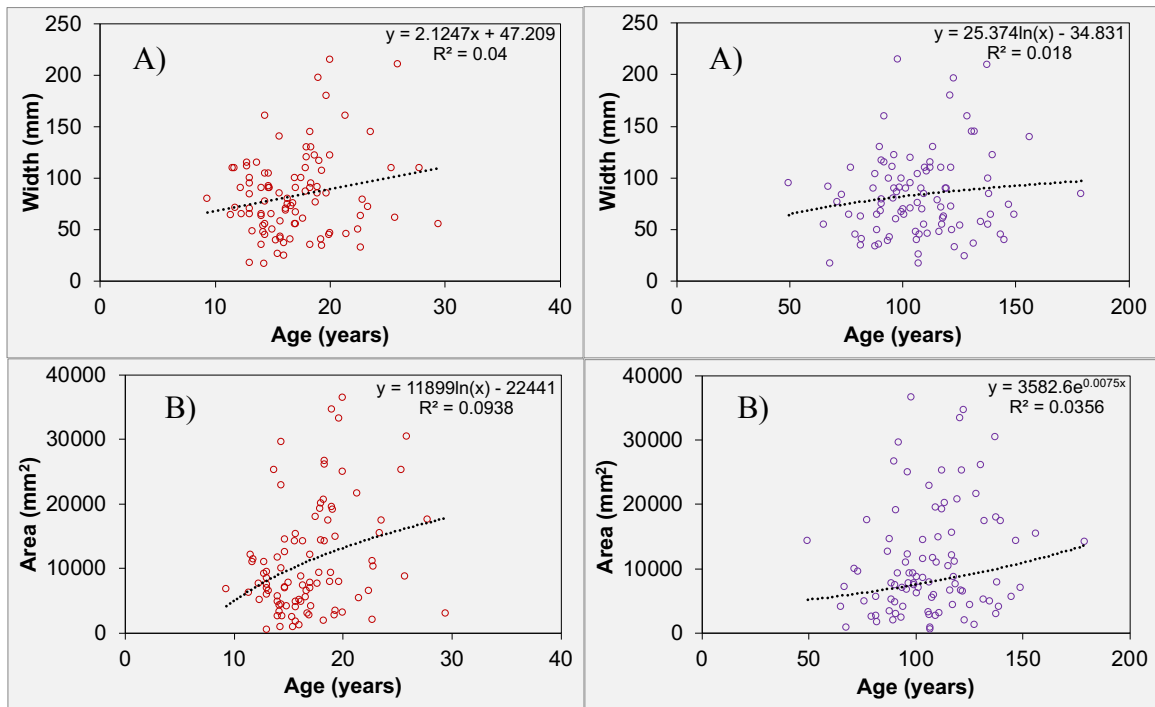
Figure A2-7.1. Ages of *Acanella arbuscula* samples (n=105) from DFO trawl surveys compared to size metrics with linear, logarithmic, or exponential regression lines plotted in black. A) width and B) area (height * width). Plots in the left column with red points are age determined from major ring counts and plots in the right column with purple points are age determined from minor ring counts.
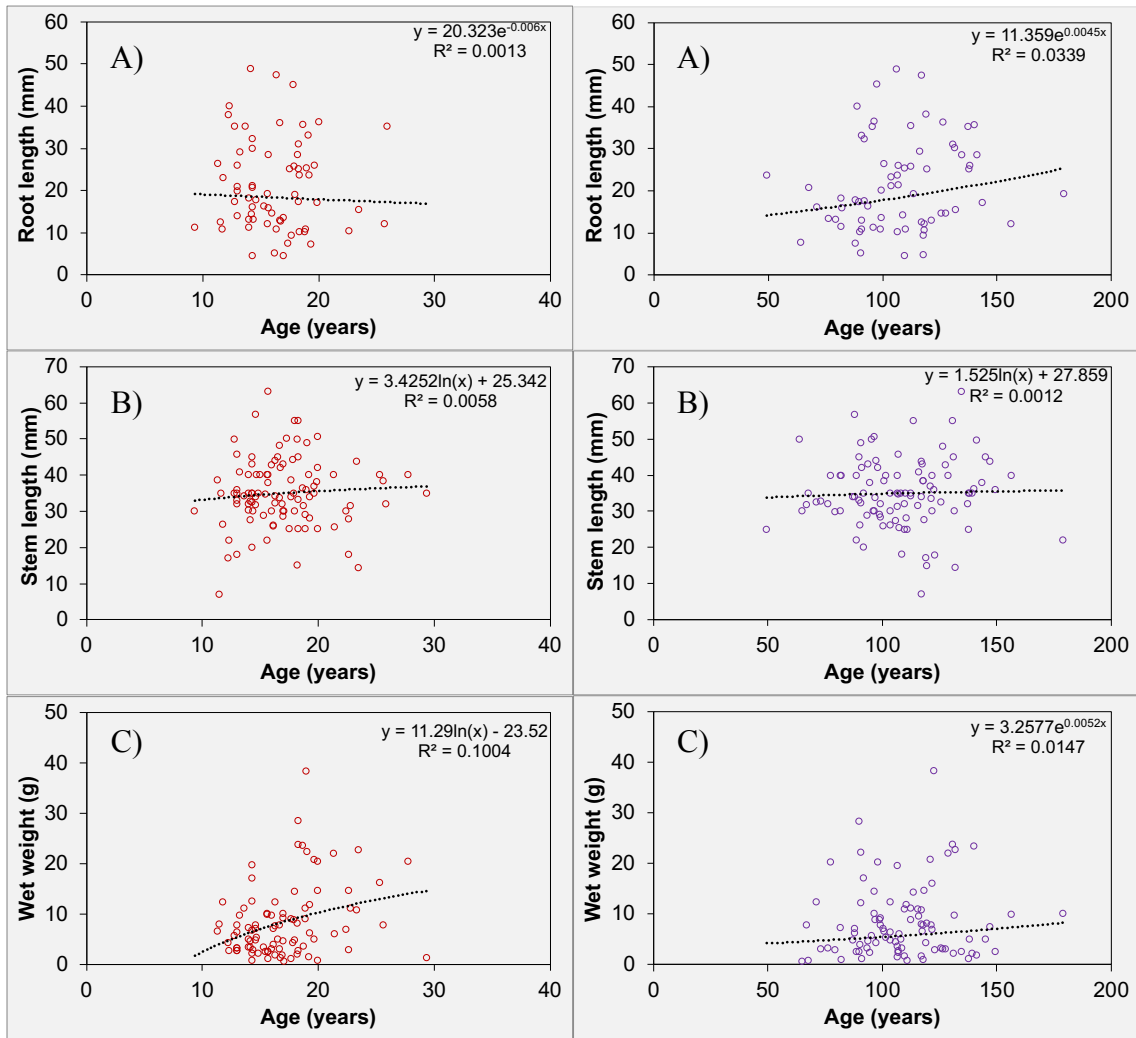
Figure A2-7.2. Ages of *Acanella arbuscula* samples (n=105) from DFO trawl surveys compared to size metrics with linear, logarithmic, or exponential regression lines plotted in black. A) root length, B) stem length, and C) wet weight. Plots in the left column with red points are age determined from major ring counts and plots in the right column with purple points are age determined from minor ring counts.
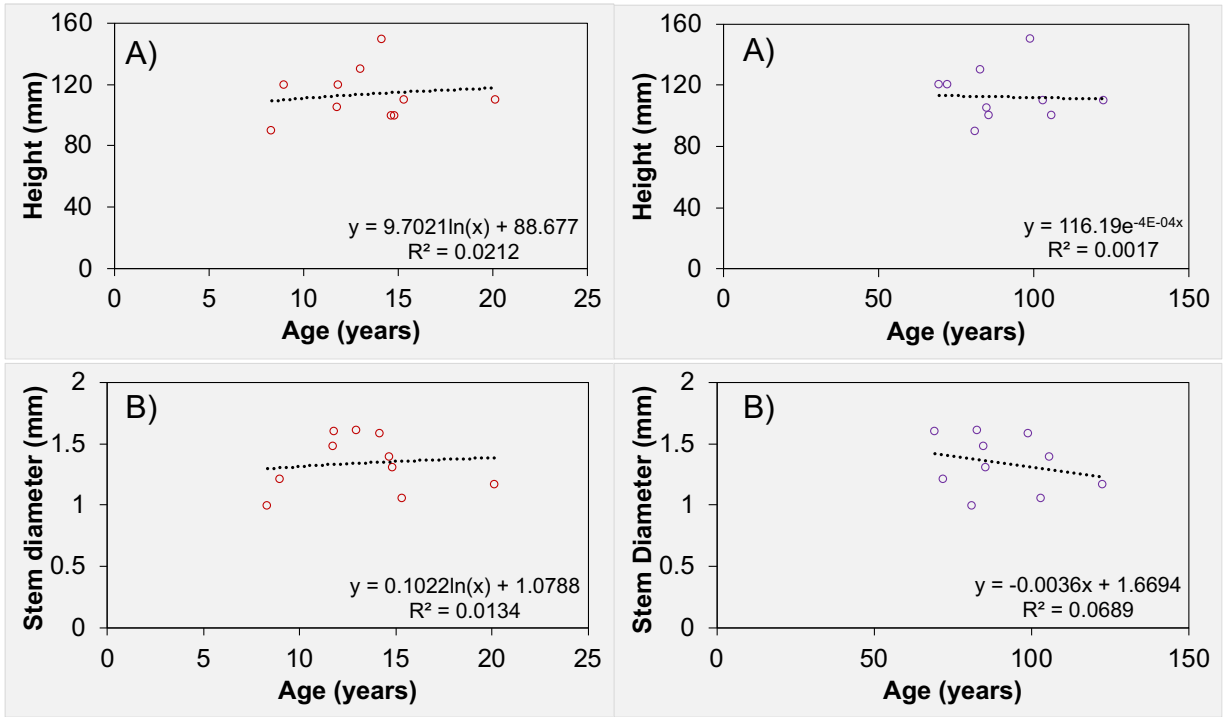
Figure A2-7.3. *Acanella arbuscula* (n = 10) collected in 2021 at Davis Strait compared to size metrics A) height and B) stem diameter. Plots in the left column with red points are age based on major rings and plots in the right column with purple points are age based on minor rings.
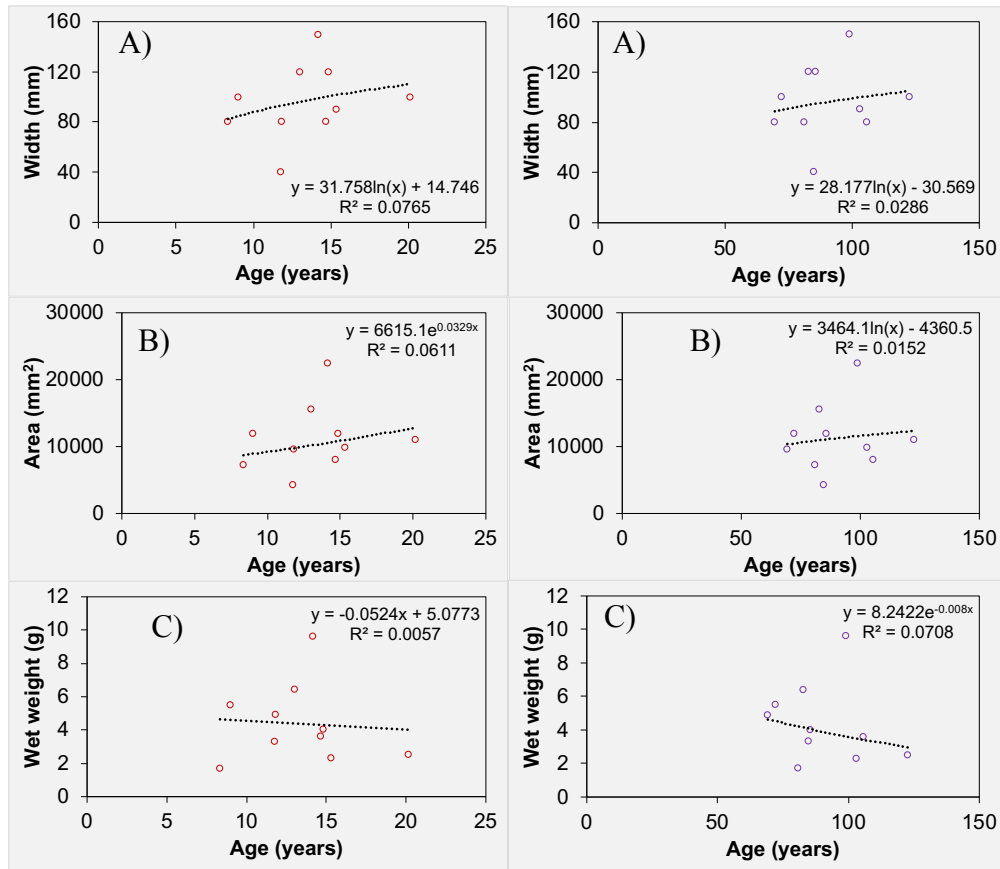
Figure A2-7.4. *Acanella arbuscula* (n = 10) collected in 2021 at Davis Strait compared to size metrics A) width, B) area (height * width), and C) wet weight. Plots in the left column with red points are age based on major rings and plots in the right column with purple points are age based on minor rings.

Appendix 2-8. Size metric data through the origin
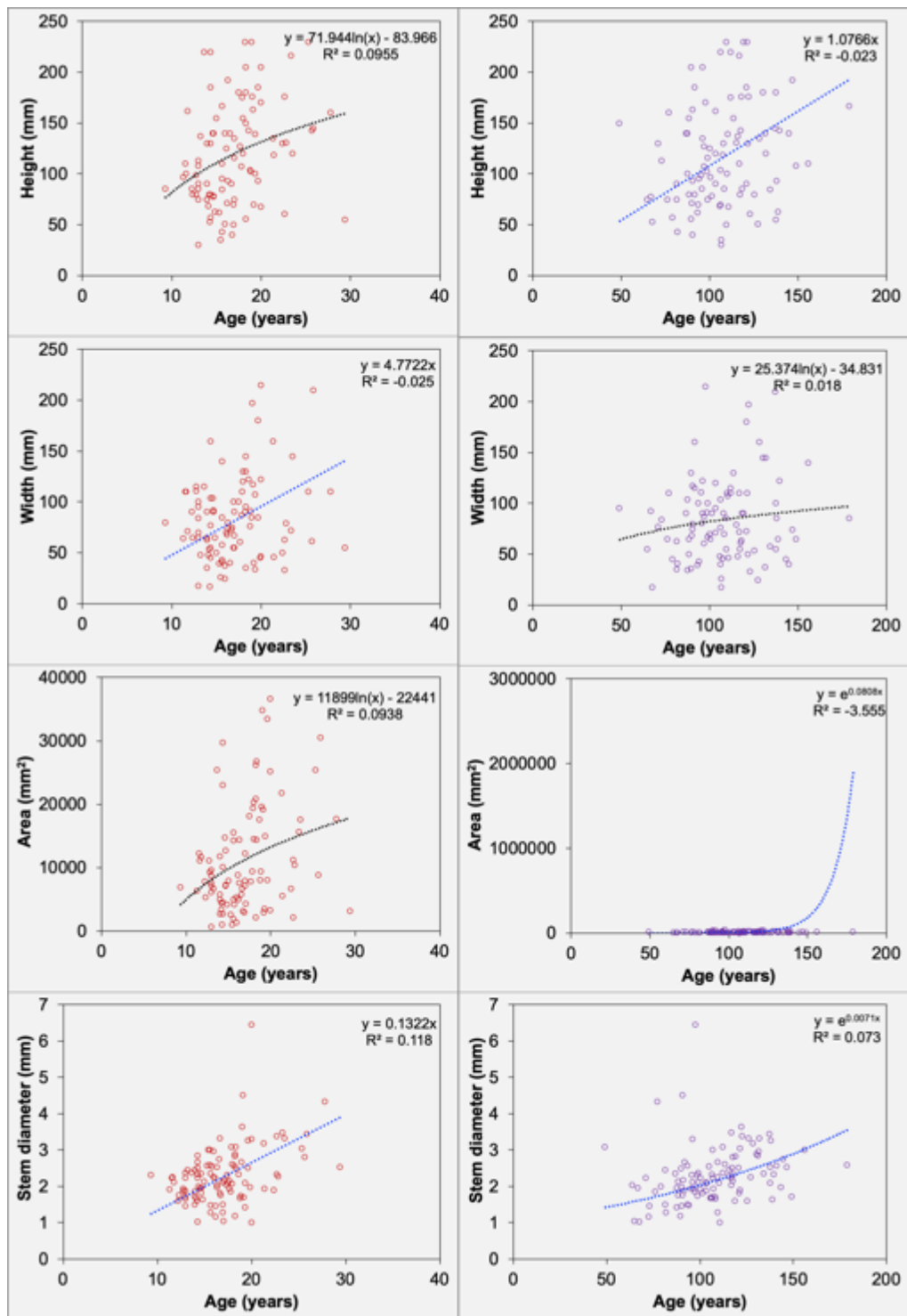
Figure A2-8.1. Some graphs through the origin (blue trend lines) and some not (black trend lines).
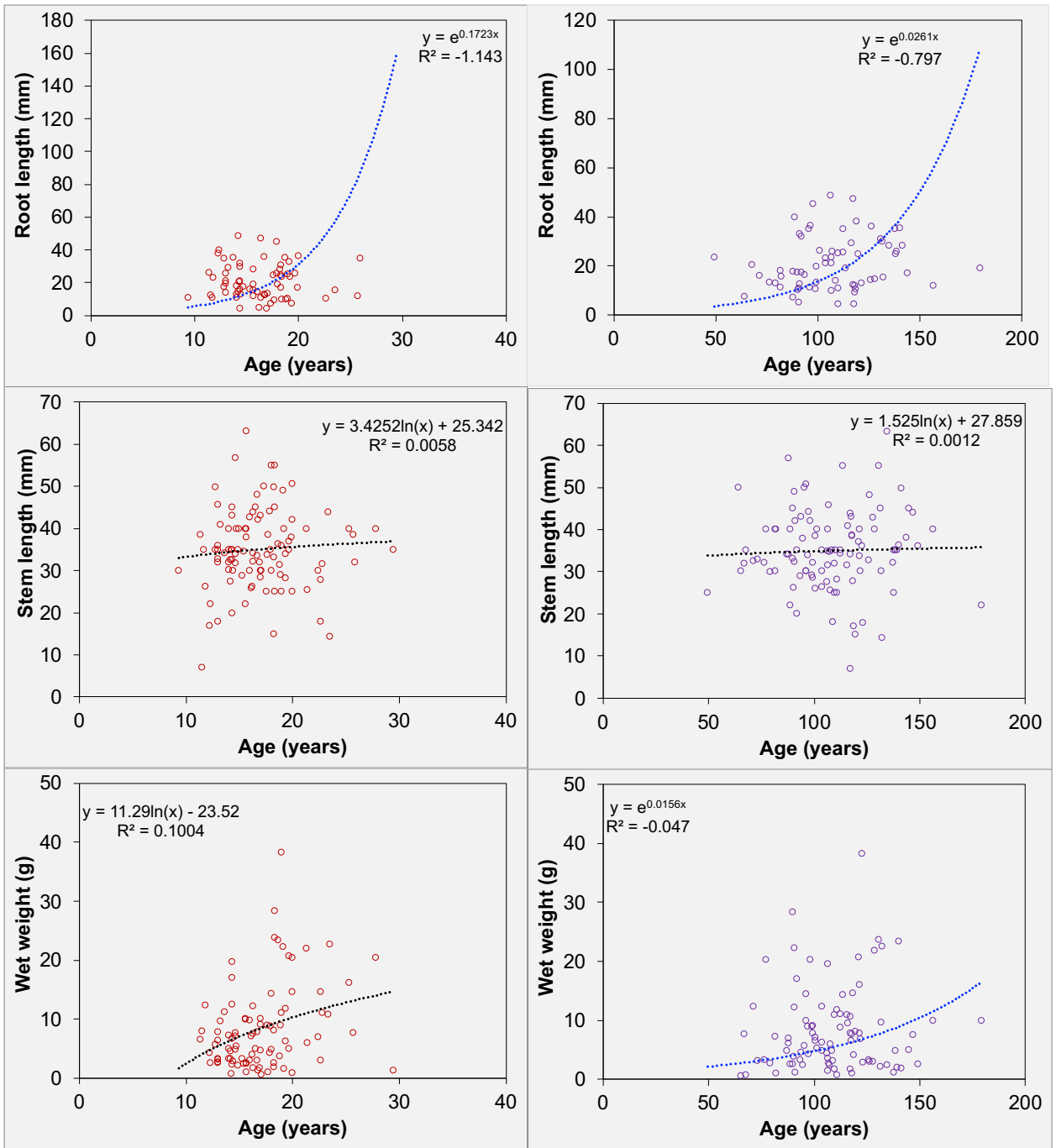
Figure A2-8.2. Some graphs through the origin (blue trend lines) and some not (black trend lines).
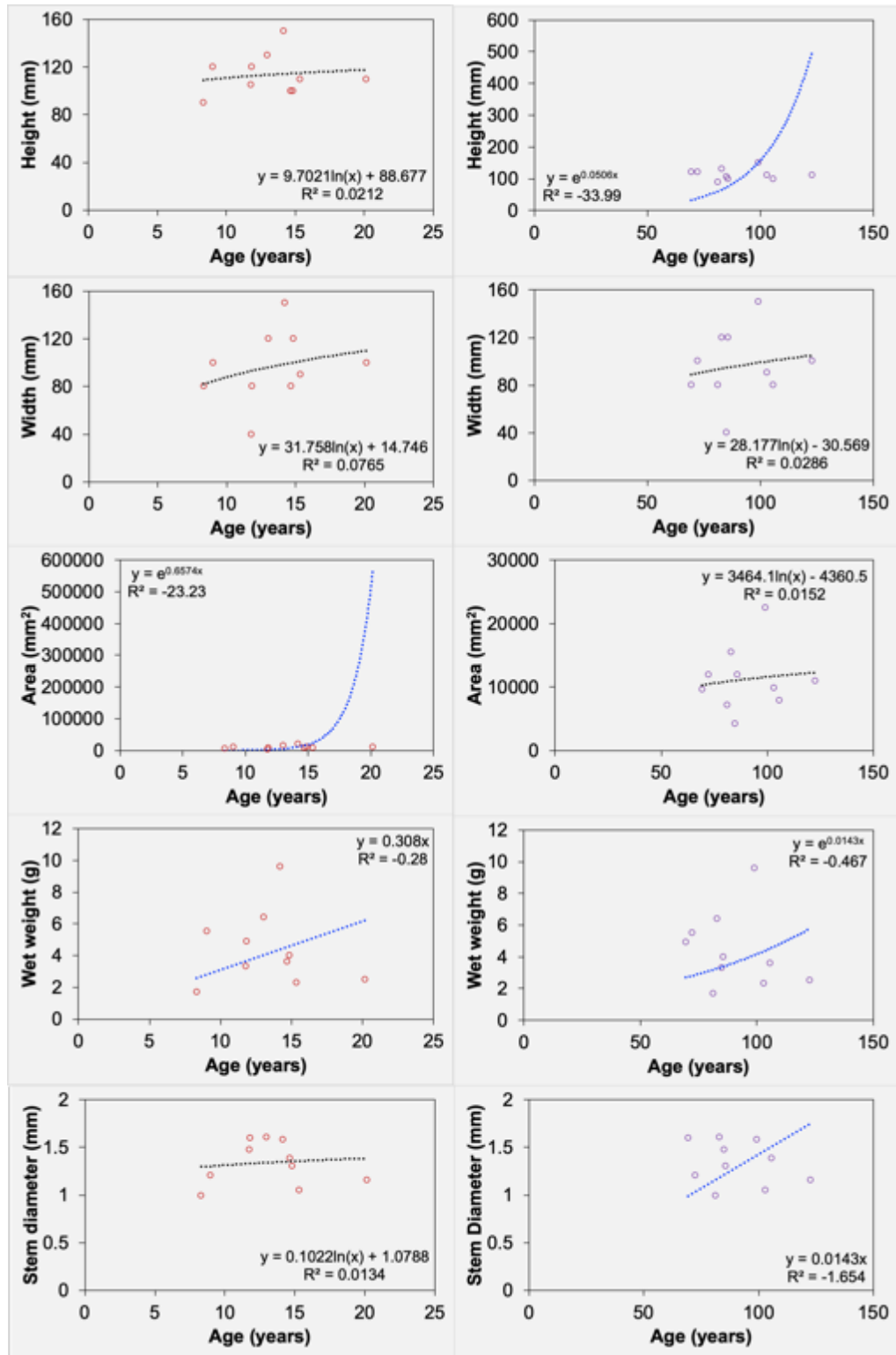
Figure A2-8.3. ROV 2021 samples with some regression lines forced through the origin (shown with blue trendlines).

Appendix 2-9. Growth ring characteristics and images

For some samples, the proteinaceous node did not extend the full sample radius, meaning the distance that growth ring counts were conducted across was also measured, since it was not always the full sample radius. With this measurement, a growth rate was determined by dividing the length of sample measured for growth rings (termed "node radius") by the number of rings counted in that area.

Figure A2-9.1. *A. arbuscula* sample 163_19_1 in thick section imaged with reflected white light. The red circle is showing the separation of protein rings by blurred material, which was observed in many samples.
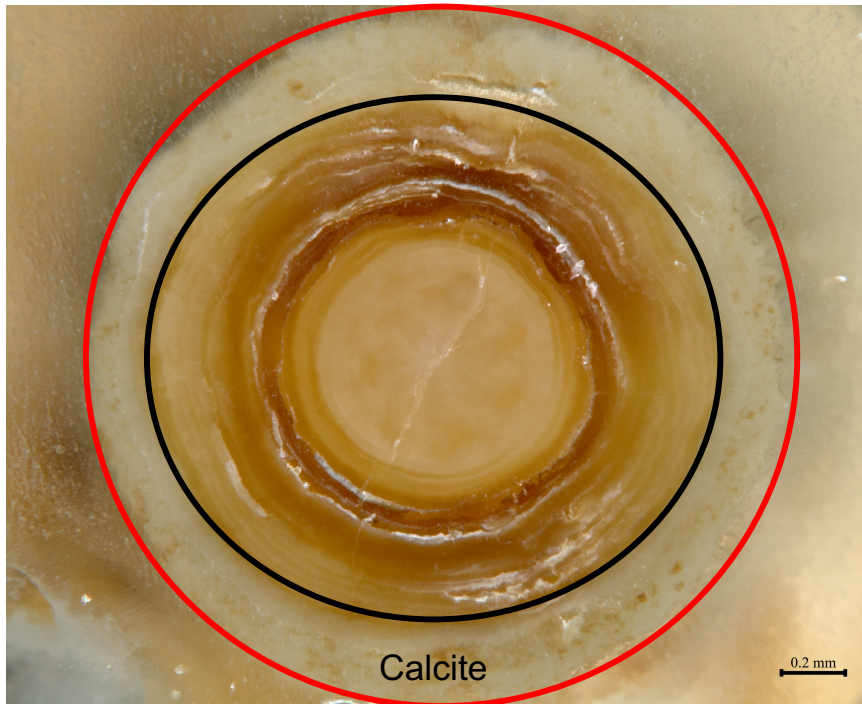
Figure A2-9.2. *A. arbuscula* sample AC 02_3 in thick section imaged with reflected white light. The area in between the black and red circles is showing the calcite material observed on the outside portion of skeleton in some *A. arbuscula* samples from this study.

Figure A2-9.3. *A. arbuscula* sample 894_1_4 in thick section imaged with reflected white light, with non-concentric growth rings on the outer portion of the skeleton.

Appendix 2-10. Scientific trawl survey samples only data analysis

Due to weak improvements observed with the Gompertz and logistic functions, only *A. arbuscula* samples collected in scientific trawl surveys were separated within the dataset and plotted with Gompertz and logistic functions. The Gompertz and logistic functions comparing age and height both showed improvements in fit of the data based on R^2 values, which was 0.1001 for the Gompertz function and 0.1019 for the logistic function. However, stem diameter and age of these select samples did not show improvement in either the Gompertz or logistic function, with R^2 values of 0.1828 and 0.1831, respectively.
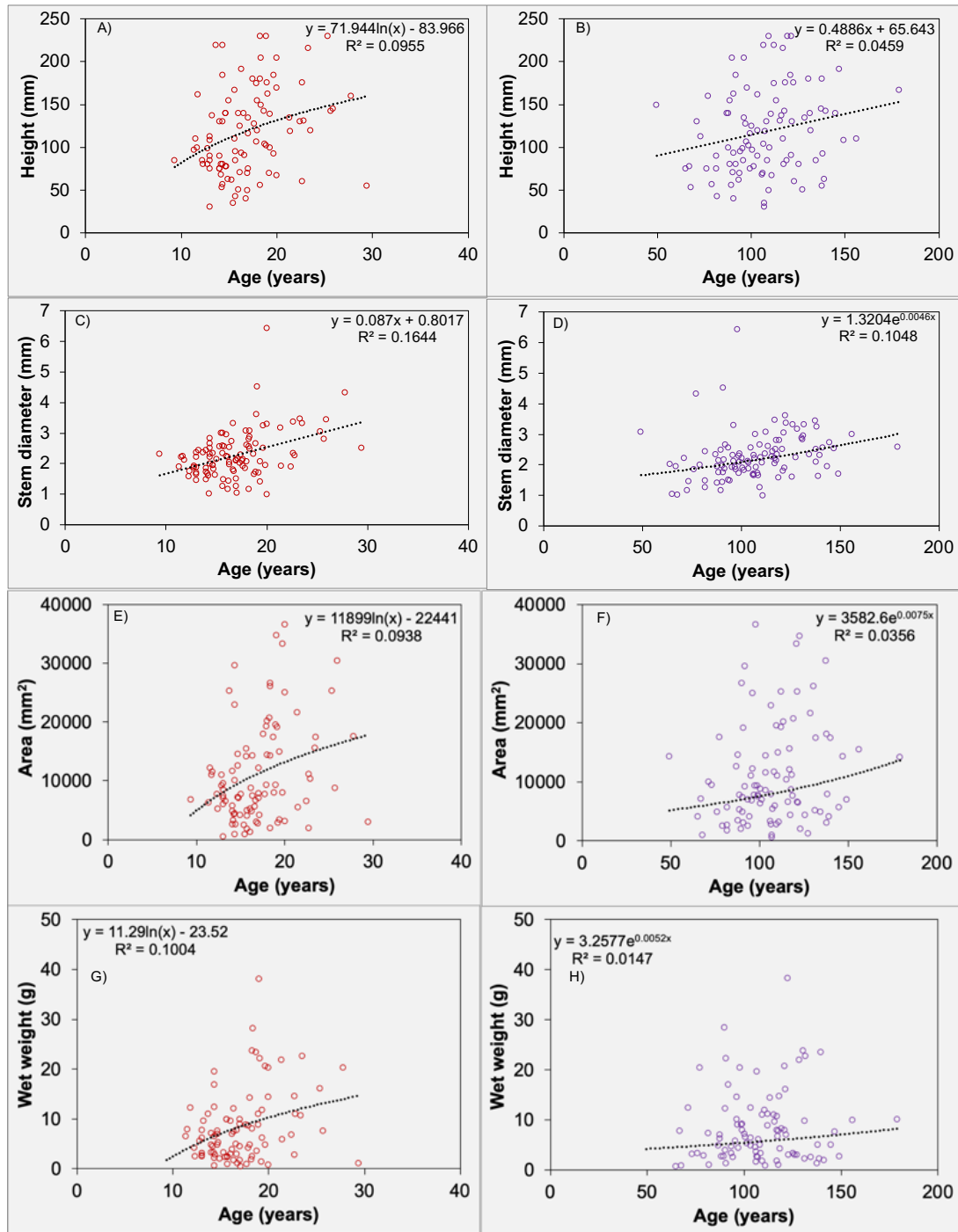
Figure A2-10.1. Ages of *Acanella arbuscula* samples (n=105) from scientific trawl surveys compared to size metrics with linear, logarithmic, or exponential regression lines plotted in black. A) height (major rings), B) height (minor rings), C) stem diameter (major rings), D) stem diameter (minor rings), E) area (major rings), F) area (minor rings), G) wet weight (major rings), H) wet weight (major rings).
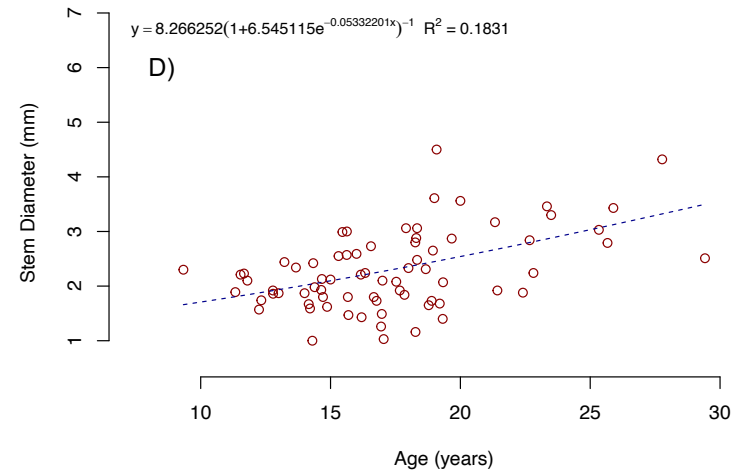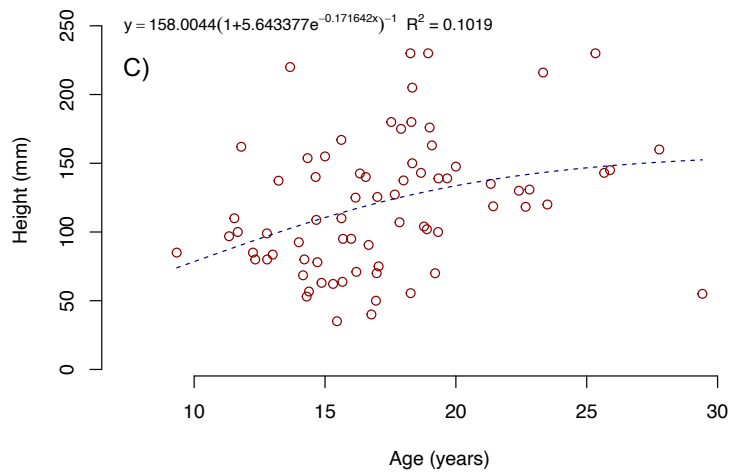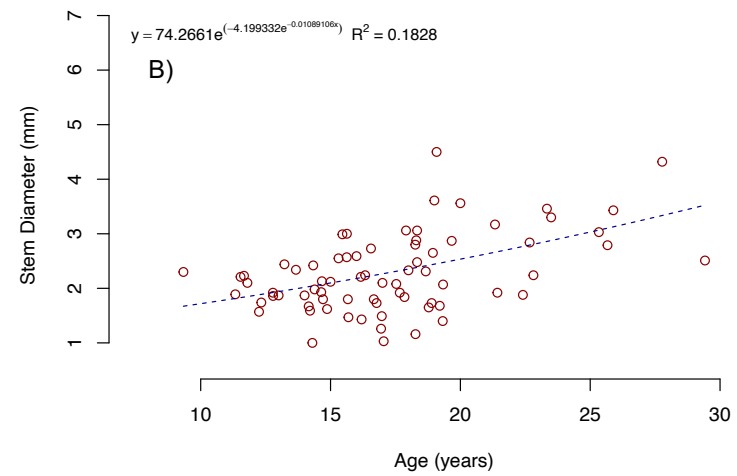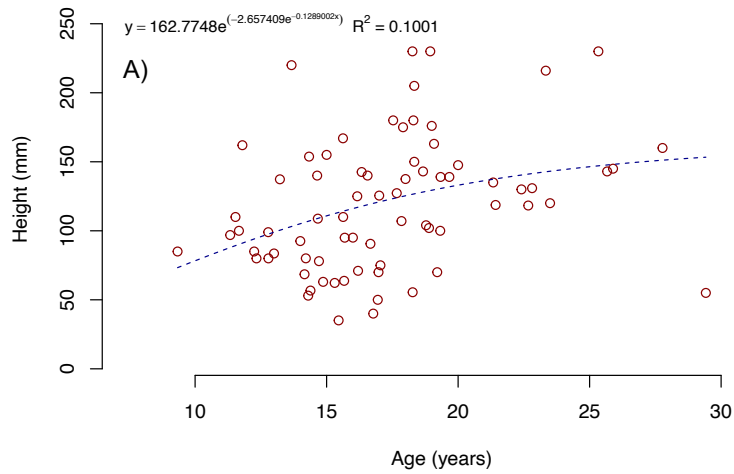
Figure A2-10.2. Age of only *A. arbuscula* samples from scientific trawl surveys, fit with Gompertz growth curves for A) height and B) stem diameter. Data fit to logistic growth curves are also shown for C) height and D) stem diameter.
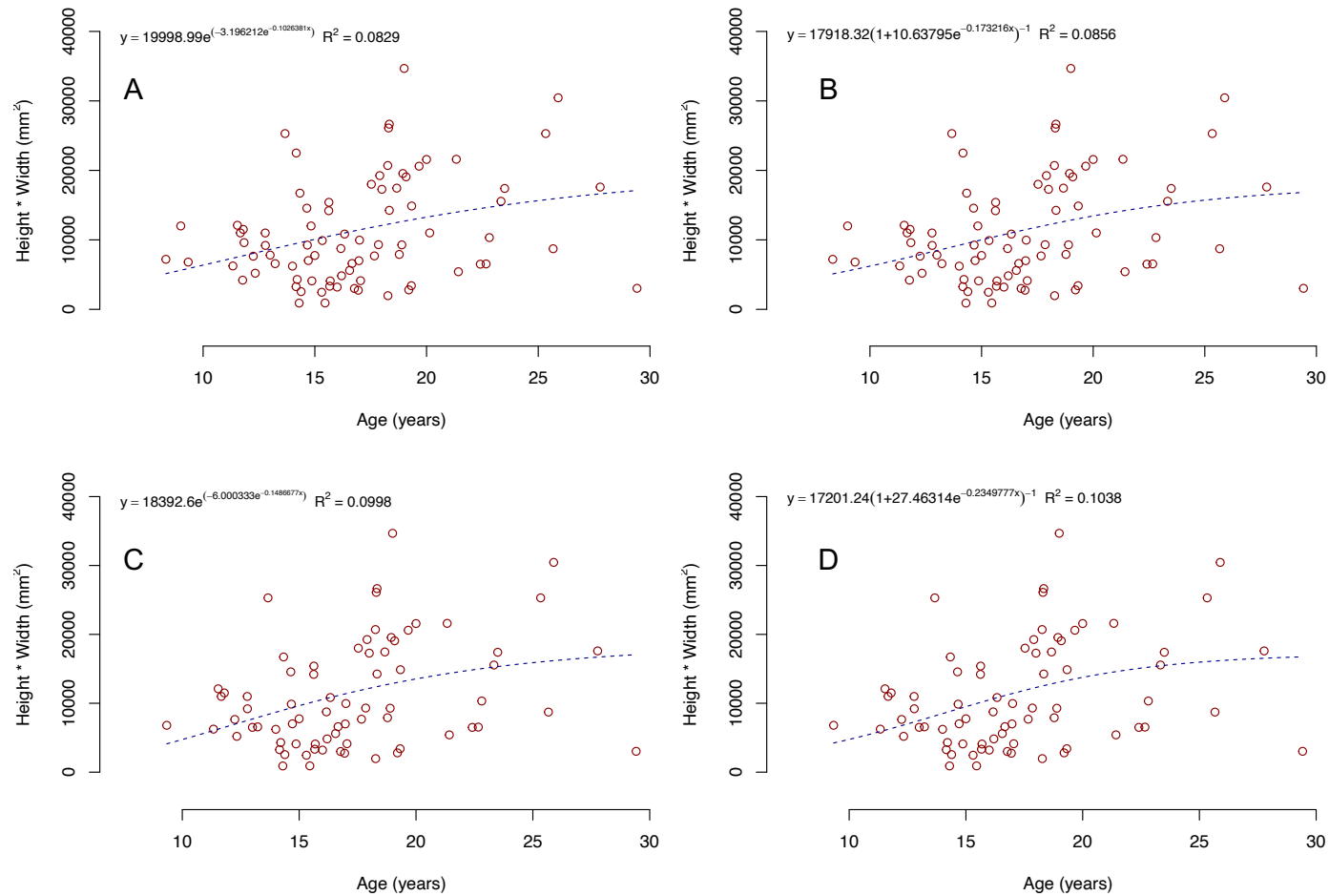
Figure A2-10.3. Height * width (area) compared to age for all *A. arbuscula* samples in this study with A) a Gompertz regression and B) a logistic regression. Height * width (area) compared with age for only *A. arbuscula* collected by scientific trawl surveys with C) a Gompertz regression and D) a logistic regression.
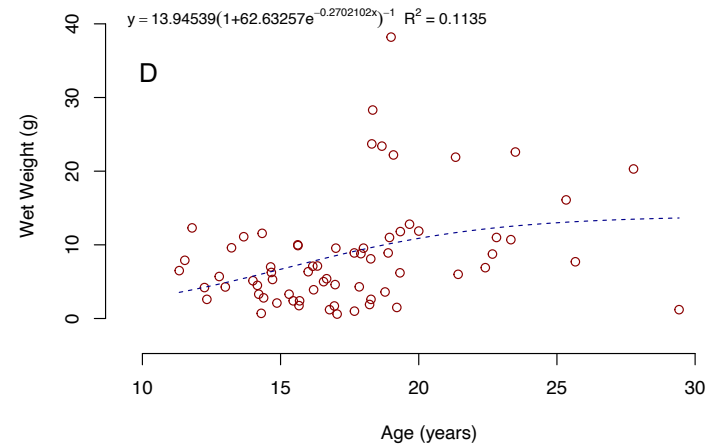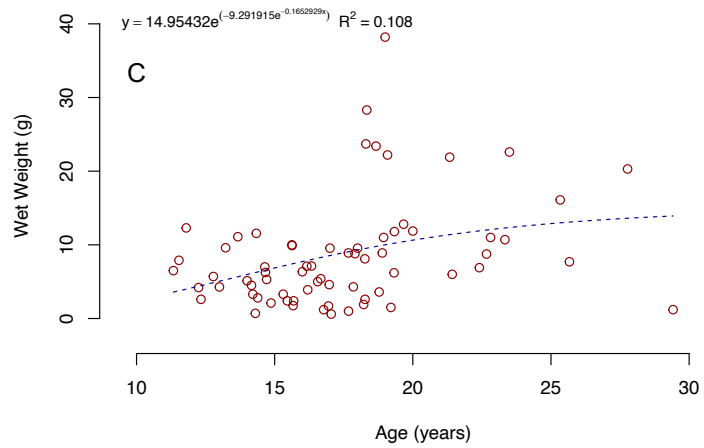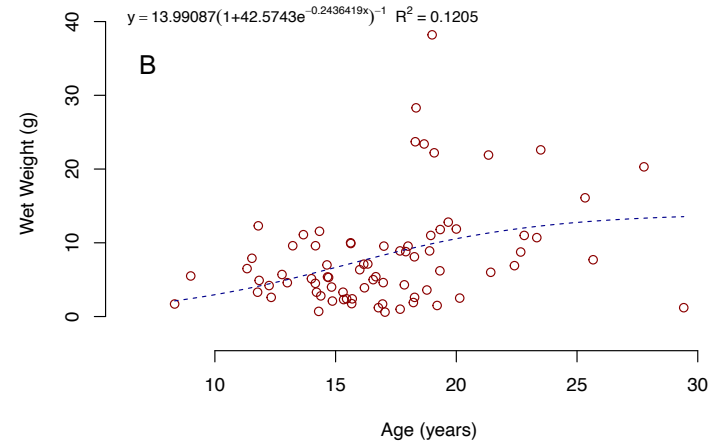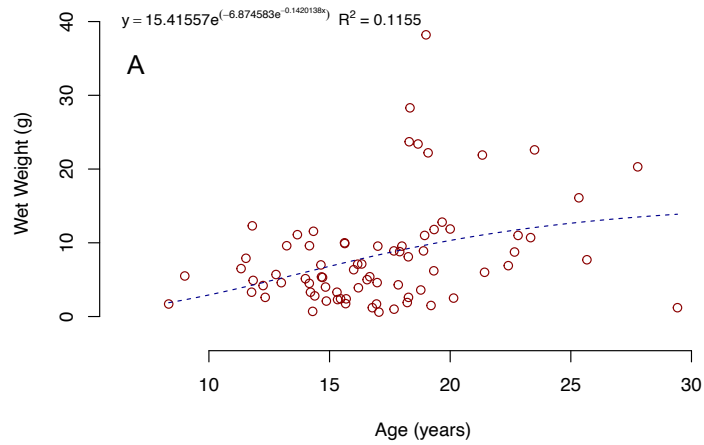
Figure A2-10.4. Wet weight compared to age for all *A. arbuscula* samples in this study with A) a Gompertz regression and B) a logistic regression. Wet weight compared with age for only *A. arbuscula* collected by scientific trawl surveys with C) a Gompertz regression and D) a logistic regression.

Appendix 2-11. Intra-location Supplementary Data

Table A2-11.1. Intra-location standard deviation and standard error values for *Acanella arbuscula* samples.

Trip/Set	Height		Width		Area		Stem Length		Root Length		Wet Weight		Stem Diameter		Rgrowth Rate		Agrowth Rate		Age	
	SD	SE	SD	SE	SD	SE	SD	SE	SD	SE	SD	SE	SD	SE	SD	SE	SD	SE	SD	SE
817_13	22	11	19	9	3992	1996	16	8.17	4.45	2.57	2.19	1.10	0.54	0.24	0.02	0.01	2.28	1.14	2.48	1.11
760_31	29	14	48	24	9802	4901	5.48	2.45	9.84	4.92	11.36	5.08	0.16	0.07	0.01	0.01	1.27	0.63	1.71	0.77
760_37	49	22	62	28	11974	5355	8.91	3.98	4.30	2.48	12.68	5.67	1.47	0.66	0.04	0.02	2.65	1.18	0.47	0.21
836_18	41	18	17	8	5764	2578	6.07	2.72	4.77	2.39	4.47	2.00	0.52	0.23	0.01	0.01	3.63	1.63	5.35	2.39
894_1	37	21	30	18	4198	2424	12.02	5.38	10.33	5.16	1.03	0.46	0.45	0.20	0.02	0.01	2.00	1.16	1.26	0.56
905_38	26	12	15	7	1952	873	4.58	2.05	4.10	2.05	3.02	1.35	0.33	0.15	0.01	0.00	1.50	0.67	1.39	0.62
905_39	15	7	14	6	1927	862	1.59	0.71	2.72	1.22	3.82	1.71	0.31	0.14	0.02	0.01	0.92	0.41	1.27	0.57
915_8	10	5	18	8	2302	1029	3.69	1.65			1.42	0.64	0.37	0.16	0.01	0.00	1.19	0.53	1.96	0.88
933_18	31	14	43	19	7125	3186	5.18	2.32			8.24	3.68	1.07	0.48	0.01	0.01	1.01	0.45	5.28	2.36

Notes and units: SD = standard deviation, SE = standard error, Rgrowth Rate = radial growth rate, Agrowth rate = axial growth rate. Height, width, stem length, root length, stem diameter – mm. Area – mm^2. Wet weight – g. Rgrowth rate and Lgrowth rate – mm/year. Age – years. Blank values represent unavailable data.

Appendix 2-12. Standard deviation measurements from chlorophyll data
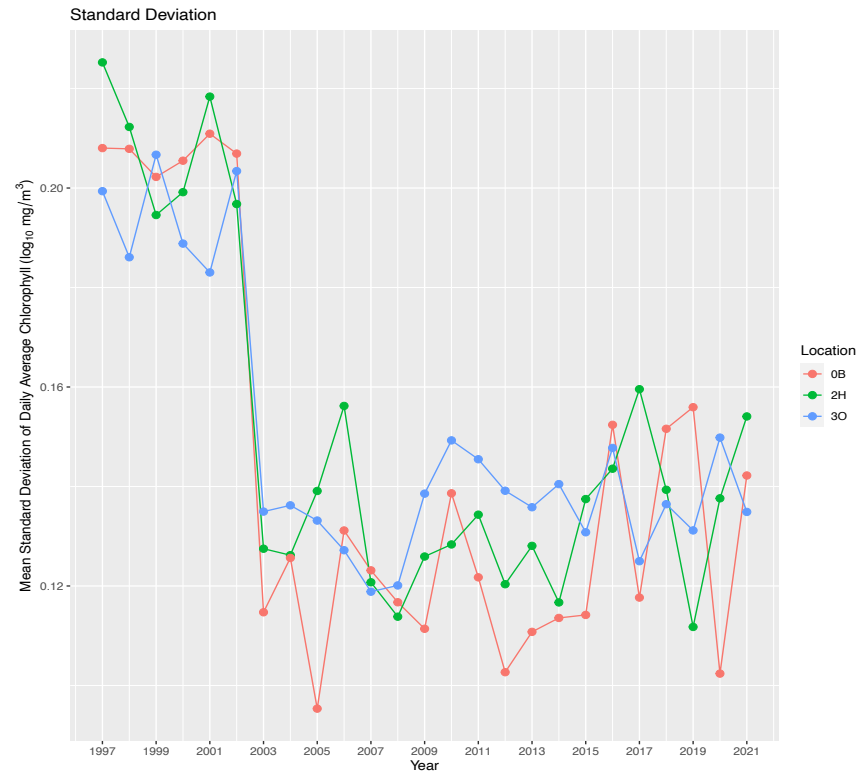
Figure A2-12.1. Comparisons of standard deviation values calculated daily from 1997-2021, and then averaged for each year. Data from years 1997-2002 are from the SeaWiFS satellite and from 2003-2021 are from the MODIS satellite. Location "0B" represents the NCLS in this study (Clay et al. 2021).

CHAPTER 3: Slow growth rates for *Keratoisis flexibilis* in muddy Arctic environments

Author list: Laura Piccirillo[1], Evan Edinger[1,2,3,4], Bárbara de Moura Neves[3,5], Meghan Burchell[1,6], Owen Sherwood[7], Shaomin Chen[7], Graham D. Layne[4]

[1]Environmental Science Program, [2]Department of Geography, [3]Department of Biology, [4]Department of Earth Sciences, Memorial University of Newfoundland and Labrador, St. John's NL, [5]Northwest Atlantic Fisheries Center, Department of Fisheries & Oceans Canada, St. John's NL, [6]Department of Archaeology, Memorial University of Newfoundland and Labrador, St. John's NL, [7]Department of Earth and Environmental Sciences, Dalhousie University, Halifax NS

ABSTRACT

The *Keratoisis* genus, defined by their alternating proteinaceous nodes and calcareous internodes, comprises many of the deep-sea bamboo corals found throughout the NW Atlantic. Two species within the genus (*K. flexibilis; K. grayi*), have been observed in the region attached to different substrates and exhibiting different growth forms, with the former observed in dense coral fields within mud-bottom habitats. *K. flexibilis* colonies have not been studied for growth rates and longevity, which are important indicators to understand when implementing protection measures from anthropogenic disturbances. Eleven *K. flexibilis* colonies were collected from SE Baffin Bay (Disko Fan Marine Refuge) using an ROV in 2021 at ~900m depth. Fragments were collected with a box core at the same location in 2018 to determine longevity and growth rates, and compare these with known ages and growth rates for *K. grayi* from the SW Grand Banks. To age corals, growth ring counts were conducted at the proteinaceous nodes of the coral skeletons. The species exhibited major and minor growth band structures, and minor growth bands were determined to represent annual banding based on age estimate and size metric comparisons with ^{14}C-dated fragments. *K. flexibilis* ages, radial, and axial growth rates ranged from 89-168 years, 0.0073-0.0267 mm/yr, and 1.5-5.3 mm/yr, respectively. Ages were comparable to previously determined *K. grayi* ages, yet radial and axial growth rates were slower for *K. flexibilis*. Data from this study reports that *K. flexibilis* is a long-lived, slow-growing species that forms important benthic habitat in primarily mud-bottom environments. Different locations with similar oceanographic conditions should be explored for observations of the slow-growing species or similar species with the same growth form.

3.1 INTRODUCTION

In the NW Atlantic, gorgonian octocorals are widespread and abundant, and usually found forming complex habitat for other organisms in muddy environments or attached to hard substrate (Gass and Willison 2005; Wareham and Edinger 2007; Neves et al. 2015). Because they are sessile animals with fragile skeletons, often with high longevities and slow growth rates, most deep-sea coral species are vulnerable to disturbance events, such as bottom-contact fishing and oil and gas exploration, in addition to ocean acidification due to climate change (Roberts and Cairns 2014). Bottom-contact fishing activities pose known risks to deep-sea coral species by removing them from their habitats or dislodging them from the seafloor (Fosså et al. 2002).

Bamboo corals are a type of gorgonian octocoral with cosmopolitan distribution, but in the NW Atlantic they have been relatively understudied in terms of growth rates and longevity when compared to larger gorgonian species, like *Primnoa resedaeformis* (Sherwood et al. 2005; Sherwood and Edinger 2009). Bamboo corals are defined by their alternating proteinaceous nodes with calcite internodes, which makes them valuable oceanographic recorders because of their organic and inorganic composition (Sherwood et al. 2008). *K. flexibilis* coral forests have been observed in multiple remotely operated vehicle (ROV) video surveys at Disko Fan within Baffin Bay (Neves et al. 2015), and are conspicuous components of the muddy environment within this location.

Bamboo coral taxonomy is continuously evolving as more species are being observed and studied for genetic differences (Heestand Saucier et al. 2021). With two different species of *Keratoisis* observed in the NW Atlantic (*K. flexibilis*; *K. grayi*),

previous studies have analyzed the biological difference between the species because classifications within the genus have been disputed and revised (France 2007; Watling et al. 2022). DNA sequences of *Keratoisis* colonies from Disko Fan (SE Baffin Bay) confirmed that it is a different species than *K. grayi* (Neves et al. 2015; Watling et al. 2022). While this previous study did not name the *Keratoisis* sp. from Disko Fan, a recent genetic study on the *Keratoisis* genus named the Baffin Bay species *Keratoisis* cf. *flexibilis* (Watling et al. 2022), and it was genetically most similar to *K. grayi*.

To understand bamboo coral growth rates and longevity in the NW Atlantic, the genus *Keratoisis* was explored in this study through sclerochronology. There are two main objectives in this study: First, to determine how long *K. flexibilis* colonies live and how fast they grow, and second to compare *K. flexibilis* growth rates and ages to *Keratoisis grayi* colonies from the SW Grand Banks and NE Saglek Bank. The first objective was met by analyzing box core fragments and colonies collected by ROV from Disko Fan in 2018 and 2021 and conducting growth ring counts and AMS-^{14}C dating. Included in the first objective was determining periodicity of growth rings in the coral skeletons, as this species presents major and minor growth rings. The second objective was met using *K. grayi* colonies previously studied and radiometrically dated for age validation (Sherwood and Edinger 2009), while the *K. flexibilis* colonies collected in 2018 and 2021 were ^{14}C dated and aged with sclerochronology techniques.

3.1.1 *Keratoisis spp.*

Keratoisis spp. have been recorded throughout the NW Atlantic (Gass and Willison 2005; Wareham and Edinger 2007; Baker et al. 2012), with the most frequently documented species in the region being *Keratoisis grayi* (accepted synonym for *Keratoisis ornata*). Globally, *Keratoisis* sp. have been observed in the Northeast Pacific (Andrews et al. 2009), in Australian and New Zealand waters (Thresher et al. 2007; Tracey et al. 2007; Thresher et al. 2009), and in various locations off the eastern US and Nova Scotia, Canada (Farmer et al. 2015).

In the NW Atlantic, *K. grayi* has been primarily observed in the SW Grand Banks attached to hard substrate in solitary formations (Edinger et al. 2011; Baker et al. 2012, 2019), and growth rates and ages for the species have been previously determined (Sherwood and Edinger 2009). *K. grayi* was also previously identified to comprise a large number of gorgonian corals caught in a bottom-trawl from 1999 in SE Baffin Bay (DFO 2007), which failed after only 9 minutes because of coral bycatch, and caused the twine to give out due to the coral weight (DFO 2007). As this report previously identified the corals to be *K. grayi*, it is likely that the species was instead *K. flexibilis*, which was later observed by ROV surveys in 2013 at the same location as the 1999 trawl (Neves et al. 2015). This report reflects on the abundance of *K. flexibilis* in the region forming dense coral fields (Neves et al. 2015), however because of the known trawl activity in the region, many colonies have likely been removed and there is no evidence of recovery for fragments of dead corals in the path of the 1999 trawl (DFO 2007; Neves et al. 2015). This suggests

that *Keratoisis* colonies does not recover quickly from disturbance events, possibly due to slow growth rates.

3.2 MATERIALS & METHODS

3.2.1 Study area & sampling: Disko Fan 2018 box cores

The Disko Fan site visited in 2018 aboard the CCGS *Amundsen* was the same location as previous ROV surveys, which highlighted the extensive existence of the bamboo coral *K. flexibilis* (Neves et al. 2015). The site in 2018 was visited primarily for gravity coring operations, while in 2013 and 2016, ROV surveys were conducted at the site (Fig. 3-1) (Neves et al. 2015). Five gravity cores were collected at the site, aiming for locations through dense portions of the *K. flexibilis* fields, and a singular box core was also collected at the site. The box core was collected at 882m depth, and a 60cm push core was taken from the box core through the section with abundant *K. flexibilis* corals on the surface (Fig. 3-1 and 3-2a). A total of 365g of *K. flexibilis* corals were measured in this box core.

3.2.2 Disko Fan 2021 ROV survey

In 2021, the Disko Fan site visited (N67° 57.9786′, W59° 29.6286′) for the ROV survey was the same location as previous studies (Fig. 3-1) (Neves et al. 2015). This site is located in SE Baffin Bay, in between Baffin Island and SW Greenland. *K. flexibilis* coral fields had been observed previously at this location, but their extent is still unknown.

The Disko Fan ROV survey was conducted on August 2, 2021 at ~900m depth, covering a ~500m transect, which was limited due to strong currents and ice cover. The

transect included video surveying, sampling of corals and other invertebrates, and deploying staining chambers using the "Astrid" ROV aboard the CCGS *Amundsen*. Twelve *K. flexibilis* colonies were collected for aging and growth rate studies, with one sample (R23-1) also being used for boron stable isotope analyses (Williams in prep) (Table 3-1). Most samples were photographed on the seafloor before collection (Fig. 3-3). A majority of the *K. flexibilis* samples collected were bycatch samples not intended for collection, but were accidently caught on the ROV while collecting transect data due to the thickness of the bamboo coral fields (Fig. 3-3). These samples were labeled as "bycatch" (R23-bycatch1-8), and their exact sampling location along the dive transect is unknown. The corals were immediately photographed on deck and measured for height, width, stem diameter, and wet weight. Any associated fauna found on the colonies were removed and will be used in other studies. After measurements were taken, the samples were stored in plastic bags at -20°C.
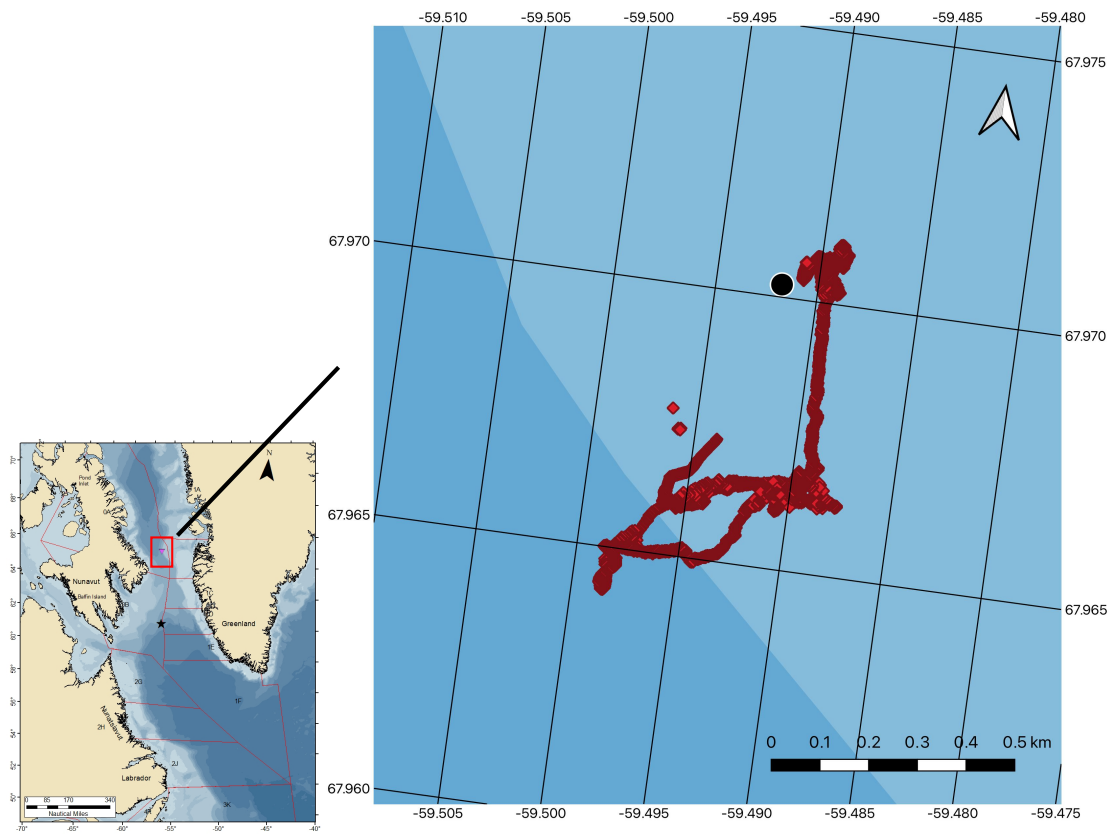
Figure 3-1. Map of the ROV dive transect (Dive 23) from 2021 at Disko Fan shown in red. The black circle represents the location of the box core sampled in 2018 (Fig. 3-2a), which the push core with *K. flexibilis* fragments was extracted from.
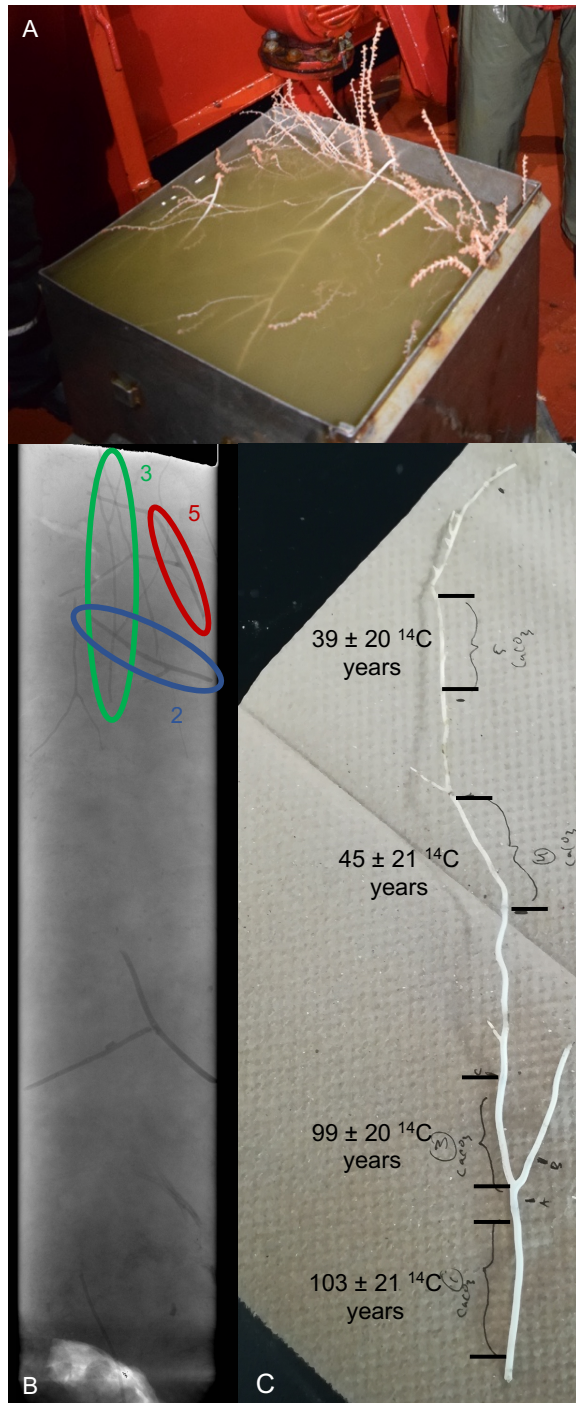
Figure 3-2. A) Box core collected in 2018 from Disko Fan at 882m depth with *Keratoisis flexibilis* corals on the surface. B) 60cm push core 9.3cm in diameter taken and x-rayed from the box core (A) and then sub-sampled for *K. flexibilis* fragments, circled and numbered in the figure (Table 3-2). C) *K. flexibilis* fragment 3 (B) with ^{14}C ages determined by AMS-^{14}C measurements indicated in the figure. This fragment is approximately 27cm in length.
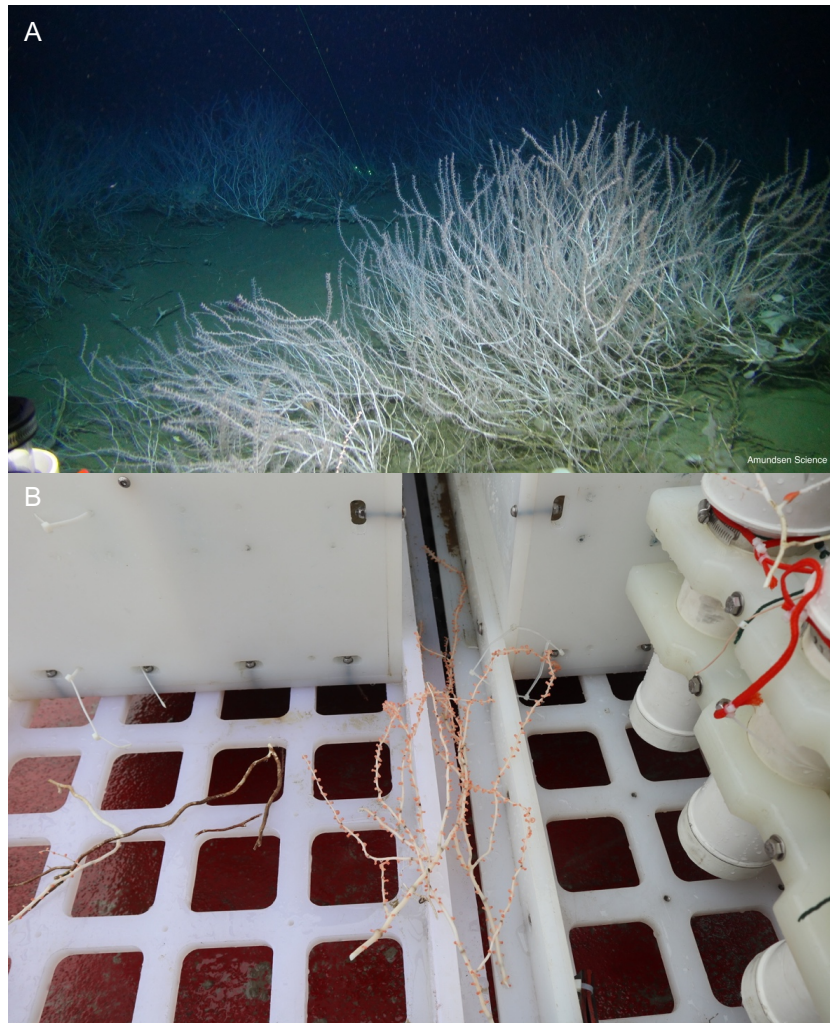
Figure 3-3. A) *Keratoisis flexibilis* coral field observed at Disko Fan during the 2021 ROV dive, forming dense thickets on a muddy bottom. B) *Keratoisis flexibilis* samples caught as bycatch samples on the front of the ROV after the Disko Fan ROV survey in 2021. 8 bycatch *K. flexibilis* colonies were collected from this dive.

3.2.3 AMS-^{14}C

Three *K. flexibilis* fragments were sub-sampled at different depths from the push core sampled from the larger box core in 2018 (Fig. 3-2; Table 3-2). They were then cut into pieces around 0.1g along the skeleton for ^{14}C analyses (Table 3-2). Some pieces contained both organic and inorganic material, which were separated during analyses.

Accelerated mass spectrometry (AMS) radiocarbon (^{14}C) analyses were conducted at the A.E. Lalonde AMS Laboratory at the University of Ottawa on a 3MV accelerator mass spectrometer, which requires at least 10mg of sample material for carbonates. Full sample methodology for the AMS-^{14}C measurements are described in Crann et al. 2017 and Murseli et al. 2019.

3.2.4 Data analysis of push core fragments

With three *K. flexibilis* samples analyzed linearly for ^{14}C, axial growth rate and age estimates were made by using the coral fragment length and the ^{14}C measurements. The following equation [1] was used to determine approximate axial growth rates:

[1] axial growth rate = coral fragment length / (oldest ^{14}C measurement – youngest ^{14}C measurement).

The uncertainty factor for the growth rates was calculated with the following equation [2]:

[2] axial growth rate ± = axial growth rate * (± of age/age)

The age was determined from the ^{14}C measurements by subtracting the youngest ^{14}C age from the oldest ^{14}C age, and the uncertainty value for age was determined by averaging the uncertainty for each ^{14}C measurement along the fragment.

Due to the thin nature of the *K. flexibilis* fragments used for ^{14}C analyses, the entire skeleton diameter was analyzed together for ^{14}C, insinuating that ^{14}C data for each location along a fragment includes all growth layers that were deposited at that section. Equation 1 was a minimum calculation for axial growth rates and ages because of the influence of younger growth layers on the determined ^{14}C measurement. Previous studies using ^{14}C to

determine ages and growth rates of bamboo corals used transects across gorgonin sections and calcite sections, which provided ^{14}C measurements ~1mm apart in different growth layers (Roark et al. 2005).

An equation was developed to account for the influence of younger growth layers on ^{14}C measurements for samples along the fragment. Towards the top of colonies, fewer growth rings are present; therefore, the ^{14}C measurement at the tips of fragments are less influenced by older growth layers. The equation is based on knowledge that *Keratoisis* colonies deposit annual, concentric growth rings simultaneously with longitudinal growth, and growth rings at the base are representative of the whole lifespan of a colony (Noé and Dullo 2006; Noé et al. 2008). Therefore, the following equation [3] was developed to adjust ^{14}C measurements taken along a fragment, except for the topmost sample, which was assumed to represent the youngest measurement without interference:

[3] adjusted ^{14}C calendar age = raw ^{14}C age from location on stem + (raw ^{14}C age –

topmost raw ^{14}C age)

The equation assumes all growth bands are deposited symmetrically and are annual and was developed by considering the likely influence of younger growth layers on the oldest growth increment, which would imply that the ^{14}C measurement is representative of the growth ring at the mid-point between the youngest and oldest growth layers. However, equation [3] does not consider the variation in mass of each growth ring deposited, which would affect the degree of the ^{14}C influence. The youngest growth rings on the outside of the sample are likely to have the highest mass, meaning their ^{14}C influence is possibly greater than older growth layers. This would suggest that the adjusted ^{14}C calendar ages

158

estimated with equation [3] represent a minimum age estimate for the oldest growth layer, but equation [3] is our most accurate attempt to present correct geometrical analyses without the capability to sample individual growth rings explicitly.

3.2.5 Sclerochronology (growth ring counts)

Sample preparation for growth ring counts of the *K. flexibilis* samples followed the same steps as the methodology described in Chapter 2, section 2.2.3. Visualization of proteinaceous nodes to section was occasionally difficult, due to calcite material on the outer skeleton. In these cases, proteinaceous nodes were located by looking for flexible portions of the skeletons, as the protein material tends to be more flexible than purely calcite material. To increase the visualization clarity of growth rings in *K. flexibilis* cross-sections, fluorescence microscopy was conducted on a Zeiss AxioZoom V.16 Telecentric Microscope, and full methodology is described in Chapter 2, section 2.2.3 (Fig. 3-4).
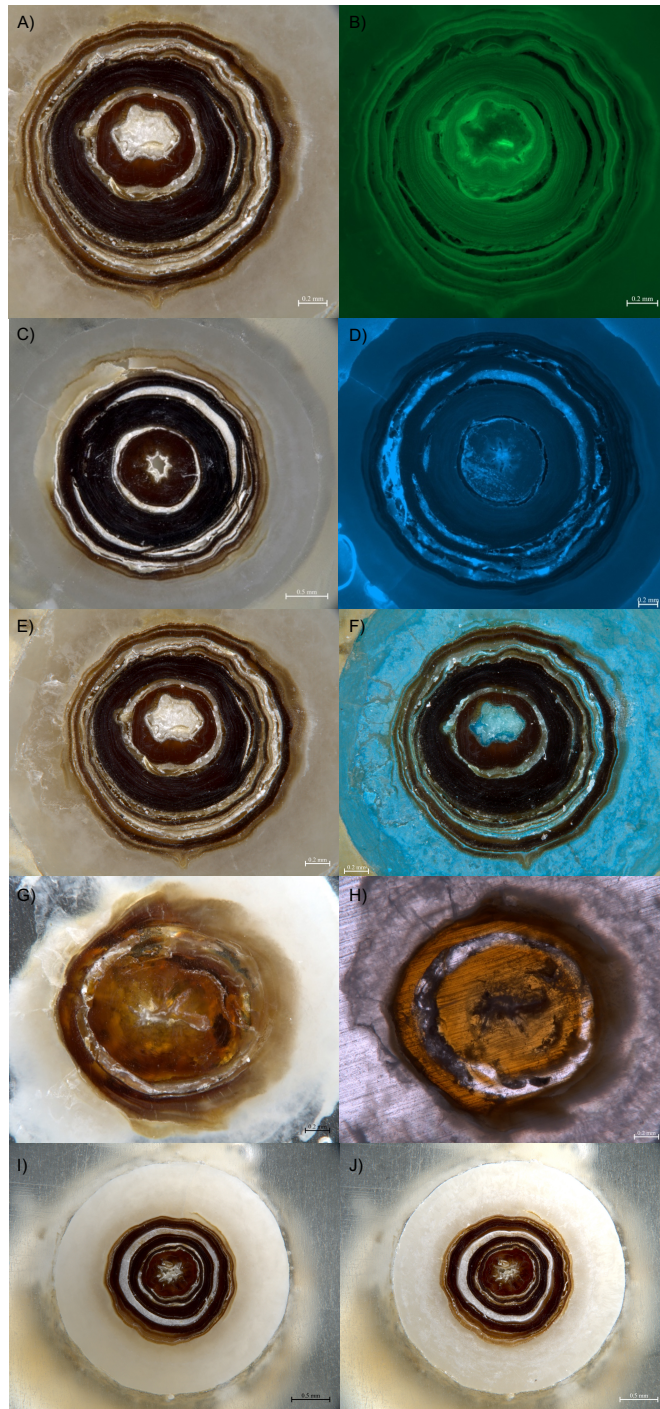
Figure 3-4. *Keratoisis flexibilis* specimens cross-sectioned at the proteinaceous nodes of the skeleton. Samples imaged in thick section with white reflected light (A, C, E, G, I) are compared to other preparation techniques used – green fluorescence microscopy (B), blue fluorescence microscopy (D), Mutvei's stain (F), thin section imaged with transmitted light (H), and etching in thick section with 5% diluted HCl (J).

3.2.6 Growth ring counting

Once all samples were imaged with reflected white light and fluorescence, growth ring counts were conducted at the proteinaceous nodes using ImageJ (Fig. 3-5). *K. flexibilis* samples exhibited both major and minor growth banding similarly to *A. arbuscula* in Chapter 2, and both structures were counted as it was unknown which structure represented annual banding (Fig. 3-5). Definitions of major and minor rings are described in Chapter 2, section 2.2.4, along with additional details of the growth ring counting methodology.
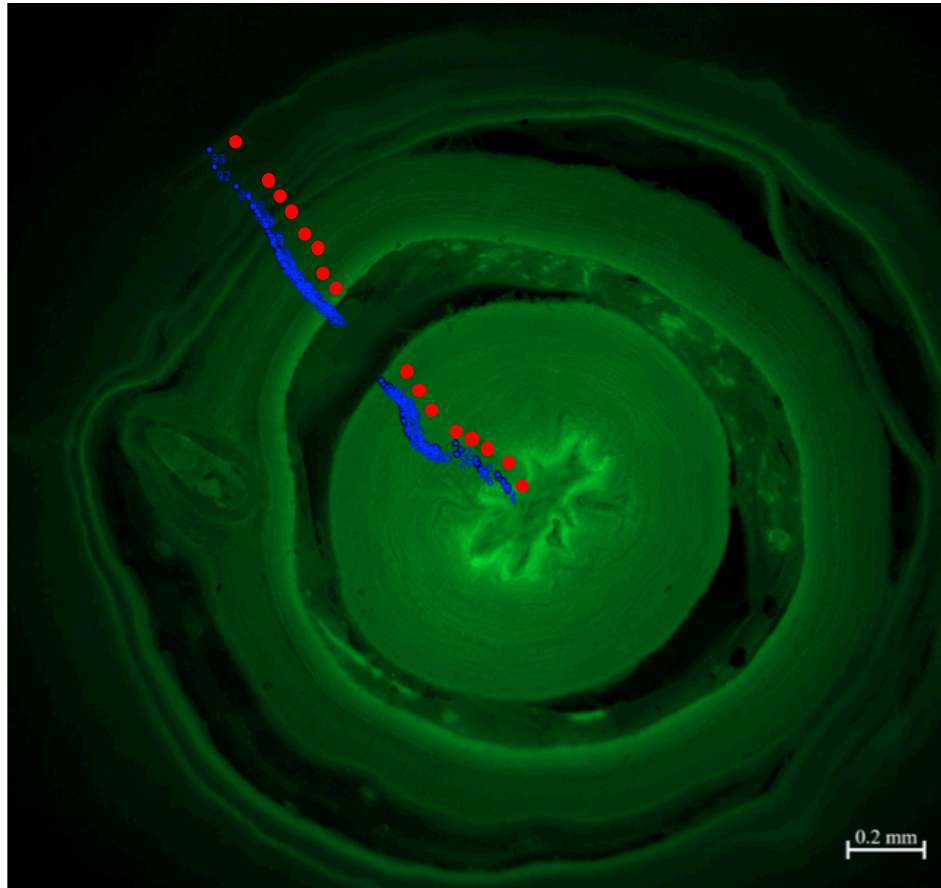
Figure 3-5. *Keratoisis flexibilis* colony R23-bycatch7_a imaged with fluorescence and counted for major (red circles) and minor (blue circles) growth rings using ImageJ software.

3.2.7 Determining growth rate and age for specimens collected by ROV

Growth ring count data were produced by three independent counters, and methodology for analyzing the data was similar to analysis for *A. arbuscula* (see Chapter 2, section 2.2.5). Because samples exhibited major and minor growth banding, *K. flexibilis* fragments collected in 2018 and ^{14}C dated, were compared to size metrics and ages for colonies from 2021, to determine which banding pattern was more likely to represent annual growth. Comparisons included linear regressions of the ^{14}C-dated specimens with colonies aged by ring counts based on major and minor rings, and observing the trend differences and R^2 values for major and minor rings.

Additionally, size metrics were compared with age based on major and minor growth ring counts. Measured size metric data for *K. flexibilis* included height, width, stem diameter, and wet weight, and colony area, which was calculated from height and width. Statistical tests included linear, logarithmic, and exponential regressions, and the R^2 value was used to compare the fit of age based on major and minor growth bands with each size metric, and to help determine which growth band pattern represented a year.

Radial and axial growth rates were then determined, similarly to methodology for *A. arbuscula* (see Chapter 2, section 2.2.5). Colonies of *K. flexibilis* that were sub-sampled and cross-sectioned twice displayed two age and growth rate estimates for one colony. The age and growth rate data were averaged for each colony with two cross-sections produced, similar to the methodology for specimens of *A. arbuscula* with two age and growth rate estimates (see Chapter 2, section 2.2.6) (Table 3-1).

3.2.8 Comparisons for K. flexibilis and K. grayi

Growth rates and ages determined for the *K. flexibilis* samples were compared to a previously studied *Keratoisis* species (cf. *Keratoisis grayi*) collected from the SW Grand Banks and NE Saglek Bank (Sherwood et al. 2008; Sherwood and Edinger 2009). The two species within the *Keratoisis* genus have different growth forms and are found in different regions, as *K. grayi* specimens have been observed with thicker skeletons (Fig. 3-6). *K. grayi* ages, growth rates, and size metrics were compared to *K. flexibilis* specimens from Disko Fan.
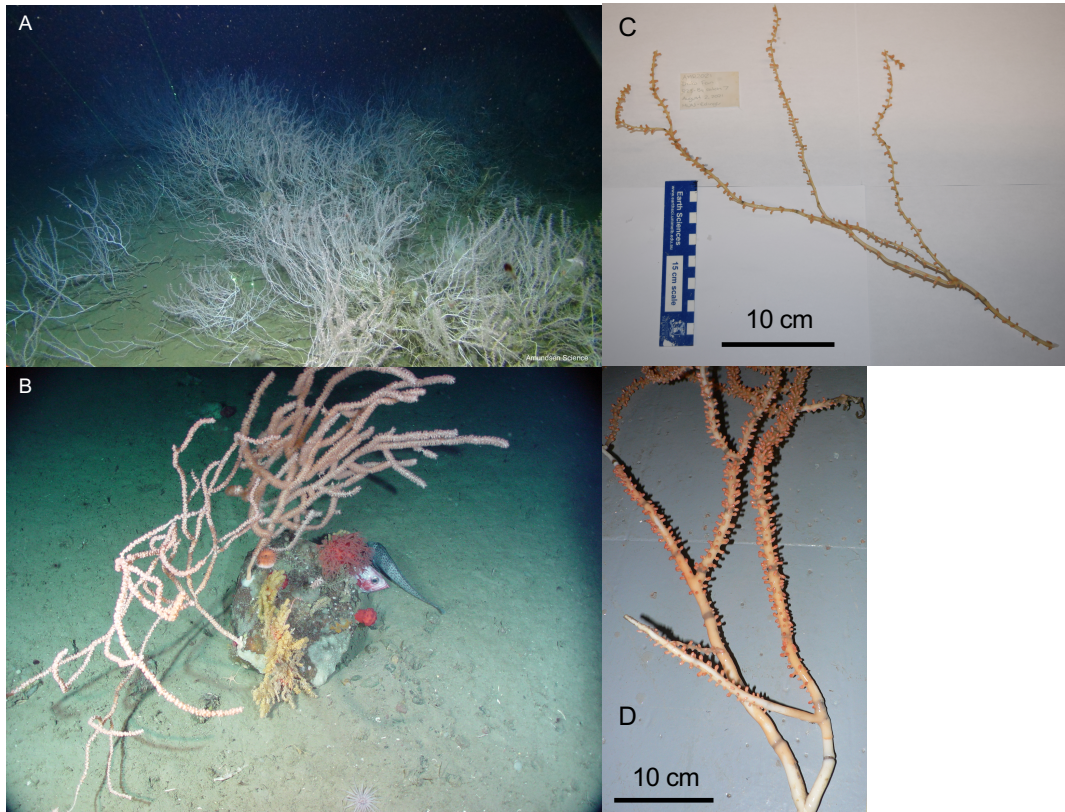
Figure 3-6. A) *Keratoisis flexibilis* colonies at Disko Fan, ~900 m depth attached to muddy bottoms and forming dense coral fields (green lasers closest in view represent 6.25cm). B) *Keratoisis grayi* colony attached to hard substrate, growing off Newfoundland, Canada imaged during ROPOS transect (R1065) in 2007. C) *K. flexibilis* colony in the lab, collected in 2021 from Disko Fan. D) *K. grayi* sample collected during ROPOS transect (R1065) in 2007.

Table 3-1. *Keratoisis flexibilis* colonies collected in 2021 Disko Fan ROV survey.

Sample	Subsample No.	Year	Latitude	Longitude	Depth	Height	Width	Diameter
R23-1	a	2021	67 57.9774	59 29.4414	885	380	160	3.18
R23-1	b	2021	67 57.9774	59 29.4414	885	380	160	2.81
R23-11	a	2021	67 57.9798	59 29.3364	875	550	210	3.27
R23-11	b	2021	67 57.9798	59 29.3364	875	550	210	2.97
R23-14	b	2021	67 57.9762	59 29.3136	879	540	300	3.06
R23-14	d	2021	67 57.9762	59 29.3136	879	540	300	3.22
R23-bycat1	c	2021	-	-	-	370	120	3.79
R23-bycat2	a	2021	-	-	-	510	140	3.10
R23-bycat2	b	2021	-	-	-	510	140	4.17
R23-bycat3	a	2021	-	-	-	290	200	2.45
R23-bycat4	b	2021	-	-	-	200	80	2.74
R23-bycat5	d	2021	-	-	-	230	65	2.03
R23-bycat6	b	2021	-	-	-	600	260	4.26
R23-bycat7	a	2021	-	-	-	650	210	3.93
R23-bycat7	b	2021	-	-	-	650	210	3.78
R23-bycat8	a	2021	-	-	-	530	170	5.71
R23-bycat8	b	2021	-	-	-	530	170	4.93

Notes & units: latitude and longitude – decimal degrees minutes, depth – meters, height – mm, width – mm, diameter - mm. Blank cells represent unknown values. Samples shaded in gray were averaged together depending on sample colony, as these are samples from the same colonies, but different proteinaceous nodes. Each colony was sampled a maximum of 2 times.

Table 3-2. *Keratoisis flexibilis* colonies measured for AMS-^{14}C with ages and growth rate determined by simplified and adjusted ^{14}C calculation.

Frag.	Mass	Length in sed	Sed position	Length total	SD	Orig. ^{14}C age BP	±	F^{14}C	±	Age BP (±)	Orig. Agrowth rate	±	Adj. ^{14}C age BP	Adj. Agrowth rate
2	0.2176	2	10-12	7	0.29	197	21	0.9758	0.0026	42 (±21)	1.7	0.85	239	0.83
2	0.2254	2	10-12	7	0.29	155	21	0.9808	0.0026	-	-	-	155	
3	0.2421	9	0-9	27	0.18	103	21	0.9873	0.0026	64 (±21)	3	0.98	167	2.11
3	0.1492	9	0-9	27	0.18	99	20	0.9877	0.0025	-	-	-	159	
3	0.1077	9	0-9	27	0.18	45	21	0.9944	0.0026	-	-	-	51	
3	0.0736	9	0-9	27	0.18	39	20	0.9951	0.0024	-	-	-	39	
5	0.1251	9	0-9	9	0.27	187	20	0.9770	0.0024	71 (±21)	1.2	0.35	258	0.63
5	0.091	9	0-9	9	0.27	116	21	0.9856	0.0025	-	-	-	116	

Notes and units: ^{14}C age BP = age before 1950. F^{14}C = fraction ^{14}C, with 1.0 = 1950, Mass – grams; Length in sed (sediment) – cm; Sed position – cm; length total – cm; SD = stem diameter – cm; "Adj" = adjusted, "Orig" = original, Age BP – years; Adjusted ^{14}C age BP (see equation 3 for calculation); adjusted Agrowth (axial growth) rate – mm/yr (see equation 3 for calculation); Agrowth– mm/yr; ± of age calculated by averaging the uncertainties of ^{14}C measurements from each measurement on a fragment; ± of axial growth rate calculated using equation 2.

3.3 RESULTS

3.3.1 Ages of ^{14}C-dated fragments

The three colonies of *K. flexibilis* sub-sampled from a push core and sampled for AMS-^{14}C measurements, were used to determine ages and axial growth rates in the species. Estimated ages of each coral fragment, determined from ^{14}C measurements of calcite from the coral skeletons were 42 ±21 years, 64 ±21 years, and 71 ±21 years (Fig. 3-2c; Table 3-2). AMS-^{14}C results indicate axial growth rates of 1.7 ±0.85 mm/yr, 3 ±0.98 mm/yr, and 1.2 ±0.35 mm/yr for coral fragments 2, 3, and 5, respectively (Table 3-2). These coral fragments were all sampled from push core "AMD2018 PT6 push" 0-12cm from the top of the core. Due to the influence of younger growth layers on the ^{14}C measurements, calculations using equation 3 showed older age estimates for each ^{14}C-dated fragment ranging from 84-142 years, and slower axial extension rates, ranging from 0.63-2.11 mm/yr (Table 3-2).

3.3.2 Growth rate comparisons for ^{14}C-dated and ring count specimens

Axial and radial growth rates were compared for the *K. flexibilis* 2021 colonies aged by ring counts and the 2018 fragments aged by ^{14}C-dating. Mean axial growth rate for the 2018 fragments was 1.97 mm/yr and for the 2021 colonies was 3.51 mm/yr (Tables 3-2 and 3-3). Radial growth rate comparisons indicated slower mean radial growth for the 2021 samples (0.014 mm/yr) when compared to the ^{14}C-dated samples (0.045 mm/yr) (Tables 3-2 and 3-3). Comparisons of axial growth rates for the adjusted ^{14}C values with colonies aged by growth ring counts showed slower mean axial growth for the ^{14}C-dated

fragments (1.19 mm/yr) than the 2021 specimens (3.51 mm/yr) (Tables 3-2 and 3-3). Radial growth rate comparisons showed more similar mean growth rates between the two groups of samples, as the ^{14}C-dated fragment mean radial growth rate was 0.023 mm/yr, and mean radial growth for the 2021 specimens aged with growth ring counts was 0.014 mm/yr (Tables 3-2 and 3-3).

3.3.3 Minor growth rings represent annual banding

Comparison of size metrics from *K. flexibilis* fragments ^{14}C-dated with colonies of *K. flexibilis* collected in 2021 and aged with growth ring counts were conducted to determine if major or minor growth banding represent annual growth in the species. Height and age based on major rings showed a negative correlation, which is not expected biologically, and does not match the positive correlation observed when analyzing *K. flexibilis* colonies from 2021 (Fig. 3-7). An analysis with age based on minor rings and height showed a positive correlation, and comparisons of height measurements had a higher R^2 value for age based on minor rings (0.351) than major rings (0.259) (Fig. 3-7). A similar relationship was observed when analyzing stem diameter and age, as the relationship for age based on major rings showed a negative correlation, while age based on minor rings showed a positive correlation (Fig. 3-7). The comparison of stem diameter and age based on major rings showed a higher R^2 value than age based on minor rings, but the negative trend indicates that minor rings record annual growth in the species. All R^2 values were too low to use as the basis for determining major or minor growth rings to be annual, but the negative slope observed for all size metrics with major rings is not biologically possible,

leading to the conclusion that minor growth rings represent annual growth in this species because of positive regression slopes.

Once equation 3 was applied to each ^{14}C measurement for fragments 2, 3, and 5, the results indicate older ages and slower axial extension rates for each fragment (Table 3-2). When compared to the samples aged with growth ring counts, minor rings representing annual growth is still most accurate, as negative trends were observed for both height and stem diameter when compared with age based on major rings (Fig. 3-7). The trends were weaker than the non-adjusted ages of the ^{14}C samples, but both non-adjusted and adjusted ^{14}C ages suggested minor rings represented annual growth (Fig. 3-7).

Additional comparisons incorporating only specimens aged by growth ring counts, analyzed relationships of all size metrics with age, determined by major and minor growth rings. Age based on minor rings showed stronger trends with size metrics, except for height, which when compared with age based on major rings showed a higher R^2 value (0.0404) than age based on minor rings (0.025) (Figs. 3-8 and 3-9; Table 3-4). The highest observed R^2 value was for width compared with age based on minor rings, which was 0.1151 (Fig. 3-9). Regression of size metrics versus age based on major or minor rings also showed higher R^2 values for logarithmic or exponential fits in some cases (Fig. 3-8 and 3-9; Table 3-4).

All comparisons and trends indicate that minor rings are more likely to represent annual growth rings in *K. flexibilis* corals collected from Disko Fan. Age based on minor rings is termed "age" in the remainder of the study, and growth rates are calculated from age based on minor rings.
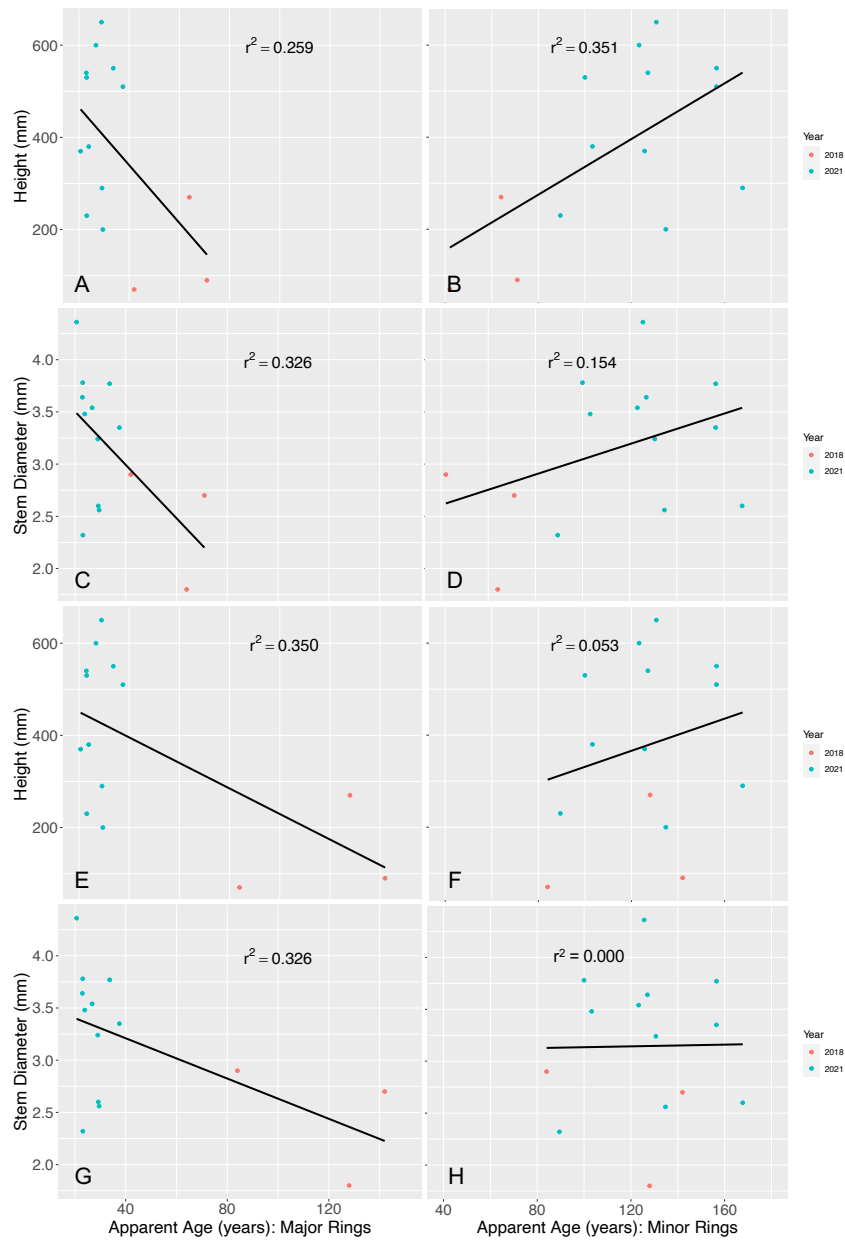
Figure 3-7. Age based on major rings for samples of *K. flexibilis* collected in 2021 from Disko Fan (A&C) and age based on minor rings for the same samples (B&D), plotted with *K. flexibilis* fragments sub-sampled from a push core and ^{14}C-dated, collected in 2018 from Disko Fan. Plots A and C are comparing age and height, and plots B and D are comparing age and stem diameter. Plots E-H represent 2018 samples re-calculated (see equation 2) to adjust age estimates of ^{14}C calendar years. Plots E and F are comparing age and height with major and minor rings, and plots G and H are comparing age and stem diameter major and minor rings. Black lines indicate the linear best fit line in each plot.
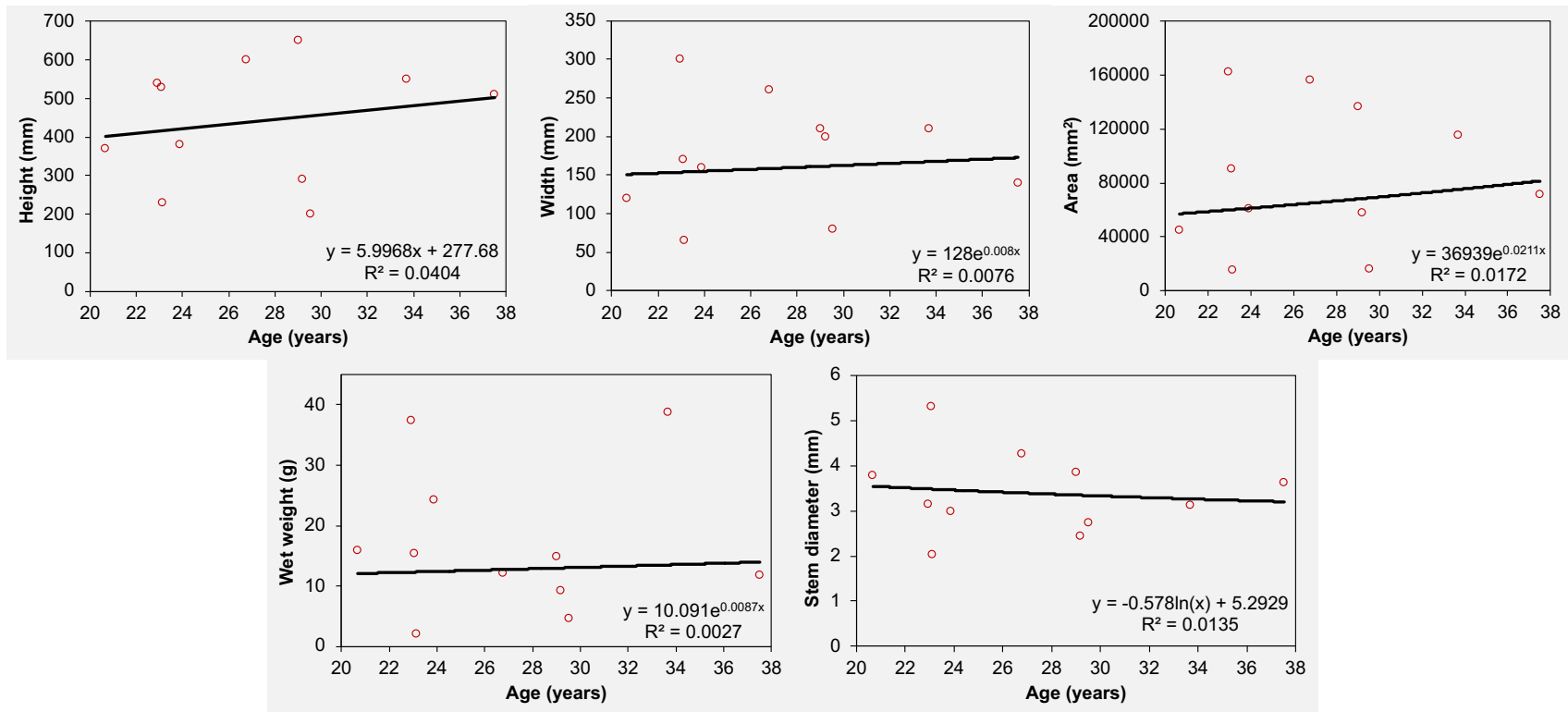
Figure 3-8. Age based on major rings for *Keratoisis flexibilis* colonies collected at Disko Fan in 2021, compared with the size metrics height, width, area (height*width), wet weight, and stem diameter. Black lines represent best fit lines for each dataset, with varying types of regression lines that showed the highest R^2 value (linear, logarithmic, exponential). Best fit line equations and R^2 values are also displayed on each plot.
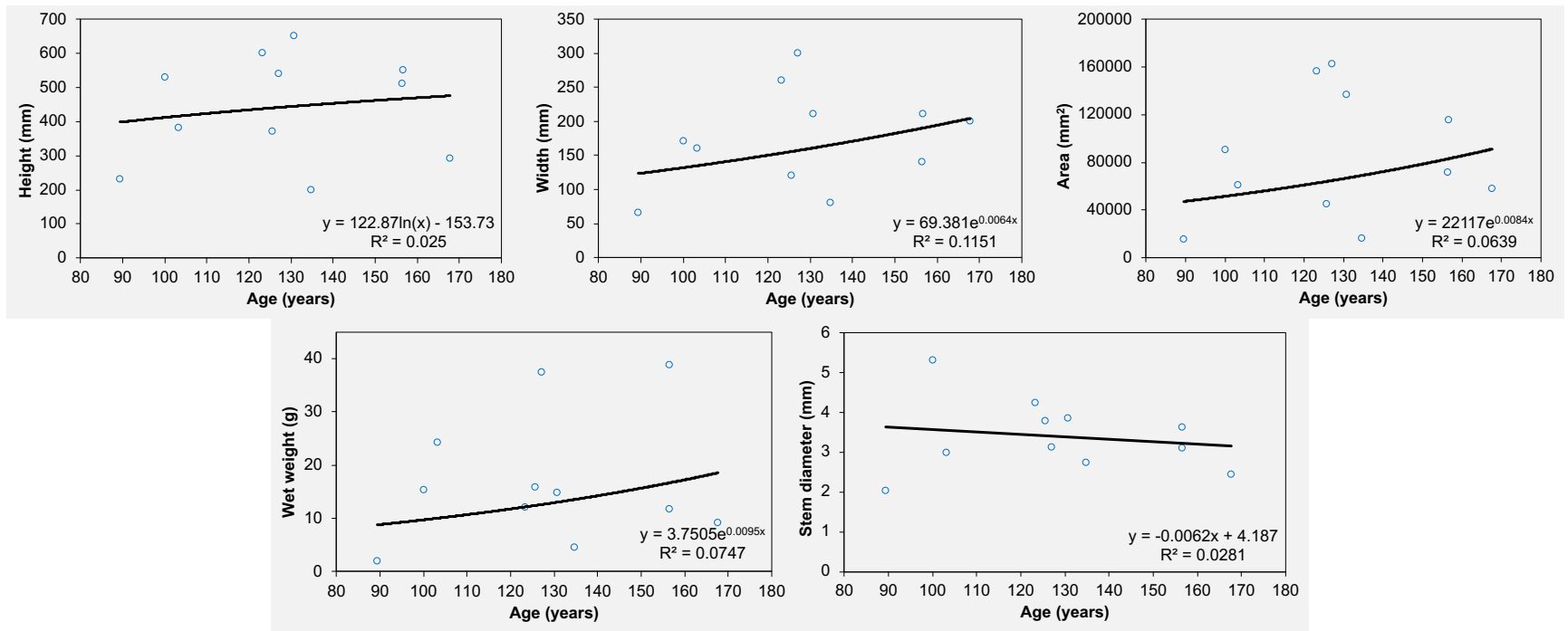
Figure 3-9. Age based on minor rings for *Keratoisis flexibilis* colonies collected at Disko Fan in 2021, compared with the size metrics height, width, area (height*width), wet weight, and stem diameter. Black lines represent best fit lines for each dataset, with varying types of regression lines that showed the highest R^2 value (linear, logarithmic, exponential). Best fit line equations and R^2 values are also displayed on each plot.

3.3.4 Growth rates and age comparisons of *K. flexibilis* and *K. grayi*

Ages for the *K. flexibilis* collected in 2021 ranged from 89-168 years, with radial growth rates of 0.007-0.027 mm/yr and axial growth rates of 1.5-5.3 mm/yr (Table 3-3). These results were compared to a different species of *Keratoisis* observed in the NW Atlantic (*K. grayi*) because differences in growth forms have been observed for the two species (Sherwood and Edinger 2009; Neves et al. 2015). These species grow on different substrate and in different formations of coral fields versus solitary colonies (Fig. 3-6). The age range for *K. flexibilis* (89-168 years) was comparable to an age range of *K. grayi* specimens previously analyzed from the SW Grand Banks of Newfoundland (94-200 years) (Tables 3-3 and 3-5) (Sherwood and Edinger 2009). Differences in radial and axial growth rates were observed, with median radial growth rates slower for *K. flexibilis* (0.013 mm/yr) than for *K. grayi* (0.074 mm/yr) (Fig. 3-10). Comparisons of axial growth rates showed the same pattern, with a median axial growth rate for *K. flexibilis* of 3.5 mm/yr and a median value for *K. grayi* of 9.6 mm/yr (Tables 3-3 and 3-5). Growth rate comparison results show consistently faster axial and radial growth rates for *K. grayi* when compared to *K. flexibilis*.
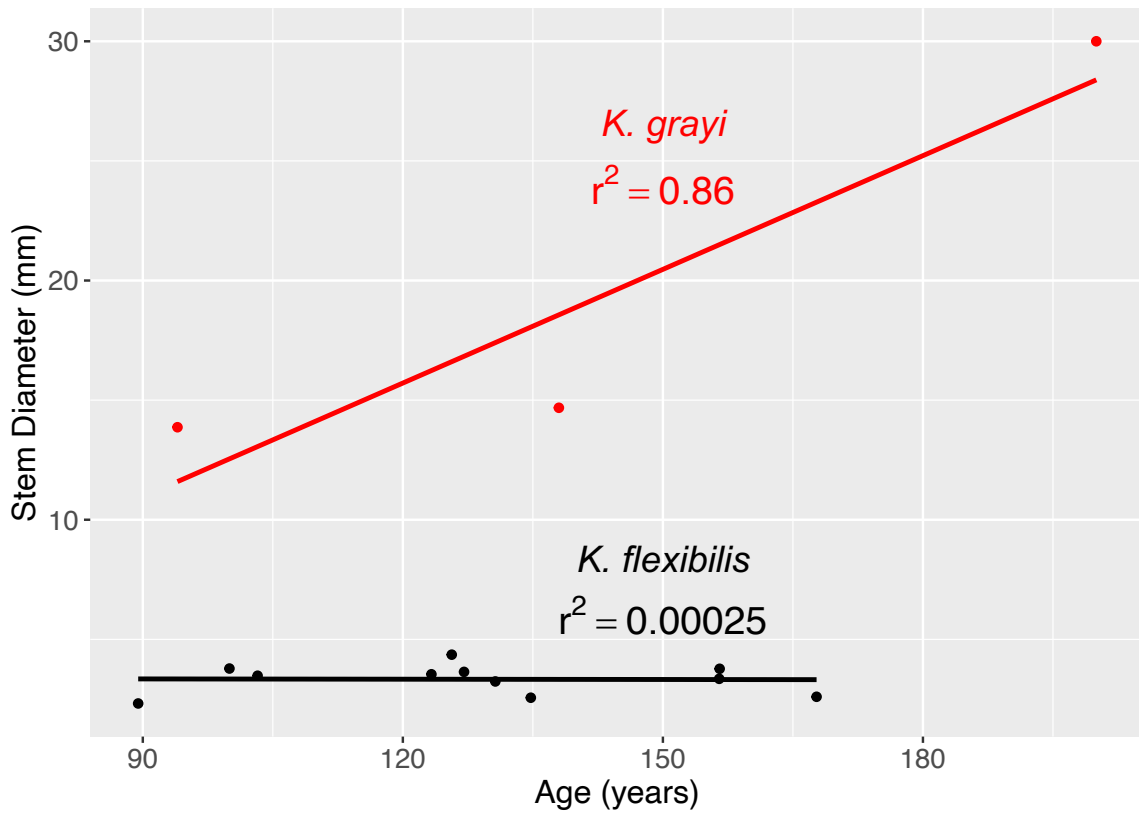
Figure 3-10. *Keratoisis flexibilis* colonies collected in 2021 from Disko Fan in black and *Keratoisis grayi* colonies from Sherwood and Edinger 2009 in red, plotted with age and stem diameter. Black and red lines indicate the linear best fit line, with R^2 values representing the fit of each line for the different species.

Table 3-3. Results of size metrics, aging, and growth rates for *Keratoisis flexibilis* colonies collected in 2021.

Sample	WW	H	W	Area	SD	MN/ MA	MA rings	MA SE	MN rings	MN SE	Rgrowth Rate (MA)	Rgrowth Rate (MN)	Agrowth Rate (MA)	Agrowth Rate (MN)	Age (MA)	Age (MN)
R23-1	24.2	380	160	60800	3.00	5.12	12.0	3.1	52.7	4.5	0.064	0.015	15.9	3.7	24	103
R23-11	38.7	550	210	115500	3.12	5.99	12.7	3.7	60.2	6.6	0.053	0.011	16.3	3.5	34	157
R23-14	37.4	540	300	162000	3.14	5.92	12.5	1.8	71.5	2.9	0.070	0.013	23.5	4.2	23	127
R23-bycat1	15.8	370	120	44400	3.79	6.29	12.3	2.0	75.0	5.6	0.092	0.015	17.9	2.9	21	126
R23-bycat2	11.8	510	140	71400	3.63	4.65	13.7	2.3	57.0	2.3	0.049	0.012	13.6	3.3	38	156
R23-bycat3	9.1	290	200	58000	2.45	5.94	13.0	2.0	74.7	7.0	0.042	0.007	9.9	1.7	29	168
R23-bycat4	4.6	200	80	16000	2.74	4.81	16.0	2.3	73.0	4.4	0.047	0.010	6.8	1.5	30	135
R23-bycat5	2	230	65	14950	2.03	4.16	12.7	1.9	49.0	3.8	0.044	0.011	9.9	2.6	23	89
R23-bycat6	12	600	260	156000	4.26	4.94	17.7	3.0	81.3	2.7	0.080	0.017	22.4	4.9	27	123
R23-bycat7	14.8	650	210	136500	3.86	4.56	19.7	2.0	88.5	5.0	0.067	0.015	22.4	5.0	29	131
R23-bycat8	15.3	530	170	90100	5.32	4.80	20.8	3.6	91.0	1.7	0.117	0.027	23.0	5.3	23	100

Notes & units: WW = wet weight (g); H = height (mm); W = width (mm); Area = height * width (mm^2); SD = stem diameter (mm); MN = minor; MA = major; SE = standard error; Rgrowth Rate = radial growth rate (mm/yr), Agrowth rate = axial growth rate (mm/yr).

Table 3-4. Regression analyses for size metrics and age (major rings and minor rings; specimens collected in 2021 only).

Size Metric	Regression Type & R^2 value			Regression Type & R^2 value		
	Major rings			*Minor rings*		
	Lin	Log	Exp	Lin	Log	Exp
Height	**0.0404**	0.0391	0.0284	0.0137	**0.025**	0.0153
Width	0.0003	0.0017	**0.0076**	0.073	0.0924	**0.1151**
Area	0.0048	0.0075	**0.0172**	0.0221	0.0374	**0.0639**
Wet Weight	0.0104	**0.0135**	0.0018	**0.0281**	0.0156	0.0063
Stem diameter	<0.0001	<0.0001	**0.0027**	0.0308	0.0406	**0.0747**

Notes: Lin = linear regression, Log = logarithmic regression, Exp = exponential regression. Bolded R^2 values represent best fit regression for each size metric for linear, logarithmic, or exponential regressions.

Table 3-5. *Keratoisis grayi* size metrics, ages, and growth rates from Sherwood and Edinger (2009).

Ref	Species	Sample	Depth	Lat (°N)	Long (°W)	Year	Dating method	Height	Radius	Age ± SE	Rgrowth Rate	Agrowth Rate
Sherwood& Edinger 2009	*K. grayi (ornata)*	2452	601	44.833	-54.469	2007	bomb-^{14}C	900	6.93	94 ± 7	0.074 ± 0.005	9.57 ± 0.713
Sherwood& Edinger 2009	*K. grayi (ornata)*	1449	1193	61.600	-60.383	2007	^{14}C		15	200 ± 30	0.075 ± 0.011	
Sherwood& Edinger 2009	*K. grayi (ornata)*	1343	713	44.133	-52.933	2006	^{210}Pb		7.34	138 ± 23	0.053 ± 0.009	

Notes & units: Depth (m), height (mm), radius (mm), age (years, SE = standard error, Rgrowth rate = radial growth rate (mm/yr), Agrowth rate = axial growth rate (mm/yr).

3.4 DISCUSSION

3.4.1 Axial growth rates from ^{14}C-dated K. flexibilis fragments

The sampling mechanism for ^{14}C of *K. flexibilis* fragments did not allow for simple calculations of axial growth rates. Equation 1 was first used as a simplified calculation, which represents a minimum ^{14}C age estimate. However, because whole diameter sub-samples were cut for ^{14}C analysis, younger growth layers likely influence the ^{14}C age given for basal samples of each fragment, as previous studies have shown that species of *Keratoisis* deposit concentric, annual growth bands simultaneously with longitudinal growth, and basal areas of the skeleton have more growth bands than top areas (Noé and Dullo 2006; Noé et al. 2008). The adjustment equation developed suggested that basal ^{14}C measurements were likely younger than the actual innermost growth ring, so they are a minimum age estimate. Therefore, equation 3 was developed to adjust ^{14}C ages. Adjusted age estimates suggest older fragments and slower axial growth rates than the original minimum age estimates (Table 3-2).

The axial growth rate and age estimates from the three fragments are similar to other axial growth rate and age estimates of a *Keratoisis* colony off Newfoundland and Labrador, which displayed an axial growth rate of 9.3 mm/yr and ages of 94-200 years (Sherwood and Edinger 2009), and *Keratoisis* colonies from the Gulf of Alaska and Davidson Seamount, which displayed axial growth rates ranging from 2.8–13.8 mm/yr and ages ranging from 87-282 years (Andrews et al. 2009). A fossil *Keratoisis* specimen collected in New Zealand displayed an age of 240 years and axial growth rate of 5 mm/yr (Noé et al. 2008). The adjusted axial growth rates in our analysis were somewhat slower

when compared to other *Keratoisis* colonies from different regions, and non-adjusted values also indicated slower axial extension in comparison with other colonies in different regions (Noé et al. 2008; Andrews et al. 2009; Sherwood and Edinger 2009). However, specimens used in our study were coral fragments and not whole colonies, meaning our age estimates only represented the individual fragments analyzed. Axial growth rates determined by ^{14}C measurements suggests that *K. flexibilis* may be a slow-growing species within the *Keratoisis* genus, potentially because of its northern location and oceanographic conditions in Baffin Bay, or because of a difference in growth form.

3.4.2 Minor growth banding representative of annual periodicity

K. grayi colonies have been previously analyzed in the SW Grand Banks, and were interpreted to contain annual growth rings, but two ring structures were not reported for the species in the previous study (Sherwood and Edinger 2009). Annual growth rings needed to be confirmed for *K. flexibilis* as it is a different species with a different growth form (Neves et al. 2015; Watling et al. 2022). *K. flexibilis* displayed both major and minor growth band structures when sectioned at proteinaceous nodes, defined as larger, more distinct growth bands and smaller, finer scaled growth bands (Fig. 3-5). A similar observation of fine growth bands within larger growth bands have been observed in other deep-sea coral species including bamboo corals (Roark et al. 2005; Tracey et al. 2007), the gorgonian corals *Primnoa pacifica* (Aranha et al. 2014) and *Primnoa resedaeformis* (Risk et al. 2002), the black coral *Bathypathes patula* (Marriott et al. 2020) and sea pens (Neves et al. 2015; K. Greeley MSc Thesis, Memorial University 2021).

177

The conclusion of minor rings representing annual growth was based on three different comparisons of data collected from this study and previous studies. *K. flexibilis* aged with growth ring counts and *K. flexibilis* fragments ^{14}C-dated showed variations in the strength of regression trends for age estimates based on major and minor rings when compared with stem diameter and height. However, only age estimates determined from minor ring counts showed positive correlations with both size metrics (Fig. 3-7). Negative correlations observed for age (major rings) with stem diameter and height are not expected biologically; therefore, the positive correlations observed for age (minor rings) with size metrics properly reflect increasing height and stem diameter as a colony gets older. An adjustment equation was applied to the ^{14}C-dated fragments (see section 3.2.8: equation 3), and the same comparisons of *K. flexibilis* colonies with the adjusted age estimates showed negative correlations for major ring age estimates with size metrics, while age based on minor rings when compared to the size metrics showed positive correlations (Fig. 3-7).

Minor growth rings are interpreted to represent annual growth banding for *K. flexibilis*. The driving factor for major ring deposition was not concluded in this study, but growth rings in *Paramuricea* sp. have also been radiometrically validated to not form annually, and instead form approximately once every 10 years (Sherwood and Edinger 2009). The interpretation of minor rings representing annual growth contradicts most other previous studies of gorgonian corals, which have determined minor growth bands to represent lunar cycles or bi-annual deposition and major growth rings to represent annual growth (Roark et al. 2005; Tracey et al. 2007), and have been validated with radiometric dating tools. However, based on radiometrically validated specimens of *K. flexibilis*, minor

growth ring age estimates show expected biological trends more clearly, and major growth rings in our specimens were not pronounced.

3.4.3 K. flexibilis comparisons of ages and growth rates with other species

Age and growth rate estimates from this study showed an age range of 89-168 years, radial growth rates of 0.007-0.027 mm/yr, and axial growth rates of 1.5-5.3 mm/yr for *K. flexibilis* aged by growth ring counts (Table 3-3). Longevity results are comparable to other studies on *Keratoisis* species and bamboo corals, but growth rates for *K. flexibilis* were slower than most previously documented growth rates within the *Keratoisis* genus. *Keratoisis* colonies from the Gulf of Alaska and Davidson Seamount displayed ages of 87-282 years, radial growth rates of 0.051-0.057 mm/yr, and axial growth rates ranging from 2.8–13.8 mm/yr (Andrews et al. 2009), a *Keratoisis* specimen collected in New Zealand with an age of 240 years and axial growth rate of 5 mm/yr (Noé et al. 2008), and bamboo corals collected from offshore California, USA and in the NW Atlantic, offshore the east coast of the USA, which showed ages ranging from 150-300 years and radial growth rates of 0.009-0.128 mm/yr (Hill et al. 2011). Farmer et al. 2015 determined radial growth rates of six *Keratoisis* colonies from the NW Atlantic using ^{14}C, which ranged from 0.012-0.078 mm/yr. This study also compared their results with a wide range of other studies that analyzed *Keratoisis* colonies and determined an overall radial growth rate range for the genus to be 0.015-0.104 mm/yr (Farmer et al. 2015).

K. flexibilis specimens from our study show similar age ranges to other *Keratoisis* colonies, but our specimens showed a slower range of radial and axial growth rates. This

may suggest that *K. flexibilis* is one of the slowest growing species within the *Keratoisis* genus, potentially due to genetic factors or environmental variables, such as temperature, current strength, or food availability in the species' location. A temperature effect on growth rates has been suggested for bamboo corals because increased growth rates were observed in warmer waters (Thresher 2009), and it has been specifically documented in the *Keratoisis* genus (Thresher et al. 2016). A comparison of published growth rates and temperatures for *Keratoisis* colonies (Thresher 2009), compared to *K. flexibilis* specimens shows the same trend, as bottom temperature measured at the *K. flexibilis* site was 1.1°C (Fig. 3-11).

We were specifically interested in comparing determined ages and growth rates for *K. flexibilis* from Disko Fan with previously analyzed *K. grayi* colonies (Sherwood and Edinger 2009), collected from the SW Grand Banks and NE Saglek Bank (Table 3-5). *K. grayi* has been observed attached to hard-bottom substrate (Baker et al. 2012) forming solitary colonies with thick skeletons, while *K. flexibilis* has only been observed in soft bottom environments anchored in muddy sediment, forming coral fields in more northern locations (Neves et al. 2015) (Fig. 3-6). Radial growth rates for *K. grayi* were one order of magnitude faster than the lower range of radial growth rates for *K. flexibilis*, and the axial growth rate measurement for *K. grayi* was faster than *K. flexibilis* (Fig. 3-10). Age estimates were similar for both species, ranging from 89-200 years all together, which suggests that *K. flexibilis* is slower-growing than *K. grayi*, yet the species have similar longevities.

Mechanisms driving the slower growth in *K. flexibilis* is likely to be either environmental factors or differences in growth form within the genus. Depth (Roark et al. 2006), bottom temperature (Tracey et al. 2007; Thresher 2009), and food availability (Thresher et al. 2016) have been documented to influence growth rates, yet depth is likely not a cause for the slower growth rates observed in *K. flexibilis* sampled at 900m, since samples of *K. grayi* ranged in depth from 601-1193m (Sherwood and Edinger 2009). Bottom temperature could be influencing the differences in growth rates because samples of *K. grayi* were not collected in waters below 3.4°C, while bottom temperature at Disko Fan is 1.1°C (Fig. 3-11). Other environmental variables such as current regime and food availability are possible drivers of growth rate differences as well.

It is important to note the distinct difference in growth forms between the species, which may foster a difference in growth rates for the two species (Fig. 3-6). As *K. flexibilis* has been observed forming coral fields in dense aggregations (Neves et al. 2015), which is optimal for low-current environments, it is possible this species does not need thick skeletons, compared to *K. grayi*, which grow as solitary colonies in higher current settings. *K. grayi* specimens also grow primarily on hard substrate (Baker et al. 2012), which may contribute to the species forming thicker skeletons for stability.

Our study suggests that *K. flexibilis* is a particularly slow growing bamboo coral species, possibly at greater risk because of their common attachment in muddy environments, dense aggregations, and thin skeletons. Because the Disko Fan location is already protected within a marine refuge (DFO 2007), a main conservation need for the species is to identify if it exists in other locations that are not protected from bottom-contact

fishing. Additionally, any deep-sea bamboo species with similar growth forms to *K. flexibilis* should be prioritized for growth rate and aging studies, and protection efforts.
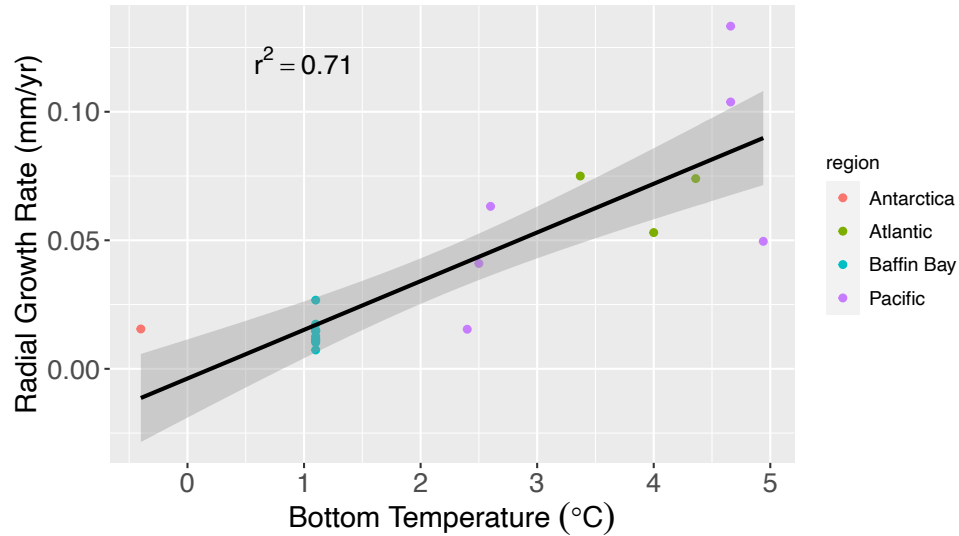
Figure 3-11. Bottom temperature and radial growth rate comparisons for *Keratoisis* colonies collected from different regions. Data in the figure is based on published studies of *Keratoisis* from the Davidson Seamount (n = 2, Andrews et al. 2007); Australia (Pacific) (n = 2, Thresher et al. 2007); New Zealand (Pacific) (n = 1, Tracey et al. 2007); Newfoundland and Labrador, Canada (Atlantic) (n = 3, Sherwood and Edinger 2009); and Antarctica (n = 1, Thresher et al. (unpubl data); most of which were recorded in Thresher (2009). Blue points represent *Keratoisis* analyzed in this study from Baffin Bay (n = 11). The black line and grey shading are the linear best fit line with 95% confidence brackets.

3.5 CONCLUSIONS & FUTURE WORK

This study represents the first age and growth rate estimates for *K. flexibilis*, as the first ROV survey at the location was conducted in 2013 following reports of abundant *Keratoisis* sp. in fisheries bycatch (DFO 2007; Neves et al. 2015). Our results indicate ages ranging from 89-168 years, radial growth rates of 0.007-0.027 mm/yr, and axial growth rates of 1.5-5.3 mm/yr for *K. flexibilis* colonies. Comparatively, these discovered growth rates for *K. flexibilis* are slower than other *Keratoisis* species previously studied globally (Noé et al. 2008; Andrews et al. 2009; Sherwood and Edinger 2009; Farmer et al.

2015), but do compare to studies on other bamboo corals not specified to genus level (Hill et al. 2011), and a *Keratoisis* colony from Antarctica (Thresher 2009). Ages determined from this study are comparable to previous studies on *Keratoisis* species and bamboo corals, which suggests the genus has multidecadal to centennial longevity. Specifically, when comparing *K. flexibilis* to *K. grayi*, we find that *K. flexibilis* is much slower growing, yet longevities are similar (Sherwood and Edinger 2009). Bottom temperature likely plays an important role in the difference in growth rates because *K. flexibilis* specimens were collected from waters around 1°C, compared to temperatures greater than 3.4°C for *K. grayi*.

K. flexibilis colonies exhibited major and minor growth banding at the proteinaceous nodes of the coral skeletons, but minor growth bands are representative of annual banding for this species. The driving mechanism behind major growth banding was not determined in this study, but it is likely to be an interannual environmental variable or climatic signal because of the frequency of major growth band deposition.

Future work on the *K. flexibilis* species should include collecting additional colonies from the Disko Fan site to increase the abundance of studied colonies within this dataset and confirm growth rate and age estimates. Samples with thick skeletons should be prioritized, as these could have potential for AMS-^{14}C dating and trace element analyses, which were not practical with the thinner skeleton samples collected and used in this study. An additional study will analyze genetic differences of *K. flexibilis* colonies growing in the coral fields to better understand how the dense aggregations of colonies are forming (Neves in prep).

3.6 LITERATURE CITED

Andrews AH, Lundstrom CC, Cailliet GM, DeVogelaere AP. 2007. Investigations of bamboo coral age and growth from Davidson Seamount. Technical Report MBNMS.

Andrews AH, Stone RP, Lundstrom CC, DeVogelaere. 2009. Growth rate and age determination of bamboo corals from the northeastern Pacific Ocean using refined ^{210}Pb dating. Marine Ecology Progress Series. 397: 173-185.

Aranha R, Edinger E, Layne G, Piercey G. 2014. Growth rate variation and potential paleoceanographic proxies in *Primnoa pacifica*: Insights from high-resolution trace element microanalysis. Deep-Sea Research II. 99: 213-226.

Baker KD, Snelgrove PVR, Fifield DA, Edinger EN, Wareham VE, Haedrich RL, Gilkinson KD. 2019. Small-scale patterns in the distribution and condition of bamboo coral, *Keratoisis grayi*, in submarine canyons on the Grand Banks, Newfoundland. Frontiers in Marine Science. 6: article 374.

Baker KD, Wareham VE, Snelgrove PVR, Haedrich RL, Fifield DA, Edinger EN, Gilkinson KD. 2012. Distributional patterns of deep-sea coral assemblages in three submarine canyons off Newfoundland, Canada. Marine Ecology Progress Series. 445: 235-249.

Crann CA, Murseli S, St-Jean G, Zhao X, Clark ID, Kieser WE. 2017. First status report on radiocarbon sample preparation techniques at the A.E. Lalonde Laboratory (Ottawa, Canada). Radiocarbon. 59(3): 695-704.

DFO. 2007. Development of a closed-area in NAFO 0A to protect narwhal over-wintering grounds, including deep-sea corals. DFO Can. Sci. Advis. Sec. Sci. Resp. 2007/002.

Edinger EN, Sherwood OA, Piper DJW, Wareham VE, Baker KD, Gilkinson KD, Scott DB. 2011. Geological features supporting deep-sea coral habitat in Atlantic Canada. Continental Shelf Research. 31: S69-S84.

Farmer JR, Robinson LF, Hönisch B. 2015. Growth rate determinations from radiocarbon in bamboo corals (genus *Keratoisis*). Deep-Sea Research I. 105: 26-40.

Fosså JH, Mortensen PB, Furevik DM. 2002. The deep-water coral *Lophelia pertusa* in Norwegian waters: distribution and fishery impacts. Hydrobiologia. 471: 1-12

France SC. 2007. Genetic analysis of bamboo corals (Cnidaria: Octocorallia: Isididae): does lack of colony branching distinguish *Lepidisis* from *Keratoisis*? Bulletin of Marine Science. 81(3): 323-333.

Gass SE, Willison JHM. 2005. An assessment of the distribution of deep-sea corals in Atlantic Canada by using both scientific and local forms of knowledge. Cold-Water Corals and Ecosystems - Erlangen Earth Conference Series.

Greeley K. 2021. MSc Thesis. Memorial University of Newfoundland.

Hill TM, Spero HJ, Guilderson T, LaVigne M, Clague D, Macalello S, Jang N. 2011. Temperature and vital effect controls on bamboo coral (*Isididae*) isotope geochemistry: A test of the "lines method". Geochemistry, Geophysics, Geosystems (G^3). 12(4).

Marriott P, Tracey DM, Bostock H, Hitt N, Fallon SJ. 2020. Ageing Deep-Sea Black Coral *Bathypathes patula*. Frontiers in Marine Science. 7: 479.

Murseli S, Middlestead P, St-Jean G, Zhao X, Jean C, Crann CA, Kieser WE, Clark ID. 2019. The preparation of water (DIC, DOC) and gas (CO_2, CH_4) samples for radiocarbon analysis at AEL-AMS, Ottawa, Canada. Radiocarbon. 61(5): 1563-1571.

Neves B de M, Edinger E, Hillaire-Marcel C, Saucier EH, France SC, Treble MA, Wareham VE. 2015. Deep-water bamboo coral forests in a muddy Arctic environment. Mar Biodiv. 45:867-871.

Neves B de M, Edinger E, Layne GD, Wareham VE. 2015. Decadal longevity and slow growth rates in the deep-water sea pen *Halipteris finmarchica* (Sars, 1851) (Octocorallia: Pennatulacea): implications for vulnerability and recovery from anthropogenic disturbance. Hydrobiologia. 759: 147-170.

Noé SU, Dullo W-Chr. 2006. Skeletal morphogenesis and growth mode of modern and fossil deep-water isidid gorgonians (Octocorallia) in the West Pacific (New Zealand and Sea of Okhotsk). Coral Reefs. 25: 303-320.

Noé SU, Lembke-Jene L, Dullo W-Chr. 2008. Varying growth rates in bamboo corals: sclerochronology and radiocarbon dating of a mid-Holocene deep-water gorgonian skeleton (*Keratoisis* sp.: Octocorallia) from Chatham Rise (New Zealand). Facies. 54: 151-166.

Risk MJ, Heikoop JM, Snow MG, Beukens R. 2002. Lifespans and growth patterns of two deep-sea corals: *Primnoa resedaeformis* and *Desmophyllum cristagalli*. Hydrobiologia. 471: 125-131.

Roark EB, Guilderson TP, Dunbar RB, Ingram BL. 2006. Radiocarbon-based ages and growth rates of Hawaiian deep-sea corals. Marine Ecology Progress Series. 327: 1-14.

Roark EB, Guilderson TP, Flood-Page S, Dunbar RB, Ingram BL, Fallon SJ, McCulloch M. 2005. Radiocarbon-based ages and growth rates of bamboo corals from the Gulf of Alaska. Geophysical Research Letters. 32: L04606.

Roberts JM, Cairns SD. 2014. Cold-water corals in a changing ocean. Current Opinion in Environmental Sustainability. 7:118-126.

Saucier EH, France SC, Watling L. 2021. Toward a revision of the bamboo corals: Part 3, deconstructing the Family Isididae. Zootaxa. 5047(3): 247-272.

Schöne BR, Dunca E, Fiebig J, Pfeiffer M. 2005. Mutvei's solution: An ideal agent for resolving microgrowth structures of biogenic carbonates. Paleogeography, Paleoclimatology, Paleoecology. 228: 149-166.

Sherwood OA, Edinger EN, Guilderson TP, Ghaleb B, Risk MJ, Scott DB. 2008. Late Holocene radiocarbon variability in Northwest Atlantic slope waters. Earth and Planetary Science Letters. 275: 146-153.

Sherwood OA, Edinger EN. 2009. Ages and growth rates of some deep-sea gorgonian and antipatharian corals of Newfoundland and Labrador. Can. J. Fish. Aquat. Sci. 66:142 152.

Sherwood OA, Scott DB, Risk MJ, Guilderson TP. 2005. Radiocarbon evidence for annual growth rings in the deep-sea octocoral *Primnoa resedaeformis*. Marine Ecology Progress Series. 301: 129-134.

Thresher RE. 2009. Environmental and compositional correlates of growth rate in deep-water bamboo corals (Gorgonacea; Isididae). Marine Ecology Progress Series. 397: 187-196.

Thresher RE, Fallon SJ, Townsend AT. 2016. A "core-top" screen for trace element proxies of environmental conditions and growth rates in the calcite skeletons of bamboo corals (Isididae). Geochimica et Cosmochimica Acta. 193: 75-99.

Thresher RE, MacRae CM, Wilson NC, Fallon S. 2009. Feasibility of age determination of deep-water bamboo corals (Gorgonacea; Isididae) from annual cycles in skeletal composition. Deep-Sea Research I. 56: 442-449.

Thresher RE, MacRae CM, Wilson NC, Gurney R. 2007. Environmental effects on the skeletal composition of deep-water gorgonians (*Keratoisis* spp.; Isididae). Bulletin of Marine Science. 81(3): 409-422.

Tracey DM, Neil H, Marriott P, Andrews AH, Cailliet GM, Sánchez JA. 2007. Age and growth of two genera of deep-sea bamboo corals (family Isididae) in New Zealand waters. Bulletin of Marine Science. 81(3): 393-408.

Wareham VE, Edinger EN. 2007. Distribution of deep-sea corals in the Newfoundland and Labrador region, Northwest Atlantic Ocean. Bulletin of Marine Science. 81:289-313.

Watling L, Saucier EH, France SC. 2022. Towards a revision of the bamboo corals (Octocorallia): Part 4, delineating the family Keratoisididae. Zootaxa. 5093(3): 337-375.

Williams T (in prep). PhD Thesis (data chapter 3). University of Southampton.

Appendix 3-1. Full sample preparation methods and results

To increase the visualization clarity of growth rings in *K. flexibilis* cross-sections, different methodologies were applied: Fluorescence microscopy; Staining samples with Mutvei's solution (Schöne et al. 2005); Thin sectioning, and etching in diluted 5% hydrochloric acid (HCl). These experiments were identical to those described in Chapter 2. Mutvei's stain (see chapter 2) was used to stain two *K. flexibilis* samples in attempt to improve growth ring clarity (Schöne et al. 2005). *K. flexibilis* samples R23-14 and R23-bycatch1 were stained for one hour in Mutvei's solution and allowed to dry before imaging under reflected light. A thin section was prepared of one *K. flexibilis* (R23-11a) sample to experiment with transmitted light and growth ring visibility. Thick sections made of *K. flexibilis* followed the first thin section methodology described in Chapter 2. Etching in 5% HCl was the final approach in attempting to increase growth ring clarity for multiple *K. flexibilis* samples, which followed the sampling methodology described in Chapter 2.

Fluorescence microscopy increased growth ring clarity in *K. flexibilis* samples, similarly to how it improved clarity in *A. arbuscula* (see Chapter 2). Comparison images with reflected light versus fluorescence show the difference in visualization capabilities of growth rings for *K. flexibilis*. Mutvei's solution was used to stain *K. flexibilis* samples for 1 hour. Results from the staining show that Mutvei's solution did not work on these samples, as the proteinaceous node portion of the skeleton did not seem to absorb the stain, causing there to be no etched or 3D appearance to the growth rings. Mutvei's stain may work on other bamboo corals, depending on composition of the skeleton and ability of the protein to absorb the stain (see chapter 2). Thin section preparation of a *K. flexibilis* sample

from a thick section showed no improvement in clarity of growth rings in the thin sections. Additionally, since the sample diameters of the *K. flexibilis* samples are small, creating level thin sections was challenging and no improvements were seen in the growth ring clarity; therefore, thin sections were not used for the remaining *K. flexibilis* samples. Nine *K. flexibilis* samples were etched with 5% HCl, and results show that etching does slightly improve growth ring clarity in some samples, but not all. In the remainder of the study, samples of *K. flexibilis* were etched if they were difficult to image for growth rings with reflected white light and fluorescence, similar to *A. arbuscula* (see Chapter 2).

Appendix 3-2. Comparison images of different sample preparation techniques
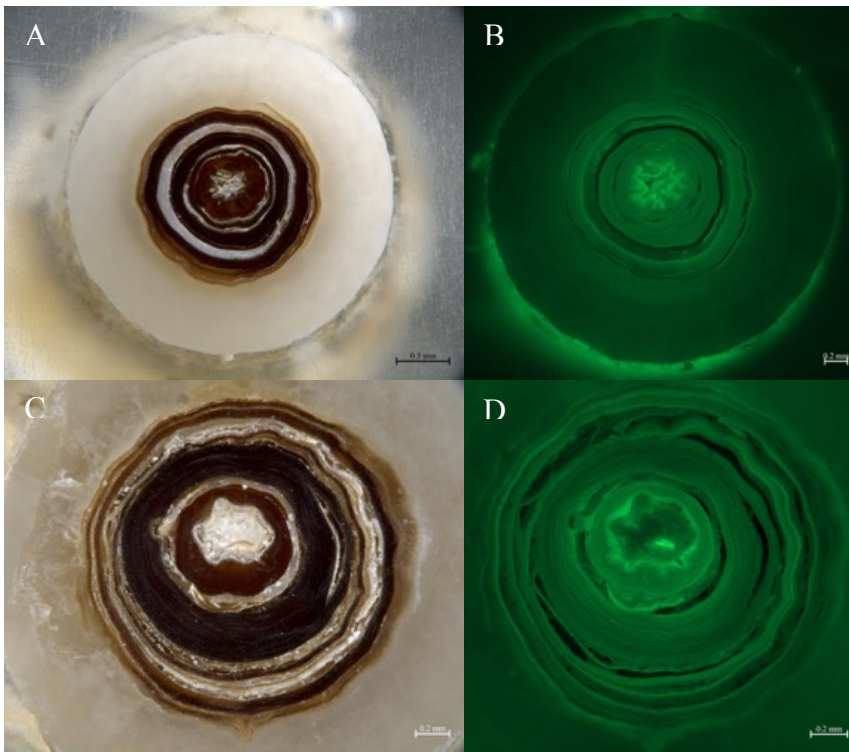
Figure A3-2.1. *K. flexibilis* sample R23-14b collected from Disko Fan in 2021 as A) sample in thick section imaged under white reflected light and B) the same sample and orientation of the sample imaged under green fluorescence (excitation wavelength: 488, emission wavelength: 509). *K. flexibilis* sample R23-14d collected from Disko Fan in 2021 as C) sample in thick section imaged under white reflected light and D) the same sample and orientation of the sample imaged under green fluorescence (excitation wavelength: 488, emission wavelength: 509).
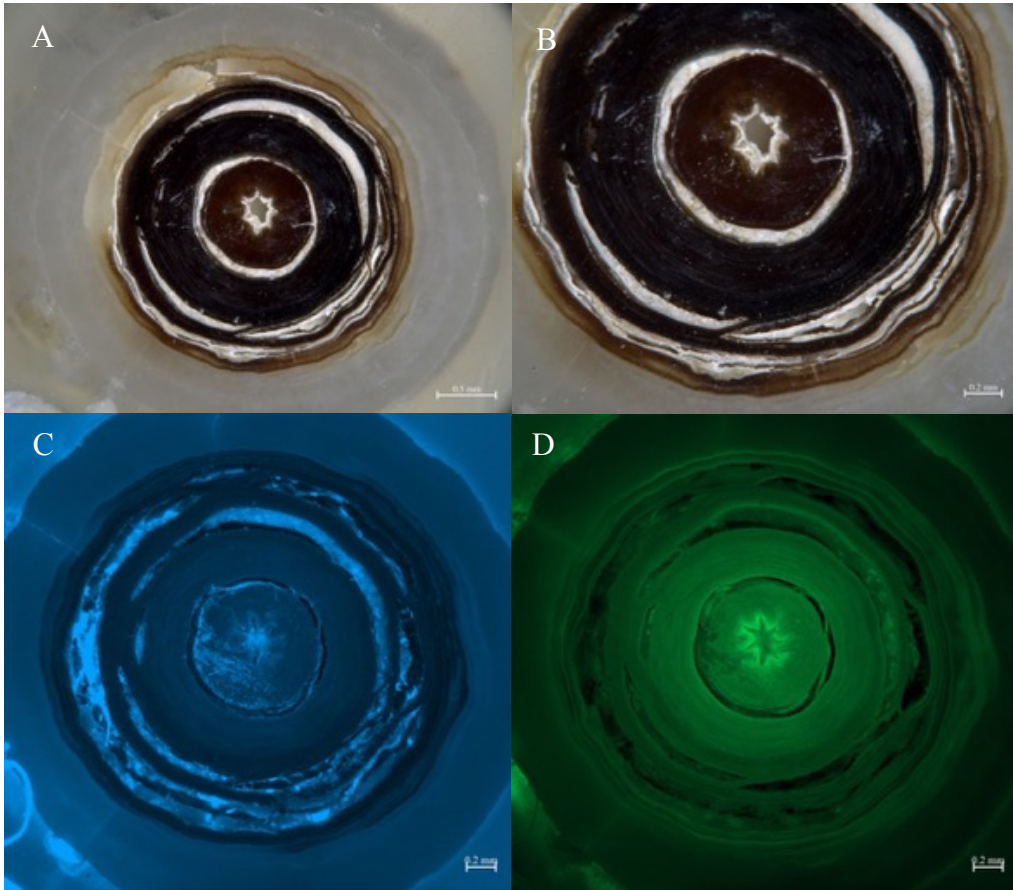
Figure A3-2.2. *K. flexibilis* sample R23-bycatch7, collected from Disko Fan in 2021. A) Sample in thick section imaged with reflected white light. B) Close-up of the proteinaceous node imaged with reflected white light. C) Sample in thick section imaged with blue fluorescence (excitation wavelength: 353, emission wavelength: 465). D) Sample in thick section imaged with green fluorescence (excitation wavelength: 488, emission wavelength: 509).
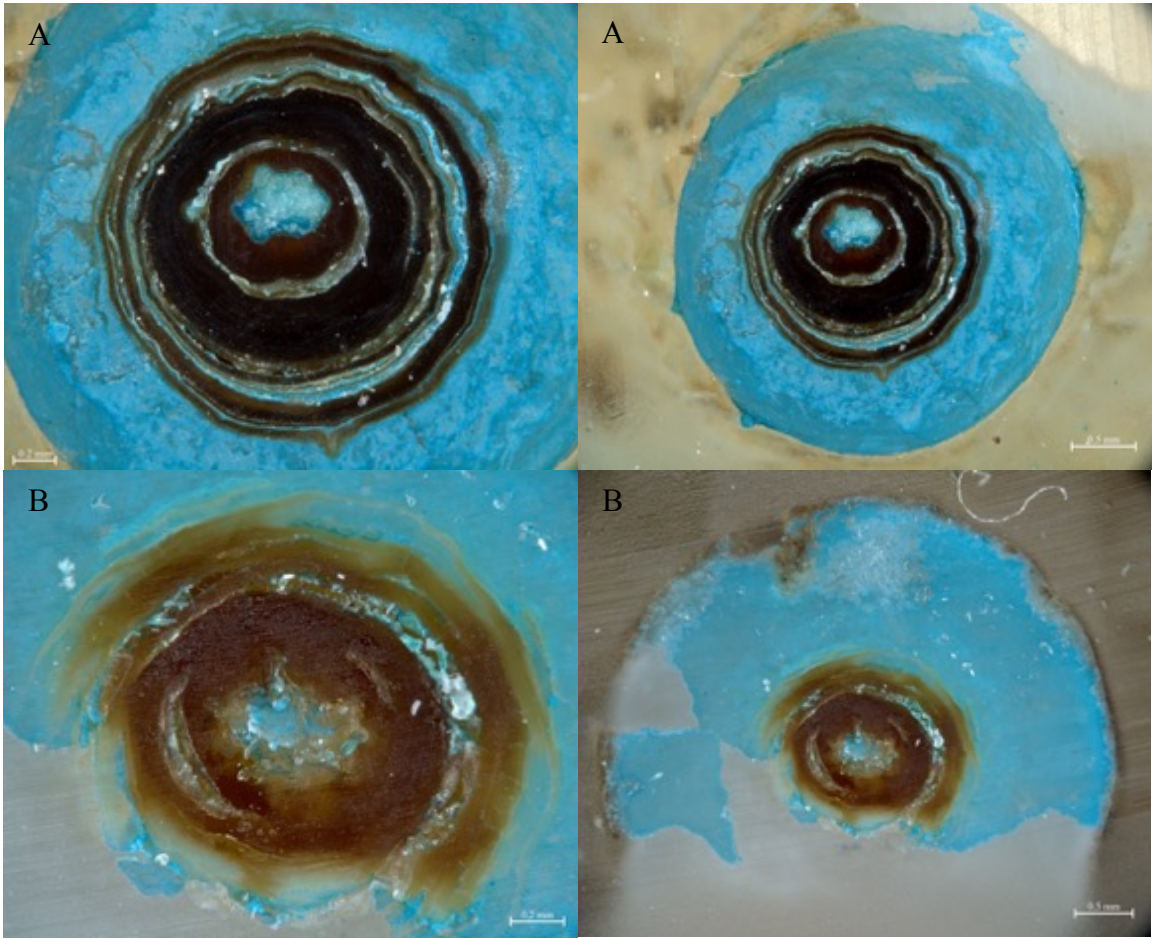
Figure A3-2.3. A) *K. flexibilis* sample R23-14 stained with Mutvei's solution for 1 hour and B) sample R23-bycatch1 stained with Mutvei's solution for 1 hour. Both samples did not absorb the stain in the proteinaceous node, but did absorb the stain in the calcite portion of the skeleton.

Figure A3-2.4. *K. flexibilis* sample R23-11a A) in thick section, imaged under reflected white light and B) in thin section imaged with transmitted light. Growth ring clarity did not improve with a thin section for this sample.
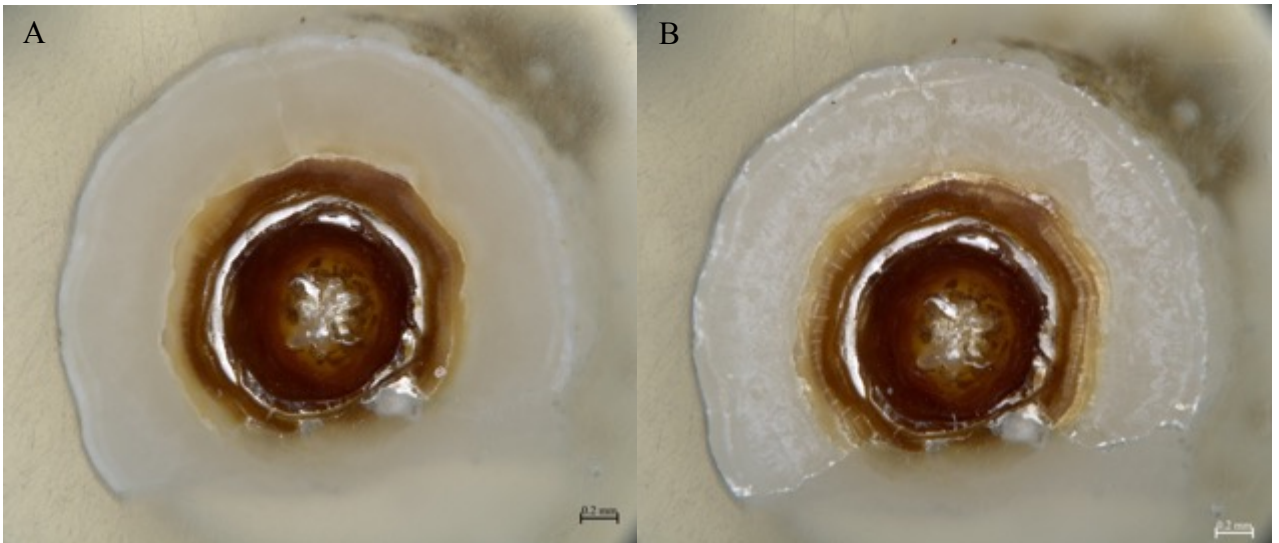
Figure A3-2.5. *K. flexibilis* sample R23-1a A) in thick section, grinded and polished, imaged with reflected white light and B) in thick section, grinded, polished, and etched with 5% HCl for about 1 minute, also imaged with reflected white light.
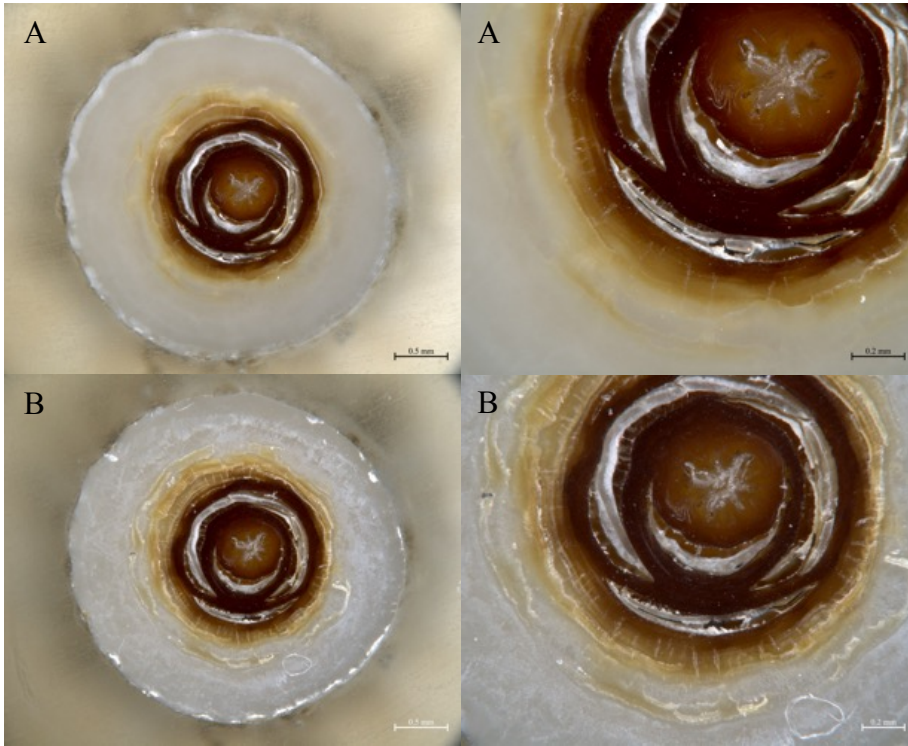
Figure A3-2.6. *K. flexibilis* sample R23-1b A) in thick section, grinded and polished, imaged with reflected white light and B) in thick section, grinded, polished, and etched with 5% HCl for about 1 minute, also imaged with reflected white light.
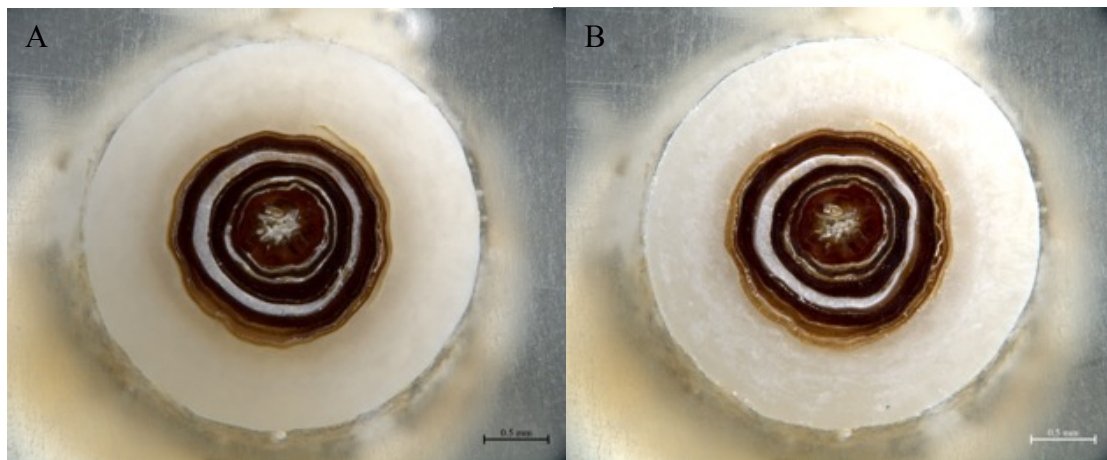
Figure A3-2.7. *K. flexibilis* sample R23-14b A) in thick section, grinded and polished, imaged with reflected white light and B) in thick section, grinded, polished, and etched with 5% HCl for about 1 minute, also imaged with reflected white light.
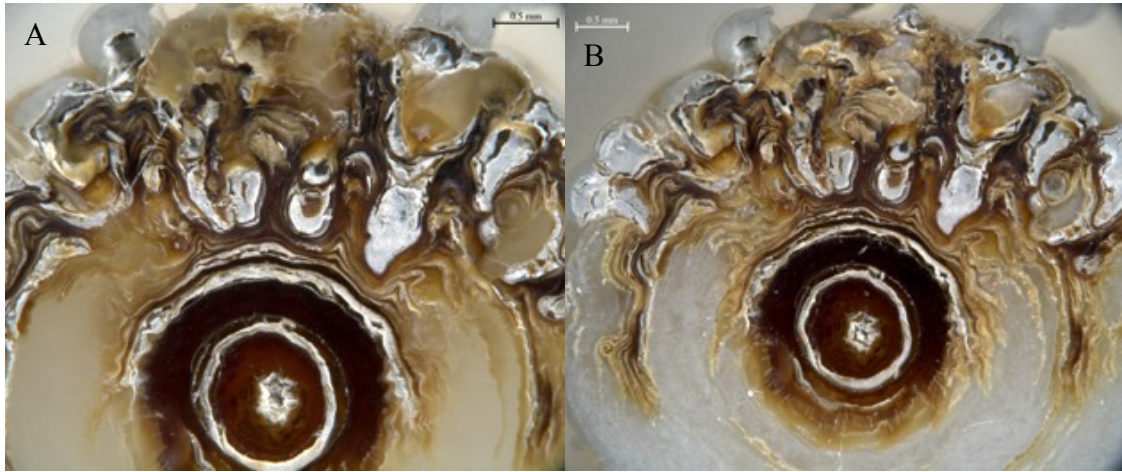
Figure A3-2.8. *K. flexibilis* sample R23-bycatch8a A) in thick section, grinded and polished, imaged with reflected white light and B) in thick section, grinded, polished, and etched with 5% HCl for about 1 minute, also imaged with reflected white light.

Appendix 3-3. Additional data of ^{14}C-dated fragments and ring count samples
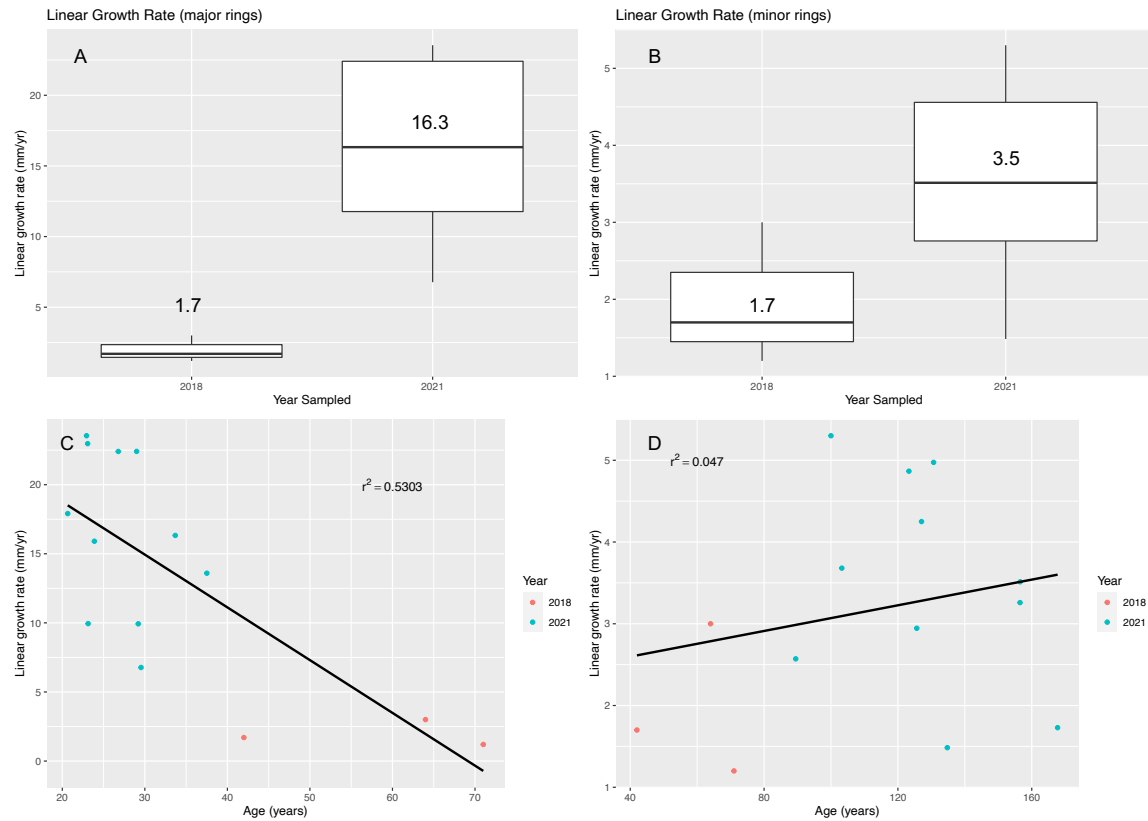
Figure A3-3.1. *Keratoisis flexibilis* samples collected as fragments from a push core at Disko Fan (2018) and collected as colonies from Disko Fan (2021). Linear growth rate is compared for both sampling methods, with age for colonies collected in 2021 based on major rings (A & C) and minor rings (B & D). Median values for each year are indicated on plots A and B. Black lines represent linear best fit lines.
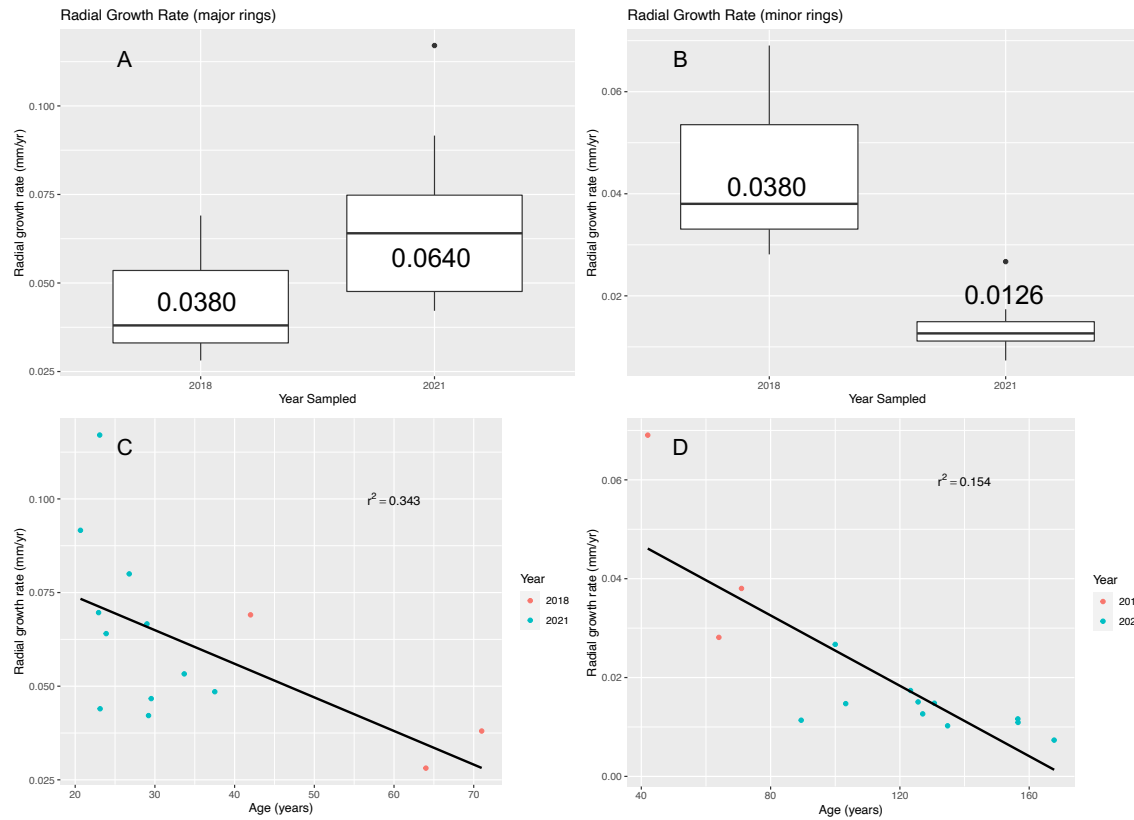
Figure A3-3.2. *Keratoisis flexibilis* samples collected as fragments from a push core at Disko Fan (2018) and collected as colonies from Disko Fan (2021). Radial growth rate is compared from each sampling year, with age for colonies collected in 2021 based on major rings (A & C) and minor rings (B & D). Median values for each year are indicated on plots A and B. Black lines represent linear best fit lines.
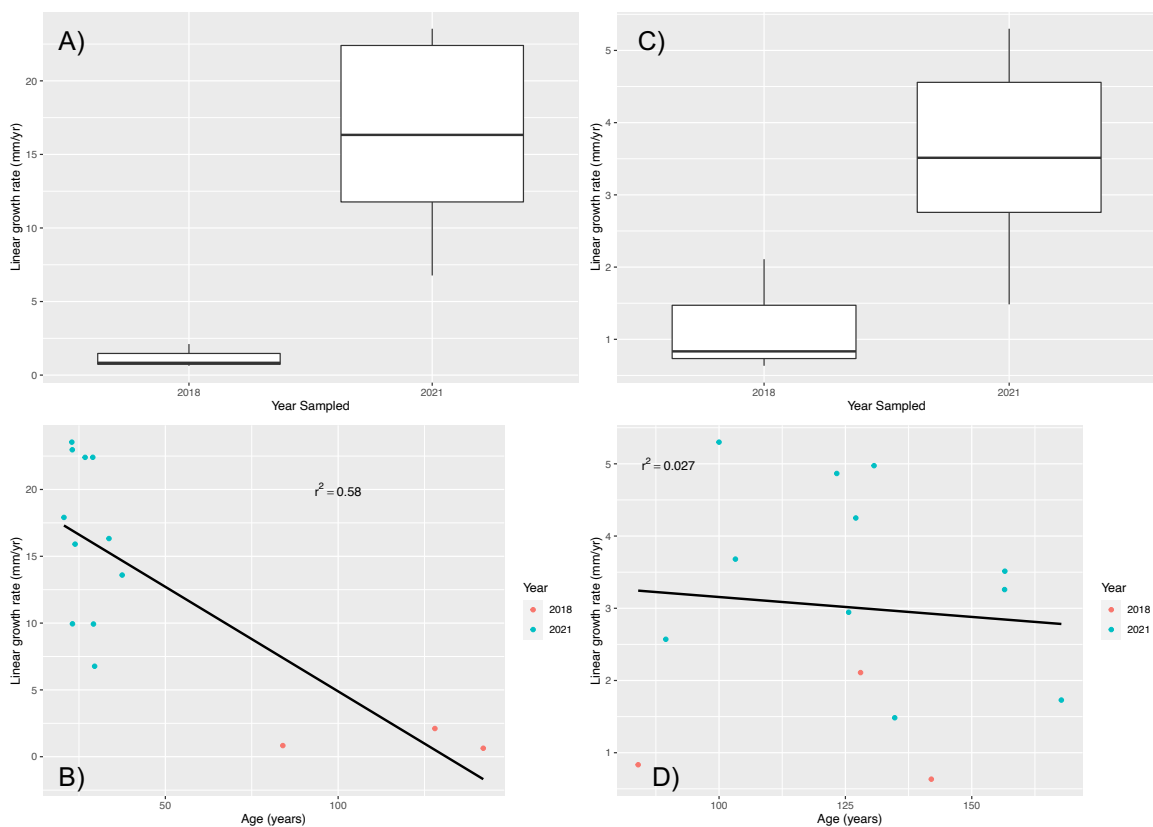
Figure A3-3.3. *Keratoisis flexibilis* samples collected as fragments from a push core at Disko Fan (2018) and collected as colonies from Disko Fan (2021). Linear growth rate is compared for both sampling methods, with age for colonies collected in 2021 based on major rings (A & B) and minor rings (C & D), and ages and linear growth rates of the 2018 samples are adjusted (see equation 2). Black lines represent linear best fit lines.
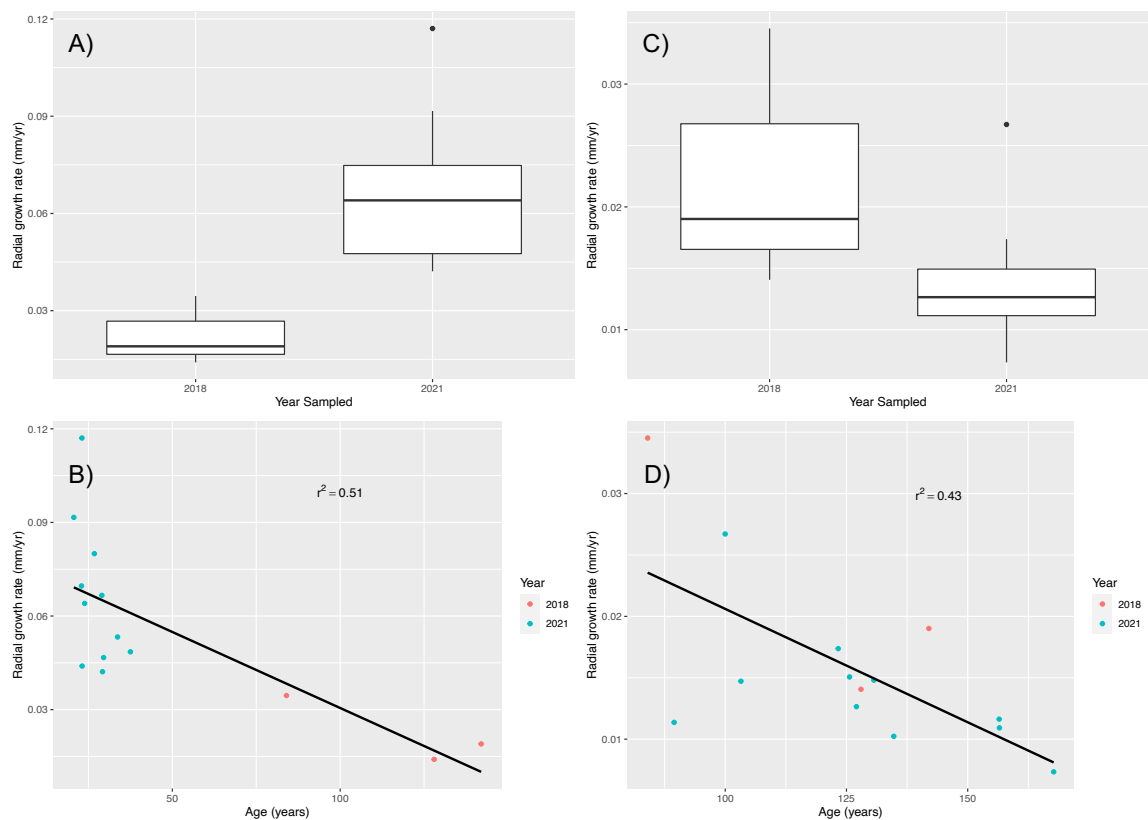
Figure A3-3.4. *Keratoisis flexibilis* samples collected as fragments from a push core at Disko Fan (2018) and collected as colonies from Disko Fan (2021). Radial growth rate is compared from each sampling year, with age for colonies collected in 2021 based on major rings (A & B) and minor rings (C & D), and ages and radial growth rates of the 2018 samples are adjusted (see equation 2). Black lines represent linear best fit lines.

Appendix 3-4. *K. flexibilis* and *K. grayi* additional comparisons
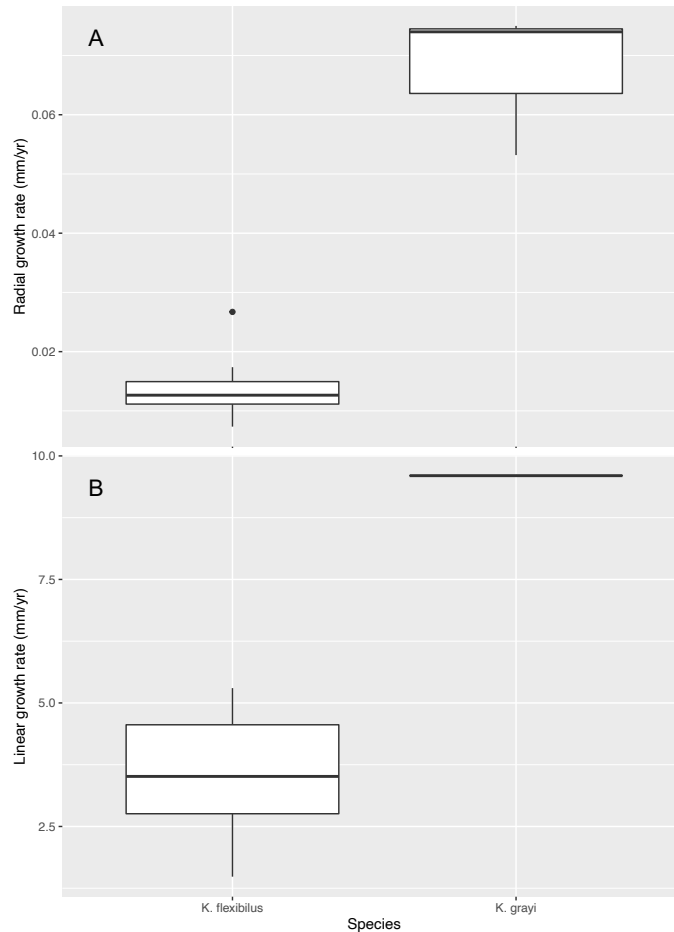
Figure A3-4.1. *Keratoisis flexibilis* (n=11) from Disko Fan and *Keratoisis grayi* (n=3 for radial growth rates; n=1 for axial growth rates) from Sherwood and Edinger 2009 compared for A) radial and B) axial growth rates.

Appendix 3-5. LA-AMS Radiocarbon Methods & Initial Results

Thick sections (varying width) of coral in epoxy were used for laser ablation accelerated mass spectrometry (LA-AMS) bomb-radiocarbon (^{14}C) analyses. Three *K. flexibilis* samples collected in 2021 were prepared for LA-AMS ^{14}C (R23-14b; R23-bycatch4b; R23-bycatch7b). These samples were chosen based on sample quality and amount of gorgonin node present, as this increases the amount of sample to analyze for ^{14}C

measurements. The samples were photographed before being analyzed using reflected white light and fluorescence. An additional sample of *K. grayi* was measured for bomb-^{14}C (sample 1343). A sample from this *K. grayi* colony was measured with AMS-^{14}C in a previous study (Sherwood et al. 2008). The sample was chosen to be analyzed to compare the different ^{14}C techniques of bomb-^{14}C from LA-AMS and bomb-^{14}C AMS, as some *Keratoisis* species are too small for bomb-^{14}C AMS.

Data analysis: LA-AMS bomb-^{14}C

As the LA-AMS bomb-^{14}C technique is still experimental with bamboo corals, data collection of bomb^{14}C was still ongoing while completing this study. The data from LA-AMS measurements will be used and composed in the future, and with it, we will hopefully be able to determine annual from sub-annual growth ring formation in the species. With the ^{14}C dates, it can be determined which banding represents annual banding by comparing the number of major and minor growth rings counted between two ^{14}C dating points. The ^{14}C results from LA-AMS will also validate age and growth rate estimates determined from growth ring counting in this study.
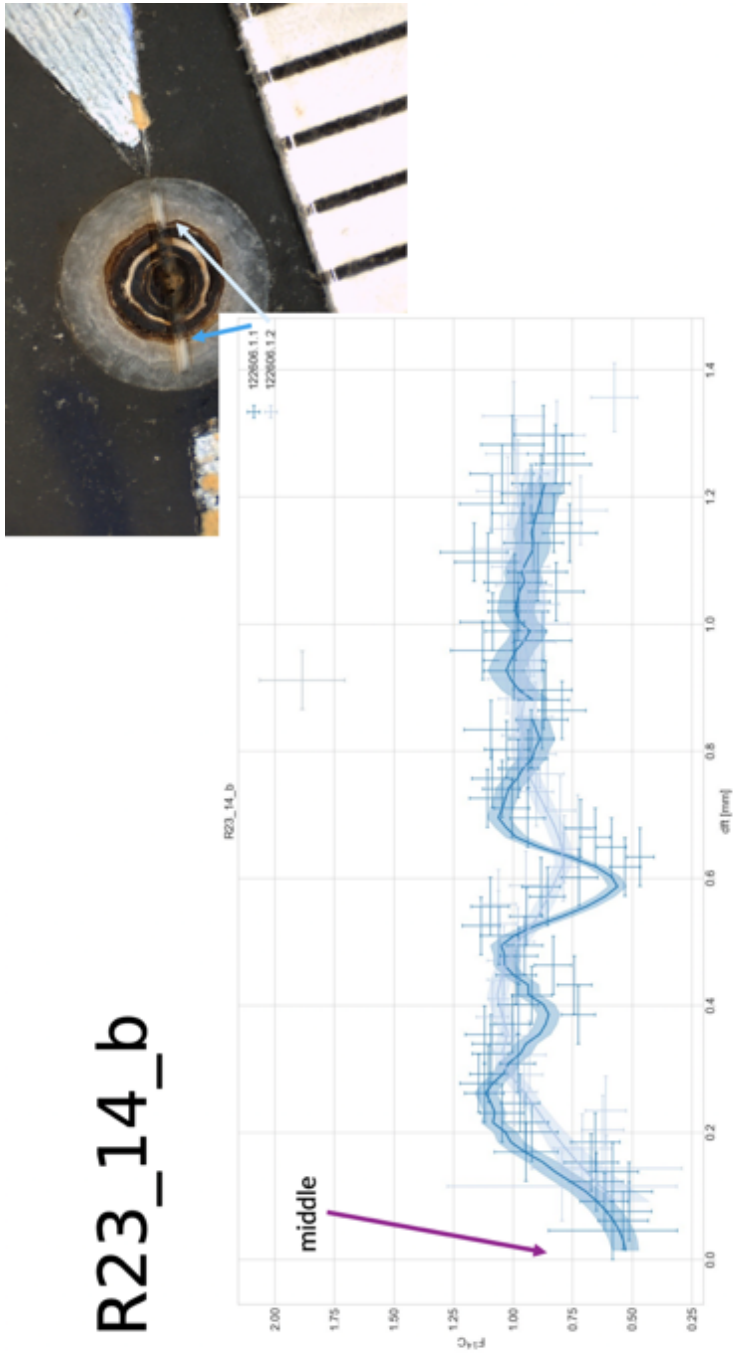
Figure A3-5.1. LA-AMS ^{14}C results for specimen R23-14b prepared by C. Welte and M. Wertnik at ETH Zürich.

Table A3-5.1. LA-AMS ^{14}C results for *K. flexibilis* specimen R23-14b

label	dft_mm	spot_mm	F14C	F14Cerror	sg	sg_err	C12 (uA)
R23_14_b			2.240217	0.694995717			0.0680569
R23_14_b			1.24635	0.582936264			0.053061
R23_14_b			0.229738	0.28282559			0.0477907
R23_14_b			0.254655	0.307400116			0.0460091
R23_14_b			0.890464	0.543261679			0.0442241
R23_14_b			1.241233	0.426018436			0.0977655
R23_14_b	0	0.0915	0.581387	0.270204936			0.1148617
R23_14_b	0.015463	0.0915	0.538757	0.104224369	0.528827	0.054689	0.7343063
R23_14_b	0.030927	0.0915	0.514177	0.094439604	0.538146	0.058143	0.8412972
R23_14_b	0.04639	0.09	0.617681	0.10185883	0.554849	0.060957	0.8577422
R23_14_b	0.061854	0.0915	0.513167	0.096755457	0.578936	0.063132	0.7866826
R23_14_b	0.077317	0.0915	0.651893	0.114464816	0.610407	0.064669	0.7067118
R23_14_b	0.09278	0.0915	0.583111	0.109172917	0.649262	0.065566	0.6944264
R23_14_b	0.108244	0.09	0.67204	0.114422751	0.696623	0.067501	0.7226163
R23_14_b	0.123707	0.0915	0.945943	0.13316954	0.760245	0.067395	0.7456237
R23_14_b	0.139171	0.0915	0.655509	0.103378157	0.825135	0.065595	0.8657503
R23_14_b	0.154634	0.0915	0.92151	0.109580218	0.878225	0.061624	1.0774394
R23_14_b	0.170098	0.0915	0.949374	0.098498509	0.951518	0.057866	1.3736367
R23_14_b	0.185561	0.09	1.046965	0.090267516	1.009648	0.053424	1.8100728
R23_14_b	0.201024	0.0915	0.972176	0.080605804	1.032563	0.048918	2.1119979
R23_14_b	0.216488	0.0915	1.120705	0.081474419	1.085143	0.047376	2.381677
R23_14_b	0.231951	0.0915	1.144571	0.078777785	1.076982	0.044977	2.6058208
R23_14_b	0.247415	0.09	1.102693	0.0779414	1.093608	0.044621	2.5646592
R23_14_b	0.262878	0.0915	0.98071	0.073307198	1.11516	0.044878	2.5849219
R23_14_b	0.278341	0.0915	1.094284	0.077392614	1.085285	0.04419	2.5822335
R23_14_b	0.293805	0.0915	1.093559	0.07807842	1.03971	0.043959	2.5320681
R23_14_b	0.309268	0.09	1.121026	0.079402535	1.020182	0.044899	2.5106923
R23_14_b	0.324732	0.0915	1.003993	0.075394486	0.969861	0.04486	2.5048137
R23_14_b	0.340195	0.0915	0.726728	0.069899134	0.946268	0.045671	2.1166937
R23_14_b	0.355659	0.0915	0.978489	0.086136043	0.888569	0.045807	1.859712
R23_14_b	0.371122	0.09	0.921161	0.083387554	0.863599	0.046225	1.8687253
R23_14_b	0.386585	0.0915	0.74296	0.072934606	0.850719	0.046298	1.9776547
R23_14_b	0.402049	0.0915	0.987173	0.085224686	0.873169	0.046586	1.9100794
R23_14_b	0.417512	0.0915	0.832523	0.077607978	0.935555	0.046813	1.951583
R23_14_b	0.432976	0.09	0.975532	0.078830961	0.937265	0.045085	2.211893
R23_14_b	0.448439	0.0915	0.950834	0.075720646	0.998613	0.044965	2.3390716
R23_14_b	0.463902	0.0915	1.058943	0.078842841	1.036123	0.044611	2.3950433
R23_14_b	0.479366	0.0915	1.134922	0.077709052	1.036592	0.043949	2.646232
R23_14_b	0.494829	0.09	0.944996	0.069485988	1.049596	0.045019	2.7667364
R23_14_b	0.510293	0.0915	1.096915	0.079299112	0.996923	0.045305	2.448453
R23_14_b	0.525756	0.0915	0.857091	0.074983017	0.906704	0.044555	2.1446008

R23_14_b	0.54122	0.0915	0.883147	0.081780211	0.79057	0.042948	1.8507632
R23_14_b	0.556683	0.09	0.723815	0.077205003	0.689743	0.041282	1.7154004
R23_14_b	0.572146	0.0915	0.530559	0.064187717	0.613854	0.039426	1.8524139
R23_14_b	0.58761	0.0915	0.466474	0.057170865	0.56222	0.037379	2.072369
R23_14_b	0.603073	0.0915	0.587111	0.06093679	0.586878	0.036594	2.2803436
R23_14_b	0.618537	0.0915	0.655865	0.0626853	0.650861	0.036254	2.3937129
R23_14_b	0.634	0.09	0.718151	0.06539862	0.75923	0.037485	2.3906743
R23_14_b	0.649463	0.0915	0.939465	0.072666825	0.888964	0.040308	2.515856
R23_14_b	0.664927	0.0915	1.005244	0.072829842	0.986538	0.043081	2.6768577
R23_14_b	0.68039	0.0915	1.108267	0.07552674	1.029026	0.044469	2.73372
R23_14_b	0.695854	0.09	1.048094	0.079448254	1.061923	0.046256	2.3250024
R23_14_b	0.711317	0.0915	1.088047	0.086518871	1.045822	0.047051	2.0273884
R23_14_b	0.72678	0.0915	0.977631	0.084271715	1.031732	0.049067	1.92125
R23_14_b	0.742244	0.0915	0.9371	0.081991712	1.019462	0.052354	1.9422197
R23_14_b	0.757707	0.09	1.026557	0.093892052	0.983235	0.054831	1.6177214
R23_14_b	0.773171	0.0915	0.923488	0.093776388	0.959806	0.056812	1.4600301
R23_14_b	0.788634	0.0915	1.092668	0.113484876	0.92038	0.058157	1.1712043
R23_14_b	0.804098	0.0915	0.879218	0.10897291	0.908244	0.060619	1.0231317
R23_14_b	0.819561	0.09	0.794341	0.100081417	0.887705	0.062706	1.0936714
R23_14_b	0.835024	0.0915	0.872779	0.105789875	0.904281	0.065353	1.0716683
R23_14_b	0.850488	0.0915	0.864409	0.111305884	0.919101	0.067487	0.9553114
R23_14_b	0.865951	0.0915	1.885428	0.179297389			0.8139395
R23_14_b	0.881415	0.09	0.999053	0.125377193	0.91957	0.068617	0.8640937
R23_14_b	0.896878	0.0915	0.997879	0.126197965	0.976215	0.071855	0.8487695
R23_14_b	0.912341	0.0915	1.126631	0.135093743	1.009294	0.074523	0.8354732
R23_14_b	0.927805	0.0915	0.876005	0.120784659	1.029116	0.076057	0.8145118
R23_14_b	0.943268	0.0915	0.989598	0.128186417	1.01127	0.075549	0.815309
R23_14_b	0.958732	0.09	1.087217	0.135250952	0.989263	0.074832	0.8030676
R23_14_b	0.974195	0.0915	0.977972	0.127742292	0.953927	0.073792	0.8100386
R23_14_b	0.989659	0.0915	0.97589	0.128548752	0.930414	0.07321	0.8000212
R23_14_b	1.005122	0.0915	0.819989	0.118777123	0.975503	0.075109	0.7876838
R23_14_b	1.020585	0.09	0.993054	0.130777644	0.990125	0.075961	0.785154
R23_14_b	1.036049	0.0915	0.897768	0.124884695	0.984076	0.075763	0.7777732
R23_14_b	1.051512	0.0915	1.105629	0.138553246	0.975756	0.075306	0.7779732
R23_14_b	1.066976	0.0915	1.1639	0.141490543	0.953351	0.074229	0.7841801
R23_14_b	1.082439	0.09	0.914563	0.124847237	0.964581	0.074405	0.7931347
R23_14_b	1.097902	0.0915	0.762432	0.112855953	0.945957	0.073489	0.8098112
R23_14_b	1.113366	0.0915	0.830446	0.117860244	0.923194	0.072415	0.8080442
R23_14_b	1.128829	0.0915	0.960288	0.127567133	0.916731	0.072081	0.7946028
R23_14_b	1.144293	0.09	1.090842	0.13565538	0.924133	0.072448	0.7974555
R23_14_b	1.159756	0.0915	0.924356	0.125015045	0.912559	0.072069	0.7970895
R23_14_b	1.17522	0.0915	0.882996	0.121676736	0.90111	0.07175	0.8036727
R23_14_b	1.190683	0.0915	1.047662	0.133399735	0.889787	0.071492	0.7925091

R23_14_b	1.206146	0.09	0.790991	0.116997041	0.878589	0.071294	0.7802965
R23_14_b	1.22161	0.0915	0.821571	0.11895153	0.867517	0.071155	0.7841901
R23_14_b	1.237073	0.0915	1.003738	0.132118219			0.7738861
R23_14_b	1.252537	0.0915	0.873046	0.122598688			0.782434
R23_14_b			1.954086	0.604032715			0.0775767
R23_14_b			1.105354	0.514904117			0.0614312
R23_14_b			0.93426	0.488854944			0.0565521
R23_14_b			1.239225	0.573271772			0.0546239
R23_14_b			1.288221	0.595044491			0.0531448
R23_14_b			0.48898	0.374638323			0.0523492
R23_14_b			0.504357	0.385594388			0.0518488
R23_14_b			0.782777	0.475174251			0.0511997
R23_14_b			1.067755	0.553826488			0.0507939
R23_14_b			0.510849	0.388861491			0.0503232
R23_14_b			0.517829	0.393736778			0.0502654
R23_14_b			0.238686	0.277025498			0.0501443
R23_14_b	0.062	0.108	0.796074	0.481613498			0.0494594
R23_14_b	0.091535	0.105	0.608168	0.317289276	0.570622	0.134458	0.0872485
R23_14_b	0.12107	0.108	0.708764	0.123272786	0.650672	0.104995	0.6784534
R23_14_b	0.150605	0.108	0.624302	0.087469493	0.724125	0.080213	1.1703489
R23_14_b	0.18014	0.108	0.612418	0.085618488	0.790983	0.060113	1.1899384
R23_14_b	0.209674	0.108	0.995438	0.094804853	0.851246	0.044695	1.5636509
R23_14_b	0.239209	0.105	0.953907	0.077102176	0.904912	0.033959	2.2638925
R23_14_b	0.268744	0.108	0.932489	0.067732705	0.964616	0.039947	2.8770483
R23_14_b	0.298279	0.108	0.975641	0.065661916	1.028151	0.039067	3.2114962
R23_14_b	0.327814	0.108	1.086273	0.06719725	1.043969	0.037082	3.4157361
R23_14_b	0.357349	0.105	1.04132	0.064314622	1.023606	0.036113	3.5872042
R23_14_b	0.386884	0.108	1.043116	0.063867204	1.048148	0.037778	3.6457533
R23_14_b	0.416419	0.108	1.038978	0.068271395	1.066906	0.03944	3.1555849
R23_14_b	0.445953	0.108	0.981573	0.071072383	1.049536	0.040081	2.7460556
R23_14_b	0.475488	0.105	1.061881	0.074863311	1.01416	0.03999	2.6740315
R23_14_b	0.505023	0.108	1.060681	0.074441841	0.96839	0.039111	2.7031639
R23_14_b	0.534558	0.108	0.947204	0.067522604	0.90705	0.037489	2.9534703
R23_14_b	0.564093	0.108	0.789339	0.05914989	0.863055	0.036165	3.2438945
R23_14_b	0.593628	0.105	0.784798	0.058419189	0.826753	0.035235	3.3212808
R23_14_b	0.623163	0.108	0.728952	0.057218661	0.789685	0.034678	3.21608
R23_14_b	0.652698	0.108	0.802102	0.063661378	0.797513	0.035368	2.8258337
R23_14_b	0.682233	0.108	0.903344	0.071135051	0.826294	0.036725	2.526209
R23_14_b	0.711767	0.105	0.855049	0.068020773	0.866878	0.038199	2.6185032
R23_14_b	0.741302	0.108	0.887983	0.068509745	0.906586	0.039654	2.6688298
R23_14_b	0.770837	0.108	0.973009	0.072829859	0.946639	0.040912	2.5840504
R23_14_b	0.800372	0.108	0.906739	0.07165409	0.964878	0.041994	2.4815358
R23_14_b	0.829907	0.105	0.9842	0.07689429	0.963731	0.043515	2.3270799

|							
R23_14_b	0.859442	0.108	1.024533	0.083979	0.963682	0.046353	2.0217179
R23_14_b	0.888977	0.108	0.970496	0.08594354	0.951487	0.049878	1.8180435
R23_14_b	0.918512	0.108	0.915407	0.093703618	0.932129	0.053606	1.4336231
R23_14_b	0.948047	0.105	0.867295	0.100822166	0.939509	0.058148	1.1651582
R23_14_b	0.977581	0.108	0.919187	0.111220965	0.958309	0.06297	1.0138143
R23_14_b	1.007116	0.108	0.956666	0.118246055	0.934746	0.065245	0.9304478
R23_14_b	1.036651	0.108	0.97097	0.120878122	0.93868	0.067607	0.9012327
R23_14_b	1.066186	0.105	1.047001	0.127359561	0.946175	0.069074	0.8737901
R23_14_b	1.095721	0.108	0.973148	0.124962469	0.965891	0.070452	0.8440392
R23_14_b	1.125256	0.108	0.716324	0.108374669	0.961408	0.071078	0.8298405
R23_14_b	1.154791	0.108	1.0225	0.130164417	0.950431	0.071149	0.8159243
R23_14_b	1.184326	0.105	0.978271	0.127658721	0.932962	0.070666	0.8122221
R23_14_b	1.21386	0.108	0.987467	0.127778423	0.909	0.069628	0.8177415
R23_14_b	1.243395	0.108	0.817725	0.117116856	0.878545	0.068034	0.8070782
R23_14_b	1.27293	0.108	0.997654	0.129070265			0.8096829
R23_14_b	1.302465	0.108	0.574707	0.09750094			0.8220199
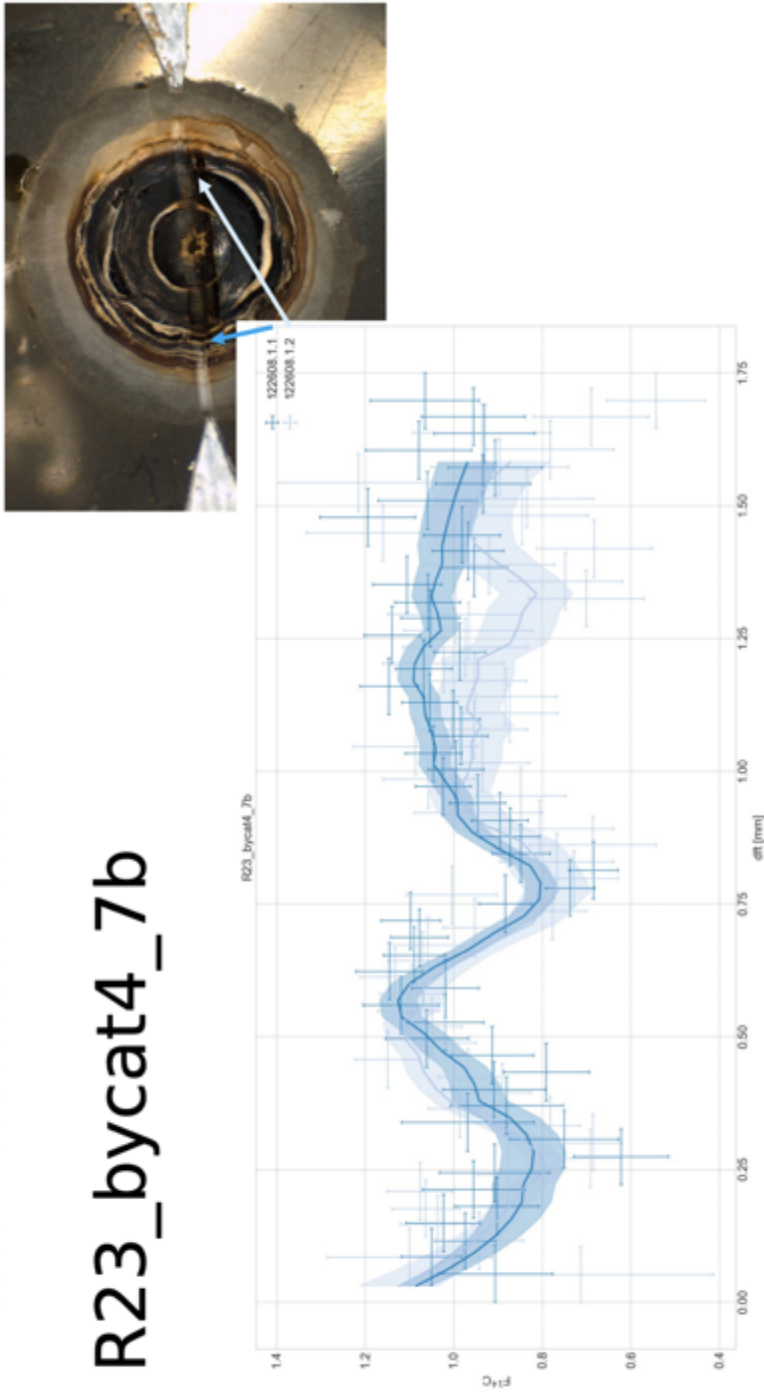
Figure A3-5.2. LA-AMS ^{14}C results for specimen R23-bycatch7b prepared by C. Welte and M. Wertnik at ETH Zürich.

Table A3-5.2. LA-AMS ^{14}C results for *K. flexibilis* specimen R23-bycatch7b.

label	dft_mm	spot_mm	F14C	F14Cerror	sg	sg_err	C12corr
R23_bycat7_b			0.797389	0.422489			0.06735
R23_bycat7_b			0.211409	0.253757			0.055943
R23_bycat7_b			0.516204	0.393147			0.051077
R23_bycat7_b			1.43437	0.658726			0.048565
R23_bycat7_b			0.563138	0.424421			0.046672
R23_bycat7_b			1.344652	0.617534			0.051954
R23_bycat7_b			0.838521	0.383823			0.081774
R23_bycat7_b	0	0.108	0.906568	0.129936			0.779068
R23_bycat7_b	0.031642	0.108	1.049878	0.068131	1.083073	0.033894	3.249073
R23_bycat7_b	0.063283	0.105	0.973887	0.068878	1.010147	0.042738	2.923069
R23_bycat7_b	0.094925	0.108	1.023418	0.083369	0.949637	0.050452	2.070443
R23_bycat7_b	0.126566	0.108	0.902043	0.094562	0.901544	0.057035	1.406052
R23_bycat7_b	0.158208	0.108	0.954868	0.115674	0.865866	0.062488	0.986909
R23_bycat7_b	0.189849	0.108	0.907727	0.125158	0.842605	0.066811	0.80432
R23_bycat7_b	0.221491	0.105	0.621933	0.10705	0.839293	0.072187	0.758591
R23_bycat7_b	0.253132	0.108	0.750038	0.123459	0.819877	0.073862	0.684982
R23_bycat7_b	0.284774	0.108	0.96824	0.149313	0.816101	0.072737	0.60504
R23_bycat7_b	0.316415	0.108	0.88002	0.128612	0.832097	0.069723	0.744282
R23_bycat7_b	0.348057	0.105	0.909005	0.115952	0.869319	0.066133	0.944671
R23_bycat7_b	0.379698	0.108	0.790752	0.09732	0.939092	0.062817	1.170805
R23_bycat7_b	0.41134	0.108	0.912535	0.093439	0.950371	0.056663	1.461948
R23_bycat7_b	0.442981	0.108	1.060494	0.093809	0.973728	0.051144	1.681768
R23_bycat7_b	0.474623	0.105	1.018792	0.086655	1.025808	0.048813	1.894792
R23_bycat7_b	0.506264	0.108	1.118767	0.085442	1.062788	0.04647	2.141834
R23_bycat7_b	0.537906	0.108	1.019175	0.075899	1.115401	0.04491	2.48397
R23_bycat7_b	0.569547	0.108	1.145554	0.075247	1.123586	0.04262	2.846317
R23_bycat7_b	0.601189	0.105	1.088831	0.069413	1.097826	0.040047	3.195192
R23_bycat7_b	0.63283	0.108	1.076946	0.065277	1.039683	0.037409	3.584585
R23_bycat7_b	0.664472	0.108	1.097128	0.066843	0.965458	0.035445	3.489533
R23_bycat7_b	0.696113	0.108	0.883214	0.060081	0.906488	0.034772	3.510065
R23_bycat7_b	0.727755	0.105	0.737223	0.055652	0.839164	0.03434	3.436775
R23_bycat7_b	0.759396	0.108	0.684299	0.055531	0.804638	0.034571	3.19418
R23_bycat7_b	0.791038	0.108	0.847571	0.066037	0.801939	0.035016	2.763811
R23_bycat7_b	0.822679	0.108	0.87193	0.066371	0.825132	0.035461	2.809098
R23_bycat7_b	0.854321	0.105	0.895423	0.064058	0.896287	0.036467	3.102295
R23_bycat7_b	0.885962	0.108	0.94625	0.063184	0.956302	0.03698	3.374759
R23_bycat7_b	0.917604	0.108	1.02374	0.063591	0.988692	0.036691	3.5989
R23_bycat7_b	0.949245	0.108	0.995163	0.063138	0.990503	0.035667	3.548321
R23_bycat7_b	0.980887	0.105	1.046331	0.063582	1.016126	0.035552	3.669563
R23_bycat7_b	1.012528	0.108	0.984145	0.061544	1.042223	0.035925	3.69575
R23_bycat7_b	1.04417	0.108	1.001569	0.061267	1.038793	0.035726	3.796066

R23_bycat7_b	1.075811	0.108	1.05399	0.062219	1.048678	0.035382	3.868599
R23_bycat7_b	1.107453	0.105	1.145932	0.065579	1.06283	0.035056	3.774973
R23_bycat7_b	1.139094	0.108	1.067899	0.063543	1.065205	0.035162	3.755362
R23_bycat7_b	1.170736	0.108	0.985788	0.058236	1.089081	0.036243	4.150959
R23_bycat7_b	1.202377	0.108	1.138922	0.063065	1.085893	0.03723	4.064024
R23_bycat7_b	1.234019	0.108	1.052921	0.066753	1.06669	0.038279	3.333307
R23_bycat7_b	1.26566	0.105	1.058801	0.073535	1.02654	0.039032	2.748334
R23_bycat7_b	1.297302	0.108	1.105463	0.077737	1.033796	0.04154	2.561757
R23_bycat7_b	1.328943	0.108	0.954228	0.07451	1.048188	0.045559	2.402822
R23_bycat7_b	1.360585	0.108	0.967705	0.080086	1.037542	0.049344	2.094518
R23_bycat7_b	1.392226	0.105	0.980929	0.087105	1.022805	0.052428	1.783677
R23_bycat7_b	1.423868	0.108	1.193878	0.107823	1.023425	0.05611	1.405175
R23_bycat7_b	1.455509	0.108	1.059136	0.112195	1.014768	0.058821	1.150325
R23_bycat7_b	1.487151	0.108	0.933306	0.106907	1.004685	0.061299	1.116066
R23_bycat7_b	1.518792	0.105	0.906158	0.106576	0.993177	0.063544	1.086666
R23_bycat7_b	1.550434	0.108	1.079175	0.119612	0.980243	0.065556	1.022983
R23_bycat7_b	1.582075	0.108	0.931057	0.114168	0.965883	0.067335	0.968787
R23_bycat7_b	1.613717	0.108	0.955823	0.117165			0.94257
R23_bycat7_b	1.645358	0.105	1.06558	0.122618			0.959113
R23_bycat7_b			0.612088	0.327811			0.087413
R23_bycat7_b			0.572591	0.353169			0.069799
R23_bycat7_b			0.192825	0.229876			0.062057
R23_bycat7_b			0.692443	0.419822			0.056552
R23_bycat7_b			0.477764	0.361932			0.05424
R23_bycat7_b			0.486458	0.367223			0.052703
R23_bycat7_b			-0.03291	-0.0013			0.051803
R23_bycat7_b			0.530839	0.399055			0.05133
R23_bycat7_b			-0.03215	-0.0013			0.050263
R23_bycat7_b			1.358759	0.621831			0.049943
R23_bycat7_b			-0.03125	-0.00129			0.04984
R23_bycat7_b			0.689381	0.416017			0.059105
R23_bycat7_b	0	0.105	0.712046	0.299432			0.113653
R23_bycat7_b	0.031037	0.108	1.099661	0.186468	1.132235	0.088336	0.452674
R23_bycat7_b	0.062074	0.108	0.942855	0.099943	1.059241	0.073041	1.346655
R23_bycat7_b	0.093111	0.108	1.036726	0.083542	0.996769	0.060217	2.113625
R23_bycat7_b	0.124148	0.105	1.063458	0.076385	0.94482	0.049863	2.592497
R23_bycat7_b	0.155185	0.108	1.076413	0.074301	0.903393	0.04198	2.778737
R23_bycat7_b	0.186222	0.108	0.878065	0.069486	0.872489	0.036566	2.607247
R23_bycat7_b	0.217259	0.108	0.690417	0.06749	0.841876	0.039173	2.191239
R23_bycat7_b	0.248296	0.105	0.685858	0.066468	0.794403	0.038905	2.248856
R23_bycat7_b	0.279333	0.108	0.781395	0.068029	0.808207	0.039133	2.427474
R23_bycat7_b	0.31037	0.108	0.985824	0.070733	0.851149	0.039361	2.813631
R23_bycat7_b	0.341407	0.108	0.890291	0.065842	0.926107	0.039729	2.933874

R23_bycat7_b	0.372444	0.105	0.967203	0.068431	1.001107	0.039876	2.943126
R23_bycat7_b	0.403481	0.108	1.149228	0.073103	1.043272	0.039706	3.054622
R23_bycat7_b	0.434519	0.108	1.018346	0.068063	1.070421	0.040045	3.130489
R23_bycat7_b	0.465556	0.108	1.048786	0.068202	1.081983	0.04078	3.208999
R23_bycat7_b	0.496593	0.105	1.101689	0.069765	1.113264	0.042123	3.223605
R23_bycat7_b	0.52763	0.108	1.094724	0.072369	1.119725	0.042626	2.965226
R23_bycat7_b	0.558667	0.108	1.132612	0.079871	1.071993	0.041893	2.504758
R23_bycat7_b	0.589704	0.108	1.070195	0.077805	1.073033	0.043234	2.49684
R23_bycat7_b	0.620741	0.105	1.05837	0.07676	1.027621	0.043705	2.537534
R23_bycat7_b	0.651778	0.108	0.952269	0.072596	0.97431	0.045625	2.56081
R23_bycat7_b	0.682815	0.108	0.776757	0.076238	0.902798	0.048728	1.889927
R23_bycat7_b	0.713852	0.108	1.00425	0.10216	0.828313	0.056069	1.350472
R23_bycat7_b	0.744889	0.105	0.728493	0.099474	0.800261	0.066739	1.035668
R23_bycat7_b	0.775926	0.108	0.767293	0.128463	0.770433	0.074485	0.647068
R23_bycat7_b	0.806963	0.108	0.685798	0.142696	0.796143	0.078935	0.467624
R23_bycat7_b	0.838	0.108	0.806424	0.167235	0.820287	0.078193	0.399044
R23_bycat7_b	0.869037	0.105	0.944445	0.144386	0.855001	0.07696	0.631539
R23_bycat7_b	0.900074	0.108	0.848138	0.101685	0.937623	0.075795	1.148192
R23_bycat7_b	0.931111	0.108	1.056293	0.103571	0.975757	0.071097	1.370128
R23_bycat7_b	0.962148	0.108	0.935492	0.108215	0.993538	0.067354	1.108702
R23_bycat7_b	0.993185	0.105	1.086488	0.14079	0.974895	0.064005	0.756209
R23_bycat7_b	1.024222	0.108	0.953403	0.12084	0.963911	0.065842	0.906063
R23_bycat7_b	1.055259	0.108	0.874099	0.108408	0.965809	0.069436	1.029913
R23_bycat7_b	1.086296	0.108	0.882723	0.116586	0.943728	0.070952	0.895664
R23_bycat7_b	1.117333	0.105	0.952368	0.116208	0.97756	0.073813	0.973101
R23_bycat7_b	1.14837	0.108	1.023159	0.13715	0.965839	0.075542	0.745459
R23_bycat7_b	1.179407	0.108	0.974275	0.140888	0.950824	0.078606	0.670472
R23_bycat7_b	1.210444	0.108	0.966677	0.145858	0.951814	0.081705	0.61816
R23_bycat7_b	1.241481	0.108	0.995264	0.151799	0.87875	0.080365	0.587269
R23_bycat7_b	1.272519	0.105	0.7005	0.129992	0.861566	0.08157	0.564402
R23_bycat7_b	1.303556	0.108	0.747381	0.128285	0.849278	0.081542	0.619365
R23_bycat7_b	1.334593	0.108	0.919498	0.145395	0.819457	0.080933	0.589753
R23_bycat7_b	1.36563	0.108	0.682288	0.131078	0.859279	0.08368	0.540059
R23_bycat7_b	1.396667	0.105	1.159323	0.172596	0.914746	0.087437	0.523965
R23_bycat7_b	1.427704	0.108	0.845644	0.149155	0.959631	0.090853	0.512878
R23_bycat7_b	1.458741	0.108	0.834236	0.149442	0.97097	0.092012	0.504645
R23_bycat7_b	1.489778	0.108	1.215443	0.180852	0.968545	0.09231	0.499231
R23_bycat7_b	1.520815	0.105	0.89637	0.155628	0.952358	0.091746	0.499268
R23_bycat7_b	1.551852	0.108	0.782271	0.144841	0.922408	0.090319	0.503595
R23_bycat7_b	1.582889	0.108	0.936134	0.155714	0.878695	0.088031	0.519941
R23_bycat7_b	1.613926	0.108	0.689931	0.130175			0.551431
R23_bycat7_b	1.644963	0.105	0.543606	0.11097			0.602544

CHAPTER 4: General Conclusions

4.1 GROWTH RINGS

Many deep-sea coral species have been documented forming annual concentric growth rings in their axes. Prior to this study, the bamboo corals *Acanella arbuscula* and *Keratoisis grayi* were documented as forming concentric growth rings that were likely deposited annually (Sherwood and Edinger 2009). This still needed to be confirmed for *Keratoisis flexibilis* as it is a different species than *K. grayi* with a distinctly different growth form.

Two growth ring structures were documented in *A. arbuscula* and *K. flexibilis* specimens cross-sectioned at the proteinaceous nodes of the coral skeletons. The growth rings were defined as larger, more distinct ring formations, which were labeled as major rings, coupled with finer rings that could only be seen with advanced microscopy techniques and many polishing steps, which were labeled as minor rings. Two varying ring structures in deep-sea bamboo coral specimens have been observed previously (Roark et al. 2005; Tracey et al. 2007), but most studies have concluded the major ring to represent annual growth.

This study concluded major rings to represent annual growth for *A. arbuscula*, but minor rings to represent annual growth for *K. flexibilis*, which were both based on comparisons of age estimates from this study with previously radiometrically dated specimens of both species (Sherwood and Edinger 2009). Major rings in *A. arbuscula* were more prominent than in *K. flexibilis* due to inconsistent spacing in between major rings in *K. flexibilis* specimens. Minor rings in *A. arbuscula* were difficult to count and

required magnification up to 258x. The cause of minor ring formation in *A. arbuscula* specimens was not determined, but fine ring structures have been suggested to represent lunar cycles in food availability (Roark et al. 2005; Aranha et al. 2014). For *K. flexibilis*, the driving factor behind major growth ring formation was not concluded, but a similar finding was reported for *Paramuricea* sp., which documented seven major growth rings in a specimen 71±6 years in age (Sherwood and Edinger 2009). A driving mechanism may be climate fluctuations that tend to occur on timescales > 1 year, which could change food availability every few years leading to major growth ring formations along with annual minor growth rings. A study conducted on a *Porites* colony from the western sub-tropical North Pacific recorded Pacific Decadal Oscillation signals using Sr/Ca and U/Ca measurements of growth bands in the coral skeletons (Felis et al. 2010), which suggests that corals can record climate signals on timescales > 1 year.

4.2 LONGEVITY & GROWTH RATES FOR *A. ARBUSCULA* & *K. FLEXIBILIS*

Growth rates and ages were based on growth ring counts at the proteinaceous nodes of the coral skeletons and were compared to radiometrically validated specimens (Sherwood and Edinger 2009). Different methods were applied for sclerochronological analyses of both species, and fluorescence microscopy improved growth ring enumeration for these bamboo corals.

Ages for *A. arbuscula* ranged from 8-29 years, while radial growth rates ranged from 0.027 – 0.160 mm/yr and axial growth rates ranged from 1.87 – 16.1 mm/yr. *A. arbuscula* ages were younger than most other deep-sea bamboo coral species that have

been studied, which mostly have recorded longevities > 100 years (Fig. 4-1) (Roark et al. 2005; Andrews et al. 2009; Sherwood and Edinger 2009). However, the radial and axial growth rates determined for *A. arbuscula* were within similar ranges to previously documented growth rates of bamboo corals, including specimens previously studied from the Atlantic (Andrews et al. 2009; Sherwood and Edinger 2009). Ages were most similar to the sea pen species *Halipteris finmarchica* (Neves et al. 2015), *Halipteris willemoesi* (Wilson et al. 2002), and *Umbellula encrinus* (Neves et al. 2018) (Fig. 4-2).

Ages for the *K. flexibilis* specimens ranged from 89-168 years, with radial growth rates of 0.007-0.027 mm/yr, and axial growth rates of 1.5-5.3 mm/yr. While ages were similar for *K. flexibilis* and *K. grayi*, *K. flexibilis* growth rates were much slower (Sherwood and Edinger 2009), which reflects a difference in growth forms for the two species, despite similarity in DNA studies conducted with both species (Watling et al. 2022). *K. flexibilis* growth rates were slower than most documented growth rates for bamboo corals, in general (Andrews et al. 2009; Hill et al. 2011) (Fig. 4-1).
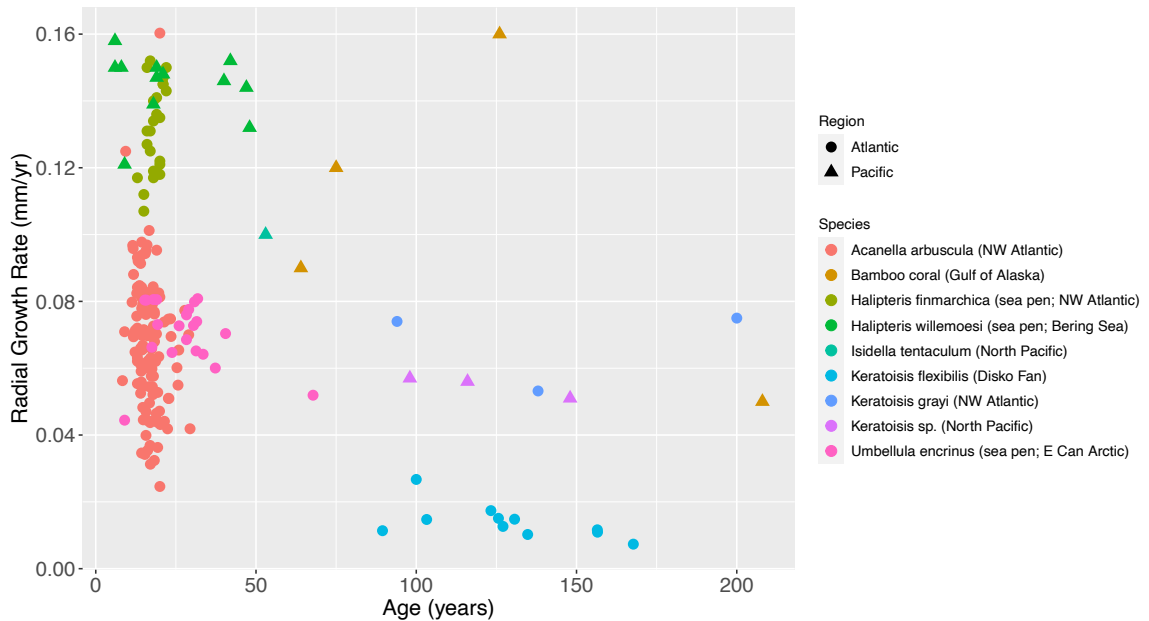
Figure 4-1. *Acanella arbuscula* and *Keratoisis flexibilis* ages and growth rates from this study, compared to *Keratoisis grayi* (Sherwood and Edinger 2009), bamboo corals (Roark et al. 2005), *Keratoisis* sp. (Andrews et al. 2009), *Isidella tentaculum* (Andrews et al. 2009), *Halipteris finmarchica* (Neves et al. 2015), *Halipteris willemoesi* (Wilson et al. 2002), *Umbellula encrinus* (Neves et al. 2018).
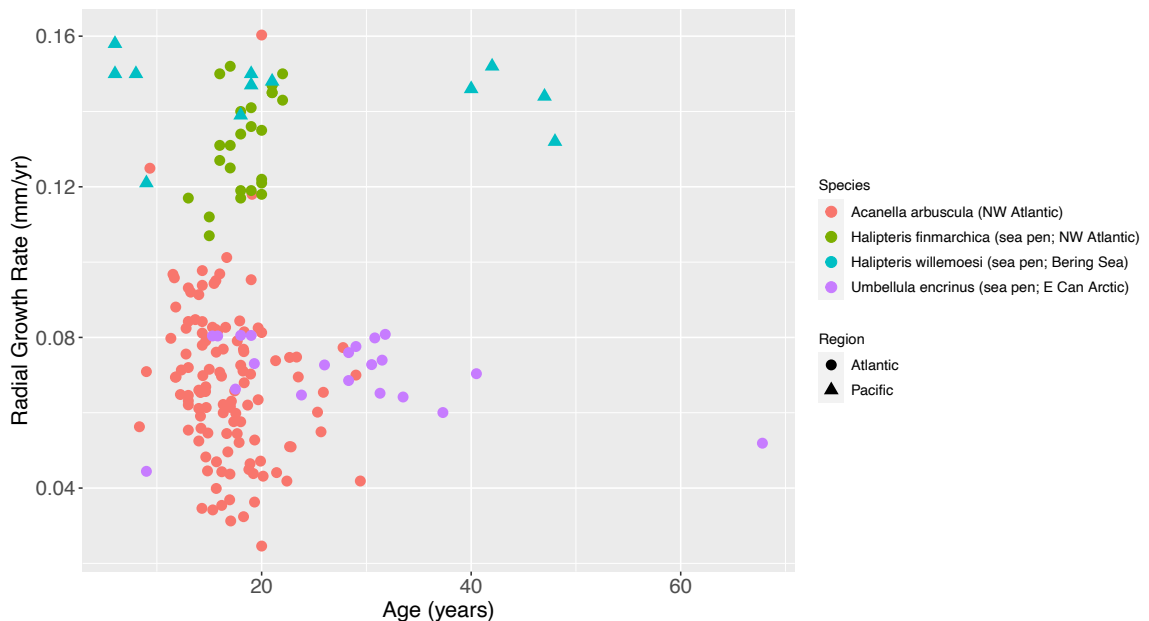

Figure 4-2. *Acanella arbuscula* colonies aged in this study compared only to sea pens from Neves et al. 2015, Wilson et al. 2002, and Neves et al. 2018.

4.3 ENVIRONMENTAL & ONTOGENETIC EFFECTS ON GROWTH RATES

4.3.1 Acanella arbuscula

A. arbuscula showed geographic differences in growth rates and longevity in the NW Atlantic when comparing the SW Grand Banks (NAFO zone 3O), the Northern Labrador Sea (NAFO zone 2H), and the SE Baffin Shelf (NAFO zone 0B). The youngest and fastest growing colonies existed on the SE Baffin Shelf, while the slowest growing and oldest colonies were found in the SW Grand Banks. Multi-factor ANOVA analyses indicated the differences in growth rates were due to ontogenetic factors, as the species seems to follow a Gompertz or logistic growth curve defined by slow growth in early and late stages of the corals' lifespan, and accelerated growth in between. Changes in growth rates throughout a corals' lifespan have been documented in previous studies on other bamboo corals as well (Andrews et al. 2009; Farmer et al. 2015).

Environmental variables were also explored in relation to *A. arbuscula* longevity and growth rates. The mean chlorophyll concentrations and phytoplankton bloom parameters were tested for relation to accelerated growth rates observed in NAFO zone 0B, but age was most strongly related, which suggests the variance in growth rates observed in the NW Atlantic was caused by ontogenetic, and not environmental factors. Figure 2-3b shows different widths of major growth rings in the species, with wider rings in the middle of the cross-section, and much thinner growth rings towards the center and outside of the section; supporting the conclusion that the species does not have consistent growth rates throughout its lifespan.

4.3.2 Keratoisis flexibilis

K. flexibilis specimens exhibited slower growth rates than most other previously documents growth rates for *Keratoisis* corals. Environmental variables, specifically bottom temperature, were concluded to be the primary cause of the difference in growth rates observed in this study. Specimens of *K. flexibilis* were collected from Disko Fan, at a bottom temperature of 1.1°C, compared to other *Keratoisis* colonies studied in the NW Atlantic, which were not collected in any temperature below 3.4°C. When comparing *K. flexibilis* to other regions, similarly most *Keratoisis* specimens were not collected in waters near 1°C, except for one specimen from Antarctica collected from a bottom temperature of -0.4°C (Thresher 2009).

The growth form observed for *K. flexibilis* colonies was also different than other *Keratoisis* species previously studied, as *K. flexibilis* has thin skeletons attached in muddy bottoms, and form dense coral fields instead of solitary colonies (Neves et al. 2015). *K. grayi* colonies observed in the SW Grand Banks have primarily been documented attached to hard substrates in solitary formations, with thick skeletons (Baker et al. 2012; 2019). The muddy environments *K. flexibilis* have been observed in are also low-current habitats, which likely contributes to their thin skeletons and slow growth rates because they do not require thick skeletons. *K. grayi* have been observed in high and low current environments on hard substrates only, which likely requires thicker skeletons for stability.

Environmental and ontogenetic factors influenced growth rates determined in this study. However, the relevance of environmental versus ontogenetic factors differed for each species, as ontogenetic factors were more applicable for growth rate variation in *A.*

arbuscula colonies, while environmental factors influenced growth rates of *Keratoisis* colonies.

4.4 FUTURE WORK

The previously under-studied bamboo corals *Acanella arbuscula* and *Keratoisis flexibilis* are slow growing species, similar to observations made for more heavily studied deep-sea corals. Longevity of *A. arbuscula* was shorter than other bamboo corals, and *K. flexibilis* growth rates were slower than previously determined growth rates for *Keratoisis* corals in the NW Atlantic. Based on the findings from this study, the following new scientific questions should be addressed:

1. Do other habitats dominated by *K. flexibilis* exist in the NW Atlantic or eastern Canadian Arctic? Since Disko Fan is protected within a marine refuge, conservation goals for the species should be focused on determining if this growth form or *K. flexibilis* colonies exist in other Arctic locations with bottom temperatures of 0-1°C, because these colonies would likely have similarly slow growth rates and fragile skeletons. If additional colonies are observed, they should be prioritized for protection because they are likely to be extremely vulnerable to disturbance events.

2. Is there a periodicity to minor growth rings in *A. arbuscula* and what causes the formation of these rings? Major growth rings were determined to represent annual growth in the species; therefore, it was not concluded what minor growth rings

217

represent, but they possibly follow lunar cycles in food availability (Roark et al. 2005).

3. Have colonies of *A. arbuscula* from other regions (i.e. Pacific) been analyzed for longevity and growth rates to compare growth rates and ages from the NW Atlantic to? Because this study determined short longevity for the species, it is of interest to expand the geographic variation compared and compare colonies from a broader range of environmental conditions that likely impact growth rates and possibly longevity.

4. What is the periodicity of major rings in *K. flexibilis* and what causes their formation? Minor growth rings were determined to represent annual growth for this species, meaning the cause for major growth ring formation is still unknown. Climate fluctuations on > 1 year timescales could possibly cause major growth rings to form, since they are present on annual to decadal increments.

5. How could radiometric dating be applied to coral specimens with diameters 1-5mm wide? Both species have small skeleton diameters, which challenges radiometric validation by traditional methods (e.g. [14]C, U-Th). Therefore; development of radiometric techniques for small deep-sea bamboo corals should be focused on in future studies to collect more information about both species (e.g. LA-AMS ^{14}C). Trace element analyses, such as Mg/Ca, Sr/Ca, and U/Ca would also be valuable in future work because trace element transects could assist in determining the periodicity of growth ring formation by constraining the timing of productivity fluxes (Felis et al. 2010; Aranha et al. 2014).

4.5 Literature Cited

Andrews AH, Stone RP, Lundstrom CC, DeVogelaere. 2009. Growth rate and age determination of bamboo corals from the northeastern Pacific Ocean using refined ^{210}Pb dating. Marine Ecology Progress Series. 397: 173-185.

Aranha R, Edinger E, Layne G, Piercey G. 2014. Growth rate variation and potential paleoceanographic proxies in *Primnoa pacifica*: Insights from high-resolution trace element microanalysis. Deep-Sea Research II. 99: 213-226.

Baker KD, Snelgrove PVR, Fifield DA, Edinger EN, Wareham VE, Haedrich RL, Gilkinson KD. 2019. Small-scale patterns in the distribution and condition of bamboo coral, *Keratoisis grayi*, in submarine canyons on the Grand Banks, Newfoundland. Frontiers in Marine Science. 6: article 374.

Baker KD, Wareham VE, Snelgrove PVR, Haedrich RL, Fifield DA, Edinger EN, Gilkinson KD. 2012. Distributional patterns of deep-sea coral assemblages in three submarine canyons off Newfoundland, Canada. Marine Ecology Progress Series. 445: 235-249.

Farmer JR, Robinson LF, Hönisch B. 2015. Growth rate determinations from radiocarbon in bamboo corals (genus *Keratoisis*). Deep-Sea Research I. 105: 26-40.

Felis T, Suzuki A, Kuhnert H, Rimbu N, Kawahata H. 2010. Pacific Decadal Oscillation documented in a coral record of North Pacific winter temperature since 1873. Geophysical Research Letters. 37(L14605).

Hill TM, Spero HJ, Guilderson T, LaVigne M, Clague D, Macalello S, Jang N. 2011. Temperature and vital effect controls on bamboo coral (*Isididae*) isotope geochemistry: A test of the "lines method". Geochemistry, Geophysics, Geosystems (G^3). 12(4).

Neves B de M, Edinger E, Hillaire-Marcel C, Saucier EH, France SC, Treble MA, Wareham VE. 2015. Deep-water bamboo coral forests in a muddy Arctic environment. Mar Biodiv. 45:867-871.

Neves B de M, Edinger E, Layne GD, Wareham VE. 2015. Decadal longevity and slow growth rates in the deep-water sea pen *Halipteris finmarchica* (Sars, 1851) (Octocorallia: Pennatulacea): implications for vulnerability and recovery from anthropogenic disturbance. Hydrobiologia. 759: 147-170.

Neves B de M, Edinger E, Wareham Hayes V, Devine B, Wheeland L, Layne G. 2018. Size metrics, longevity, and growth rates in *Umbellula encrinus* (Cnidaria: Pennatulacea) from the eastern Canadian Arctic. Arctic Science. 00: 1-28.

Roark EB, Guilderson TP, Flood-Page S, Dunbar RB, Ingram BL, Fallon SJ, McCulloch M. 2005. Radiocarbon-based ages and growth rates of bamboo corals from the Gulf of Alaska. Geophysical Research Letters. 32: L04606.

Sherwood OA, Edinger EN. 2009. Ages and growth rates of some deep-sea gorgonian and antipatharian corals of Newfoundland and Labrador. Can. J. Fish. Aquat. Sci. 66:142 152.

Thresher RE. 2009. Environmental and compositional correlates of growth rate in deep-water bamboo corals (Gorgonacea; Isididae). Marine Ecology Progress Series. 397: 187-196.

Tracey DM, Neil H, Marriott P, Andrews AH, Cailliet GM, Sánchez JA. 2007. Age and growth of two genera of deep-sea bamboo corals (family Isididae) in New Zealand waters. Bulletin of Marine Science. 81(3): 393-408.

Watling L, Saucier EH, France SC. 2022. Towards a revision of the bamboo corals (Octocorallia): Part 4, delineating the family Keratoisididae. Zootaxa. 5093(3): 337-375.

Wilson MT, Andrews AH, Brown AL, Cordes EE. 2002. Axial rod growth and age estimation of the sea pen, *Halipteris willemoesi* Kölliker. Hydrobiologia. 471: 133-142.

Appendix 4-1: Determining periodicity of growth ring formation in two species of bamboo corals: calcein staining experiment preliminary results & methodology

INTRODUCTION

In the Northwest (NW) Atlantic, fishing activities have posed threats to deep-sea corals for many years due to bottom trawling. A warming climate has led to increased anthropogenic activity in these areas, which includes expansion of oil and gas exploration, and a migration of fishing efforts into deeper waters (Roberts and Hirshfield 2004; Roberts and Cairns 2014). With an increase in anthropogenic activities, more species are at risk for disturbance, which includes vulnerable deep-sea corals. Corals are particularly vulnerable because of their sensitivity to environmental parameters in order to calcify successfully (Roberts and Cairns 2014), and their tendency to have slow growth rates and high longevities, meaning recovery from disturbance is slow and not guaranteed (Wareham and Edinger 2007).

Two abundant bamboo corals in the NW Atlantic are *Keratoisis* species (sp.) and *Acanella arbuscula* (Wareham and Edinger 2007). A previous study on deep-sea corals of Newfoundland and Labrador determined that *Keratoisis grayi* (*ornata*) colonies from the SW Grand Banks exhibit annual growth banding in their skeleton, which can be counted to age the samples (Sherwood and Edinger 2009). However, a different species of *Keratoisis* colonies exist at Disko Fan (c.f. *Keratoisis flexibilis*). One sample of *A. arbuscula* was also analyzed in this study, which suggested that *A. arbuscula* also exhibit annual growth bands (Sherwood and Edinger 2009). However, the periodicity of growth

ring formation in both *A. arbuscula* and *K. flexibilis* needs to be confirmed to validate data collected using growth ring counts.

Calcein solution has been used in previous studies to stain cold-water corals. Species previously stained with calcein include the reef-building corals, *Lophelia pertusa* and *Madrepora oculata* (Lartaud et al. 2017), and the red coral, *Corallium rubrum* (Marschal et al. 2004). These previous studies did not stain the samples *in situ*, but instead removed the corals from their habitat and stained them at the surface, and then returned them to the seafloor to continue growing. Alizarin red has also been used previously to stain corals for growth banding studies (Lartaud et al. 2017), but calcein solution has proven to be the least toxic for corals, thus allowing successful growth post-staining. This study aims to determine the periodicity of growth band formation for *A. arbuscula* and *K. flexibilis* using calcein solution to stain the corals *in situ*, and then allowing the stained corals to continue growing on the seafloor for 2-3 years.

METHODOLOGY

Making Calcein Solution

Two different concentrations of calcein solution (150 mg/L and 60 mg/L) were created for staining experiments with dead *A. arbuscula* and *K. flexibilis*. Filtered or DI water with Instant Ocean sea salt was mixed with the appropriate mass of calcein powder for each desired concentration of solution. Two higher concentration bottles were also made at 24 g/L (3g/125mL).

Calcein staining with dead samples

Previously collected samples stored at -20°C of *A. arbuscula* and *K. flexibilis* were used to test the staining effect of different calcein solution concentrations and for different lengths of staining time. This experiment was not a test of toxicity to the corals since these samples were already dead. 13 samples of *K. flexibilis* and 13 samples of *A. arbuscula* were first measured for wet weight and photographed. Different staining time and concentrations were experimented with, summarized in Table A4-1.1. Concentrations were chosen based on calcein solutions used in previous studies (Lartaud et el. 2017; Marschal et al. 2004), as it was previously concluded that these concentrations would likely not be toxic to corals when stained *in situ*. Variations in staining duration were chosen based on the amount of time corals would likely be stained *in situ*, which is limited due to the duration of the remotely operated vehicle (ROV) survey.

Samples were stained in glass beakers for 4 – 24 hours at different concentrations. Once removed from solution, samples were photographed again for any visible calcein solution remaining on the outside of the skeleton. To compare the effect of staining time and concentration, samples were observed using fluorescence microscopy on a Zeiss AxioZoom V.16 Telecentric Microscope (excitation wavelength: 488, emission wavelength: 509). Only the outside of the skeletons was observed for calcein uptake with these samples.

Staining experiment with living soft coral

Calcein stain was experimented with on a living soft coral, conducted at DFO by Bárbara Neves. Results of the staining indicated that the calcein solution was not toxic to the living soft coral.

Creating solution for CCGS Amundsen 2021

Most of the calcein solution concentrations were created at Memorial University before the 2021 *Amundsen* cruise due to the difficulties of preparing accurate concentrations of solution on board the ship. However, some additional solution was required to be made on board the ship. Concentrations created, which were chosen based on the success of the stain on dead samples, were three bottles of 3g/125mL and three bottles of 0.2g/125mL. The specific mass of calcein powder was chosen based on the volume of seawater used, and based on the 21L staining chambers the solutions would be dispersed in during the *in situ* staining. The concentration used in all *in situ* staining during the 2021 *Amundsen* cruise was 150 mg/L (Lartaud et al. 2017).

Acanella arbuscula in situ staining during 2021 Amundsen cruise

The first attempt of deploying the staining chambers was conducted on the SE Baffin Shelf (Davis Strait - *Acanella arbuscula* site) at about 1300 m depth. The completed transect length of the ROV dive with the *Astrid* ROV was about 1400 m, and covered a depth range of 1336-1293 m (Fig. 2-2). Bottom temperature at this site was 3.5°C and salinity was 34.8 PSU (Amundsen Science 2021 Leg 2 Cruise Report).

Two coral staining chambers were deployed during the ROV dive, which had calcein solution inside a balloon at a concentration of 150mg/L, mixed with seawater (Fig. A4-1.1). This was the first *in situ* attempt to stain bamboo corals with calcein in Canadian waters. Both staining chambers were deployed on small *A. arbuscula* colonies. The first staining chamber contained an *A. arbuscula* colony about 10 cm in height and 10 cm wide. At first attempt, the calcein solution was too buoyant and did not sink within the chamber (Fig. A4-1.2). The ROV then maneuvered the chamber, lifting it slightly off of the seafloor to mix the solution, which was successful. The first chamber stained the *A. arbuscula* colony for about 7 hours before being recovered at the end of the dive.

The second chamber was deployed on a different *A. arbuscula* colony, which was about 7 cm wide. The balloon containing calcein was punctured before the chamber was on the seafloor in an attempt to make the solution sink. Because of this, some of the calcein solution leaked out of the bottom of the chamber before being set down on the seafloor, meaning the final concentration of calcein solution within the second chamber is unknown (Fig. A4-1.2). The second chamber was recovered at the end of the dive and stained the *A. arbuscula* colony for about 6.5 hours. Three tent stakes were placed around each of the stained coral colonies and a floating marker was also placed near the colonies (Fig. A4-1.2). The stained corals will be revisited and collected in 2-3 years.
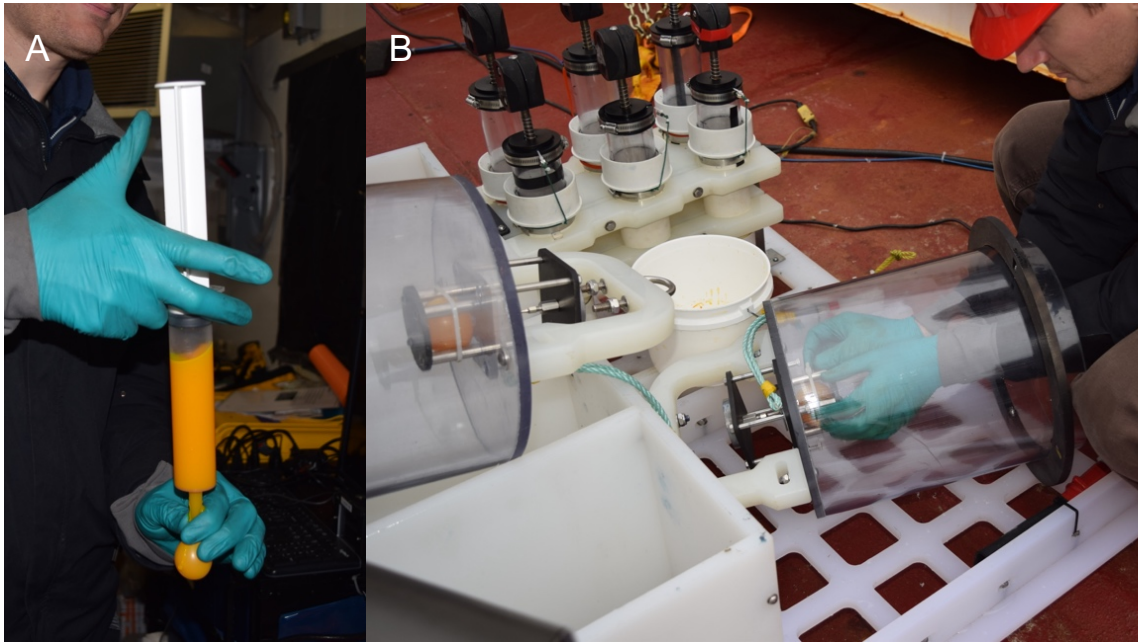
Figure A4-1.1. A) A balloon being filled with calcein solution in preparation for *in situ* staining on board the *Amundsen* in 2021. B) Both 21L staining chambers on the front porch of the "Astrid" ROV. Peter Lockhart (CSSF) is shown preparing the balloon filled with calcein solution for *in situ* staining.
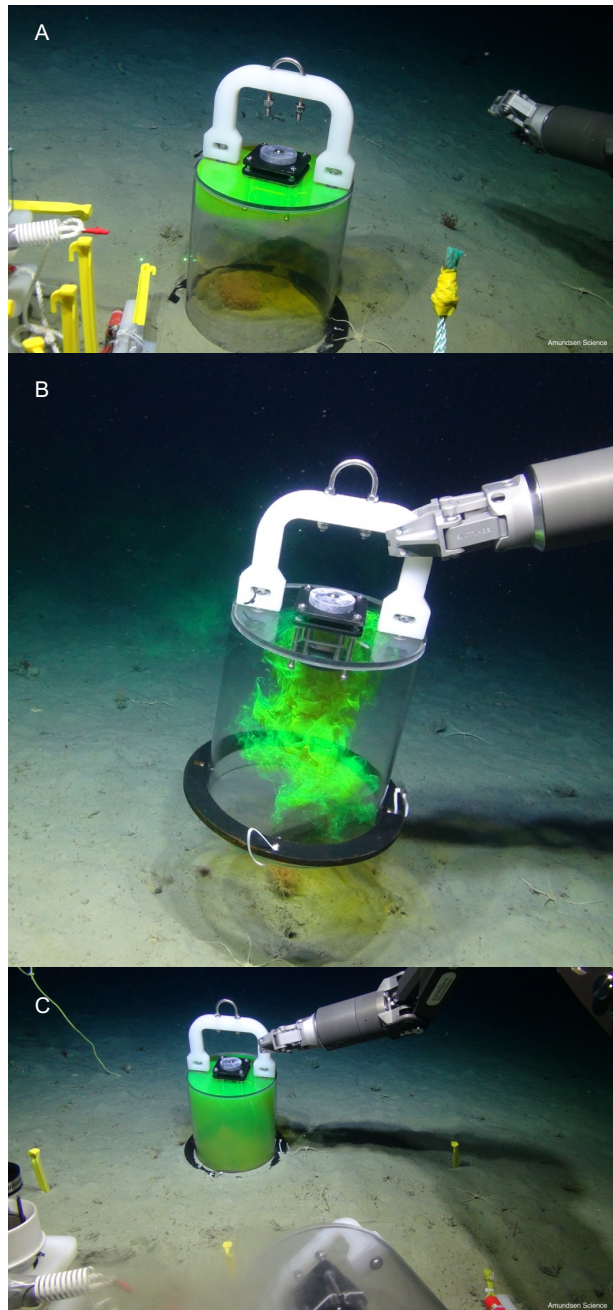
Figure A4-1.2. First *in situ* staining attempt at Davis Strait on an *A. arbuscula* colony on July 29, 2021. A) Calcein solution was too buoyant at first and remained at the top of the chamber. B) The balloon filled with calcein solution was punctured before placing the staining chamber on the seafloor due to difficulties in attempt 1 with stain buoyancy. Some solution escaped from the chamber, meaning the exact concentration used to stain this colony is unknown. C) Yellow tent stakes and floating marker shown to help relocate the colony in a future expedition.

Keratoisis flexibilis in situ calcein staining during 2021 Amundsen cruise

The second attempt to stain bamboo corals was conducted at Disko Fan at about 900 m depth (Fig. 3-1). This site had been previously visited by ROV surveys and abundant *K. flexibilis* samples forming dense coral fields had been observed and sampled previously (Neves et al. 2015). Originally a site located about 10 km from this site was chosen based on Fisheries Observer data, but due to lack of coral presence in box cores and drop cameras deployed at this new site, the ROV dive was instead conducted at the same location as previous dives in the area (Neves et al. 2015). Ice cover in the area also restricted the location and length of this dive, as ice poses abrasion threats to the ROV cable (Amundsen Science 2021 Leg 2 Cruise Report).

Two coral staining chambers were deployed during the dive, which had calcein solution inside a balloon at a concentration of 150mg/L, mixed with seawater. Before the dive, the calcein solution was altered to make it hypersaline, with approximately 1g of salt added to the solution (exact amount is unknown due to difficulty of getting accurate mass measurements on board the ship). This was an attempt to increase density of the solution so it did not remain at the top of the chamber as it did during the *A. arbuscula* staining attempt (Fig. A4-1.2). The staining chambers were also altered to include a plunging device, which could be operated with the ROV arm (Fig. A4-1.3). This allowed for mixture of the solution once the chamber was placed on the seafloor.

Both staining chambers during this dive were deployed on *K. flexibilis* colonies. Due to the size of *K. flexibilis* colonies, the staining chamber did not fit ideally over the colonies for staining (Fig. A4-1.4). The first deployed chamber stained the *K. flexibilis*

colony for about 4 hours due to limitations of the dive caused by ice cover complications. The second chamber stained a *K. flexibilis* colony for about 3.5 hours. The second stained colony was dislodged upon removal of the staining chamber; therefore, recollection of the stained sample in the future may be challenging. Three tent stakes were placed around each of the stained coral colonies and a floating marker was also placed near the colonies (Fig. A4-1.4). The stained corals will be revisited and collected in 2-3 years.

Figure A4-1.3. Staining chamber altered with plunging disc and rope, completed by Peter Lockhart (CSSF).
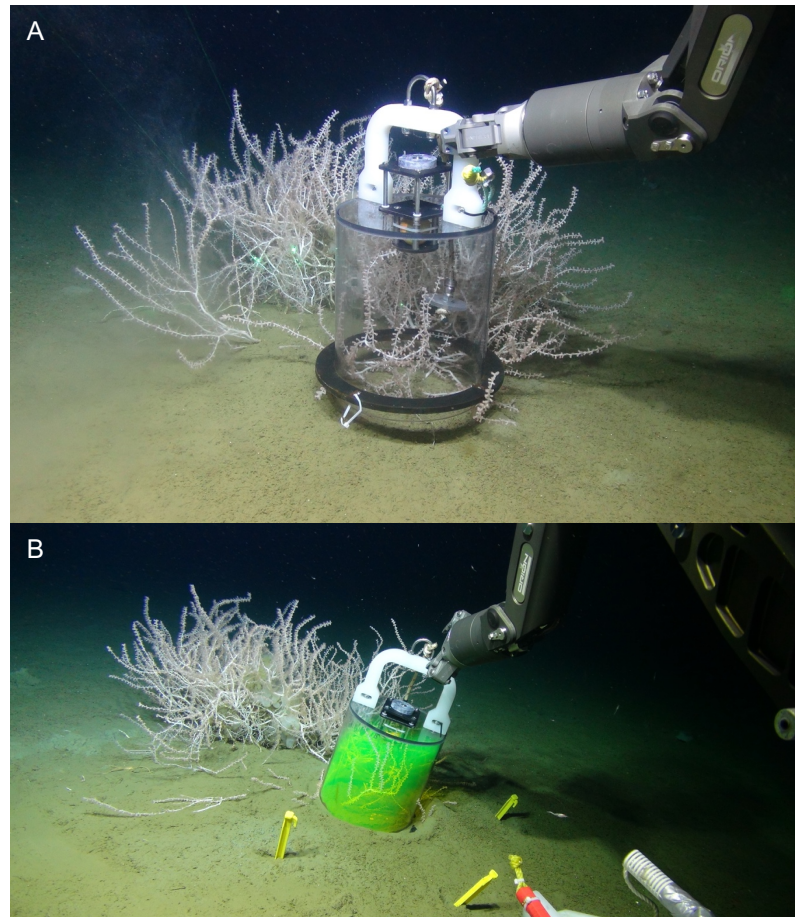
Figure A4-1.4. A) Staining chamber being placed on a *K. flexibilis* colony during the Disko Fan ROV dive in 2021. The size and density of *K. flexibilis* colonies made it challenging to stain individual colonies. B) Stain released on a *K. flexibilis* colony during the Disko Fan ROV dive in 2021. 3 yellow tent stakes are also shown, which will be used during future collection to relocate the stained colonies.

Aquaria experiments on board the Amundsen in 2021

The first experiment conducted in aquaria on board the *Amundsen* was with a colony of *Primnoa resedaeformis* collected from Saglek Bank (sample R19-19). This sample was stained to test for any toxicity indicators with the planned stain concentration for the *in situ* staining, and this experiment was conducted before the *in situ* staining of *A. arbuscula* and *K. flexibilis*. The colony was stained for about 8 hours in 150 mg/L calcein

solution in an aquarium with an aerator, located in a 4°C room (Fig. A4-1.5). The colony was then placed in a different aquarium with an aerator and bottom water from Saglek Bank and monitored for any signs of distress (Fig. A4-1.5).

With two live-collected *A. arbuscula* corals (R21-10, R21-16) from the Davis Strait ROV dive, a test was done on board the ship for effectiveness of the calcein solution in marking the coral skeletons. Once the ROV was recovered, the samples intended for staining on board were first photographed, and then placed in an aquarium with an aerator and 150mg/L calcein solution in a 4°C room. The samples were stained for 6 hours, and then placed in a different aquarium, with an aerator and bottom water from Davis Strait, which was collected with the CTD-Rosette on board the *Amundsen*. The samples were monitored for 2 days before being removed from the seawater and stored in plastic bags at -20°C.

A similar test was done with *K. flexibilis* samples (R23-bycatch2, R23-bycatch3) collected at Disko Fan. Samples were photographed once the ROV was recovered and then placed in an aquarium with 150 mg/L calcein solution and an aerator in a 4°C room (Fig. A4-1.5). The samples were stained for about 4 hours and then placed in an aquarium with bottom water from Disko Fan and an aerator in a 4°C room. The samples were monitored for 2 days post-staining for any signs of distress.

The samples stained on board the ship in aquaria were then analyzed under fluorescence microscopy (excitation wavelength: 488, emission wavelength: 509) using a Zeiss AxioZoom V.16 Telecentric Microscope for any signs of calcein marking on their skeletons. After this analysis, they were sectioned at a proteinaceous node of their skeleton

and embedded in epoxy. After allowing the samples to dry for at least 12 hours, samples were cut with an IsoMet low-speed saw and grinded and polished on a Buehler Meta-Serv 250 Grinder and Polisher. Cross-sections were then also analyzed under fluorescence microscopy for calcein marking on the growth rings.
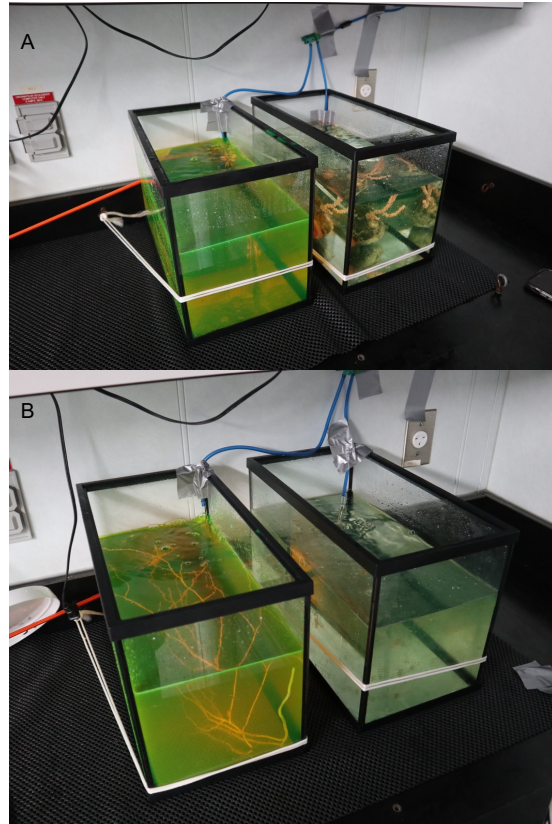

Figure A4-1.5. A) Colony of *P. resedaeformis* in an aquarium with bottom water from Saglek Bank. The colony was stained in calcein solution for about 8 hours before being placed in the aquaria with seawater. B) *K. flexibilis* samples R23-bycatch2 and R23-bycatch3 staining in 150 mg/L calcein solution on board the *Amundsen* after the Disko Fan ROV dive. These samples were stained for about 4 hours.

Table A4-1.1. Summary different concentrations and lengths of staining time experimented.

Concentration/Time Stained	*A. arbuscula*	*K. flexibilis*
150 mg/L, 4 hr	A 1-4	K 2-3
150 mg/L, 5 hr	A 1-1	K 2-4
150 mg/L, 6 hr	A 1-7	K 2-2
75 mg/L, 4 hr	A 1-8	K 3-5
75 mg/L, 5 hr	A 1-12	K 3-1
75 mg/L, 6 hr	A 1-13	K 3-2
60 mg/L, 4 hr	A 1-5	K 1-2
60 mg/L, 5 hr	A 1-3	K 3-3
60 mg/L, 6 hr	A 1-6	K 1-1
40 mg/L, 4 hr	A 1-10	K 1-3
40 mg/L, 5 hr	A 1-11	K 1-4
40 mg/L, 6 hr	A 1-9	K 3-4
10 mg/L, 24 hr	A 1-2	K 2-1

PRELIMINARY RESULTS

Summary of results and problems with first in situ staining attempt

The first *in situ* attempt to stain bamboo corals in deep Canadian waters was successful. Main problems with the techniques used was the buoyancy of the calcein solution during the Davis Strait ROV dive, which was resolved for the Disko Fan ROV dive by creating a hypersaline solution. Other difficulties included the size of the staining chamber because *A. arbuscula* and *K. flexibilis* colonies differ in size, meaning the staining chamber was not suited for both species. A sample of *K. flexibilis* was dislodged upon retrieval of the staining chamber, which may lead to difficulties with recollecting this sample in the future.

Live corals stained in aquaria on board the Amundsen in 2021

Based on observations, the *A. arbuscula* and *K. flexibilis* specimens collected live and stained in aquaria on board the *Amundsen* were alive post-staining, but their polyps were closed when removed from the seawater. Also, some tissue material had been shed during staining and afterwards when in seawater. A possible reason for the decline in coral health could have been lack of food, as we did not provide food for the corals while in the seawater post-staining.

The *A. arbuscula* samples stained in aquaria showed some fluorescing at the proteinaceous nodes only (Fig. A4-1.6). *K. flexibilis* samples were also imaged with fluorescence microscopy, and the internode sections of the *K. flexibilis* skeletons were fluorescing, but not the proteinaceous nodes (Fig. A4-1.6).

Cross-sections of the stained samples at the proteinaceous nodes, analyzed under fluorescence microscopy, showed fluorescing of the growth rings in both species (Fig. A4-1.7). Cross-sections at the calcite internodes did not show any fluorescing in the stained *A. arbuscula* samples, but the *K. flexibilis* calcite internodes did fluoresce slightly (Fig. A4-1.7).

Unstained samples of both species also showed fluorescing at the proteinaceous nodes, specifically along the growth lines (Fig. A4-1.8). Fluorescence was used for all remaining samples to enhance growth ring clarity for ring counts, aging, and growth rate assessments. Since the species tend to have fluorescent growth rings naturally, this may make visualizing the staining mark once samples stained *in situ* are collected much more

difficult. However, the stain may enhance the fluorescence significantly, which would
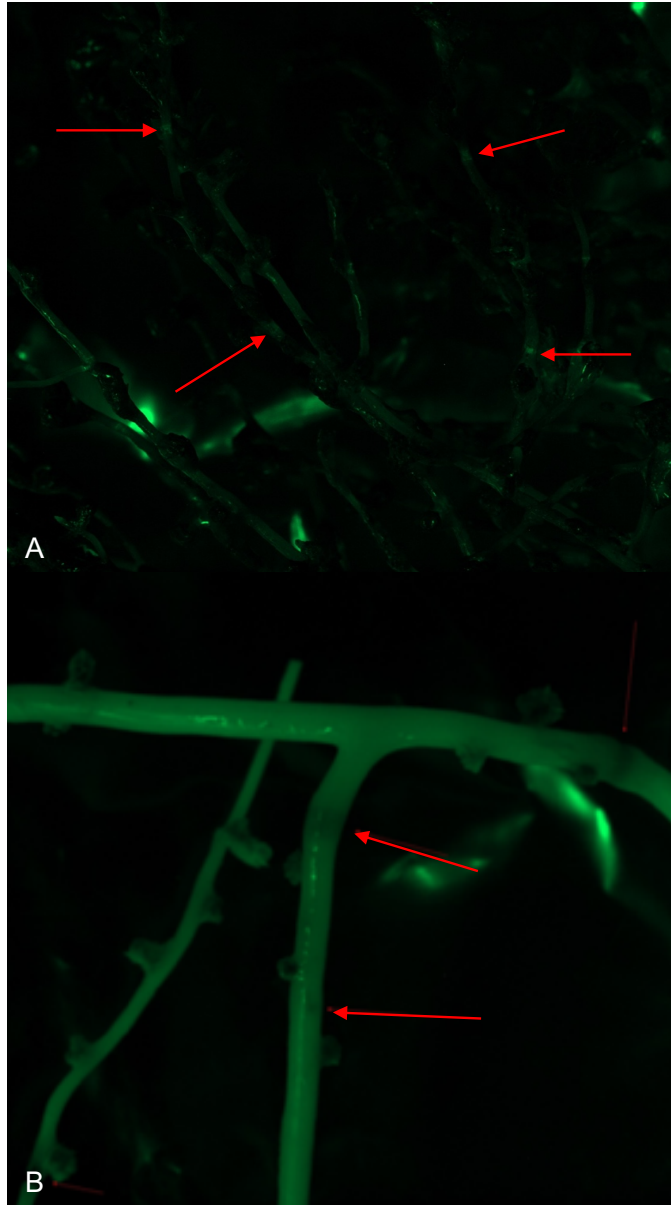
simplify visualizing the staining mark.

Figure A4-1.6. A) *A. arbuscula* colony R21-16 analyzed under fluorescence microscopy. Red arrows indicate slight fluorescing at the proteinaceous nodes of the skeleton. B) *K. flexibilis* sample R23-bycatch3 analyzed under fluorescence microscopy. The image shows fluorescing of the outside calcite skeleton. The red arrows are pointing to proteinaceous nodes of the skeleton, which do not seem to be visually fluorescing from outside the skeleton.
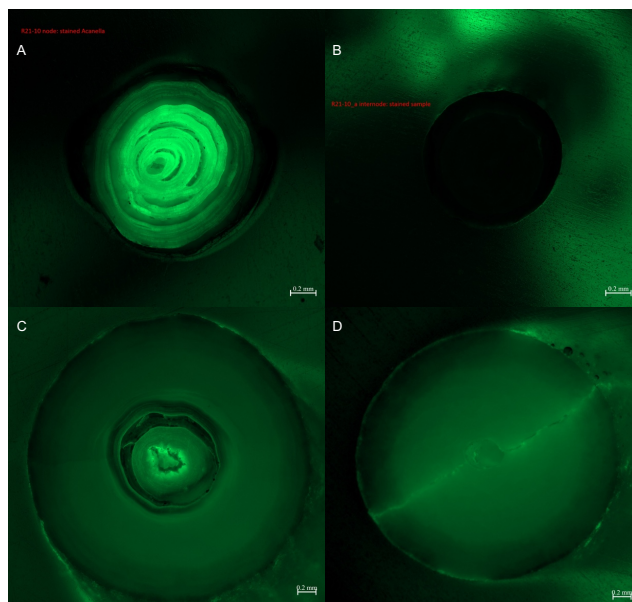
Figure A4-1.7. A) Cross-section of a proteinaceous node of an *A. arbuscula* sample (R21-10), which was stained with calcein solution on board the *Amundsen* in an aquarium. B) Cross-section of a calcite internode from the same *A. arbuscula* sample (R21-10). The internode did not fluoresce. C) Cross-section of a proteinaceous node of a *K. flexibilis* sample (R23-bycatch2) stained with calcein solution on board the *Amundsen* in an aquarium. D) Cross-section of a calcite internode of the same *K. flexibilis* sample (R23-bycatch2). The internodes showed some fluorescing in the calcite.
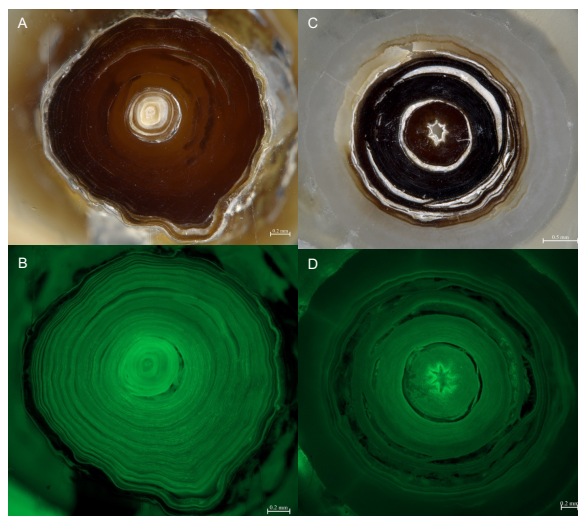

Figure A4-1.8. A) *A. arbuscula* (836_18_1) not stained with calcein shown in cross-section under normal reflected white light and B) the same cross-section under fluorescence microscopy, which improved growth ring clarity. C) *K. flexibilis* (R23-bycatch7b) not stained with calcein solution under reflected white light and D) the same cross-section under fluorescence microscopy.

FUTURE WORK

Collection of in situ stained samples

A. arbuscula and *K. flexibilis* corals stained *in situ* in 2021 with calcein solution will be collected in a future scientific mission. GPS coordinates of the stained corals were taken during staining to assist in relocating the samples. A floating marker and yellow markers in the sediment were also placed at the time of staining to help relocate the exact colonies that were stained. Photos from the staining will assist in finding the samples as well. The corals will be collected with the "Astrid" ROV aboard the *Amundsen*. Upon collection, the samples will immediately be measured for height, width, wet weight, and stem diameter, and stored in plastic bags at -20°C.

Analyses of in situ samples upon collection

Once collected, samples will be analyzed under fluorescence microscopy. The samples will first be analyzed for calcein stain marking on the outside of their skeleton. Samples will then be sectioned at the thickest proteinaceous nodes for analysis of staining marks within the growth rings.

Literature Cited

Lartaud F, Meistertzheim AL, Peru E, Le Bris N. 2017. *In situ* growth experiments of reef building cold-water corals: The good, the bad and the ugly. Deep-sea Research I. 121: 70-78.

Marschal C, Garrabou J, Harmelin JG, Pichon M. 2004. A new method for measuring growth and age in the precious red coral *Corallium rubrum* (L.). Coral Reefs. 23: 423-432.

Neves B de M, Edinger E, Hillaire-Marcel C, Saucier EH, France SC, Treble MA, Wareham VE. 2015. Deep-water bamboo coral forests in a muddy Arctic environment. Mar Biodiv. 45: 867-871.

Roberts JM, Cairns SD. 2014. Cold-water corals in a changing ocean. Current Opinion in Environmental Sustainability. 7: 118-126.

Roberts S, Hirshfield M. 2004. Deep-Sea Corals: Out of Sight, but No Longer out of Mind. Frontiers in Ecology and the Environment. 2: 123-130.

Sherwood OA, Edinger EN. 2009. Ages and growth rates of some deep-sea gorgonian and antipatharian corals of Newfoundland and Labrador. Can. J. Fish. Aquat. Sci. 66: 142 152.

Wareham VE, Edinger EN. 2007. Distribution of deep-sea corals in the Newfoundland and Labrador region, Northwest Atlantic Ocean. Bulletin of Marine Science. 81: 289-313.